Late Quaternary Sedimentation Processes and Sediment Accumulation Changes off Portugal

Dissertation
zur Erlangung des Doktorgrades
der Naturwissenschaften

im Fachbereich 5 Geowissenschaften
der Universität Bremen

vorgelegt von
Ulrich Alt-Epping
Bremen im Januar 2008

Tag des Kolloquiums:

2. Oktober 2008

Gutachter:

Prof. Dr. Dierk Hebbeln

Prof. Dr. Ralph Schneider

Table of Contents

Summary

Changes in the marine and continental environment comprise variations in climatic, hydrographic, biological or sedimentological parameters. Furthermore, such environmental changes occur on different timescales, ranging from seasons to millennia. Hence, a synoptic environmental reconstruction requires the combined interpretation of several parameters, which stand for specific environmental "boundary conditions" – such as temperature, wind strength, precipitation or biological productivity – plus an account for different temporal resolutions by an appropriate sampling design.

One of the dominating environmental mechanisms, that exceed a strong influence on European environmental conditions, is the North Atlantic Oscillation (NAO). Particularly over the Iberian Peninsula, the NAO determines precipitation as well as wind strength and hence the intensity of coastal upwelling along the western Portuguese margin. These environmental variations are finally recorded in sediments of the western Portuguese shelf, which combine marine and continental inputs from the Portuguese coastal realm and from the Iberian hinterland. Additionally to the high sensibility of shelf sediments to environmental fluctuations, the combined deposition of marine and continental material leads to high sedimentation rates, allowing paleoenvironmental reconstructions on a high temporal resolution.

To identify the present day situation of sediment supply from riverine and marine sources, surface samples from four different regions along the western Portuguese shelf are analysed in terms of the provenance of their organic matter.

In the northern sampling region off the Douro River mouth, river discharged, continental input is combined with marine, autochthonously produced material. Sediments close to the Nazaré Canyon contain small amounts of continental material, which is probably transported southwards along the coast. Surface sediments inside the Tagus Estuary show a clear imprint of continental organic material, but also evidence for anthropogenic and agricultural pollution. The decrease of continental organic contributions on the Tagus Prodelta is visible by an increasingly marine source signature in the organic matter off the Tagus Estuary mouth, including a preferential transport of estuarine material southward towards the canyons. The southern sampling region off Cape Sines is characterised by exclusively marine input, due to the absence of major rivers in the vicinity.

Supplementary, visual and hydroacoustic investigations with a remotely operated vehicle (ROV) and with a parametric echosound system along the coast reveal a highly variable sediment texture with sharp boundaries between different sediment textures.

An evaluation of changing sediment properties during the past 3000 years on a high temporal resolution is obtained by a multi-proxy analysis of a 5.4m long gravity core from the Tagus Prodelta (GeoB 8903). Data from this core shows no changes in hydrographic conditions nor in the quantity of terrigenous organic matter input through time. Instead, physical sediment properties such as magnetic susceptibility and grain-size indicate changes in sediment supply and transport mechanisms around 2000yrs BP and 600yrs BP (i.e.

AD1400). A detailed analysis of the grain-size spectra yields three lithic end-members of the sediment, which are clearly related to organic and inorganic sediment properties. The magnetic susceptibility signal is carried by the finest end-member, organic carbon is related to an intermediate end-member and the calcium carbonate correlates with the coarsest sediment component. These results allow inferences about sources and transport mechanisms of each end-member and of the associated proxy. The end-members also show a correlation with the North Atlantic Oscillation, which has a strong impact on environmental conditions in the research area. These findings further emphasise the importance of an integrated interpretation of multi-proxy data by revealing a clear association of organic and inorganic sediment properties to a specific grain-size spectrum.

A long-term view on regional environmental changes is obtained by the analysis of a deep sea core MD03-2698 and its comparison to a piston core from the Tagus prodelta. These cores cover the Holocene and the last Deglaciation. The comparison between the deep sea and shelf record reveals differences, but also similarities between deep water and shelf environments. In the deep realm, long-term processes, such as changes in thermohaline circulation play a major role by affecting deep-water mass properties particularly during the Deglaciation. Changes in sea level affect the settings of both sediment cores by quantitatively changing the supply of terrigenous sediment to the deep sea and by changing the volume of sediment accommodation space on the shelf. Additionally, the postglacial sea level rise leads to a relocation of the upwelling cells from the shelf edge onto the shelf, which becomes evident by nutrient budget proxies.

The effect of tsunamis on shelf sediments is spatially inhomogeneous, with stronger evidence for sediment reworking, interpreted as a results of tsunamis, in sediments from the southern Tagus prodelta. Contrary, in western sediment records a tsunami impact is not clearly evident.

Zusammenfassung

Veränderungen im marinen und kontinentalen Lebensraum beinhalten Variationen klimatischer, hydrographischer, biologischer und sedimentologischer Parameter. Zudem finden solche Veränderungen in verschiedenen zeitlichen Dimensionen statt – von saisonal bis zu Jahrtausenden. Eine synoptische Rekonstruktion früherer Umweltbedingungen erfordert daher eine Kombination von Daten, die indikativ für bestimmte Umweltparameter sind, sowie die Berücksichtigung der verschiedenen relevanten Zeiträume durch eine angemessene Beprobungsstrategie.

Einen wichtigen Einfluss auf die Umweltbedingungen in Europa hat die Nordatlantische Oszillation (NAO). Besonders auf der Iberischen Halbinsel bestimmt die NAO Niederschlag und Windstärke; letzteres wiederum beeinflusst die Intensität des küstennahen Auftriebs entlang der portugiesischen Westküste. Variationen dieser Parameter können in Sedimenten, z.B. entlang des westlichen portugiesischen Schelfs, aufgezeichnet werden. Die in diesem Fall kombinierte Ablagerung marinen und kontinentalen Materials führt zu einer höheren Sensibilität der Sedimente gegenüber Umweltveränderungen im marinen und kontinentalen Bereich, sowie außerdem zu hohen Sedimentationsraten, die zeitlich hochauflösende Rekonstruktionen ermöglichen.

Die heutige Verteilung mariner und kontinentaler Sedimente wird beispielhaft in vier Gebieten entlang der portugiesischen Westküste untersucht, indem die Herkunft organischen Materials analysiert wird. Im nördlichsten Gebiet vor der Mündung des Douro Flusses zeigen die geochemischen Eigenschaften der Oberflächensedimente einen deutlichen terrigenen Flusseintrag. Am nördlichen Rand des Nazaré Canyons dagegen enthalten die Sedimente bzw. das darin enthaltene organische Material einen geringen Anteil terrigener organischer Substanz, die vermutlich küstenparallel südwärts transportiert wurde und aus dem Flusseintrag des nördlichen Schelfs stammt. Sedimente aus dem Tagus Ästuar sind eindeutig kontinentaler Herkunft, einschließlich eines Signals landwirtschaftlicher Nutzung im Einzugsgebiet. Außerhalb des Ästuars nimmt der Anteil terrigener organischer Substanz mit zunehmender Entfernung von der Ästuarmündung ab. Dort lässt sich der bevorzugte Transport ästuarinen Materials südwärts in Richtung des Lisbon und Setubal Canyons nachweisen. Im südlichsten Probengebiet vor Kap Sines besteht das Sediment ausschließlich aus marinem Material, da hier kein nennenswerter Flusseintrag existiert.

Zusätzliche visuelle und hydroakustische Untersuchungen des Meeresbodens durch einen unbemannten Tauchroboter (ROV) sowie durch hochauflösende Seismik zeigen, dass die Sedimentstrukturen am Meeresboden sehr variabel sind und dass strukturell homogene Bereiche scharf gegeneinander abgegrenzt sind.

Zeitlich hochauflösende Veränderungen der Sedimenteigenschaften während der letzten 3000 Jahre werden durch die Analyse eines 5.4m langen Schwerelot-Kerns vom Tagus Prodelta rekonstruiert (GeoB 8903). Hydrographische Bedingungen sowie die Herkunft organischen Materials blieben demnach konstant. Veränderungen werden jedoch in physikalischen Eigenschaften wie magnetischer Suszeptibilität und Korngrößenspektrum beobachtet, was als Resultat veränderter Transportmechanismen sowie einer veränderten Herkunft der anorganischen Sedimentfraktion jeweils ca. 2200 und 600 Jahre vor heute interpretiert wird. Detaillierte Korngrößenanalysen zeigen drei

lithische Komponenten, die eng mit anderen Sedimentparametern gekoppelt sind. Eine feine Komponente korreliert mit magnetischer Suszeptibilität, während eine Komponente mittleren Korngrößenspektrums mit Gehalt organischen Kohlenstoffs zusammenhängt. Eine gröbste Komponente korreliert stark mit dem $CaCO_3$-Gehalt. Diese Zusammenhänge erlauben Rückschlüsse über Transportmechanismen und somit über die Herkunft der einzelnen Sedimentbestandteile. Zusätzlich zeigen die relativen Anteile dieser drei lithischen Sedimentfraktionen, sowie die magnetische Suszeptibilität und die durchschnittliche Korngröße des Sediments eine Korrelation mit dem NAO Index. Dieser Zusammenhang zwischen Proxies, Korngrößenspektra und externer Umwelteinflüsse zeigt die Notwendigkeit, eine Vielzahl von Parametern in die Interpretation zu integrieren.

Durch den Vergleich eines Tiefseekerns (MD03-2698) mit einem Schelfkern (D13882) zeigen sich langfristige regionale Umweltveränderungen. Die Kerne umfassen das Holozän sowie das Ende der letzten Eiszeit und zeigen Unterschiede, aber auch Gemeinsamkeiten in den jeweiligen Gebieten. In der Tiefsee spielen langfristige Prozesse, wie Variationen der thermohalinen Zirkulation eine Rolle, speziell gegen Ende der letzten Eiszeit. Meeresspiegelschwankungen beeinflussen sowohl Tiefsee, als auch den Schelfbereich durch Veränderungen des küstennahen Akkomodationsraums und durch die daraus folgenden Schwankungen terrigenen Eintrags. Auch das Auftriebsmuster wird durch Meeresspiegelvariationen beeinflusst, indem sich durch den postglazialen Anstieg des Meeresspiegels das Zentrum des Auftriebs von der Schelfkante auf den Schelf verlagert.

Der Einfluss von Tsunamis – z.B. AD1755 – auf die Schelfsedimente ist räumlich nicht homogen und im Umfang unklar. In Sedimenten des südlichen Tagus Prodeltas finden sich stärkere Hinweise auf tsunami-generierte Umlagerung, während in Sedimenten des westlichen Prodeltas solche Anhaltspunkte fehlen.

1 Introduction

1.1 Scientific Rationale

The reconstruction of past environmental conditions is an essential prerequisite, to view present environmental changes in an objective way. In order to obtain a synoptic picture of the past environmental setting and its changes, information about the various relevant environmental parameters must be gathered. These comprise e.g. climatic, geological, biological or hydrological conditions and processes, which are usually closely connected by feedback mechanisms, but should still be considered individually. Suitable sources of information, which combine signals from various sources and thus allow a distinction between the individual climatic parameters, are shelf sediments. Due to their location at the continent-ocean interface, they record continental and marine environmental parameters combined. By the analysis of these sediments, it is possible to reconstruction continental and marine environmental parameters and to assess the interactions between relevant environmental processes.

Fig. 1.1 shows some examples of relevant processes in a shelf setting, which affect the amount and composition of shelf sediments and that are eventually recorded in the sediments. Relevant boundary conditions include climatic parameters, such as temperature, precipitation or wind regime, as well as hydrographic, biological, anthropogenic and sedimentological factors. These are closely connected, e.g. sea level changes affect the coastal upwelling regime, hence marine productivity and have therefore an influence on the larger biosphere. Despite these close feedbacks, analysing a range of indicative properties of the shelf sediments can differentiate important environmental parameters. However, such a multi-proxy approach must also integrate biasing effects of sediment transport processes and (post-) depositional mechanisms. Chemical and physical sediment properties such as organic carbon content or magnetic susceptibility can often be related to grain-size and may thus be biased by sorting processes prior, during or after deposition. It is therefore essential, to include information about the sediment grain-size spectrum and to evaluate a potential dependence of sediment properties on grain-size.

Changes in environmental conditions occur on different timescales, which may range between months and millennia (Fig. 1.2). Examples for this in a climatic context are centennial climatic oscillations such as the Medieval Warm Period or the Little Ice Age, which are superimposed on long-term glacial/interglacial cycles. Accordingly, different timescales must be considered during sample acquisition in order to obtain a complete image of environmental changes. Reconstructions of short-term environmental conditions and changes require sediment records with a high temporal resolution. As these often cover only a relatively short time span, records with a lower temporal resolution are needed to evaluate long-term processes. Thus it is possible to account for the different time scales, on which environmental processes occur.

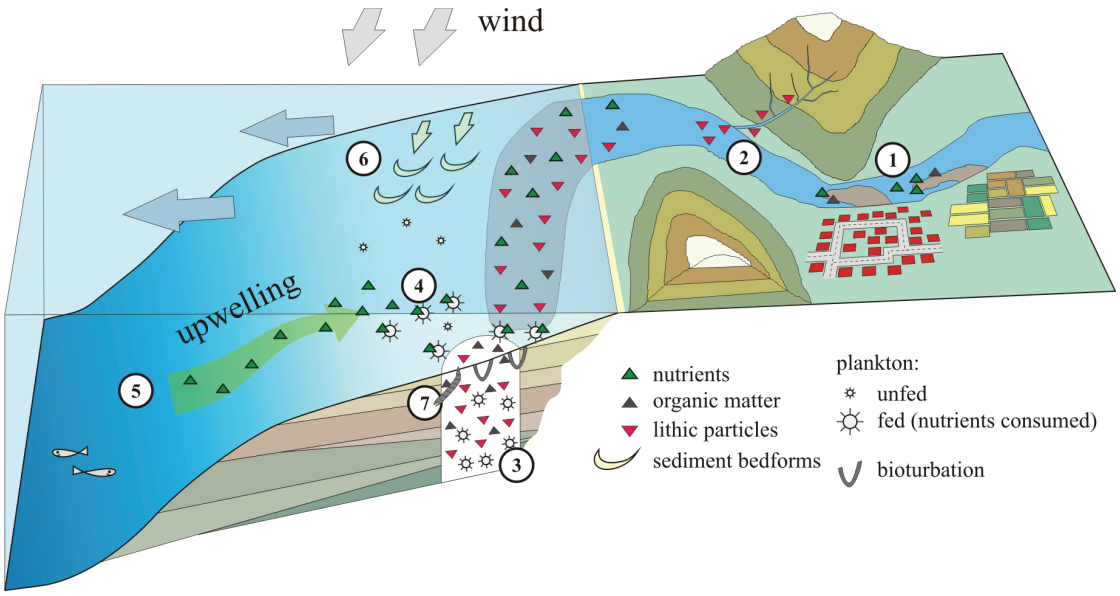

Fig. 1.1: Some relevant processes in a coastal environment, which are eventually recorded in marine shelf sediments. Riverine material is discharged onto the shelf, transporting terrigenous organic matter (black triangles), fertilising matter from agricultural or urban sources (green triangles, 1) and inorganic components from the hinterland (red triangles, 2). Wind-driven upwelling provides fresh deep-water nutrients (green triangles, 5), thereby increasing marine productivity on the shelf (4). Material from these various sources is deposited as shelf sediment and eventually recovered in a sediment core (3). Sorting processes and postdepositional reworking of sediment are the results of possibly wind-induced bottom currents (6) or bioturbation (7).

1.2 Implementation

To achieve the desired goals, suitable sediment archives must be obtained. These ideally come from a region, which combines inputs of material from marine and continental sources, with both source regions being sensitive to environmental processes and changes. Furthermore, the sampling region must be characterised by high sedimentation rates, which allow high-resolution studies. Such conditions are found along the western Portuguese shelf, where large amounts of sediment from both, marine and continental sources are deposited. The hinterland, the Iberian Peninsula, is under a strong influence of the NAO, which determines precipitation and wind strength, thus influencing the input of continental material to the shelf (e.g. HURRELL and LOON, 1997; TRIGO et al., 2004). The NAO affects also hydrographic conditions in the marine realm on different spatial and temporal scale, e.g. by influencing the intensity of wind-driven, coastal upwelling (e.g. SKINNER and SHACKLETON, 2004, for a basin-wide approach; ABRANTES et al., 2001, for a local perspective). High sedimentation rates on the shelf allow analyses on high temporal resolutions. Nevertheless, considerable

amounts of marine and continental sediments are transported across the shelf into the deep sea. Here, they accumulate more slowly and record environmental variations on a lower temporal resolution, recording additional environmental information from the oceanic realm, such as changes in the geological and sedimentological setting (MILLIMAN, 1990; WEAVER et al., 2000; DIAS et al. 2002b, HOLZ et al., 2004), including sea level variations (DIAS et al., 2000).

The broad spectrum of influences as well as their interconnections demands a broad methodological approach, which is achieved by the combined interpretation of elemental and stable isotope ratios of organic carbon and nitrogen, abundance of major and trace elements, magnetic susceptibility and detailed grain-size analysis, including numerical modelling of potential end-members of the sediment grain-size spectrum. Additionally, acoustic and visual surveys of the sea floor were conducted with a parametric echosound system and a remotely operated vehicle (ROV).

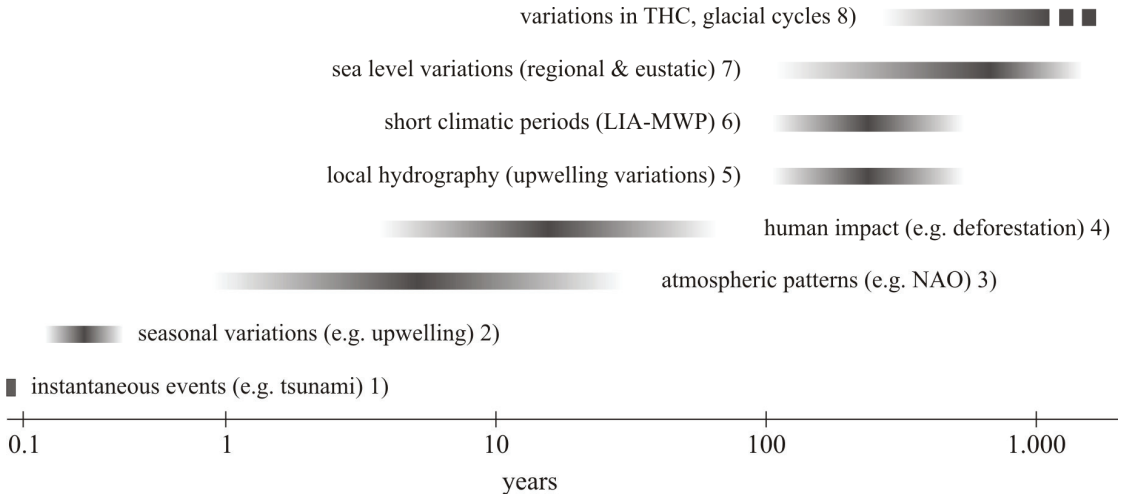

Fig. 1.2: Dependence of environmental processes on the timescale, with a focus on the Portuguese margin. References: 1) ANDRADE et al., 2003; ABRANTES et al., 2005. 2) FIUZA, 1983. 3) TRIGO et al., 2002; VICENTE-SERRANO et al., 2004. 4) DESPRAT et al., 2003. 5) SOARES et al., 2006. 6) BARTELS-JONSDOTTIR et al., 2006. 7) DIAS et al., 2000. 8) BIANCHI et al., 1999; D'ABREU et al., 2003.

The association of environmental processes and changes to a specific timescale (Fig. 1.2) is accounted for during sample acquisition. In a first stage, recent surface sediments from four regions along the western Portuguese margin are analysed for the content of terrigenous sedimentary organic matter based on C_{org}/N_{total} ratios and $\delta^{13}C_{org}$ values, as well as for the spatial pattern of seasonal upwelling along the coast, based on sedimentary $\delta^{15}N$ values. Past variations on multidecadal and centennial timescales are reconstructed from physical and chemical properties of a sediment core off the Tagus Estuary mouth, where high sedimentation rates provide paleoenvironmental information on a high temporal resolution. Finally, a

long piston core from the Tagus Canyon levée is investigated on a centennial and millennial scale resolution and correlated to a second shelf record. This combination enables the comparison and correlation of long-term changes on the shelf and in the oceanic realm.

2 Portuguese Margin

The Portuguese shelf can be divided into three sections, which are distinct by their predominant sediment type and sedimentological character (Fig. 2.1).

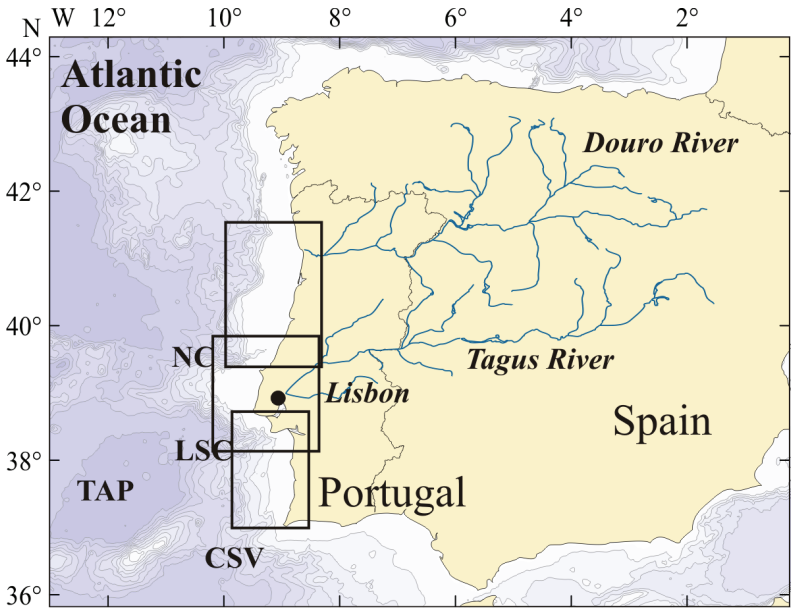

Fig. 2.1: Overview map of the Iberian Peninsula. Rectangles indicate the enlargements, shown in Figs. 2.2, 2.3 and 2.5. NC: Nazaré Canyon; LSC: Lisbon and Setubal Canyons; CSV: Cape S. Vicente; TAP: Tagus Abyssal Plain.

2.1 Northern Shelf

The northern part of the Portuguese shelf is 30-50km wide and covered by dominantly sandy sediments (DIAS et al., 2002b). The reduction of current velocities by cretaceous outcrops on the shelf leads to the accumulation of silty sediments, which form elongate mud belts parallel to the coast (JOUANNEAU et al., 1998; DIAS et al., 2002b) (Fig. 2.2). These mud belts are particularly pronounced in front of the Douro River mouth, where a ca. 5m thick silt layer covers an area of ca. 500km^2. The mean grain size on the mud belt ranges from 10 to 40µm, with a slight fining trend towards offshore (JOUANNEAU et al., 2002; DRAGO et al. 1999; OLIVEIRA et al., 1999).

Average sedimentation rates on the northern shelf are around 0.01cm/yr (BAAS et al., 1997). In the Douro mud patch sedimentation rates vary between 0.05 and 0.4cm/yr (JOUANNEAU et al., 2002; DIAS et al., 2002a), locally 0.57cm/yr (DRAGO, 1999). The Nazaré Canyon forms the southern boundary of the northern shelf section. It incises the shelf almost up to the coast and serves thus as an efficient drainage for shelf sediments to the deep sea.

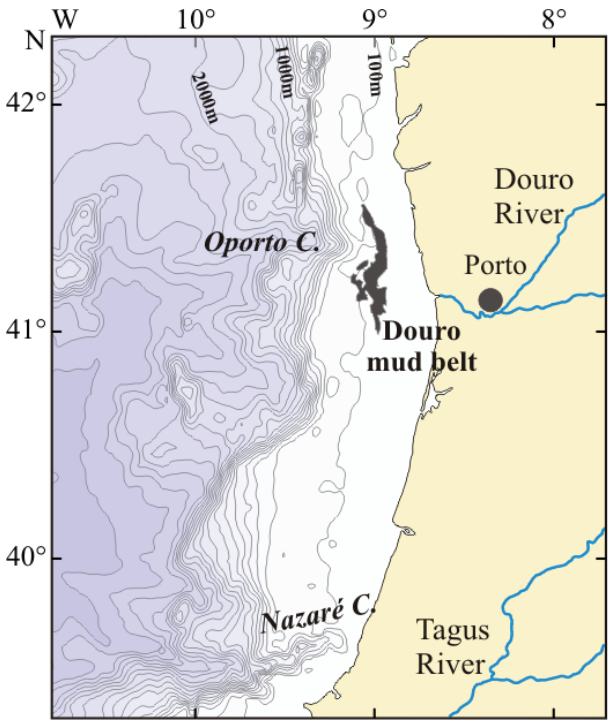

Fig. 2.2: Map of the northern part of the Portuguese shelf, showing the Oporto and Nazaré Canyons and a part of the Douro mud belt.

The Douro River is the main source for terrigenous sediment to the northern shelf (ARAUJO et al., 1994; DIAS, 1987; DIAS et al., 2002a), draining 95.700km^2 of mountainous hinterland with precipitation rates of more than 1000mm/yr (LOUREIRO and MACEDO, 1986) (Fig. 2.1). 67% of the river's catchment are used as cropland and 10% are covered by urban and industrial areas (WATER RESOURCE E-ATLAS: http://earthtrends.wri.org). The river discharges on average 420m^3/s water directly into the sea (VIEIRA and BORDALO, 2000; OLIVEIRA et al., 2002), showing a strong seasonality. Annual sediment discharge is estimated to be around 2.25million tons (OLIVEIRA et al., 1982), constituting 80% of total riverine sediment supply onto the northern shelf (DIAS et al., 2002b) and leading to recent shelf sediment accumulation (OLIVEIRA et al., 1982). A surface nepheloid layer during summer, which may extend 30km offshore, and a bottom nepheloid layer during winter indicate the transport of suspended sediment by the Douro River onto the shelf (DRAGO et al., 1998; JOUANNEAU et al., 1998).

2.2 Central Shelf

The central part of the shelf is located between the Nazaré and Lisbon Canyon (Fig. 2.3). Sediment accumulates on a 560km^2 large mud patch west of the Tagus Estuary mouth with sedimentation rates around 0.47cm/yr (ABRANTES et al., 2005), locally reaching more than 2cm/yr (JOUANNEAU et al., 1998), compared to around 0.02cm/yr (BAAS et al., 1997) on the Tagus prodelta. Although sedimentation rates on the shelf are high, a considerable fraction of sediment is transported through the Lisbon and Setubal Canyons to the Tagus Abyssal Plain (JOUANNEAU et al., 1998).

Sediments and nutrients are supplied to the shelf by the Tagus River, which is with ca. 1000km the longest river of the Iberian Peninsula, draining a ca. 80.600km^2 large watershed (Fig. 2.1). Vegetation in its watershed is strongly influenced by agricultural activity and dominated by C3 plants. Almost 50% of the catchment area is utilised as cropland whereas urban and industrial areas cover ca. 17% of the catchment area (WATER RESOURCE E-ATLAS: http://earthtrends.wri.org). Precipitation rates in the catchment area are about 900mm/yr in the North and 650mm/yr in the South (LOUREIRO and MACEDO, 1986).

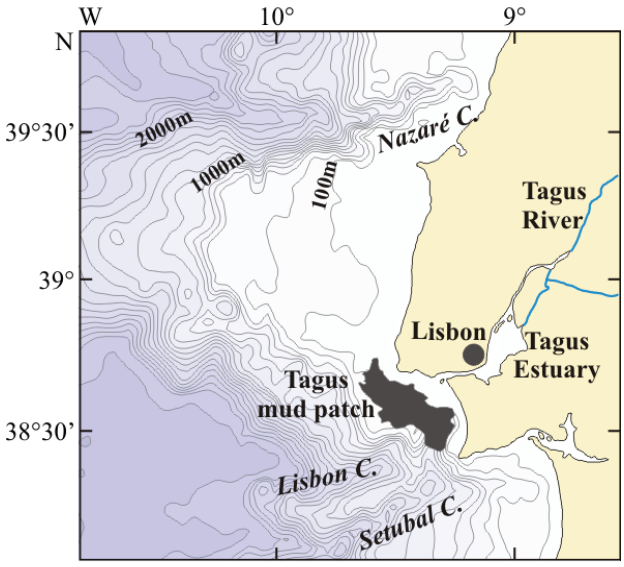

Fig. 2.3: Central part of the Portuguese margin off the Tagus River mouth, bordered by the Nazaré and Lisbon/ Setubal Canyos. Mud patch outline is according to JOUANNEAU et al. (1998).

The discharge is on average 364m^3/s, oscillating from 80m^3/s in summer months to 720m^3/s in winter months (LOUREIRO, 1979). The suspended matter carried by the Tagus outflow (Fig. 2.4) is transported across the Tagus mud patch and reaches as far as to the Lisbon Canyon (JOUANNEAU et al., 1998). The associated nepheloid layer is subject to seasonal variations with an extensive surface nepheloid layer during summer, extending up to 14km offshore, and a bottom nepheloid layer during winter (JOUANNEAU et al., 1998). An

estimated amount of between 0.4 and 1 million tons suspended material is exported to the shelf annually (JOUANNEAU et al., 1998). River discharged nutrients fertilise marine productivity on the Tagus prodelta and lead to a perennially high chlorophyll concentration (Fig. 2.6).

Fig. 2.4: Space image, showing the plume of the Tagus River, extending across the shelf and the Tagus mud patch. Image Science and Analysis Lab, NASA (earth.jsc.nasa.gov/sseop/EFS/ photoinfo.pl? PHOTO=STS047-85-95).

The Tagus feeds into the Atlantic Ocean through a large mesotidal estuary. The estuary is ca. 50km long and 350km^2 large. In the upper part it is 15km wide and has a water depth of around 15m, whereas the lower part is only ca. 2km wide, forming a channel with a water depth around 40m. The tidal range varies between 1 and 4m, resulting in current velocities of up to 2m/s (JOUANNEAU et al., 1998). The tidal reverse flow reaches 50km upstream (Vila Franca de Xira) and drives the estuarine water circulation (CABECADAS, 1999), resulting in a well mixed salinity distribution (LEMOS, 1984; VALE and SUNDBY, 1987). The turbidity of the estuarine waters shows a maximum in the uppermost part of the estuary, between Vila Franca da Xira and Santa Iria, where the suspended particle load reaches more than 200mg/l. Upstream and seawards this value decreases, reaching 20-40mg/l in the lower estuary channel (CASTANHEIRO, 1982). This trend coincides with a salinity gradient from 3‰ close to Vila Franca de Xira to 30‰ south of Sacavém (half the length of the upper estuary) (CASTANHEIRO, 1982) and is therefore assigned to flocculation of riverine, dissolved organic material.

Chlorophyll-*a* concentration in the lower estuary is 0.5-4.3mg/m^3, indicating a daily primary production between 30 and 135mgC/m^2 (CABECADAS, 1999). Sedimentation rates inside the estuary are highly variable, ranging from 0.7cm/yr in Seixal Bay in the southern estuary (FREITAS et al., 1999) as well as in the upper estuary (CASTANHEIRO, 1982) to 3.4cm/yr at the southern bank of the estuary channel (CASTANHEIRO, 1982). Although the estuary acts on average as a depocentre, the sedimentary evolution is characterized by varying erosion and redeposition, leading to a high spatial and temporal variability of the bathymetry (CASTANHEIRO, 1982).

2.3 Southern Shelf

The shelf between Setubal Canyon and Cape St. Vicente is relatively broad with no major fluvial contributions (Fig. 2.5) and sediments are mainly sandy. The usually planar sea floor of the southern shelf is perturbed by the Principes d'Avis Spur, which forms an approximately 400m high elevation on the sea floor between 37.65°N and 37.83°N / 9.38°W and 9.43°W in ca. 1000m water depth. During a ROV survey rocky outcrops have been observed at the same latitude close to the coast. These may be foothills or eastward extensions of the Principes d'Avis Spur.

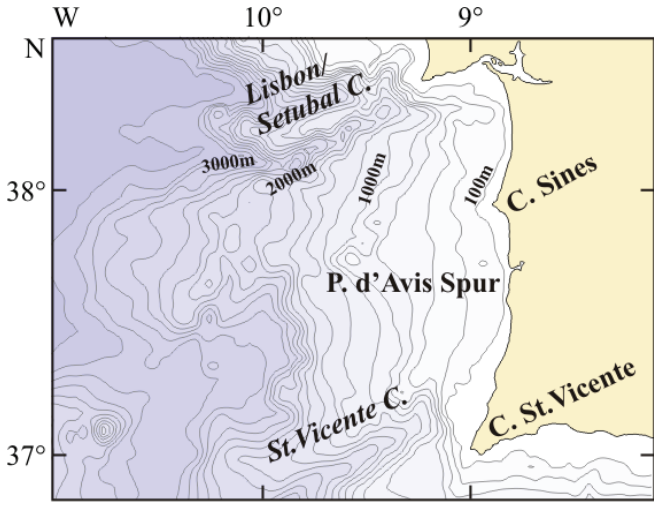

Fig. 2.5: Southern Portuguese margin off Cape Sines, between Setubal and St. Vicente Canyons.

2.4 Hydrography and Marine Productivity

The deep water masses along the Portuguese margin are constituted by North Atlantic Deep Water, flowing southward below 1500m water depth (VAN AKEN, 2000a/b; FIUZA et al., 1998). Mediterranean Outflow Water (MOW) flows northward along the slope between 500 and 1500m depth, creating contourites and active winnowing in its shallow part along the southern shelf (ZENK and ARMI, 1990; SCHÖNFELD, 1997). North Atlantic Central Water overlies the MOW, reaching 70m below the sea surface. The dominating large scale surface current is the southward directed Portugal Current (or Canary Current). The Portugal Coastal Current flows northward during upwelling (FIUZA, 1983) and the Portuguese Coastal Counter-current flows southward during downwelling (PELIZ and FIÚZA, 1999). Hence, the direction of these shallow coastal currents, which also control coastal sediment transport, is controlled by wind direction (DRAGO et al., 1998).

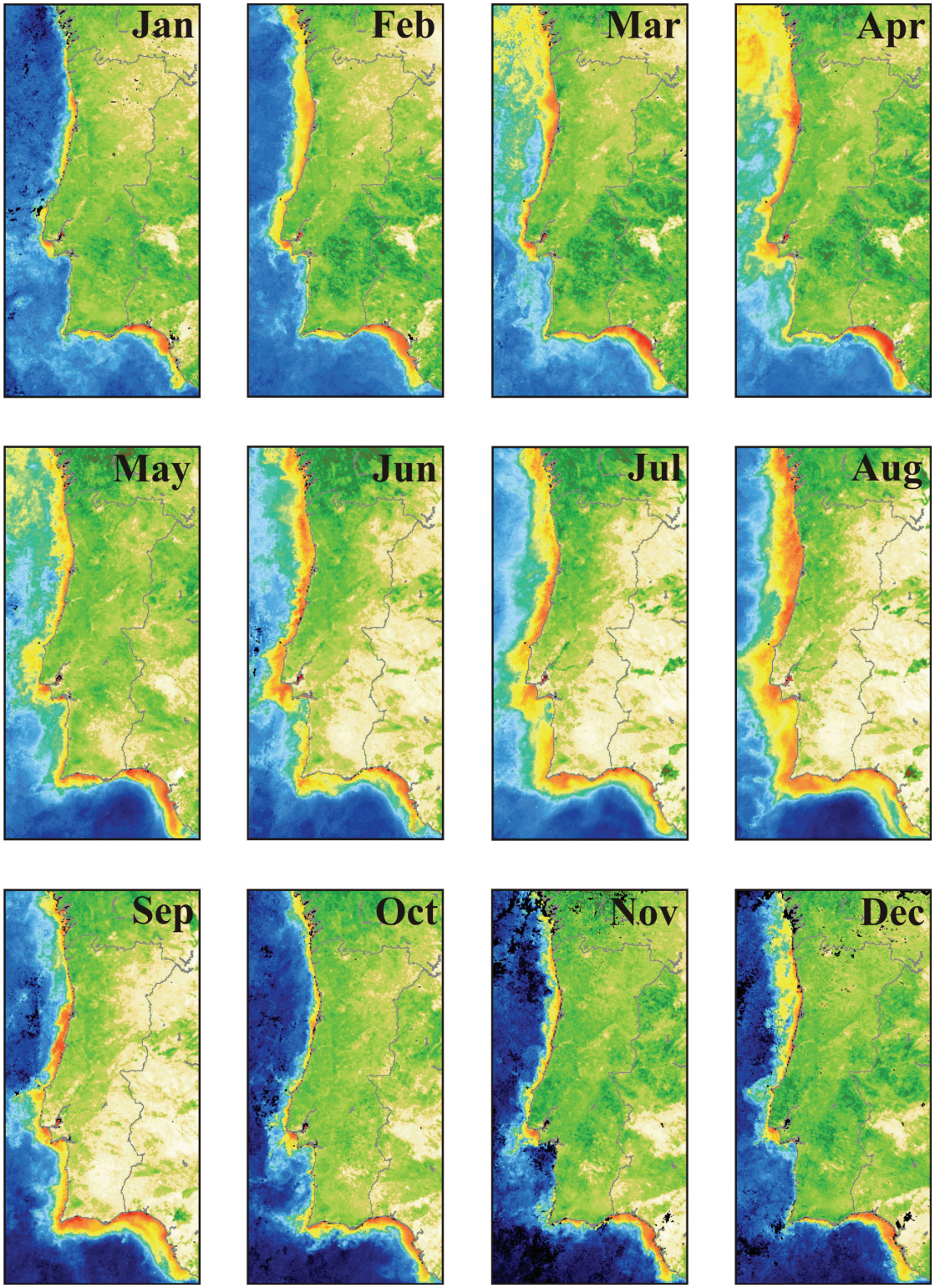

Fig. 2.6: Chlorophyll-a concentration from SeaWifs and Modis during the year 2002. Increased marine productivity, fertilised by seasonal upwelling and perennial discharge of the Tagus River are visible (http://oceancolour.jrc.ec.europa.eu/).

Southerly winds, caused by the location of the Azores High off the northwest African coast during winter months, generate downwelling conditions. During spring and summer, the seasonal relocation of the Azores high-pressure system closer to the Iberian coast causes northerly winds, triggering upwelling along the Portuguese margin (FIÚZA, 1983; Fig. 2.6). During winter months the Azores High is located off the northwest African coast, resulting in southerly winds, which favour downwelling conditions. Upwelling of cold, nutrient rich waters from depths between 60 to 120m (FIUZA, 1982) occurs along the coast mainly from May to September and is especially pronounced along the Galician coast, north of the Nazaré Canyon, at the Tagus River mouth and south of Cape Sines, as observed by satellite remote sensing (Fig. 2.6). A less pronounced phytoplankton bloom occurs also around January and February (DIAS 2002a), which is fertilised by the increased riverine input of terrigenous nutrients. Fig. 2.6 shows diffuse patches of elevated chlorophyll concentration during spring off the northern coast. Marine primary productivity is around 600mgC/m^2/day (year average) along the Portuguese coast, reaching up to 900mgC/m^2/day during high productivity periods (http://www.seaaroundus.org).

2.5 North Atlantic Oscillation

The North Atlantic Oscillation (NAO) is an atmospheric pattern, which has a profound impact on European climate. It is generated by oscillating atmospheric pressure gradients between the Iceland Low and the Azores High pressure systems (Fig. 2.7). With respect to reference stations in southwest Europe (mostly Lisbon, Gibraltar or Ponta Delgada, Azores) and northwest Europe (mostly Reykjavik, Iceland), the offset to a reference value is defined as NAO-Index (NAOI, Fig. 2.8). The effect of the NAO on e.g. precipitation on the Iberian Peninsula becomes evident by correlating the NAO index with precipitation rates. Correlation coefficients range from -0.2 in the eastern and northern part of Iberia to -0.6 in the Southwest (VICENTE-SERRANO and HEREDIA-LACLAUSTRA, 2004). Accordingly, a negative NAO leads to increased precipitation over the Iberian Peninsula (TRIGO et al., 2004) and to enhanced river runoff (BENITO et al., 2003 for the Tagus River). Generally, the NAO has a similar effect on temperatures over Europe, but on the Iberian Peninsula correlation coefficients between NAO index and temperature are around 0 (VISBECK at al., 2001). A positive NAO index results in stronger winds due to the stronger gradient between the Iceland Low and Azores High. As the coastal current system, including upwelling, is mainly wind driven, stronger wind intensity leads consequently to higher current velocities and stronger upwelling (Fig. 2.7).

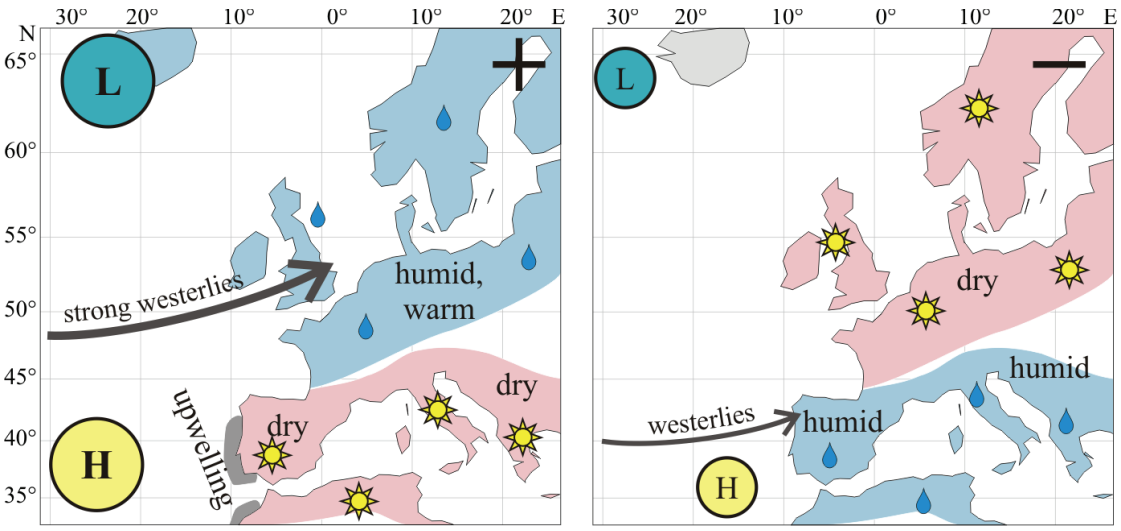

Fig. 2.7: Weather conditions during positive (left) and negative (right) NAO states, showing the impact of the NAO on weather and climate in Europe and over the Iberian Peninsula.

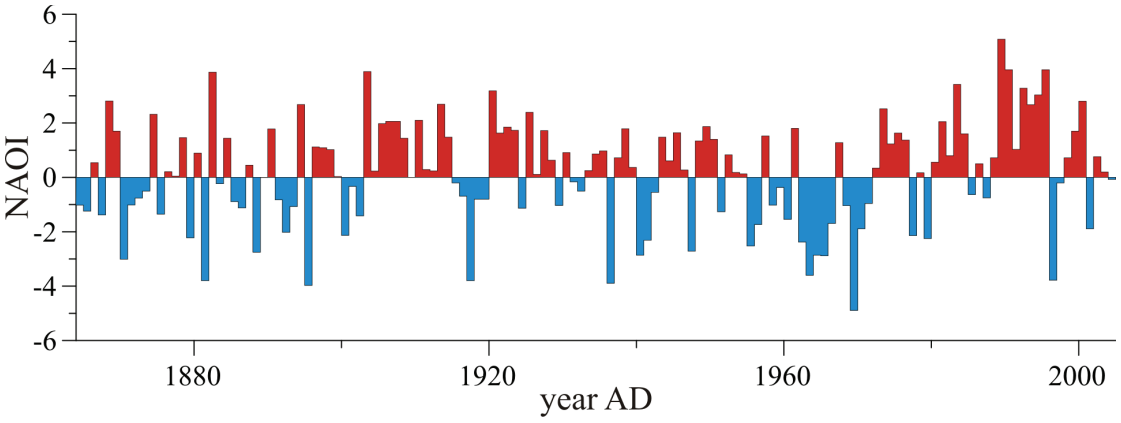

Fig. 2.8: North Atlantic Oscillation Index: Difference between Lisbon and Reykjavik (Iceland) sea level pressure, 1864-2005. Values are normalised to the average 1864-1994, annual values are averages of December through March, ascribed to each January (after HURREL and LOON, 1997).

2.6 Previous work

Considerable research has been conducted on environmental parameters, which are relevant for the Portuguese margin. Atmospheric conditions, namely the NAO, have been reconstructed by HURREL and LOON (1997) and their feedback on the environment on the Iberian Peninsula has been investigated e.g. by TRIGO et al. (2004) or – including a spatial component – by VICENTE-SERRANO and HEREDIA-LACLAUSTRA (2004). The results show consistently high rainfall during NAO negative phases, although the degree of correlation between NAO and precipitation varies across Iberia.

Oceanographic changes on a long term, i.e. regarding centennial and millennial variations of the North Atlantic section of the global thermohaline circulation, were reconstructed e.g. by SKINNER and SHACKLETON (2004), concentrating on Termination I. SOARES and DIAS (2006) investigated the regional impact of millennial scale hydrographic variability on regional radiocarbon reservoir ages. They were thus able to distinguish periods of stronger or weaker upwelling, although on a varying temporal resolution. Similarly, ABRANTES et al. (2001) reconstruct the local upwelling history by a multi-proxy analysis of marine sediments.

A detailed record of sea level changes and its effect along the Portuguese margin is provided by DIAS et al. (2000) based on sedimentological data. The distribution of shelf sediments is described e.g. by DIAS et al. (2002b) and by JOUANNEAU et al. (1998, 2002), concentrating on the mud belts off the Douro and Tagus Rivers. A detailed analysis of abundance and relative changes of grain-size end-members from marine sediments off the NW African margin (HOLZ et al., 2004) allows a first evaluation of sources and transportation pathways of the lithic sediment fraction also off the Portuguese margin, which is in more detail presented in this study.

Attempts to reconstruct past variations of sea surface temperature (SST) on the Tagus prodelta have so far been not convincing (see chapter 3), as they yield large offsets (for a compilation see e.g. BARTELS-JONSDOTTIR et al., 2006). These are likely to be caused by salinity variations on the shelf due to varying freshwater discharge through the Tagus River and Estuary.

Locally, various multi-proxy studies have been conducted on Tagus prodelta sediments and applied to paleoenvironmental interpretations for the past two millennia (e.g. ABRANTES et al., 2005; BARTELS-JÓNSDÓTTIR et al., 2006; GIL et al., 2006; LEBREIRO et al., 2006). Selected results are compiled in Fig 2.9, showing reconstructed climate phases on a centennial timescale. It becomes obvious, that e.g. the Little Ice Age (LIA) is relatively well confined, despite a likely disturbance of the shelf sediments by the AD1755 tsunami (ABRANTES et al., 2005), whereas the older boundary of the Medieval Warm Period (MWP) is less well defined. Despite this lack of consistency regarding the reconstructed timing of environmental changes, a synchronous timing exists between sediment parameters of a stacked sediment record from the Tagus prodelta (LEBREIRO et al., 2006) and records from the

eastern and northern North Atlantic (e.g. HEBBELN et al., 2006, EIRÍKSSON et al., 2006), emphasising the significance of the Tagus prodelta records and suggesting the existence of a common driving mechanism for environmental changes in the eastern North Atlantic realm. Latter could e.g. be atmospheric patterns, which provide a link between the continent and the marine realm as well as between northern and southwestern Europe.

Evidence for the AD1755 tsunami, that devastated Lisbon, could be identified in a sediment core from the south-western prodelta (ABRANTES et al., 2005; ABRANTES et al., submitted, see chapter 8), whereas no clear evidence of the tsunami could be found neither in a record from the western prodelta (see chapter 6), nor inside the estuary (ANDRADE et al., 2003). The possible effect of the AD1755 and other tsunamis is discussed in chapter 9.

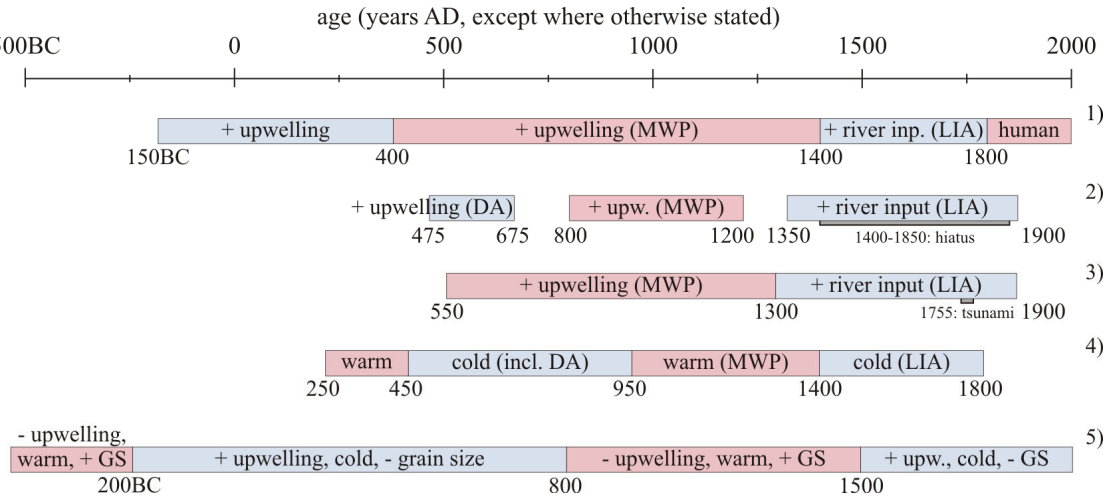

Fig. 2.9: Major climatic and hydrographic episodes of the past 2000 years, compiled from various literature sources. References: 1) BARTELS-JÓNSDÓTTIR et al., 2006; 2) GIL et al., 2006; 3) ABRANTES et al., 2005; 4) DESPRAT et al., 2003; 5) MARTINS et al., 2006.

3 Material and Methods

3.1 Material

3.1.1 Surface Samples

The present day situation along the Portuguese margin in terms of sediment and organic matter properties is evaluated by analysing surface samples from four different sampling regions (Fig. 3.1), which were provided by the Marine Geology Department of the Geological and Mining Institute of Portugal (IGM-DGM; now INETI: Instituto Nacional de Engenharia, Tecnologia e Inovação). A list of the surface samples is given in Tab 3.1. Additionally to the samples listed in Tab. 3.1, core top samples of gravity core GeoB 8903 and of box cores Plutur and PO287, listed in Tab. 3.2 are integrated into the surface sample dataset.

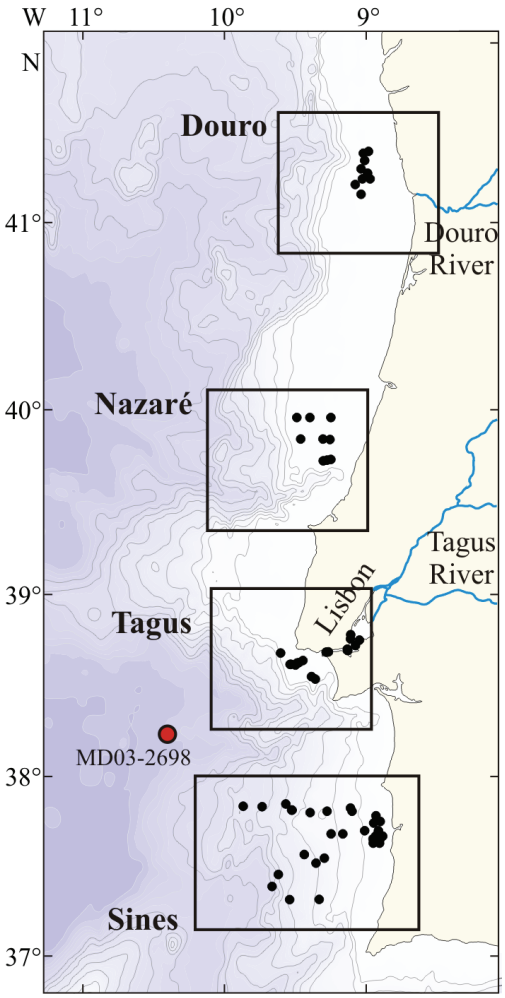

Fig. 3.1: Locations of the samples in the four sampling regions along the western Portuguese margin. The red dot marks deep-sea core MD03-2698, obtained from the Tagus Canyon levée.

Tab. 3.1: Surface samples from four regions along the Portuguese margin. All PO287 samples are box core tops, TJ and TV samples are gravity core tops.

	sample name	latitude (°N)	longitude (°W)	water depth (m)	project (sample holder)
Douro region	PO287-04	41.38	8.96	78	Paleo-1 cruise (INETI)
	PO287-05	41.37	9.00	87	
	PO287-06	41.34	8.99	84	
	PO287-08	41.29	9.01	88	
	PO287-09	41.27	8.97	77	
	PO287-010	41.24	8.95	67	
	PO287-011	41.24	9.01	80	
	PO287-012	41.21	9.06	97	
	PO287-013	41.16	9.01	81	
Nazaré region	PO287-014	39.74	9.23	94	Paleo-1 cruise (INETI)
	PO287-015	39.74	9.25	111	
	PO287-016	39.73	9.28	120	
	PO287-017	39.85	9.44	134	
	PO287-018	39.85	9.28	115	
	PO287-019	39.85	9.23	103	
	PO287-020	39.97	9.23	100	
	PO287-021	39.97	9.38	128	
	PO287-022	39.97	9.47	138	
Tagus region	TJ 17	38.77	9.09	7	Euromargin (INETI)
	TJ 38	38.69	9.25	10	
	TV 29	38.79	9.09	8	
	TV 55	38.70	9.11	16	
	TV 62	38.73	9.05	9	
	TV 65	38.76	9.03	10	
Sines region	PO287-029	37.64	8.93	134	Paleo-1 cruise (INETI)
	PO287-030	37.64	8.88	115	
	PO287-031	37.66	8.88	104	
	PO287-032	37.66	8.93	134	
	PO287-033	37.68	8.91	119	
	PO287-034	37.68	8.86	90	
	PO287-035	37.71	8.89	106	
	PO287-036	37.71	8.99	145	
	PO287-037	37.75	8.93	128	
	PO287-038	37.76	8.88	92	
	PO287-040	37.69	9.23	493	
	PO287-043	37.83	9.09	292	

3.1.2 Sediment Cores

From the Tagus prodelta, five box cores (PLUTUR) were acquired by the Hydrographic Institute, Portugal during the OMEX1 project and provided by the University of Bordeaux (J.M. Jouanneau) (Fig. 3.2, Tab. 3.2). Top samples of these box cores were measured and included in the surface sample dataset. Downcore variations of sediment parameters in the box cores were integrated into the interpretation of the Tagus prodelta records on a 1cm resolution.

Although not included in the manuscripts, the elemental and isotopic carbon and nitrogen ratios of four box cores were analysed every 1cm (Fig. 3.2; Tab. 3.2; Chapter 10). This material (PO287) was acquired during the Paleo-1 project. Three box cores were obtained from the Tagus Prodelta and one core from inside the estuary.

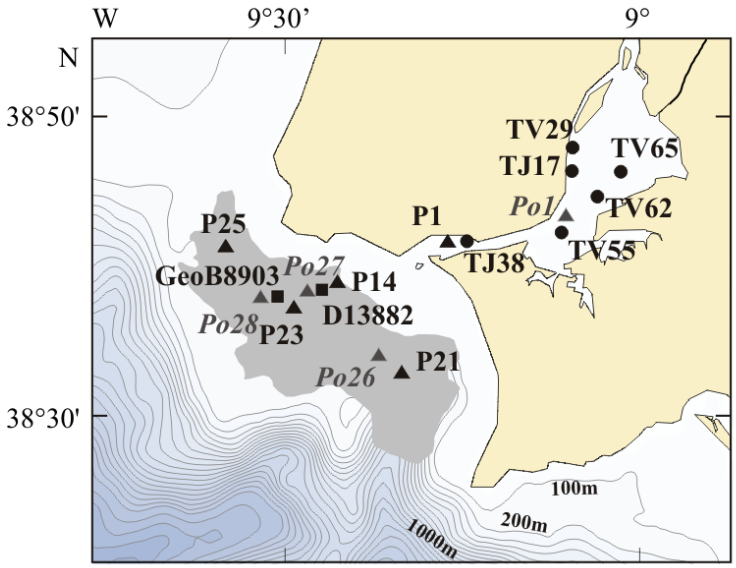

Fig. 3.2: Samples from the Tagus Estuary and prodelta. Circles: surface samples. Triangles: box cores. Squares: gravity/piston cores. Grey triangles: complementary box cores. Po: Po287, P: Plutur.

For a high-resolution study of the Tagus prodelta sediments, a gravity core was recovered from the mud belt (GeoB 8903) off the estuary mouth (Fig. 3.2, Tab. 3.2) and sampled every 5cm. Additionally the top 55cm were sampled in 1cm steps. This core was acquired for the ESF-EUROMARGINS SEDPORT project and covers the past 3200 years. An additional gravity core D13882 from the Tagus prodelta (Fig. 3.2) was provided by the INETI and sampled in irregular intervals between 5 and 10cm down to a depth of 1370cm. The lowest section of core D13882 below 12m core depth was disturbed during coring and is thus omitted. An additional deep-sea record MD03-2698 (Fig. 3.1), obtained for the EUROMARGINS SEDPORT project in 2003, was sampled in irregular intervals between 4 to 20cm down to a core depth of 866cm. These two latter records are used for reconstructions of Holocene environmental changes.

Tab. 3.2: Sediment cores from the Tagus prodelta (italics: maximum sampling depth; core is actually longer) (Figs. 3.1, 3.2) GC: gravity core; PC: piston core; BC: box core

sample name	latitude (°N)	longitude (°W)	water depth (m)	length (cm)	project (sample holder)
D13882 (GC)	38.63	9.45	85	*1370*	Discovery (INETI)
MD03-2698 (PC)	38.24	10.4	4 602	*866*	SEDPORT (RCOM)
GeoB 8903 (GC)	38.63	9.51	102	540	
Plutur6-1 (BC)	38.69	9.26	19	20	OMEX 1 (Instituto Hydrographico, Portugal; University Bordeaux)
Plutur6-14 (BC)	38.65	9.42	54	14	
Plutur6-21 (BC)	38.55	9.34	101	15	
Plutur6-23 (BC)	38.62	9.48	100	9	
Plutur6-25 (BC)	38.69	9.58	101	7	
PO287-1 (BC)	38.71	9.11	13	24	Paleo-1 (INETI)
PO287-026 (BC)	38.56	9.36	94	35	
PO287-027 (BC)	38.63	9.47	86	38	
PO287-028 (BC)	38.63	9.52	104	36	

3.2 Methods – Introduction and Application

The analysed sediment properties are interpreted as being indicative for specific environmental variables. This connection is outlined in Fig. 3.3, showing exemplarily the relation between some sediment properties and environmental processes:

- Magnetic susceptibility (MS) indicates lithic, continental supply, which increases with increasing precipitation in the hinterland, leading to higher erosion rates and higher sediment export to the shelf through rivers.
- Grain-size (GS) increases with increasing current strength: on land due to higher precipitation and thus fluvial energy; on the shelf by stronger, possibly wind-driven shelf currents.
- Ca ($CaCO_3$ content) is indicative for marine productivity.
- $\delta^{18}O$ of foraminifera tests is representative for salinity and temperature of seawater.
- C_{org}/N_{total} and $\delta^{13}C_{org}$ indicate relative fractions of marine and terrigenous organic matter.
- $\delta^{15}N$ is controlled by NO_3^- budget in the marine realm (supply versus consumption), hence an indication of the relation between upwelling strength and marine productivity. It may also be biased by agricultural and anthropogenic DIN inputs from land.

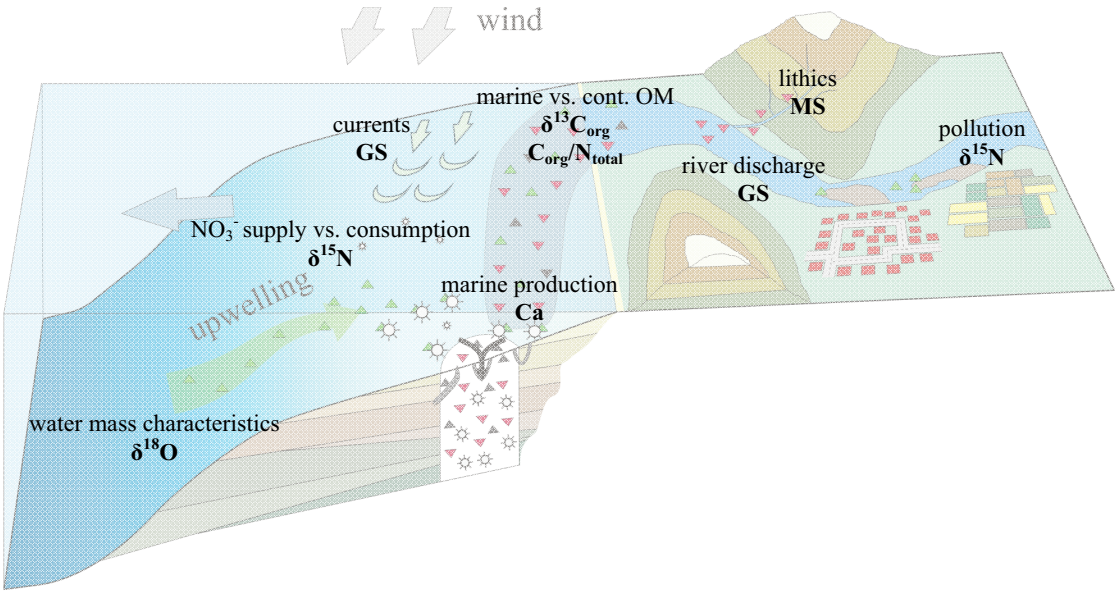

Fig. 3.3: Overview of some connections between sediment properties and environmental parameters. For explanation see text.

3.2.1 Carbon, Nitrogen and $CaCO_3$ Content

C_{org} and N_{total} values are often interpreted as productivity proxies. High productivity results in high C_{org} fluxes and a high associated N_{total} content. However, the origin of the organic material can be evaluated by the C_{org}/N_{total} weight ratio. Marine organic matter has typically a C_{org}/N_{total} ratio of 6-7 (REDFIELD et al., 1963; Appendix 1), whereas terrigenous organic matter has commonly C_{org}/N_{total} ratios above 15 (e.g. MEYERS, 1994; Appendix 1).

The simple mixing between marine and terrigenous organic matter can be biased by inputs of organic matter from other sources, such as bacterial biomass with significantly lower C_{org}/N_{total} ratios (BORDOVSKIY, 1965). C_{org}/N_{total} ratios may also be subject to early diagenetic degradation of organic matter, leading to postdepositional increases in C_{org}/N_{total} ratios, because nitrogen components are considered more labile. Such early diagenetic alteration can be prevented by high sedimentation rates, which protects organic matter against degradation (MÜLLER and SUESS, 1979; HEDGES and KEIL, 1995). Terrestrial C_{org}/N_{total} ratios can be lowered by the substitution of ammonium (NH_4^+) for potassium (K^+) in clay minerals, e.g. Illite or Vermiculite, thus binding N to the inorganic sediment fraction (MÜLLER, 1977; SCHEFFER and SCHACHTSCHABEL, 2002). As NH_4^+ is more abundant on land, particularly in agricultural areas, and K^+ is more concentrated in seawater, this adsorption of NH_4^+ to clays occurs predominantly in the continental realm (SCHUBERT and CALVERT, 2001).

$CaCO_3$ in sediments along the Portuguese shelf is assumed to be of marine origin. Inputs of clastic $CaCO_3$ are considered minor, as the river drains no significant areas with limestone bedrock.

The samples presented in this study were measured for their total carbon (C_{total}), organic carbon (C_{org}) and total nitrogen (N_{total}) content with an Elementar Vario-EL3 element analyser according to the procedure described by MÜLLER et al. (1994). All samples were freeze-dried, ground and homogenized prior to measurement. 25 mg of bulk sediment were filled into tin containers, folded and combusted in the analyser to obtain C_{total} and N_{total}, reported in wt% (percent dry weight). Organic carbon (C_{org}) was measured on 25 mg sample material, which was filled into silver containers, treated with 1-molar HCl to remove carbonate and dried at 60°C in an oven previous to combustion. Samples were not washed after treatment with HCl to prevent the loss of suspended material (Schubert and Nielsen, 2000). The analytical error, obtained by repetitive measurements, is 2% relative. Precision was ensured by continuous control measurements of a lab internal standard. The calcite content was calculated using the equation $CaCO_3 = 8.33*(C_{total}-C_{org})$.

3.2.2 Stable Carbon Isotope Ratios ($\delta^{13}C_{org}$)

Stable isotope ratios of organic carbon ($\delta^{13}C_{org}$) are applied as provenance proxy. They depend dominantly on the isotopic composition of the food source. In the marine realm this is dissolved inorganic carbon (DIC), which consists mainly of marine bicarbonate (HCO_3^-, $\delta^{13}C$ = 0‰). After biological fractionation, marine $\delta^{13}C_{org}$ values are typically between -18 and -22‰ (e.g. Smith and Epstein, 1977; Appendix 1), depending on CO_2 concentration and thus also on water temperature and pH (GEARING, 1975; DENIRO and EPSTEIN, 1978). In the continental realm the main carbon source is atmospheric CO_2 ($\delta^{13}C$ ca. -7‰), but terrigenous $\delta^{13}C_{org}$ values also depend on the photosynthetic pathway of CO_2-fixation in the plant. In C3 plants, which are most relevant in this study, $\delta^{13}C_{org}$ ratios are between -26 and -28‰, whereas C4 plants, which are common e.g. in salt marshes, have a $\delta^{13}C_{org}$ of ca. -13‰ or higher (e.g. SMITH and EPSTEIN, 1977; Appendix 1). A third group, CAM plants, combine the C3 and C4 pathway and thus have intermediate $\delta^{13}C_{org}$ values. The resulting ambiguity of $\delta^{13}C_{org}$ values requires a combined interpretation with C_{org}/N_{total} ratios (Fig. 3.4).

As marine $\delta^{13}C_{org}$ values depend strongly on CO_2 concentration, which in turn depends on water temperature, a temperature effect of between 0.2‰/°C (SACKETT et al., 1965) and 0.5‰/°C (FONTUGNE and DUPLESSY, 1981) may bias the organic matter $\delta^{13}C$, with lighter values in colder water.

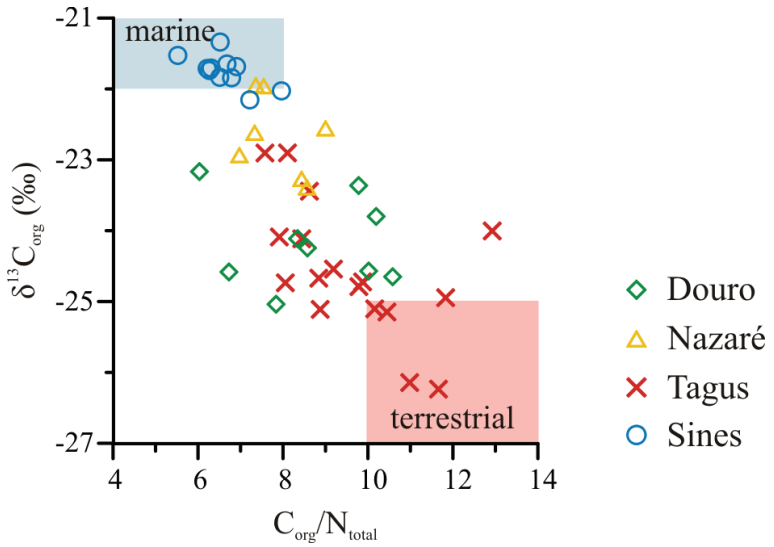

Fig. 3.4: C_{org}/N_{total} versus $\delta^{13}C_{org}$: The measured values scatter between the terrigenous and marine end-member, indicating a mixture of at least two end-members. References for end-member ranges are compiled in chapter 11: Appendix 2.

The isotopic composition of organic carbon ($\delta^{13}C_{org}$) was measured on decalcified samples, following the procedure described by MÜLLER et al. (1994). The material was combusted to CO_2 in an HERAEUS elementar analyser, cleaned in a trapping box system and measured with a FINNIGAN DELTA E mass spectrometer against an internal standard gas, which was calibrated against NBS19. The error of measurements is ±0.1‰, based on long-term calibration curves. Isotopic values are given in standard notation with reference to PDB.

Sampling resolution is 1 cm for the box cores and 5 cm for gravity core GeoB 8903. Cores D13882 and MD03-2698 are sampled at irregular intervals between 2 cm and 10 cm.

3.2.3 Nitrogen Isotope Ratios ($\delta^{15}N$)

Sedimentary $\delta^{15}N$ values depend mainly on the isotopic composition of the food source and the degree of its assimilation. Generally, organisms prefer the light isotope (^{14}N) during nutrient uptake, resulting in an isotopic fractionation between product and substrate, which is quantitativly determined by the fractionation coefficient ε and eventually reflected in the sediments (e.g. ALTABET and FRANCOIS, 1994) (Fig. 3.5). This allows an estimation of the degree of nutrient assimilation by organisms and an estimation of the relation between nutrient supply and nutrient consumption by sedimentary $\delta^{15}N$. In a closed system, i.e. without supply of fresh nutrients, and according to Rayleigh fractionation, complete nutrient

assimilation results in a product-$\delta^{15}N$ equal to the source-$\delta^{15}N$ (Fig. 3.5). In an open system, i.e. with sufficient supply of fresh nutrients, product-$\delta^{15}N$ is by ε lower than source-$\delta^{15}N$.

The isotopic composition of the food source determines the initial δ-value, at which the fractionation begins. In the eutrophic marine realm, e.g. in upwelling regions, marine NO_3^- with a $\delta^{15}N$ between 5 and 6‰ (LIU and KAPLAN, 1989) is the main nitrogen source. In the oligotrophic ocean NO_3^- is generated by bacterial fixation of atmospheric N_2, which has a $\delta^{15}N$ of 0‰ (MARIOTTI, 1983). Accordingly the process of N-fixation results in low $\delta^{15}N$ around 0‰. This also applies for the terrestrial realm. In estuaries, organic matter is often repeatedly recycled, and as the product-$\delta^{15}N$ increases with every trophic step by ca. 3‰ (DENIRO and EPSTEIN, 1981), estuarine organic matter often has high $\delta^{15}N$ values, which can be used as provenance indicator (OWENS, 1985).

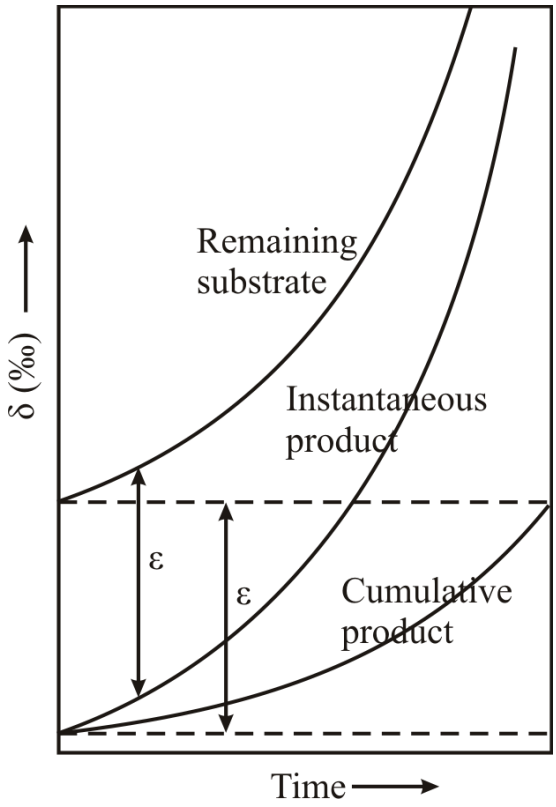

Fig. 3.5: Development of δ-values of the instantaneus (i.e. POM) and cumulative product (i.e. sediment) and the remaining substrate (i.e. remaining nutrient pool). Dashed lines show open system conditions, i.e. infinite nutrient supply, resulting in a constant offset of ε between product and substrate. Closed system conditions (solid lines), i.e. limited nutrient supply, result in initial depletion of the product and according enrichment of the remaining substrate. This, in turn, results in enrichment of the products, until the substrate is used up and the cumulative product has an equal δ-value as the initial substrate. Redrawn after KENDALL et al. (1998).

The situation in the Portuguese upwelling system can be compared to closed system conditions, because marine productivity is fuelled by seasonal, coastal upwelling and the NO_3^- supply is a temporally limited event. The spatial as well as temporal pattern of upwelling and associated productivity can be recorded in the sediments by a spatial and temporal $\delta^{15}N$ gradient. Spatially, sedimentary $\delta^{15}N$ values are lightest at the upwelling centre, where fresh ^{14}N is assimilated. The remaining ^{15}N is advected to the outer regions of the upwelling cell, where it is also assimilated and transferred to the more distal sediments, which then have a heavier $\delta^{15}N$ signature. In a temporal way, fresh ^{14}N is assimilated during the early stage of a bloom, leading to an increase in $\delta^{15}N$ during the course of the bloom. (e.g. ALTABET and FRANCOIS, 1994; HOLMES et al., 1998; FREUDENTHAL et al., 2001a).

In sub- and anoxic environments, denitrification (reduction of NO_3^- to N_2) can be a major oxygen source, leading to a nitrogen fractionation of -20‰ in the water column, but to no net fractionation within the sediment, as intra-sediment diffusion coefficients of NO_3^- are lower (BRANDES and DEVOL, 1997).

Selective degradation of labile organic compounds can shift the $\delta^{15}N$ towards lighter values. The difference between labile organic components and bulk sediment can reach 3‰ (LEHMANN et al., 2002)

The nitrogen isotope ratio ($\delta^{15}N$) was measured by combusting bulk sediment in a CARLO-ERBA elementar analyser to N_2, which was then led into the FINNIGAN DELTA E mass spectrometer in a continuous flow mode, using He as carrier gas. Precision is ±0.2 to 0.3‰; internal calibration was performed the same way as for $\delta^{13}C$. Isotopic values are given in standard notation against $\delta^{15}N_{air}$ (=0‰, MARIOTTI, 1983). The use of bulk sediment for nitrogen isotope analysis instead of decarbonized material is justified by the observation that decarbonization has no effect on the nitrogen isotopic composition (LAVIK, 2001). Sampling intervals are equal to those of $\delta^{13}C_{org}$ analyses.

3.2.4 Oxygen Isotope Ratios ($\delta^{18}O$)

$CaCO_3$ that precipitates from seawater, e.g. by marine microorganisms, incorporates oxygen with an isotopic signature ($\delta^{18}O$), which is a function of water temperature and $\delta^{18}O$ of the surrounding water. If the latter is known, the $\delta^{18}O$ of calcareous microfossil tests can be used to assess past variations in seawater temperature. Seawater $\delta^{18}O$ is on a long term affected by global sea ice volume and on a short term to a lesser extend e.g. by changes in salinity, particularly close to river mouths.

In this study, $\delta^{18}O$ has been measured on monospecific samples of the planktonic foraminifera *G. bulloides*. Thus species-depending effects are avoided and it is ensured, that the obtained signal is representative for surface waters. Samples were analysed at the Leibniz Laboratory, Kiel, Germany, with a FINNIGAN MAT 251 mass spectrometer with the Carbo Kiel device (Kiel I type).

3.2.5 Element Abundance – XRF Spectroscopy

The determination of major and trace element abundance is performed by XRF (X-Ray Fluorescence) spectrometry at the RCOM Bremen (JANSEN et al., 1998). The sample material is irradiated with X-rays and subsequently excites a secondary X-ray fluorescence with element specific wavelengths. The analysis of the emitted wavelength gives a qualitative indication of the elemental composition of the sample material. Certain elements can be interpreted as provenance indicators, e.g. Fe and Ti for a terrigenous and Ca for a marine origin.

The AVAATECH core scanner of the Research Center Ocean Margins (RCOM) Bremen was used to measure the abundance of elements between mass number 19 (K) and 38 (Sr) in a non-destructive way. Measurements were performed on split sediment sections of cores GeoB 8903 and MD03-2698 on a 1cm resolution.

3.2.6 Magnetic Susceptibility

Magnetic susceptibility (MS) describes the degree of magnetisation of a material in response to an applied magnetic field. It mainly depends on the abundance of potentially magnetic minerals, such as Magnetite, Hematite, Pyrite or Pyrrhotite and therefore usually parallels Fe abundance, which is obtained e.g. by XRF scanning. Accordingly it is applied as a proxy for lithic, continental input. However, iron sulfides may also form in anoxic marine sediments.

In this study, split sediment core sections of cores GeoB 8903 and MD03-2698 were measured on a 1cm resolution with a GEOTEK Multi-Sensor-Core-Logger (MSCL), which includes a BARTINGTON point sensor Kappabridge, obtaining volume specific susceptibility in a non-destructive way (GUNN et al., 1998).

3.2.7 Grain-Size Analyses and Modelling

The bulk grain-size of the sediment depends on the sediment sources, transport mechanisms and postdepositional processes and is applied as a proxy for energetic conditions in the hydro- and atmosphere. Furthermore, the comparison between bulk sediment grain-size and grain-size of the terrigenous sediment fraction allows a first estimate about the origin and transport mode of the sediment. Thereby the terrigenous, lithic sediment fraction is defined as bulk sediment minus organic matter, $CaCO_3$ and biogenic opal.

The sediment is commonly derived from a variety of sources and may be affected by different transport mechanisms, postdepositional influences and sorting processes in general (e.g. winnowing). This commonly results in a polymodal grain-size spectrum, which contains several subpopulations. By identifying these subpopulations, it may be possible to reconstruct the transport and sorting processes and hence the source of the sediments. Additionally, possible associations of other proxies with a certain grain-size spectrum are revealed, e.g. an association of organic matter with fine material, thus biasing the C_{org} content by sediment-dynamic processes. This reconstruction of sediment components is achieved by end-member modelling (WELTJE, 1997), which yields several possible subpopulations with a characteristic, ideally unimodal grain-size spectrum. These are eventually interpreted in terms of provenance, transport mechanism and postdepositional alteration (e.g. STUUT et al., 2002; HOLZ et al., 2004; Chapter 6, this study).

Grain-size of core GeoB 8903 was measured with a Coulter LS200 on a 5cm resolution on bulk and terrigenous material. Additionally bulk sediment of the top 55cm of the core was sampled and measured on a 1cm resolution. The terrigenous fraction was obtained by treating bulk sediment with 10ml 10% hydrochloric acid to remove $CaCO_3$, 10ml 35% hydrogen peroxide to remove organic matter and 6mg sodium hydroxide (NaOH) to remove biogenic opal. All samples were dispersed with sodium pyrophosphate ($Na_4P_2O_7*10H_2O$) prior to measurement. Mean grain-sizes were calculated with the software GRADISTAT (BLOTT and PYE, 2001) after the FOLK and WARD (1957) method. End-member modelling of possible lithic subpopulations of the grain-size spectrum was performed according to WELTJE (1997).

4 Provenance of organic matter and nutrient conditions on a river- and upwelling influenced shelf: A case study from the Portuguese Margin

U. Alt-Epping[a], M. Mil-Homens[b], D. Hebbeln[a], F. Abrantes[b], R.R. Schneider[c]

Marine Geology 243 (2007)

[a] DFG-Research Center Ocean Margins, University of Bremen, PO Box 330440, 28334 Bremen, Germany

[b] Department of Marine Geology, Instituto Nacional de Engenharia, Tecnologia e Inovação (INETI), Estrada da Portela, 2721-866 Alfragide, Portugal

[c] Department of Geosciences, Christian-Albrecht University Kiel, Ludewig-Meyn-Str. 10, 24118 Kiel, Germany

4.1 Abstract

Organic matter contained in surface sediments from four regions on the western Portuguese shelf, which are influenced by coastal upwelling and fluvial input, was analysed with respect to elemental organic carbon (C_{org}) and nitrogen (N_{total}) content and isotopic carbon and nitrogen ratios ($\delta^{13}C_{org}$, $\delta^{15}N$). C_{org}/N_{total} weight ratios and $\delta^{13}C_{org}$ values are interpreted in terms of terrigenous or marine organic matter sources, supported by $CaCO_3$ content. Organic matter in the shelf sediments is mainly of marine origin, with increasing terrigenous components only close to rivers and estuaries. In the northern shelf region the data indicates significant terrigenous supply by the Douro River. North of the Nazaré Canyon organic matter composition implies a mainly marine origin, with a higher terrestrial influence close to the canyon head. Organic matter composition in the central shelf region, which is dominated by the Tagus Estuary and the Tagus Prodelta, reveals a change from a continental-type signature within the estuary to a more marine-type signature further to the west and south of the estuary mouth. In the southern region near Cape Sines the geochemical properties clearly reflect the marine origin of sedimentary organic matter.

Sedimentary $\delta^{15}N$ values are interpreted to reflect various degrees of assimilation of seasonally upwelled nitrate, in relation to the upwelling centres. In the estuarine environment, inputs of agriculturally influenced dissolved inorganic nitrogen are reflected in the sediments. No evidence for N_2-fixation or denitrification is found. On the central shelf north of the

Nazaré canyon, sedimentary $\delta^{15}N$ values are close to marine $\delta^{15}NO_3^-$ and thus indicate complete NO_3^- assimilation and N-limitation of marine production. Light $\delta^{15}N$ values in distal sediments off the Douro River mouth and in samples south of Cape Sines reflect high NO_3^- supply and a close proximity to the seasonal upwelling centres. Particularly in sediments form the Sines region, light $\delta^{15}N$ values in southern samples reflect stronger upwelling further south.

4.2 Introduction

The stable carbon isotope ratio ($\delta^{13}C_{org}$) and the C_{org}/N_{total} weight ratio of sedimentary organic matter has often been used as a first provenance proxy to distinguish between a marine or terrestrial organic matter source (e.g. SACKETT and THOMPSON, 1963; BORDOVSKIY, 1965; FONTUGNE and JOUANNEAU, 1987; MIDDELBURG and NIEUWENHUIZE, 1998). The basic assumption for this approach considers organic matter to comprise a particular range of $\delta^{13}C_{org}$ and C_{org}/N_{total} ratios (e.g. CRAIG, 1953, REDFIELD et al., 1963), which depends on a variety of metabolic and environmental parameters (e.g. ALTABET and FRANCOIS, 1994; FONTUGNE and JOUANNEAU, 1987; SACKETT et al., 1965). Terrestrial organic matter typically has a $\delta^{13}C_{org}$ between -26‰ and -28‰, if C3 plants are the dominating organic constituents, or around -13‰, if C4 plants are prevailing (PETERS et al., 1978; MIDDELBURG and NIEUWENHUIZE, 1998). Typical terrestrial C_{org}/N_{total} ratios are >10, with the exact ratio depending on the specific organic material (SMITH and EPSTEIN, 1971; WADA et al., 1987; MIDDELBURG and NIEUWENHUIZE, 1998). Terrigenous C_{org}/N_{total} values may be lowered by the adsorption of N to clay minerals, in which NH_4^+ substitutes for K^+. This effect occurs preferentially on land, as the high K^+ abundance in the marine realm prevents the substitution (SCHUBERT and CALVERT, 2001). Marine organic matter has a $\delta^{13}C_{org}$ of around -22‰ (e.g. FONTUGNE and DUPLESSY, 1981; WADA et al., 1987; MIDDELBURG and NIEUWENHUIZE, 1998), depending on water temperature, which controls dissolved CO_2 levels in surface waters (SACKETT et al, 1965; FONTUGNE and JOUANNEAU, 1987). The cited value is valid for the mid-latitudes. C_{org}/N_{total} ratios of marine organic matter are around 6-7, but may be significantly lower, if protein rich organisms (e.g. bacteria) dominate (REDFIELD et al., 1963; BORDOVSKIY, 1965).

Sedimentary $\delta^{15}N$ values are strongly determined by the isotopic composition and assimilation of N-containing nutrients. In oligotrophic ocean regions bacterial fixation of atmospheric N_2 is an important NO_3^- source, resulting in particulate $\delta^{15}N$ values around 0‰. The primary nitrogen source in upwelling regions is marine NO_3^- with a typical $\delta^{15}N$ between 5-6‰ (LIU and KAPLAN, 1989). As organisms assimilate preferentially ^{14}N, the remaining nitrate pool is gradually enriched in ^{15}N. This enrichment is finally reflected in the sediments (ALTABET and FRANCOIS, 1994; FREUDENTHAL et al., 2001), leading to a temporal $\delta^{15}N$ gradient of increasingly heavier $\delta^{15}N$ values during the course of a bloom as well as to a

spatial $\delta^{15}N$ gradient of heavier $\delta^{15}N$ with increasing distance to the upwelling centre (e.g. FREUDENTHAL et al., 2001).

The spatial distribution of geochemical parameters for organic matter in the surface sediments along the Portuguese margin is evaluated and their elemental composition and isotopic C_{org} signature is attributed to the mixing or exclusive supply of organic matter from marine and terrestrial sources. Nitrogen isotope ratios are used to evaluate possible nitrogen sources, such as deep water NO_3^- or agriculturally affected dissolved inorganic nitrogen (DIN), as well as the degree of marine NO_3^- utilisation. For this purpose geochemical parameters (C_{org}, N_{total}, $CaCO_3$ content, $\delta^{13}C_{org}$, $\delta^{15}N$ and C_{org}/N_{total} ratio) of surface sediments from four different regions along the western Portuguese margin are mapped (Fig. 4.1). Two of these areas are located in front of river mouths, the Douro and Tagus Rivers, with the latter region including a large estuary. Here a large continental and estuarine influence on sedimentary properties can be expected, especially in estuarine samples. The Nazaré sampling region is located close to the Nazaré Canyon, away from major rivers and thus under primarily marine influence, but possibly including laterally advected terrigenous material. On the southern shelf, organic sediment properties are expected to be of entirely marine origin, as any lateral input of terrigenous sediment is intercepted by canyons north and south of the sampling region and riverine inputs are largely absent. In case of regularly reoccurring upwelling patterns, the spatial distribution of NO_3^- supply is expected to be reflected in sedimentary $\delta^{15}N$ values.

4.3 Regional Setting

4.3.1 Shelf Sediments

The northern and central parts of the western Portuguese shelf are between 30 and 50km wide and covered dominantly by sandy sediments (DIAS and NITTROUER, 1984). Mesozoic and Cenozoic rock outcrops on the shelf off the Douro River act as traps for fine sediment, resulting in the formation of a mud belt northwest of the Douro River mouth at about 100m water depth. This mud belt covers an area of about 500km^2 with a sediment layer of 2 to 5m thickness (DRAGO et al., 1999). Lateral sediment transport between the northern and central shelf is intercepted by the Nazaré Canyon, which cuts the central shelf and removes laterally transported sediments into the deep sea (VAN WEERING et al., 2002) (Fig. 4.1). Off the Tagus Estuary mouth a mud belt developed, which covers an area of 560 km2 with maximal 15m thick silty sediments (JOUANNEAU et al., 1998). South of the Tagus mud belt the shelf is incised by the Lisbon and Setubal Canyons, which deliver a significant amount of river discharged sediment towards the Tagus Abyssal Plain. Nevertheless sedimentation dominates on the shelf, resulting in sedimentation rates around 0.2cm/yr (JOUANNEAU et al., 1998). The

southern part of the western shelf is ca. 20km broad, separated from the central part by the Setubal Canyon and bordered southwards by the S. Vicente Canyon. Sediments are dominated by calcareous marine sands and lack significant riverine contributions.

4.3.2 Marine Productivity

Northerly winds, caused by the periodic relocation of the Azores high-pressure system closer to the Iberian coast, generate seasonal upwelling along the Portuguese margin between May and September (FIÚZA, 1983). Cold and nutrient rich waters, upwelled from depths between 60 to 120m, form ca. 50km wide bands along the coast (FIÚZA, 1983), occasionally extending offshore some hundred kilometers through filaments. Upwelling enhances marine productivity, which can reach 60 to 90gC/m^2yr (FIÚZA, 1983; ABRANTES and MOITA, 1999). A less pronounced upwelling also occurs around January and February (DIAS et al., 2002), resulting in a phytoplankton bloom along the Portuguese Margin, which is fertilised by the input of river derived nutrients. Therefore, a persistently high productivity, evidenced by high chlorophyll concentration, is observed off the Tagus River (MOITA et al. 2003). Upwelling off the Douro River is characterised by a large offshore extend (Fig. 4.1), while in the Nazaré region upwelling shows a high interannual variability. Generally, upwelling north of the Nazaré Canyon is relatively strong. South of C. Sines upwelling is restricted to a narrow band close to the coast, becoming stronger southward and reaching a maximum around Cape S. Vicente (Fig. 4.1).

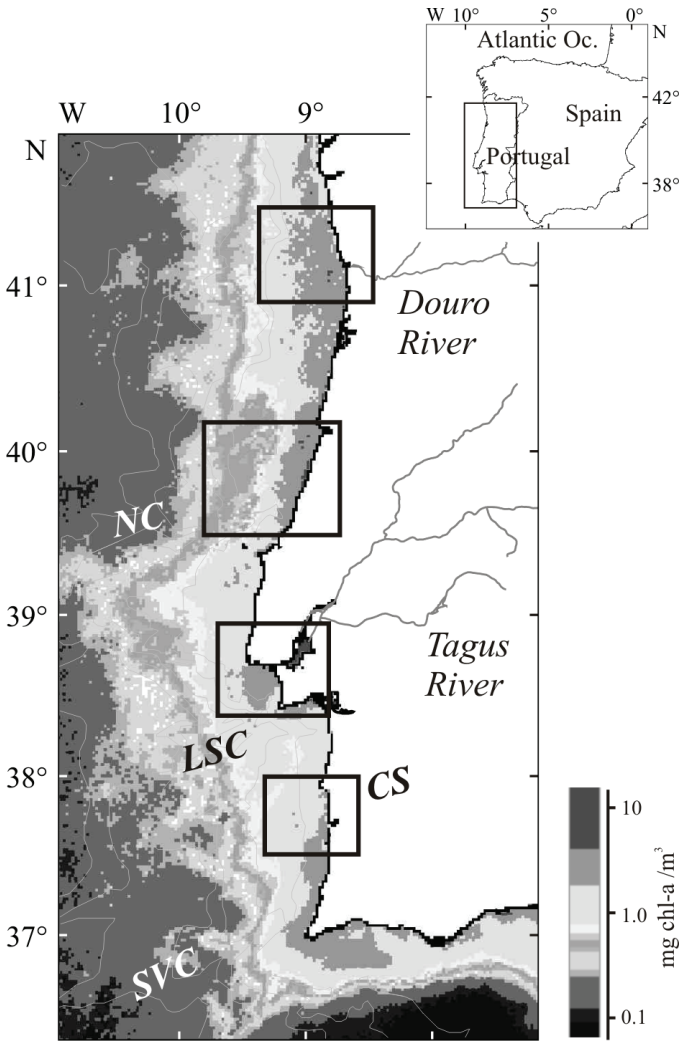

Fig. 4.1: Average chlorophyll-a concentration during August 2002 (SEAWIFS), showing the typical pattern of upwelling related marine productivity along the Portuguese western margin. Sampling regions are shown by rectangles. Centers of upwelling are north of the Nazaré Canyon, off the Tagus Estary mouth and around C. San Vicente. Major morphological features are indicated: NC - Nazaré Canyon, LSC - Lisbon and Setubal Canyons, CS - Cape Sines, SVC - St. Vicente Canyon. Fluvial sediment input is expected to occur mainly through the Douro and Tagus rivers.

4.3.3 Fluvial Supply

The Douro River is the main source of terrigenous sediments on the northern shelf (DIAS and NITTROUER, 1984), draining 95 700km^2 of mountainous hinterland. The mean river discharge is about 420m^3/s (OLIVEIRA et al., 2002), showing a strong seasonality. Sediment discharge is estimated to be around 1.8*10^{6}t/yr through the Douro River, compared to a total riverine

sediment supply to the northern shelf of ca. $2.25*10^6$t/yr (OLIVEIRA et al., 1982). Hence, the contributions of other rivers along the northern coast are minor (DIAS et al., 2002).

In the central part of the shelf the Tagus River is the source for riverine input. With about 1 000km length it is the longest river of the Iberian Peninsula and drains a watershed of about 80 600 km^2, which is strongly influenced by agricultural activity and dominated by natural and cultured C3 plants. Therefore, an influence of agriculturally affected dissolved inorganic nitrogen (DIN) can be expected particularly in the estuarine sediments. The Tagus River feeds into the Atlantic Ocean through a $350km^2$ large, mesotidal estuary, which is characterised by a seasonally varying oxygen saturation of 60-130% (FERREIRA et al., 2001). The course of the suspended matter carried by the Tagus Estuary outflow can be traced outside the estuary by a nepheloid layer, stretching over the Tagus mud belt and extending towards the Lisbon Canyon (JOUANNEAU et al., 1998).

On the southern shelf south of the Lisbon and Setubal Canyons large rivers are absent, thus fluvial contributions can be neglected.

4.4 Material and Methods

All PO287, TV and TJ samples are surface samples. TV and TJ samples were collected with Van Veen and Shipeck sediment sampler. Plutur samples are taken from box core tops and the GeoB 8903 sample is a gravity core top. Locations of all sampling sites are compiled in the PANGEA database (www.pangea.de).

Measurements of elemental C and N content were performed following the procedure described by MÜLLER et al. (1994), using an Elementar Vario-EL3 element analyser. All samples were freeze-dried, ground and homogenized. 25mg of bulk sediment were filled into tin containers, folded and combusted in the analyser to obtain total carbon (C_{total}) and nitrogen (N_{total}) content, reported in wt% (percent dry weight). Organic carbon (C_{org}) was measured on 25mg sample material, which was filled into silver containers, treated with 1-molar HCl to remove carbonate and dried at 60°C in an oven previous to combustion. Samples were not washed after treatment with HCl to prevent the loss of suspended material (SCHUBERT and NIELSEN, 2000). The analytical error, obtained by repetitive measurements, is 2% relative. Precision was ensured by continuous control measurements of a lab internal standard. The calcite content was calculated using the equation $CaCO_3 = 8.33*(C_{total}-C_{org})$. The isotopic composition of organic carbon ($\delta^{13}C_{org}$) was measured on decalcified samples, following MÜLLER et al. (1994). The material was combusted to CO_2 in an HERAEUS elementar analyser, cleaned in a trapping box system and measured with a FINNIGAN DELTA E mass spectrometer against an internal standard gas, which was calibrated against NBS19. The error of measurements is ±0.1‰, based on long-term calibration curves. Isotopic values are given in standard notation with reference to PDB. The nitrogen isotope ratio ($\delta^{15}N$) was measured by

combustion of bulk sediment in a CARLO-ERBA elementar analyser to N_2, which was then led into the FINNIGAN DELTA E mass spectrometer in a continuous flow mode, using He as carrier gas. Precision is ±0.2 to 0.3‰; internal calibration was performed the same way as for $\delta^{13}C$. Isotopic values are given in standard notation against $\delta^{15}N_{air}$ (=0‰).

Grain sizes of TV and TJ -samples were obtained at the Marine Geology Department of the INETI, by sieving and settling methods and are reported as fine fraction (<63µm), sand fraction (63µm-2mm) and gravel (>2mm). Grain sizes of PO287 samples were measured with a Coulter LS320 (MIL-HOMENS, 2006). Grain sizes of Plutur samples were determined by JOUANNEAU et al. (2004) and grain size of core GeoB 8903 was measured with a Coulter LS320 at the RCOM, Bremen, Germany. Except for the sediments from the Tagus region, grain sizes are expressed as fractions clay (<4µm), silt (4-63µm), sand (63µm-2mm) and gravel (>2mm).

4.5 Results

4.5.1 Douro Region

The surface sediments in the vicinity of the Douro river (Fig. 4.2a-f) contain 3-6wt% $CaCO_3$, with slightly higher values offshore. The C_{org} content is between 0.4 and 1.3wt% and the total N content is between 0.06 and 0.12wt% (not shown in figure). For both parameters, higher values are observed in offshore samples. C_{org}/N_{total} weight ratios range between 6 and 10.6. Lowest values are observed in the central part of the Tagus mud complex and closest to the Douro River mouth. The $\delta^{13}C_{org}$ values vary between -23.2 and -25‰ with lower values in the northern samples. $\delta^{15}N$ is between 7.9‰ closest to the Douro River mouth and 4.1‰ ca. 5km away (Fig. 4.2). Offshore samples have about 2‰ lower $\delta^{15}N$ values than the four coastal samples.

The sediment texture is mainly silty, with a silt content between 34 and 74% and a sand content between 19 and 63% (MIL-HOMENS, 2006). The clay fraction reaches maximal 7%. C_{org} and N_{total} contents are higher in the fine fraction (R^2=0.9 for both). However, the correlation between C_{org}/N_{total} and fine fraction is statistically not significant (R^2=0.47), as the removal of only one data point leads to an R^2 below 0.3. Similarly, no significant correlation is evident between fine fraction and $\delta^{13}C_{org}$ or $\delta^{15}N$ (R^2=0.29 and 0.3, respectively) (Tab. 4.2).

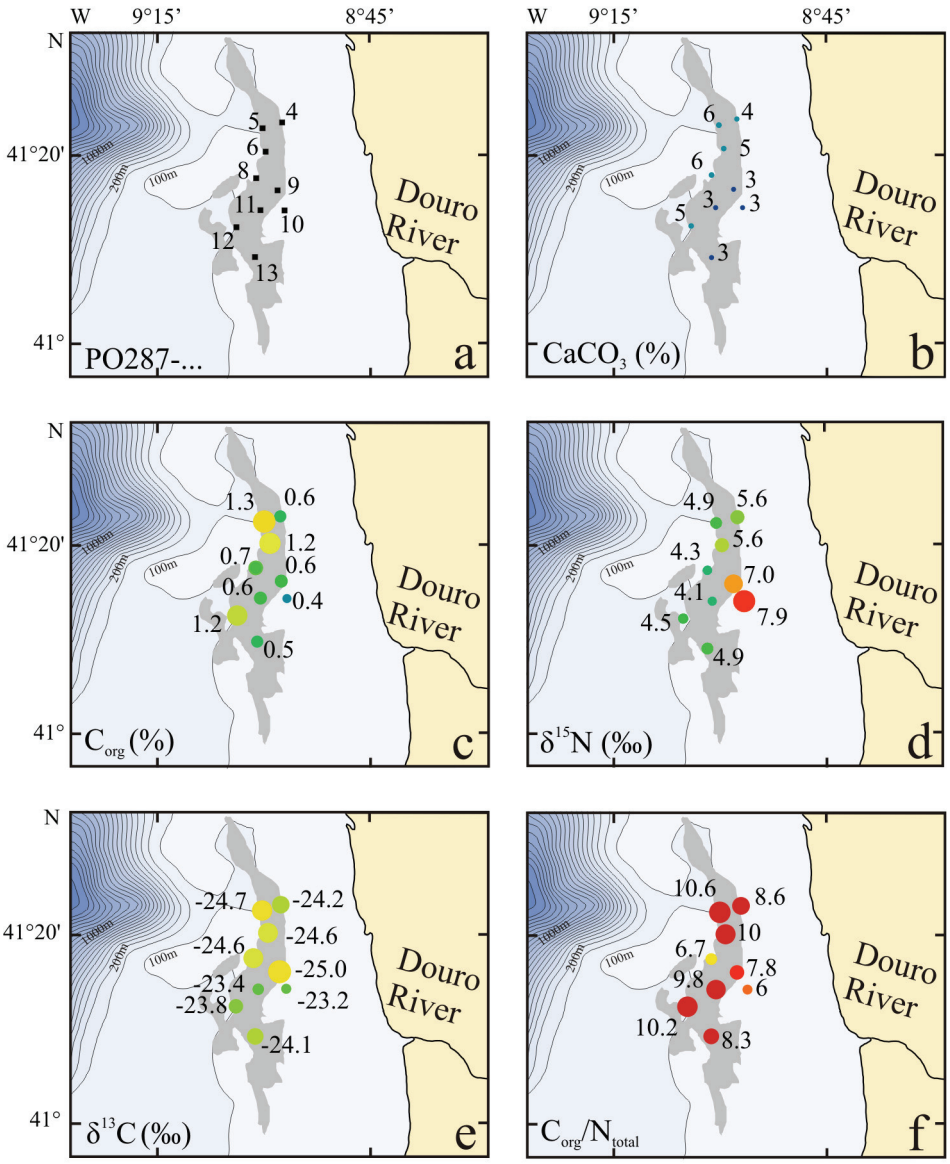

Fig. 4.2: Distribution of sediment properties in the Douro region. a) sample name, b) $CaCO_3$ content, c) C_{org} content, d) sedimentary $\delta^{15}N$, e) $\delta^{13}C_{org}$, f) C_{org}/N_{total} ratio. Shaded area on the shelf indicates the limits of the Douro mud belt adapted from DRAGO et al. (1999).

4.5.2 Nazaré Region

In the surface sediments close to the Nazaré Canyon (Fig. 4.3a-f) the $CaCO_3$ content varies between 49 and 5wt%, with higher values in the northwestern, distal samples. The C_{org} content ranges from 0.2 to 1.3wt% and the N_{total} content ranges from 0.02 to 0.19wt% (not shown in figure). Both parameters reach their highest value in the central sample, where the samples contain the highest fine-fraction contents, indicating the tendency of organic matter to

accumulate with fine-grained material (MIL-HOMENS, 2006). Lowest values are found in the samples close to the coast. C_{org}/N_{total} weight ratios are between 4 and 9. $\delta^{13}C_{org}$ in the Nazaré samples varies between -23.4‰ and -21.9‰ an. That is close to typical marine $\delta^{13}C_{org}$ values. Samples in the south, close to the canyon head, are relative to the northern samples 0.6‰ lighter. $\delta^{15}N$ varies between 4.5 and 5.5‰, with slightly lower values close to the coast (Fig. 4.3).

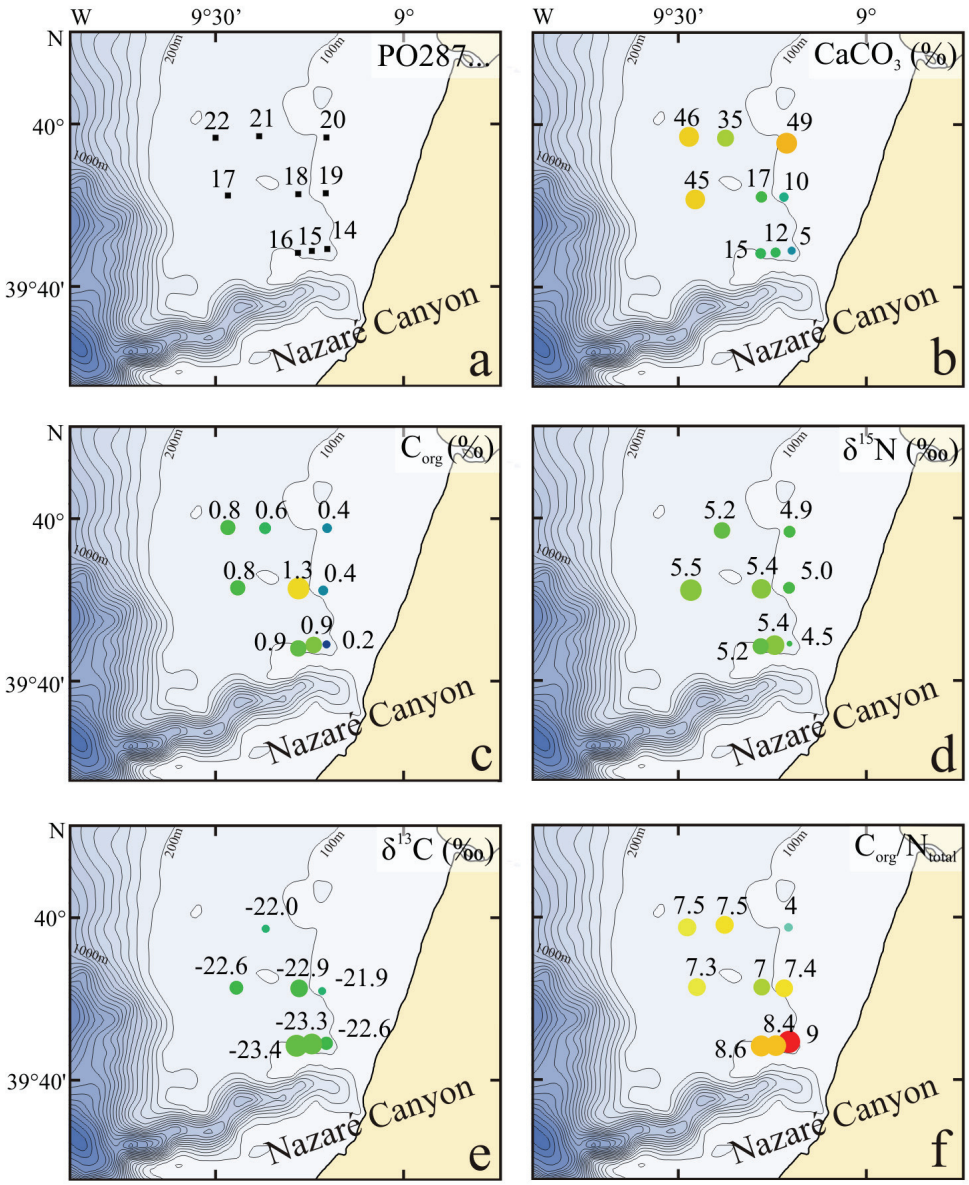

Fig. 4.3: Distribution of sediment properties in the Nazaré region. a) sample name, b) $CaCO_3$ content, c) C_{org} content, d) sedimentary $\delta^{15}N$, e) $\delta^{13}C_{org}$, f) C_{org}/N_{total} ratio.

The grain size is highly variable, with a sand content between 14 and 86% and a silt content between 14 and 69% (MIL-HOMENS, 2006). Two samples were collected furthest

offshore contain 15 and 18% gravel composed of shell fragments. The clay fraction can reach 17% but averages 8%. No significant correlation exists between grain size and C_{org}/N_{total}, $\delta^{13}C_{org}$ or $\delta^{15}N$ (Tab. 4.2).

4.5.3 Tagus Region

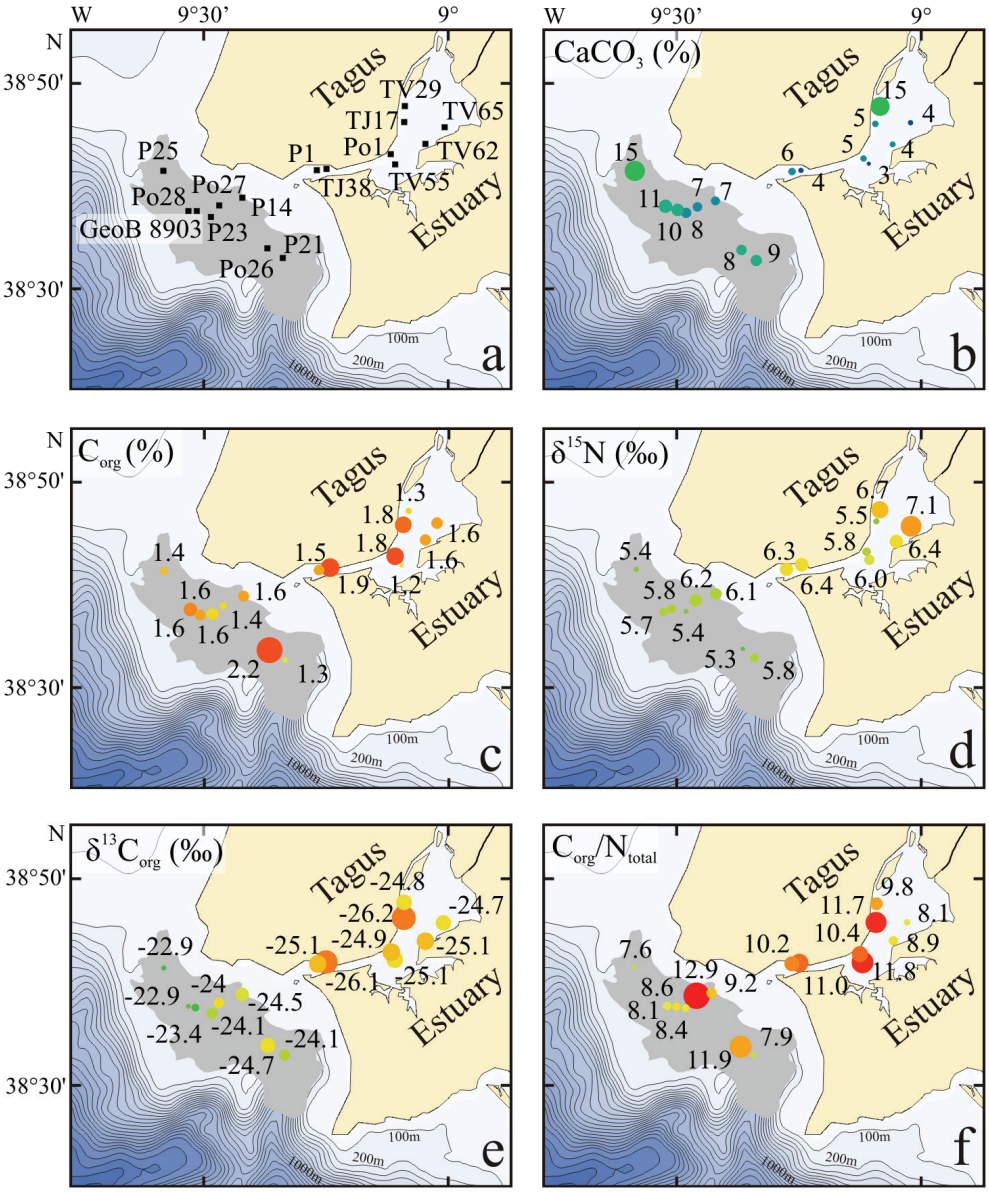

Fig. 4.4: Distribution of sediment properties in the Tagus region. a) sample name (Pl. = Plutur, Po = Po287), b) $CaCO_3$ content, c) C_{org} content, d) sedimentary $\delta^{15}N$, e) $\delta^{13}C_{org}$, f) C_{org}/N_{total} ratio. Shaded area on the shelf indicates the Tagus Prodelta mud belt adapted from JOUANNEAU et al. (1998).

In surface sediments from the Tagus region (Fig. 4.4a-f) the $CaCO_3$ content varies between 3 and 15wt% and is considerably lower inside the estuary, compared to mud belt samples. The C_{org} content in the Tagus estuary and on the prodelta is between 1.2 and 2.2wt% and the N_{total} content ranges between 0.1 and 0.2wt% (not shown in figure). Both parameters have similar values inside and outside the estuary. C_{org}/N_{total} weight ratios range between 7.6 and 12.9. Values inside the estuary are generally higher, although also low values (8.1) are observed in the north-eastern part of the estuary (Fig. 4.4). On the Tagus mud belt lowest C_{org}/N_{total} ratios below 8 occur at the western and eastern fringes of the mud belt and highest C_{org}/N_{total} ratios above 11 were measured in the central part.

The $\delta^{13}C_{org}$ of sediments inside the estuary varies between -26.2‰ and -24.7‰. This is significantly lower, than $\delta^{13}C_{org}$ of mud belt samples, which range between -24.7 and -22.9‰. $\delta^{15}N$ values are between 5.5 and 7.1‰ inside the estuary and between 5.3 and 6.3‰ on the mud belt, where higher $\delta^{15}N$ and lower $\delta^{13}C_{org}$ values are found in the central part, compared to southeastern and northwestern values (Fig. 4.4).

The amount of material finer than 63µm is between 41 and 98%, with an average of 82% (JOUANNEAU et al., 2004). LIMA (1971) identified illite as the dominant clay mineral in this area, varying between 34 and 62% of the clay fraction. No relation between fine fraction (<63µm) and C_{org}, $\delta^{13}C_{org}$ nor $\delta^{15}N$ exists in the Tagus surface samples. Fine sediments however have lower C_{org}/N_{total} ratios (R^2=0.79), which is caused by a higher N_{total} content in finer sediments (R^2=0.78) (Tab. 4.2).

4.5.4 Sines Region

The $CaCO_3$ content in Sines surface samples ranges from 24 to 52wt%. C_{org} content ranges from 0.2 to 0.6wt% and the N_{total} content varies between 0.04 and 0.15wt% (not shown in figure). C_{org}/N_{total} weight ratios are very low, ranging from 5.5 to 8. $\delta^{13}C_{org}$ values range between -21.3‰ to -22.2‰ and $\delta^{15}N$ values are low, with values between 3.6 to 5.4‰, which slightly increase northwards (Fig. 4.5).

Surface sediments from the Sines region contain between 49 and 88% sand (average 77%) and between 7 and 41% silt (average 18%) (MIL-HOMENS, 2006). The clay content does not exceed 10% and the gravel content is maximal 5%. In the Sines surface samples, no correlation between fine fraction and C_{org}, N_{total}, C_{org}/N_{total}, $\delta^{13}C_{org}$ or $\delta^{15}N$ is observed, as all R^2 values are below 0.2.

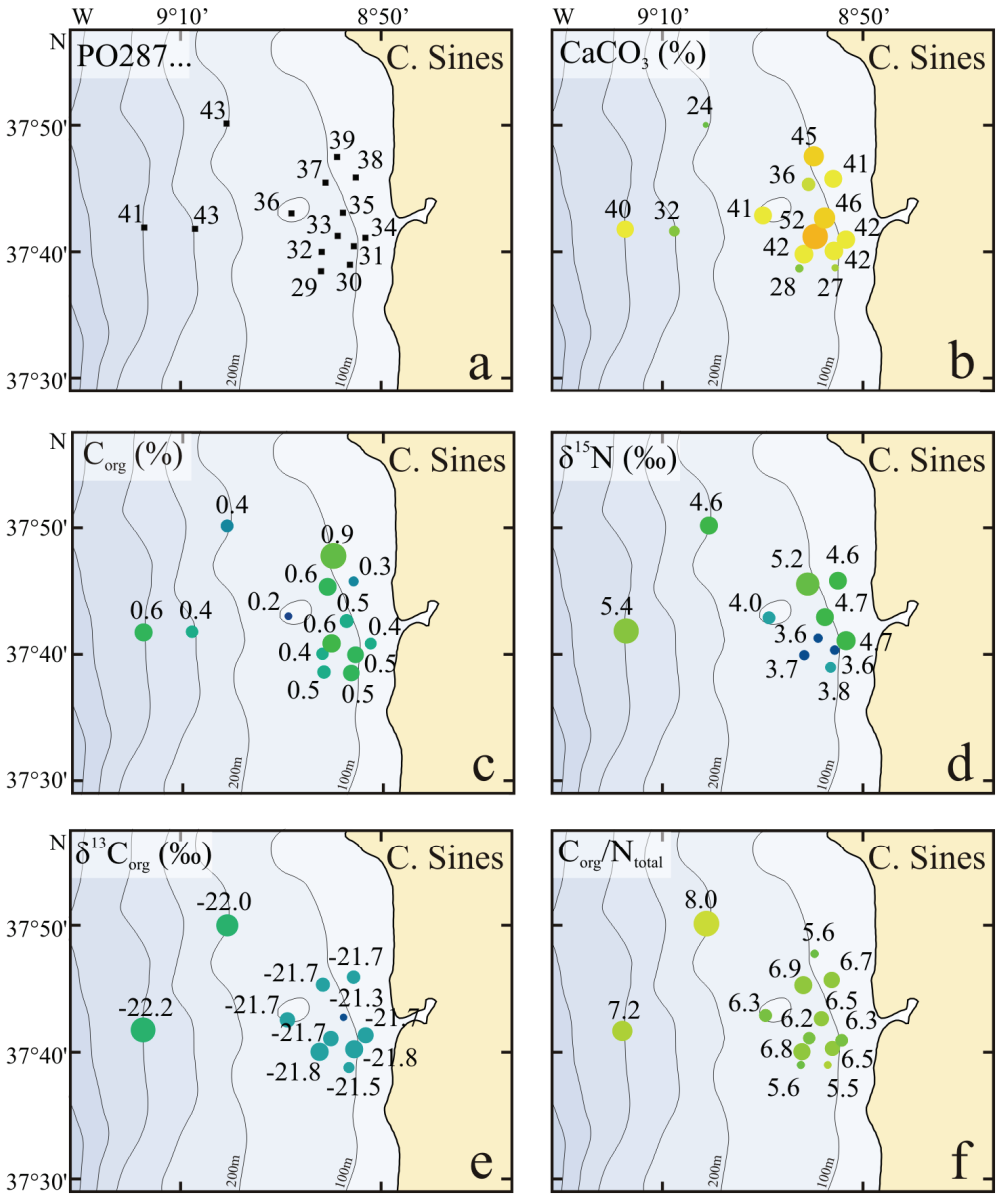

Fig. 4.5: Distribution of sediment properties in the Sines region. a) sample name, b) $CaCO_3$ content, c) C_{org} content, d) sedimentary $\delta^{15}N$, e) $\delta^{13}C_{org}$, f) C_{org}/N_{total} ratio.

Tab. 4.1: Compilation of minimum, maximum, mean values and standard deviation (SD) of elemental and isotopic C and N data as well as $CaCO_3$.

	C_{org} (%)	N_{total} (%)	C_{org}/N_{total}	$\delta^{13}C_{org}$ (‰)	$\delta^{15}N$ (‰)	$CaCO_3$ (%)
Douro samples						
Minimum	0.4	0.06	6	-25.0	4.1	3
Maximum	1.3	0.12	10.6	-23.2	7.9	6
Mean	0.8	0.09	8.7	-24.2	5.4	4
SD	0.4	0.03	1.6	0.6	1.3	1
Nazaré samples						
Minimum	0.2	0.02	4	-23.4	4.5	5
Maximum	1.4	0.19	9	-21.9	5.5	49
Mean	0.7	0.1	7.4	-22.7	5.2	26
SD	0.4	0.05	1.4	0.6	0.3	18
Tagus samples						
Minimum	1.2	0.11	7.6	-26.2	5.3	3
Maximum	1.9	0.2	12.9	-22.9	7.1	15
Mean	1.6	0.16	9.6	-24.6	6.0	7
SD	0.2	0.03	1.5	0.9	0.5	4
Sines samples						
Minimum	0.2	0.04	5.5	-22.2	3.6	24
Maximum	0.9	0.15	8.0	-21.3	5.4	52
Mean	0.5	0.08	6.6	-21.8	4.4	38
SD	0.14	0.03	0.8	0.2	0.6	8

4.6 Discussion

4.6.1 Organic Matter Sources

Although sedimentary $\delta^{13}C_{org}$ and C_{org}/N_{total} values do not always reflect organic matter provenance (MILTNER et al., 2005), the clear relation between $CaCO_3$ content, which is regarded as of marine origin, and $\delta^{13}C_{org}$ values implies, that $\delta^{13}C_{org}$ values can be interpreted in terms of organic matter provenance (Fig. 4.6).

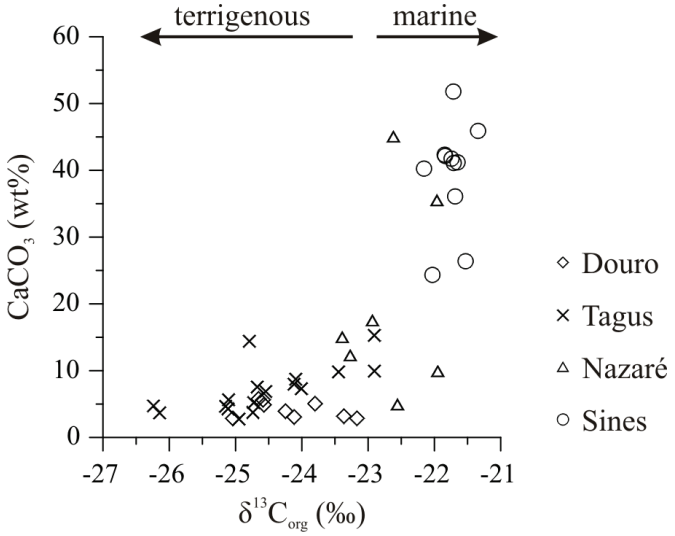

Fig. 4.6: $\delta^{13}C_{org}$ versus $CaCO_3$ content, showing the dependence of $\delta^{13}C_{org}$ on sediment provenance.

Discrete C_{org}/N_{total} and $\delta^{13}C_{org}$ values for each organic matter source are needed, in order to quantify the fraction of terrigenous organic material. Defining terrigenous organic matter to have a C_{org}/N_{total} ratio of 15 and a $\delta^{13}C_{org}$ value of -27‰, and marine organic matter to have a C_{org}/N_{total} ratio of 6 and a $\delta^{13}C_{org}$ value of -22‰ (e.g. MIDDELBURG and NIEUWENHUIZE, 1998) allows the calculation of the terrigenous organic matter fraction, assuming conservative and linear mixing, by

$$f_t = [\delta^{13}C_{org} - (\delta^{13}C_{mar} * f_m)]/\delta^{13}C_{terr}$$

with f_t and f_m as terrigenous and marine organic matter fraction, respectively, $\delta^{13}C_{org}$ as measured value and $\delta^{13}C_{terr}$ and $\delta^{13}C_{mar}$ as terrigenous and marine $\delta^{13}C$-endmember values.

Generally, the range of C_{org}/N_{total} and $\delta^{13}C_{org}$ values in the four sampling regions indicate a dominantly marine origin of organic matter, except in the close vicinity of the Douro and Tagus river mouths. The marine endmember is represented by sediments from the

Sines region, where $\delta^{13}C_{org}$ and C_{org}/N_{total} values indicate a fraction of only 5% terrigenous organic matter (Fig. 4.5). In the Nazaré region 10-15% of the sedimentary organic matter is of terrigenous origin (Fig. 4.3), whereas in the Douro region as well as on the Tagus Prodelta a terrigenous fraction of 30-40% is calculated (Fig. 4.2, 4.5). As expected, highest terrigenous contributions of 50-65% are reconstructed inside the Tagus Estuary. Slightly increased C_{org}/N_{total} ratios and lowered $\delta^{13}C_{org}$ values in prodelta samples southwest of the estuary mouth indicate a higher terrigenous organic matter fraction in these samples, which is interpreted as the trace of the Tagus River plume (Fig. 4.4).

Low correlation coefficients between $\delta^{13}C_{org}$ and fine sediment fraction indicate no major effect of grain size on $\delta^{13}C_{org}$ values in any of the sampling regions (Tab. 4.2). This applies also to the relation between fine fraction and C_{org}/N_{total} ratio, except inside the Tagus Estuary, where fine material has lower C_{org}/N_{total} ratios (R^2=0.84) (Tab. 4.2). This correlation is caused by a higher N content of fine material (R^2=0.79), whereas the C_{org} content is indepentent of grain size (R^2 of C_{org} versus fine fraction = 0.25). In agriculturally influenced regions, such as the Tagus hinterland, the substitution of NH_4^+ for K^+ is particularly important, as NH_4^+ is a common constituent of fertilizers. As the total N content in estuarine sediments consists of 10-20% inorganic N, obtained from the N_{total} intercept on a C_{org} versus N_{total} plot (GOÑI et al., 1998), the C_{org}/N_{total} ratios particularly in fine sediments are probably lowered by the adsorption of inorganic N to clay minerals and thus reflect the input from agricultural sources.

In the other regions the amount of inorganic N is insignificantly low, implying, that the nitrogen content in the sediments is associated to the organic matter.

Tab. 4.2: Correlation coefficients R^2 between fine fraction <63µm and C_{org}/N_{total}, $\delta^{13}C_{org}$ and $\delta^{15}N$ of the four sampling regions.

	C_{org}/N_{total}	$\delta^{13}C_{org}$	$\delta^{15}N$
Douro	0.47	0.29	0.3
Nazaré	0.06	0.5	0.38
Tagus	0.79	0.16	0.01
Sines	0	0.16	0.09

4.6.2 Stable Nitrogen Isotopes

No evidences for N_2-fixation are found in any of the sampling regions, since C_{org}/N_{total} ratios around 6 and higher indicate no influence of nitrogen rich, bacterial biomass. Further, high O_2 concentrations and saturation in the water column along the coast as well as inside the Tagus Estuary (MOITA, 2001; FERREIRA et al., 2001) indicate, that water column denitrification plays no major role. Additionally there is no effect of grain size on sedimentary $\delta^{15}N$ observed. Therefore marine sedimentary $\delta^{15}N$ values are interpreted as results of isotopic fractionation during NO_3^- uptake.

Close to the Douro and Tagus river mouths and inside the Tagus Estuary sedimentary $\delta^{15}N$ values are relatively high (6-7‰) (Fig. 4.2, 4.5). Particularly the Tagus River drains a watershed, that is dominated by agricultural land. This is observed by high DIN concentrations in the upper estuary (FERREIRA et al., 2001) as well as by the strong relation between N_{total} content and grain size (R^2=0.79), which can be interpreted as an effect of the substitution of NH_4^+ for K^+ in clays (MÜLLER, 1977). $\delta^{15}N$ values of estuarine sediments may hence be increased by contributions of agriculturally derived DIN, which is particularly evident by two slightly heavier $\delta^{15}N$ values in the uppermost estuary (samples TV29 and TV65), where also DIN concentrations are highest (FERREIRA et al., 2001). Alternative explanations for enhanced $\delta^{15}N$ values inside the estuary are contaminations with sewage from the Lisbon urban area or water column denitrification. Sewage is mainly discharged outside the Tagus Estuary (SILVA et al., 2002), close to samples Plutur14 and Po287-27, which show no increased $\delta^{15}N$ (Fig. 4.4) and give no evidence for contamination. Water column denitrification can be excluded, as oxygen concentrations are with between 6 and 9.5mg/l high (oxygen saturation between 60 and 130%: FERREIRA et al., 2001).

Heavy $\delta^{15}N$ values in sediments directly off the Tagus Estuary and Douro River mouths are interpreted as the traces of estuarine and riverine discharge, transporting an agriculturally influenced $\delta^{15}N$ signal to the shelf.

Intermediate $\delta^{15}N$ values between 5 and 6‰ are found in the marine dominated sediments of the Nazaré region and of the northwestern and southeastern parts of the Tagus Prodelta. These $\delta^{15}N$ values are within the range of marine $\delta^{15}NO_3^-$ (5-6‰, LIU and KAPLAN, 1989), which is the dominant NO_3^- source during coastal upwelling (Fig. 4.3, 4.5). A gradient towards heavier $\delta^{15}N$ values offshore (R^2=0.41) justifies the interpretation of sedimentary $\delta^{15}N$ values in terms of NO_3^- utilisation. However, the fact that the surface sediment $\delta^{15}N$ is most likely an integrated signal of several upwelling seasons, combined with the spatial variability of upwelling in the Nazaré region blurs the gradient from proximal light $\delta^{15}N$ to distal heavier $\delta^{15}N$. Instead, $\delta^{15}N$ values in the range of marine $\delta^{15}NO_3^-$ imply spatially averaged complete NO_3^- assimilation. The consequent NO_3^- limitation of productivity is supported by water column NO_3^- concentrations close to zero during summer and autumn, but coevally higher concentrations of other nutrients (phosphate, silica) (MOITA, 2001).

$\delta^{15}N$ values below 5‰ are observed in the offshore Douro samples and in the southern Sines region (Fig. 4.2, 4.6). In both regions, relatively high C_{org}/N_{total} ratios indicate no bacterial inputs (BORDOVSKIY, 1965) and thus no influence of N_2-fixation. Hence, the $\delta^{15}N$ values imply a close proximity to the upwelling centre and a high NO_3^- utilisation of 80-95% (ALTABET and FRANCOIS, 1994; MONTOYA, 1994). In the Douro region, satellite chlorophyll images show a regularly large offshore extend of high chlorophyll concentrations and thus upwelling (Fig. 4.1). Hence, the Douro surface sediments are located within the relatively static upwelling centre.

In the Sines area upwelling is largely restricted to the coast (Fig. 4.1), generating low $\delta^{15}N$ values. Particularly in southern samples $\delta^{15}N$ values are below 4‰ (Fig. 4.5). These match with high chlorophyll and NO_3^- concentrations between C. San Vicente and south of C. Sines (Fig. 4.1, MOITA, 2001), extending over the southern part of the Sines sampling area. Accordingly low $\delta^{15}N$ values in the southern Sines samples reflect stronger upwelling southward. N_2-fixation, which could lead to low $\delta^{15}N$ during oligotrophic, non-upwelling phases is contradicted by C_{org}/N_{total} ratios, which are in a reasonable marine range (MIL-HOMENS, 2006 and references therein).

4.7 Summary

Organic matter along the Portuguese margin appears to be primarily of marine origin, except where large rivers contribute significant amounts of terrigenous sediment to the shelf. Here marine and terrigenous organic matter mixes, resulting in intermediate C_{org}/N_{total} and $\delta^{13}C_{org}$ values. This is the case in the coastal Douro and Tagus samples, where heavy $\delta^{15}N$ values in coastal and estuarine sediments indicate an input of agriculturally affected DIN. Particularly inside the uppermost part of the Tagus Estuary, the geochemical signature reflects thorough mixing of marine and terrigenous organic matter. Estuarine $\delta^{15}N$ values appear to be affected by the influx of agriculturally affected DIN. Sediment discharge through the Tagus Estuary mouth occurs mainly westwards to the Tagus mud belt, reflected by a stronger terrigenous source signature and relatively heavy $\delta^{15}N$ values in samples west of the estuary mouth, compared to sediments of the southern and northern Tagus Prodelta. In the Douro region, more offshore samples show also a considerable terrestrial organic matter fraction, but $\delta^{15}N$ values indicate a close proximity to the upwelling centre, which regularly extends considerably offshore.

Sediments in the Nazaré region show mainly marine provenance of organic matter, with small contributions of terrigenous material close to the canyon top. $\delta^{15}N$ values in the range of marine $\delta^{15}NO_3^-$ indicate complete NO_3^- assimilation, which is supported by the almost complete depletion of surface water NO_3^- during upwelling. Spatial and temporal

variability of upwelling and the time-averaged $\delta^{15}N$ signal in surface sediments results in an only slight gradient towards heavier $\delta^{15}N$ values offshore.

Surface sediments from the Sines region show a clear marine provenance. Stronger upwelling in the southern part of the Sines region, extending southward towards C. San Vicente, is evidenced by light $\delta^{15}N$ values.

The interpretation of sedimentary $\delta^{15}N$ values as result of fractional NO_3^- utilisation is justified by the absence of processes like N_2-fixation or water column denitrification, which would be reflected by low C_{org}/N_{total} ratios or oxygen deficiency. However, a higher spatial coverage along the Portuguese margin, particularly offshore, is required to substantiate the interpretation in terms of NO_3^- utilisation and the effect of the supply of upwelled marine NO_3^-.

4.8 Acknowledgements

The work was conducted as a part of the SEDPORT project (Sedimentation Processes on the Portuguese Margin: The Role of Continental Climate, Ocean Circulation, Sea Level, and Neotectonics) and funded by the German Science Foundation (DFG) as part of the EUROMARGINS/ EUROCORES program. Samples were provided by the Marine Geology department of the Instituto Nacional de Engenharia, Tecnologia e Inovação (INETI, former IGM), Lisbon, Portugal.

Thanks are also due to the crew of RV Poseidon during the cruise PO304, to A. Völker, S. Lebreiro, E. Salgueiro, I. Gil, J. Köster and C. Wienberg for discussions and additional informations as well as to H. Buschhoff, M. Segl and B. Meyer-Schack for technical support.

4.9 References

Abrantes, F., M.T. Moita (1999): Water column and recent sediment data on diatoms and coccolithophorids, off Portugal, confirm sediment record of upwelling events. Oceanologica Acta 22(3): 319-336.

Altabet, M.A., R. Francois (1994): Sedimentary nitrogen isotopic ratio as a recorder for surface ocean nitrate utilization. Global Biogeochemical Cycles 8(1): 103-116.

Bordovskiy, O.K. (1965): Sources of organic matter in marine basins. Marine Geology 3: 5-31.

Craig, H. (1953): The geochemistry of the stable carbon isotopes. Geochimica et Cosmochimica Acta 3: 53-92.

Dias, J.M.A., C.A. Nittrouer (1984): Continental shelf sediments of northern Portugal. Continental Shelf Research 3(2): 147-165.

Dias, J.M.A., J.M. Jouanneau, R. Gonzalez, M.F. Araujo, T. Drago, C. Garcia, A. Oliveira, A. Rodrigues, J. Vitorino, O. Weber (2002a): Present day sedimentary processes on the northern Iberian shelf. Progress in Oceanography 52: 249-259.

Drago, T., F. Araujo, P. Valerio, O. Weber, J.M. Jouanneau (1999): Geomorphological control of fine sedimentation on the northern Portuguese shelf. Boletin Instituto Espanol de Oceanografia 15(1-4): 111-122.

Ferreira, J.G., T. Simas, J.P. Nunes (2001): Production and fate of organic matter: Organic matter cycling models in estuaries. European Salt Marsh Modelling – EUROSSAM Final Report. DGXII–Environment Programme: Part 2, Task 4. Project ENV4-CT97-0436. 63 p.

Fiúza, A.F.G. (1983): Upwelling patterns off Portugal. In: Suess, E., J. Thiede (Eds.): Coastal Upwelling: Its Sediment Record. New York, NATO Conference Series IV: 85-98.

Fontugne, M.R., J.C. Duplessy (1981): Organic carbon isotopic fractionation by marine phytoplankton in the temperature range -1 to 31°C. Oceanologica Acta 4(1): 85-90.

Fontugne, M.R., J.M. Jouanneau (1987): Modulation of the particulate organic carbon flux to the ocean by a macrotidal estuary: evidence from measurements of carbon isotopes in organic matter from the Gironde system. Estuarine, Coastal and Shelf Science 24: 377-387.

Freudenthal, T., S. Neuer, H. Meggers, R. Davenport, G. Wefer (2001): Influence of lateral particle advection and organic matter degradation on sediment accumulation and stable nitrogen isotope ratios along a productivity gradient in the Canary Islands region. Marine Geology 177(1-2): 93-109.

Goñi, M.A., K.C. Ruttenberg, T.I. Eglinton (1998): A reassessment of the sources and importance of land-derived organic matter in surface sediments from the Gulf of Mexico. Geochimica et Cosmochimica Acta 62(18): 3055-3075.

Jouanneau, J.M., C. Garcia, A. Oliveira, A. Rodrigues, J.A. Dias, O. Weber (1998): Dispersal and deposition of suspended sediment on the shelf off the Tagus and Sado estuaries, S.W. Portugal. Progress in Oceanography 42: 233-257.

Jouanneau, J.M. and OMEX-I Project members (2004): Grain size analysis of sediment core Plutur6-BoxT01 to 25, PANGAEA, doi:10.1594/PANGAEA.217915

Lima, L. (1971): Distribuição dos Minerais Argilosos na Plataforma Continental entre os Cabos Raso e Espichel. 1º Congresso Hispano-Luso-Americano de Geologia Económica, Madrid.

Liu, K.-K., I.R. Kaplan (1989): The eastern tropical Pacific as a source of 15N-enriched nitrate in seawater off southern California. Limnology and Oceanography 34(5): 820-830.

Middelburg, J.J., J. Nieuwenhuize (1998): Carbon and nitrogen stable isotopes in suspended matter and sediments from the Schelde estuary. Marine Chemistry 60(3-4): 217-225.

Mil-Homens, M. (2006): Assessment of heavy metal contamination in three areas of the Portuguese shelf. Ph.D. thesis, Department of Geology, Earth Science Centre, Göteborg University: 128 pages.

Miltner, A., K.-C. Emeis, U. Struck, T. Leipe, M. Voss (2005): Terrigenous organic matter in Holocene sediments from the central Baltic Sea, NW Europe. Chemical Geology 216: 313-328.

Moita, M.T. (2001): Estrutura, variabilidade e dinâmica do fitoplâncton na costa de Portugal continental. Ph..D. thesis, Faculdade de Ciências da Universidade de Lisboa: 272 pages.

Moita, M.T., P.B. Oliveira, J.C. Mendes, A.S. Palma (2003): Distribution of chlorophyll a and Gymnodinium catenatum associated with coastal upwelling plumes off central Portugal. Acta Oecologica. Proceedings of the Plankton Symposium, Espinho, Portugal 24 (Supplement 1): S125-S132.

Montoya, J.P. (1994): Nitrogen isotope fractionation in the modern ocean: implications for the sedimentary record. In: Zahn, R. T.F. Pedersen, M.A. Kaminski, L. Labeyrie (Eds.): Carbon Cycling in the Glacial Ocean: Constraints on the Ocean's Role in Global Change. NATO ASI Series 17, Springer, Berlin: 259-279.

Müller, P.J. (1977): C/N ratios in Pacific deep-sea sediments: Effect of inorganic ammonium and organic nitrogen compounds sorbed by clays. Geochimica et Cosmochimica Acta 41: 765-776.

Müller, P., R.R. Schneider, G. Ruhland (1994): Late Quaternary pCO_2 variations the Angola Current: Evidence from organic carbon $\delta^{13}C_{org}$ and alkenone temperatures. In: Zahn, R., T.F. Pedersen (Eds.): Carbon Cycling in the Glacial Ocean: Constraints of the Ocean's Role in Global Change. NATO ASI Series, Vol. 1(17), Springer: 343-366.

Oliveira, I., A. Valle, F. Miranda (1982): Littoral problems in the Portuguese west coast. Coastal Engineering Proceeding III: 1951-1969.

Oliveira, A., J. Vitorino, A. Rodrigues, J.M. Jouanneau, J.A. Dias, O. Weber (2002): Nepheloid layer dynamics in the northern Portuguese shelf. Progress in Oceanography 52: 195-213.

Peters, K.E., R.E. Sweeney, I.R. Kaplan (1978): Correlation of carbon and nitrogen stable isotope ratios in sedimentary organic matter. Limnology and Oceanography 23(4): 598-604.

Redfield, A.C., B.H. Ketchum, F.A. Richards (1963): The influence of organisms on the composition of seawater. In: Hill, M.N. (ed.), The Sea, Vol. 2, Wiley, New York: 26-79.

Sackett, W.M., R.R: Thompson (1963): Isotopic organic carbon comnposition of recent continental derived clastic sediments of the East Gulf Coast, Gulf of Mexico. American Association of Petroleum Geologists Bulletin 47: 525-532.

Sackett, W.M., W.R. Eckelmann, M.L. Bender, W.H. Bé (1965): Temperature dependence of carbon isotope composition in marine plankton and sediments. Science 148: 235-237.

Schubert, C.J., S.E. Calvert (2001): Nitrogen and carbon isotopic composition of marine and terrestrial organic matter in Arctic Ocean sediments: implications for nutrient utilization and organic matter composition. Deep-Sea Research I 48: 789-810.

Schubert, C.J., B. Nielsen (2000): Effects of decarbonation treatments on $\delta^{13}C_{org}$ values in marine sediments. Marine Chemistry 72: 55-59.

Silva, J.F.d., R.W. Duck, T.S. Hopkins, J.M. Anderson (2002): Airborne Observations of Water Circulation in the Nearshore Zone of the Aveiro Coast, Northern Portugal. Littoral 2002, The Changing Coast, Porto, Portugal.

Smith, B.N., S. Epstein (1971): Two categories of $^{13}C/^{12}C$ ratio for higher plants. Plant Physiology 47: 380-384.

van Weering, T.C.E., H.C. de Stigter, W. Boer, H. de Haas (2002): Recent sediment transport and accumulation on the NW Iberian margin. Progress in Oceanography 52(2-4): 349–371.

Wada, E., M. Minagura, H. Mizutani, T. Tsuji, R. Imaizumi, K. Karasawa (1987): Biogeochemical studies on the transport of organic matter along the Otsuchi River watershed, Japan. Estuarine, Coastal and Shelf Science 25: 321-336.

5 Variations in sediment provenance during the past 3000 years off the Tagus River, Portugal

Ulrich Alt-Epping[a], Jan-Berend W. Stuut[a], Dierk Hebbeln[a], Ralph Schneider[b]

Submitted to Marine Geology

[a] DFG-Research Center Ocean Margins, University of Bremen, PO Box 330440, 28334 Bremen, Germany
[b] Department of Geosciences, Christian-Albrecht University Kiel, Ludewig-Meyn-Str. 10, 24118 Kiel, Germany

5.1 Abstract

A high-resolution multi proxy study has been carried out on a 5.4m long gravity core and five box cores from the Tagus prodelta on the western Portuguese margin. Geochemical (C_{org}/N_{total} ratios, $\delta^{13}C_{org}$, $\delta^{15}N$, $\delta^{18}O$, C_{org} and $CaCO_3$ content) and physical sediment properties (magnetic susceptibility, grain-size) are interpreted in terms of environmental changes in the hinterland and in the marine realm.

Subsurface data of the five box cores indicate no major effect of early postdepositional alteration. Surface data show a higher fraction of terrigenous organic material close to the river mouth and in the southern prodelta. Gravity core GeoB 8903 covers the last 3.2kyrs with a temporal resolution of at least 0.1cm/yr. Very high sedimentation rates between 69 and 140cm core depth indicate a possible disturbance of the record by the AD1755 tsunami, although no evidence for a disturbance is observed in the data, e.g. in grain-size. The local budget of marine NO_3^- as well as the provenance of organic matter remained virtually constant during the past 3.2kyrs. Latter is interpreted as an effect of thorough mixing of marine and freshwater inside the Tagus Estuary.

A positive correlation between magnetic susceptibility (MS) and North Atlantic Oscillation (NAO) is evident for the past 250years, coinciding with a negative correlation between mean grain-size and NAO. This is assigned to a constant riverine supply of fine material with high MS, which is diluted by the riverine input of a coarser, low-MS component during NAO negative, high-precipitation phases. End-member modelling of the lithic grain-size spectrum supports this concept, also revealing a third, coarse lithic component. The high

abundance of this coarse end-member prior to 2kyr BP is interpreted as the result of stronger bottom currents, concentrating the coarse sediment fraction by winnowing. Because shelf currents are mainly wind driven, stronger winds before 2kyr BP initiate additionally stronger upwelling, thus explaining a coincidently high $CaCO_3$ content. As continental climate was more arid prior to 2kyr BP (Subboreal), the coarse end-member may also consist of dust from local sources, transported by stronger winds. A decrease in grain-size and $CaCO_3$ content after 2kyr BP is interpreted as a result of decreasing wind strength, providing less dust and weakening upwelling and winnowing. The onset of a fining trend and a further decrease in $CaCO_3$ around AD900 occurs simultaneous to climatic variations, reconstructed from eastern North Atlantic records. A strong increase in MS between AD1400 and AD1500 indicates higher lithic terrigenous input, caused by deforestation in the hinterland.

5.2 Introduction

The sedimentary record off the Tagus Estuary on the central western Portuguese shelf comprises inputs of marine and continental sources, as it is under the influence of seasonal coastal upwelling (FIÚZA, 1983) and of continental contributions from the Tagus River and Estuary (JOUANNEAU et al., 1998). Additionally, aeolian or current-transported material may contribute to the sediments (e.g. MAHOWALD et al., 1999; MORENO et al., 2002). Past environmental changes in the marine realm and in the continental hinterland as well as variations in atmospheric circulation intensity will most likely be recorded in these sediments and will have an influence on physical and geochemical properties of the shelf sediments. As sedimentation rates are high, interaction between continental and marine environmental processes can be resolved on a high temporal resolution. Sediment parameters that are indicative of environmental changes in continental and marine realm include elemental and stable carbon and nitrogen isotope ratios as proxies for organic matter provenance and NO_3^- budget (e.g. THORNTON and MCMANUS, 1994; MIDDELBURG and NIEUWENHUIZE, 1998, for organic matter provenance; ALTABET and FRANCOIS, 1994; FREUDENTHAL et al., 2001, for $\delta^{15}N$ as proxy for nutrient utilisation) as well as planktonic foraminiferal $\delta^{18}O$ as proxy for sea surface temperature (SST) and -salinity (SSS) (MCCREA, 1950; NIEBLER et al., 1999; WOLFF et al., 1999; BONWAY and MIX, 2004). Inorganic sediment properties, such as grain-size and magnetic susceptibility (MS), act as indicators for changes in sedimentological conditions and lithic sediment supply. Particularly a detailed grain-size analysis, including modelling of potential end-members of the grain-size spectrum, allows the evaluation of different sources of lithic sediment material (STUUT et al., 2002). The combined interpretation of these parameters allows an integrated view on environmental changes in the region.

Climatic conditions over large parts of Europe are largely determined by the North Atlantic Oscillation (NAO), which describes the varying air-pressure gradient between the

Azores High and the Iceland Low (e.g. HURREL, 1995). Precipitation over the Iberian Peninsula correlates negatively with the NAO index (TRIGO et al., 2004; VICENTE-SERRANO and HEREDIA-LACLAUSTRA, 2004), whereas wind strength, which drives coastal upwelling along the Portuguese margin, shows a positive correlation with NAO (OSCHLIES, 2001). Although variations in NAO occur on short timescales, high local sedimentation rates allow an assessment of the influence of the NAO on the marine sediment record.

Previous studies from the Tagus Prodelta (GIL et al., 2006; BARTELS-JÓNSDÓTTIR et al., 2006) lack a synchronous phasing of environmental changes. Nevertheless, a prodelta record (LEBREIRO et al., 2006) has been successfully correlated to records from the eastern and northern North Atlantic (HEBBELN et al., 2006; EIRÍKSSON et al., 2006), showing synchronous environmental but opposed changes in southwest and northern Europe. Hence, despite the apparent heterogeneity of sediment properties on the shelf, this suggests the existence of large scale driving mechanisms for environmental changes, e.g. by varying atmospheric circulation patterns.

This on one hand, and the large potential of the region to record continental and marine environmental variations on a high temporal resolution on the other hand, makes this region particularly interesting for paleoenvironmental studies.

In this study a gravity core from the central part of the western Portuguese shelf is analysed with respect to its geochemical (C_{org}/N_{total}, $\delta^{13}C_{org}$, $\delta^{15}N$, $\delta^{18}O$, $CaCO_3$ content) and physical (grain-size, MS) sediment properties in order to evaluate environmental variations on the Iberian Peninsula and in the adjacent marine realm as well as sedimentological changes in the depositional area. The downcore information is complemented by surface and subsurface data from five nearby box cores, which yield information about the recent spatial distribution and possible early diagenetic alterations of the analysed parameters.

5.3 Regional Setting

The central part of the western Portuguese margin is bordered to the North by the Nazaré Canyon and to the South by the Lisbon and Setubal Canyons. These canyons intercept the ca. 20-30km broad shelf and prevent major coast-parallel sediment transport.

The major source for continental sediments to the shelf is the Tagus River, which is 1 000km long and drains about 80 600km^2. It discharges into the Atlantic Ocean at ca. 30°40'N close to the city of Lisbon through a 350km^2 large, mesotidal estuary. The Tagus Estuary is the third largest estuary in Europe and acts as a depocenter for river-discharged sediments with sedimentation rates of locally around 80cm/kyr (e.g. at the southern brim of the estuary, FREITAS et al., 1999). The sediments discharged to the shelf are partly deposited on a ca. 550km^2 large mud belt on the shelf in front of the estuary mouth and partly transported south to the Lisbon Canyon, through which it is discharged into the deep sea. The

course of suspended matter carried by the Tagus outflow can be traced by a bottom nepheloid layer, stretching over the Tagus mud belt and extending towards the Lisbon Canyon (JOUANNEAU et al., 1998).

Marine productivity is determined by upwelling from May to September, which is driven by the periodic relocation of the Azores high-pressure system closer to the Iberian coast (FIÚZA, 1983) and associated northerly winds. During summer months cold and nutrient rich waters are upwelled from 60 to 120m depth and form ca. 50km wide bands along most parts of the Portuguese coast (FIÚZA, 1983), occasionally extending offshore some hundreds of kilometers through filaments. Upwelling increases marine productivity to 60 to 90gC/m^{2}yr (FIÚZA, 1983; ABRANTES and MOITA, 1999). During winter months the Azores High is located south off the northwest African coast, resulting in southerly winds, which favour downwelling conditions.

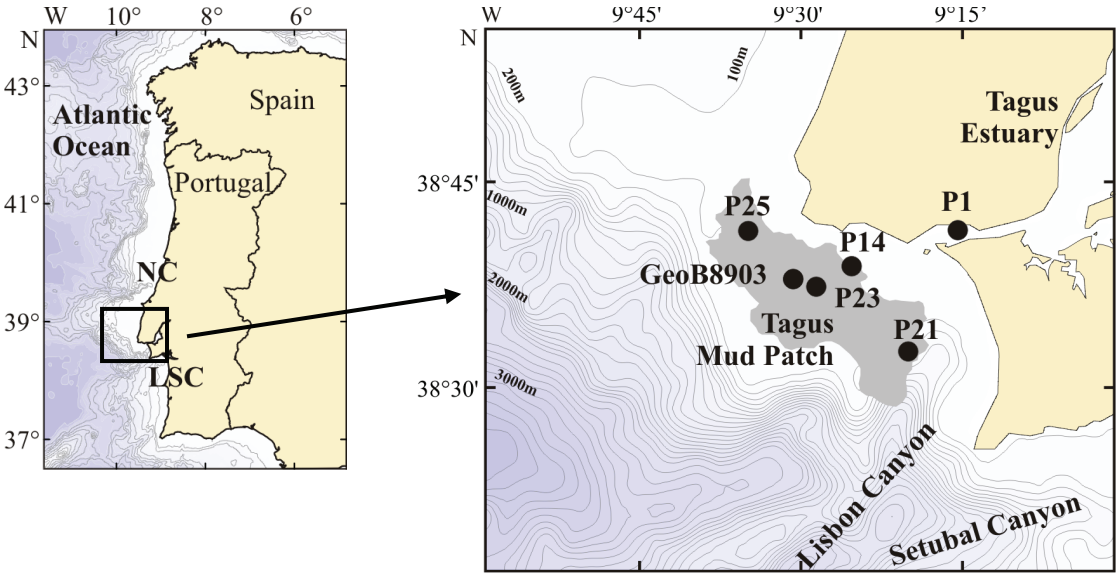

Fig. 5.1: Map of the area of investigation and sampling locations. Grey shaded area shows the mud belt redrawn after JOUANNEAU et al. (1998). NC: Nazaré Canyon, LSC: Lisbon and Setubal Canyons, Pxx: plutur samples.

5.4 Materials and Methods

A 5.4m long gravity core (GeoB 8903) and five box cores (Plutur-1, -14, -21, -23, -25) with a length between 7 and 20cm were collected from the Tagus prodelta (Fig. 5.1, Tab. 5.1). Samples for elemental and isotope analyses were taken every 5cm from the gravity core, whereas the box cores were sampled in 1cm steps.

The elemental C and N content was analysed following the procedure described by MÜLLER et al. (1994) at the RCOM, Bremen. The freeze-dried sediment was ground and 25mg of material was filled into tin containers and analysed in an Elementar Vario-EL3 element analyser to obtain the total carbon and nitrogen content. To measure organic carbon and nitrogen, 25mg of sediment was filled into silver containers and treated with 1-molar HCL to remove carbonate. Samples were not washed after treatment to prevent the loss of suspended material (SCHUBERT and NIELSEN, 2000). The N content of carbonate-containing and carbonate-free samples was compared in order to detect offsets that might indicate loss of sediment material during treatment or effects of decarbonatization on the N content. The offsets were all in a tolerable range (maximum rel. 3%), confirming only minor and non-systematic effects of decarbonatization on the N content. Precision was ensured by continuous control measurements of a lab internal standard. The calcite content was calculated using the equation $CaCO_3 = 8.33*(C_{total}-C_{org})$.

The isotopic composition of organic carbon ($\delta^{13}C_{org}$) was measured on carbonate-free samples. The material was combusted to CO_2 in a Heräus element analyser, cleaned in a trapping box system and measured with a Finnigan Delta E mass spectrometer against an internal standard gas, which was calibrated against NBS19. Absolute measuring error is ±0.1‰, based on long-term calibration curves. Isotopic values are given in standard notation with reference to PDB. Nitrogen isotope ratios ($\delta^{15}N$) were measured by combusting bulk sediments in a Carlo Erba element analyser to N_2, which was then led into the Finnigan Delta E mass spectrometer in a continuous flow mode, using He as carrier gas. Absolute precision is ±0.2 to 0.3‰, based on repetitive measurements. Internal calibration was performed the same way as for $\delta^{13}C$. Isotopic values are given in standard notation against $\delta^{15}N_{air}$ (=0‰, MARIOTTI, 1983). The use of bulk sediment for nitrogen isotope analysis instead of decarbonized material is justified by the observation that decarbonization has no effect on the nitrogen isotopic composition (LAVIK, 2001).

Grain-size was measured on gravity core GeoB 8903 every 5cm with a Coulter LS200 on bulk and terrigenous material, resolving grain-size spectra between 0.4 and 2000µm. Bulk sediment of the top 55cm was additionally measured on a 1cm resolution. The terrigenous fraction was obtained by treating bulk sediment with 10ml 10% hydrochloric acid to remove $CaCO_3$, 10ml 35% hydrogen peroxide to remove organic matter and 6mg sodium hydroxide (NaOH) to remove biogenic opal. All samples were dispersed with sodium pyrophosphate ($Na_4P_2O_7*10H_2O$) prior to measurement. Mean grain-sizes were calculated with the software GRADISTAT (BLOTT and PYE, 2001) after the FOLK and WARD (1957) method. End-

member modelling was performed to distinguish several possible lithic subpopulations of the grain-size spectrum (WELTJE, 1997).
Magnetic susceptibility (MS) was measured on gravity core GeoB 8903 in 1cm steps with a GEOTEK Kappabridge at the RCOM, Bremen.

Tab. 5.1: Compilation of investigated cores. IH: Hydrographic Institute, Lisbon, Portugal. OMEX: Ocean Margin Exchange. SEDPORT: Sedimentation processes on the Portuguese margin: the role of continental climate, ocean circulation, sea level and Neotectonics. RCOM: Research Center Ocean Margins, Bremen, Germany.

core name	latitude (decimal °N)	longitude (decimal °W)	water depth (m)	length (m)	project (sample holder)
Plutur1	38.692	9.261	19	0.2	
Plutur14	38.646	9.424	54	0.14	
Plutur21	38.545	9.337	101	0.15	OMEX I (IH)
Plutur23	38.622	9.477	100	0.09	
Plutur25	38.688	9.582	101	0.07	
GeoB8903	38.631	9.514	102	5.4	SEDPORT (RCOM)

The age model of core GeoB 8903 is based on ten ^{14}C AMS datings obtained from samples comprising between 3.9 and 7.5 mg of multispecies planktonic foraminifera, and measured at the Leibniz Laboratory of the University Kiel, Germany (NADEAU et al., 1997) (Tab. 2). Radiocarbon ages were corrected for a reservoir effect of 400 years (ABRANTES et al., 2005), regardless of biasing influences of changing upwelling or river freshwater discharge, and calibrated with the software Calib 5.0.1 (STUIVER and REIMER, 1993), using the "intcal04" calibration curve.

5.5 Results

5.5.1 Plutur Box Cores

In the box cores the C_{org} content is between 1.3 and 1.7wt%, with higher values (2.1wt %) in the upper 4cm of core Plutur-1 (Fig. 5.2). The N_{total} content decreases downcore in a parallel way in all five cores from between 0.15 and 0.19wt% at the core tops to ca. 0.13wt%. C_{org}/N_{total} ratios increase slightly with depth, ranging between 8 and 10 at the core tops and between 9 and 10 at the core bases. Plutur-1 shows a high variability, with C_{org}/N_{total} values of up to 12 in the upper 4cm and at 20cm depth. The $CaCO_3$ content is virtually constant in each core, varying between 4wt % in the box core most proximal to the estuary (Plutur-1) and 16 wt % in the distal box core (Plutur-25). However, Plutur-23, which is located on the shelf

south of the estuary mouth, shows intermediate $CaCO_3$ values between Plutur-14 and Plutur-23. The $\delta^{13}C_{org}$ of the box cores decreases clearly with decreasing distance to the estuary mouth, ranging from -26‰ in Plutur-1 to -22.5‰ in Plutur-25. $\delta^{13}C_{org}$ values of Plutur-14, -21 and -23 are similar. The $\delta^{15}N$ values show a comparable pattern, as they decrease with increasing distance to the estuary mouth. Plutur-1 shows highest $\delta^{15}N$ values of around 7‰, Plutur-21, Plutur-23 and Plutur-25 show similar values between 5 and 6‰ (Fig. 5.2).

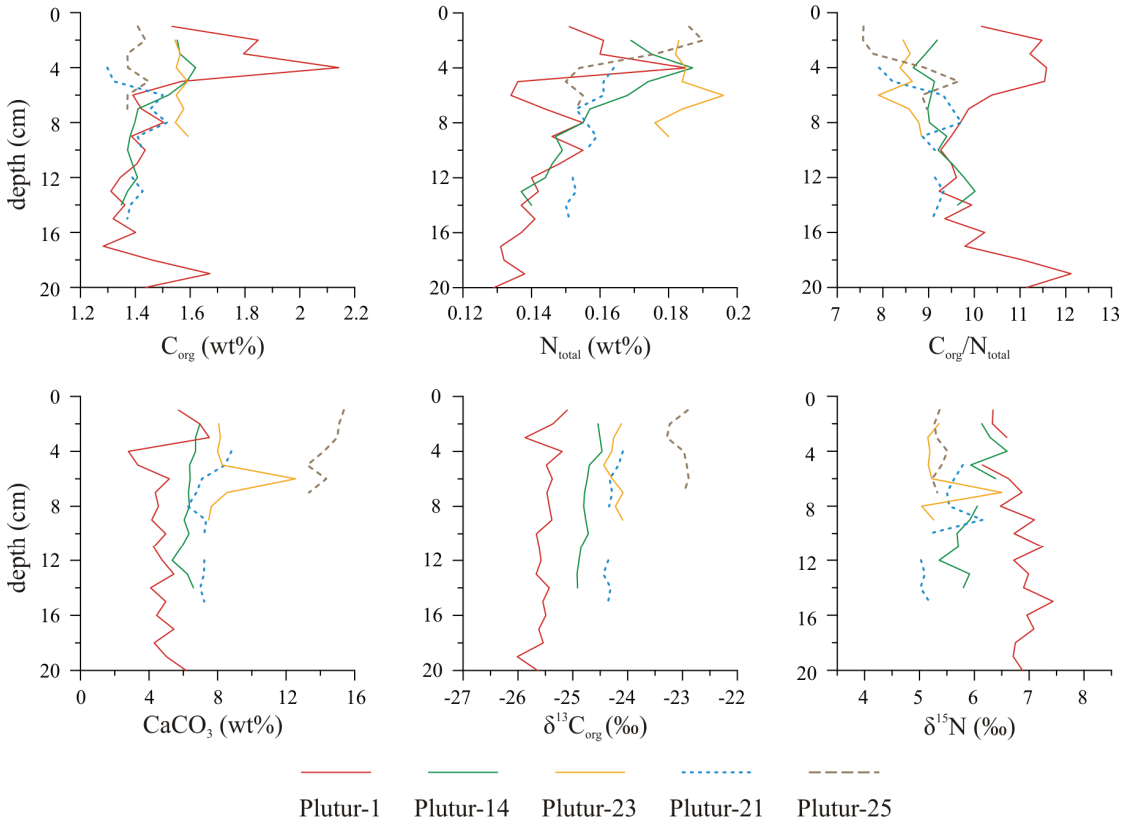

Fig. 5.2: Data of the five Plutur box cores.

5.5.2 GeoB 8903

C_{org} content (Fig. 5.4F) is ca. 1wt% below 500cm, before increasing to 1.4wt% between 470 and 300cm and further to 1.6wt% between 300 and 250cm. A decrease to 1.4wt% at 170cm is followed by constant values until 50cm, above which C_{org} content increases to 1.6wt% at the core top. C_{org}/N_{total} ratios (Fig. 5.3D) are around 10.5 between 450cm and the core base before they increase to a maximum value of 11 at 450cm. Above 450cm the C_{org}/N_{total} values decrease to around 9.5 at the core top. This trend is interrupted by two intervals of relatively constant C_{org}/N_{total} values between 350 and 250cm and between 170 and 100cm. $\delta^{13}C_{org}$ values

(Fig. 5.3C) vary between -23.2 and -24‰, with heavier values around 470cm, between 370 and 300cm and above 60cm. Relatively light $\delta^{13}C_{org}$ values are observed below 490cm, between 450 and 400cm and between 230 and 60cm. $\delta^{15}N$ values (Fig. 5.3B) vary between 5 and 5.8‰ with slightly heavier values and three positive peaks between 350 and 250cm. At 150cm a sharp increase from 5.2 to 5.6‰ is observed, otherwise variations in $\delta^{15}N$ are minor. The $CaCO_3$ content (Fig. 5.4D) decreases from 24wt% at the core base to 14-18wt% between 470cm and 300cm. Above 300cm the $CaCO_3$ content decreases to 10wt% at 170cm and remains constant until the core top.

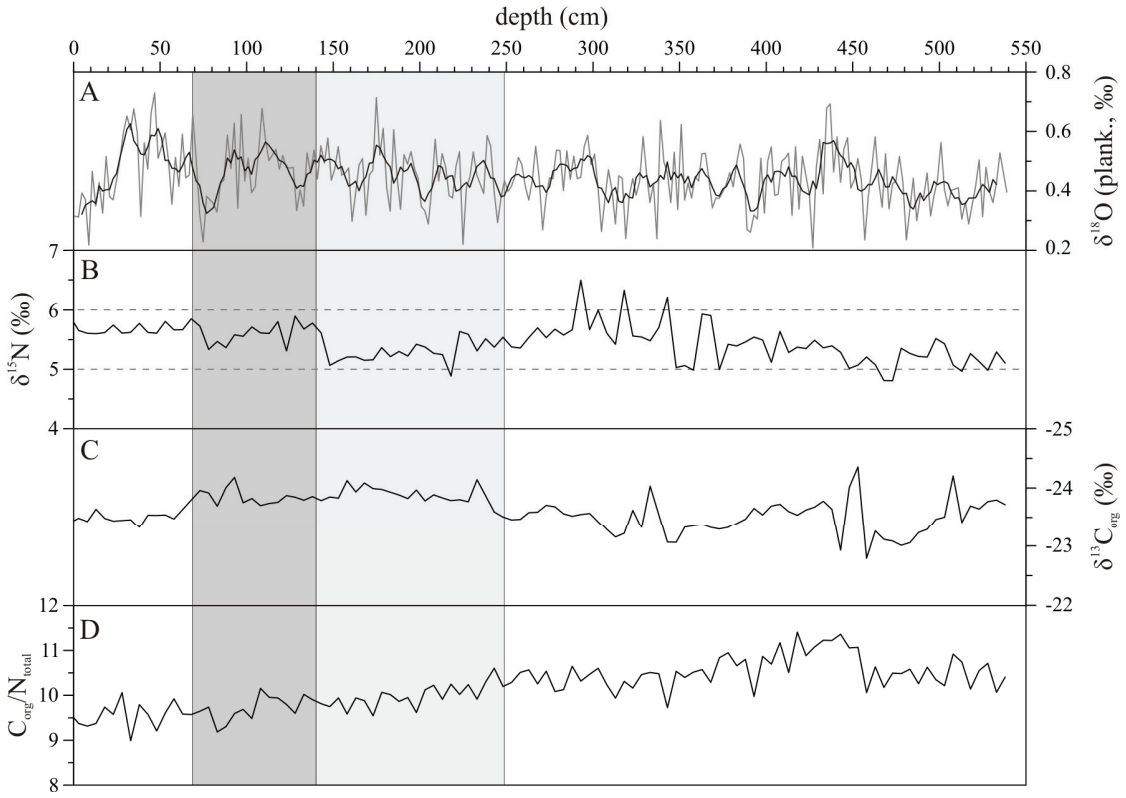

Fig. 5.3: Selected sediment parameters (from top to bottom: planktonic $\delta^{18}O$, $\delta^{15}N$, C_{org}/N_{total}, $\delta^{13}C_{org}$,), which are indicative for oceanographic conditions (SST, SSS, nutrient budget) and organic matter provenance. Red line in the $\delta^{18}O$ plot shows the 9-point running average. Dashed, horizontal lined in $\delta^{15}N$ plot indicate upper and lower limits of typical deep-water $\delta^{15}NO_3^-$ (5-6‰, LIU and KAPLAN, 1989).

The MS of core GeoB 8903 (Fig. 5.4B) is below $5*10^{-5}$ until 320cm, interrupted by two positive excursions to values around $10*10^{-5}$ between 470 and 480cm and to values around $5*10^{-5}$ at 400cm. At 320cm MS increases to ca. $10*10^{-5}$, before increasing further to 30-35$*10^{-5}$ from 250 to 200cm. This high level is maintained until the core top, interrupted by a short excursion to $25*10^{-5}$ at 140cm.

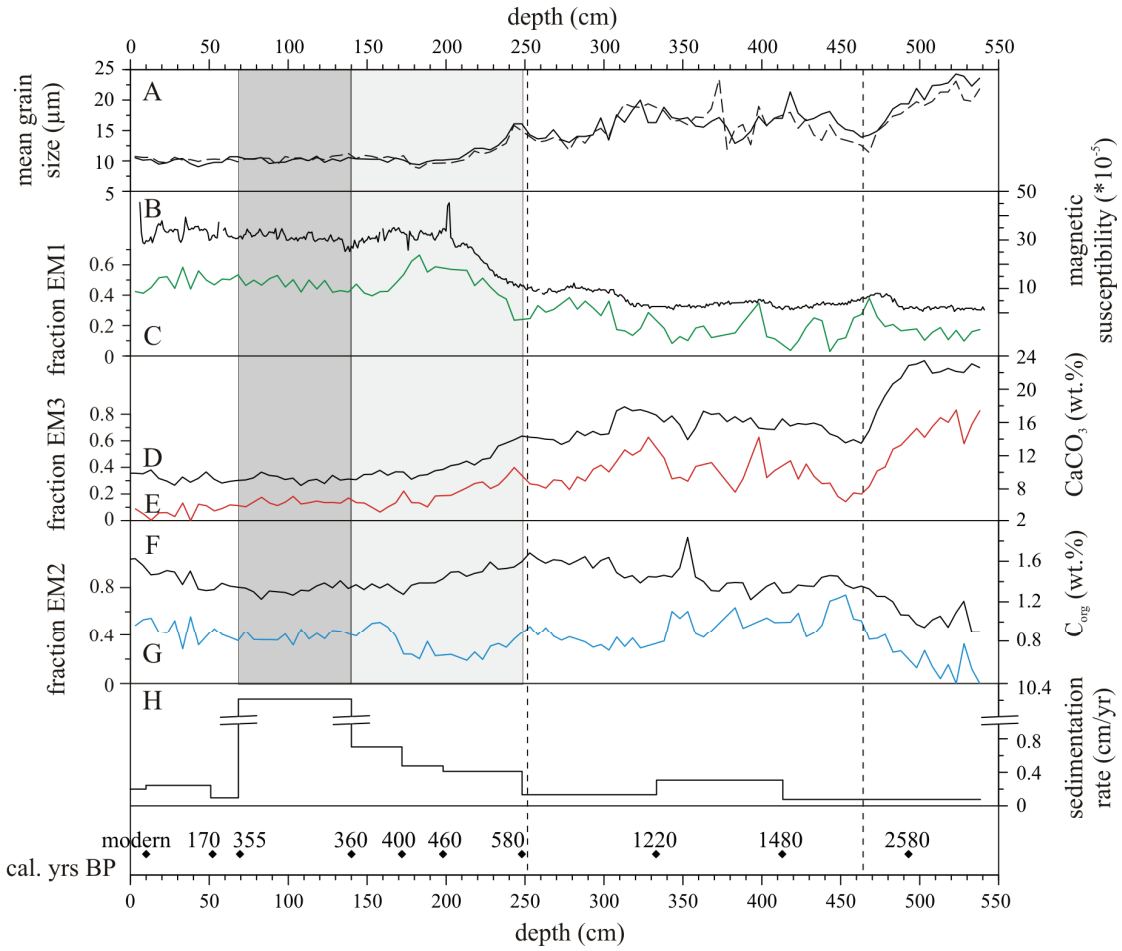

Fig. 5.4: Sediment properties versus age. A: mean grain-size (bulk sediment: solid line, terrigenous fraction: dashed line), MS (B) and EM1 (C), $CaCO_3$ content (D) and EM3 (E) and between C_{org} (F) and EM2 (G). Sedimentation rates (H) and datings are shown below. The interval, which is omitted from interpretation, is shaded in dark grey, whereas the light grey box marks the section, in which a tsunamigenic influence cannot be excluded. Dashed lines separate the three environmental phases, described in the text.

The $\delta^{18}O$ values (Fig. 5.3A) range between 0.2 and 0.7‰ and thus vary not significantly, except for a constant decline from 0.6‰ to 0.3‰ in the top 30cm.

Mean bulk grain-size of core GeoB 8903 (Fig. 5.4A) decreases from 24µm at the core base to 15µm around 450cm core depth, fluctuating around this value until 240cm. Two slight increases in mean grain-size are observed around 420cm (20µm) and 320cm (18µm). Above 240cm, values decrease to 10µm until the core top. The mean grain-size of the terrigenous

sediment fraction is similar, with ca. 1-2µm finer values between 420cm and the core base (Fig. 5.4A).

End-member modelling of the grain-size spectrum of the terrigenous sediment fraction results in several potential lithic subpopulations. With two subpopulations, 77% of the variance of the grain-size spectrum can be explained. Three end-members give a correlation coefficient R^2 of 0.86, whereas four end-members results in an only slightly improved correlation coefficient of 0.91. Therefore, the three end-member model is chosen to explain the sediments grain-size distribution in an optimal way. End-member 1 (EM1) is defined as the finest subpopulation, which is poorly sorted with a mean grain-size of 6µm (Fig. 5.5A). End-member 2 (EM2) has a mean grain-size of 12µm, end-member 3 (EM3) has a mean grain-size of 25µm and is better sorted. These values apply for the low-resolution model (5cm spacing), but are equal for the separately obtained high-resolution model (1cm spacing), showing the good reproducibility of the modelling results. The abundance of each end-member changes with depth, showing a max. 80% abundance of EM3 in the lowest 80cm and an increased EM3 fraction of ca. 60% also between 350 and 300cm (Fig. 5.5B). Above 300cm, the fraction of EM3 decreases to below 20% at 200cm and to around 10% at the core top. EM2 shows generally an abundance of around 40%, with lower values below 470cm, higher values between 470 and 340cm and again lower values between 220 and 170cm. EM1 comprises a low abundance in the lower half of the record (10-30%) and values between 40 and 70% above 240cm (Fig. 5.5B).

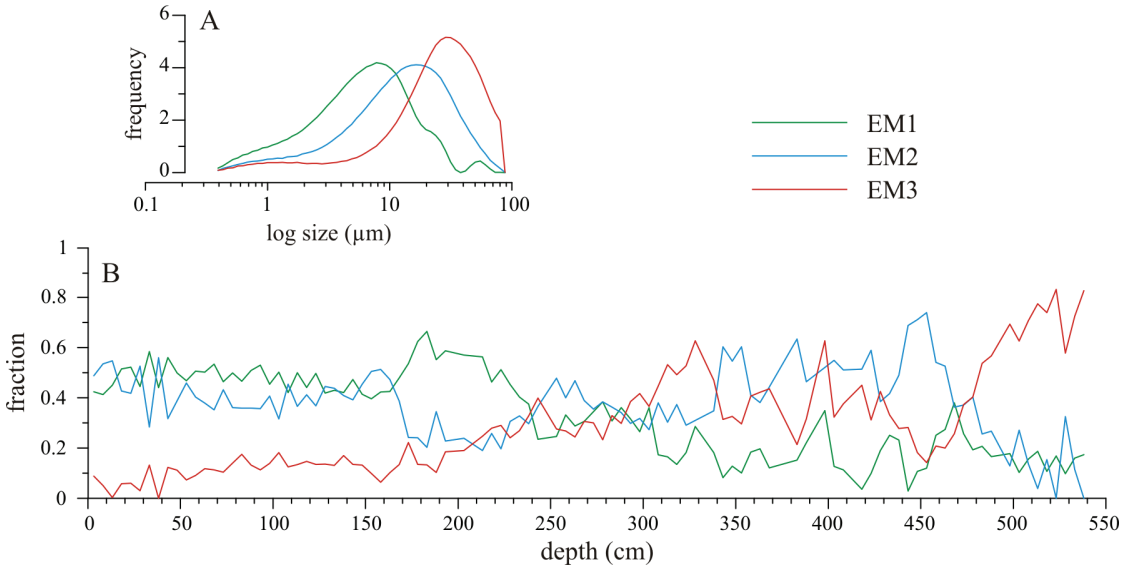

Fig. 5.5A, B: Grain size spectra of the three modelled end-members (Fig. 5.5A) and downcore variation of the end-members (Fig. 5.5B).

The reservoir corrected and calibrated age model of core GeoB 8903 (Tab. 5.2, Fig. 5A, B) has an oldest date of 628BC close to the base of the core. Resulting sedimentation rates (SR) are with 0.08cm/yr lowest in the bottom part of the core before they increase to 0.3cm/yr between 413 and 333cm depth. Until 248cm SR reach 0.13cm/yr and increase to 0.1-0.7cm/yr in the upper 248cm. These sedimentation rates are in accordance to values reported by JOUANNEAU et al. (1998) and ABRANTES et al. (2005) from the Tagus prodelta. A sedimentation rate of 10cm/yr between 69 and 140cm is probably unrealistic and discussed below.

5.6 Discussion

5.6.1 Plutur Box Cores

Decreasing C_{org}/N_{total} values as well as increasing $\delta^{13}C_{org}$ and $CaCO_3$ values along the transect Plutur-1 - Plutur-14 - Plutur-23 imply decreasing terrigenous organic matter inputs with increasing distance to the estuary mouth. Furthermore, decreasing $\delta^{15}N$ values indicate decreasing amounts of estuarine organic matter (OWENS, 1985). Plutur-25, located in the northwestern part of the prodelta, shows typical marine properties (high $CaCO_3$ content, heavy $\delta^{13}C_{org}$). Plutur-21, located in the southern part of the prodelta, shows intermediate values similar to Plutur-23, implying that the sampling location is within a major transport pathway for terrigenous sediment from the estuary to the Lisbon Canyon (JOUANNEAU et al., 1998).

The slight downcore increase of C_{org}/N_{total} ratios reflects the degradation of labile, N-rich organic substances, such as proteins, which is caused by a decrease in N_{total} (not shown). Isotope ratios are constant, showing no downcore trend and thus no sign for early diagenetic alterations.

The high variability of the data of Plutur-1 is caused by its location inside the estuary channel, where current speeds are highest and the sediment surface is frequently disturbed by anthropogenic activities (e.g. dredging) or natural processes (e.g. channel migration).

5.6.2 GeoB 8903

5.6.2.1 Age Model

The complete recovery of the core top of gravity core GeoB 8903 is indicated by a post-AD1950 radiocarbon age at 10cm core depth as well as by a similar magnitude and pattern in MS in a nearby, ^{210}Pb-dated box core (ABRANTES et al., 2005).

Between 69 and 198cm four dated samples comprise an identical range of possible ages between 300 and 490 cal. yrs BP (Fig. 5A, B). Particularly the 69cm-dating yields an age reversal, suggesting a disturbance of the sedimentary record in this interval. This is possibly caused by the AD1755 tsunami, as this date corresponds well to the 51cm-dating level, which may hence represent the upper limit of the tsunamigenic sediment layer. The definition of the lower boundary is problematic, because although the dating results are all in a similar range, suggesting a lower boundary of the tsunamigenic layer of at least 198cm core depth, it is possible to construct a plausible linear age-depth relation between 140 and 248cm (Fig. 5.6B). Omitting the 51cm- and the 69cm-datings, this line also intersects the origin and the resulting sedimentation rates of less than 0.7cm/yr are in a realistic range for this region (JOUANNEAU et al., 1998; ABRANTES et al., 2005). Furthermore, the strong change in MS between 250 and 200cm (Fig. 5.4B) is visible in other cores along the central Portuguese margin (e.g. ABRANTES et al., 2005, ABRANTES, pers. comm) and therefore not an artefact of the tsunami. Hence, the interval 51-140cm should be considered as disturbed, whereas the interval 140-248cm should be interpreted carefully, especially above 198cm.

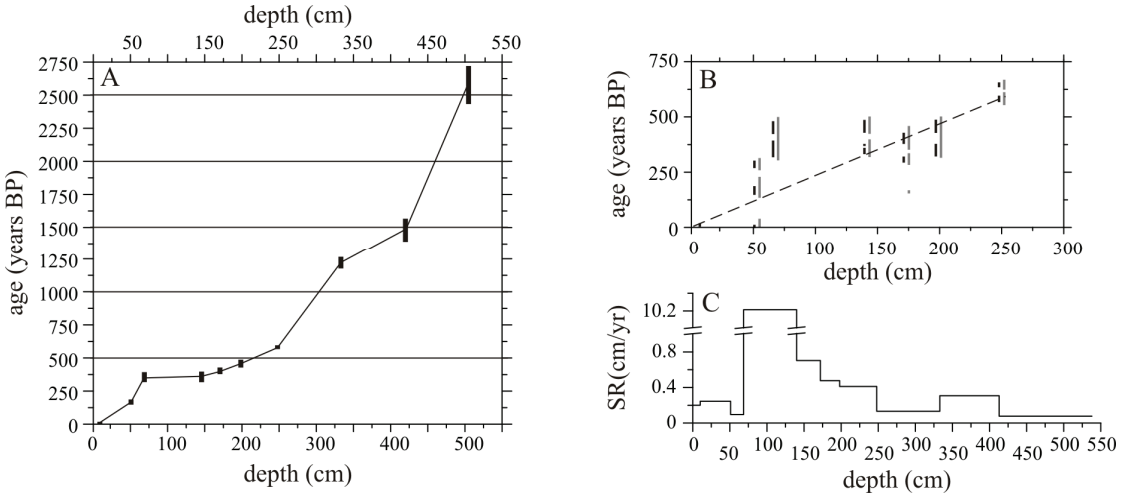

Figs. 5.6A, B, C: Age model (Figs. 5A and B) and sedimentation rates (Fig. 5C) for core GeoB 8903. Fig. 5A shows calibrated (STUIVER and REIMER, 1993) and reservoir corrected (400 years, ABRANTES et al., 2005) ages. Lengths of bars represent the dating error. Fig. 5B shows the enlarged dating results of the upper part of the sediment record. Black bars indicate the 1sigma interval; grey bars the 2sigma intervals. The length of each bar represents the probability for each date. Fig. 5C shows the sedimentation rates.

Tab. 5.2: Compilation of dated samples and dating results. ^{14}C ages are corrected by 400yrs reservoir effect (ABRANTES et al., 2005) and calibrated with Calib5.0.1, using the "intcal04" calibration dataset (STUIVER and REIMER, 1993).

depth (cm)	^{14}C age (yrs BP)	calibrated yrs BP	age (yrs AD)	half error (yrs)	sed. rate (cm/yr) (interval, cm)
10	modern	modern	modern		0.2 (0-10)
51	610	170	1780	18.5	0.25 (10-51)
69	735	350	1600	18	0.1 (51-69)
140	760	360	1590	40	10.21 (69-140)
172	685	405	1545	24.5	0.7 (140-172)
198	760	455	1495	30	0.48 (172-198)
248	1035	580	1370	17.5	0.41 (198-248)
333	1660	1220	730	44.5	0.13 (248-333)
413	2000	1480	470	88.5	0.31 (333-413)
498	2885	2580	-630	144	0.08 (413-498)

Erosion of 39cm sediment and subsequent, instantaneous deposition of 19cm sediment in a gravity core from the southern prodelta has been reconstructed by interpreting grain-size and MS data and explained by the AD1755 tsunami (ABRANTES et al., 2005). However, sediment parameters of core GeoB 8903 show no evidence for a disturbance (Fig. 5.3, 5.4). Particularly the grain-size is constant in this interval. This is similar to observations by ANDRADE et al. (2003) inside the Tagus Estuary, stating that the tsunami left no relevant textural contrast in the sediments. Furthermore, BAPTISTA et al. (2003) modelled a tsunami wave height of around 5m at Oeiras, close to Lisbon outside the Tagus Estuary. This is relatively low, considering the shallow water depth and compared to a 12m high tsunami wave at C. San Vicente, SW Portugal (BAPTISTA et al., 2003). Due to the possible overestimation of the tsunamigenic impact on the shelf sediments and because in core GeoB 8903 neither grain-size nor MS data evidence a tsunami impact, the age model is applied according to Fig. 5A and Tab. 2. However, the interval 51-140cm is omitted from interpretation, accounting for the extreme sedimentation rates and the interval 140-248cm is regarded with care, as a tsunamigenic disturbance cannot be excluded.

5.6.2.2 Hydrography, Organic Matter Provenance and Nutrient Conditions

Planktonic foraminifera $\delta^{18}O$ values show no significant variability, indicating no major local variations in salinity and sea surface temperature during the past 3.2kyrs (Fig. 5.3A). Also sedimentary $\delta^{15}N$ values are relatively constant, indicating a stable relation between nutrient supply (e.g. upwelling intensity) and nutrient consumption (i.e. marine productivity) as well as no varying influences of $\delta^{15}N$ affecting processes, such as e.g. denitrification or N_2-fixation

(Fig. 5.3B). However, $\delta^{18}O$ values may be biased by changing water characteristics, caused e.g. by variations in upwelling or riverine freshwater discharge. Local $\delta^{15}N$ values are affected by agricultural inputs from the hinterland, which has been shown for estuarine sediments (ALT-EPPING et al., 2007) and is liklely to apply for shelf sediments as well. Hence, further research is necessary to provide a reliable interpretation of this data.

$\delta^{13}C_{org}$ and C_{org}/N_{total} values in core GeoB 8903 are similar to those of the marine dominated core Plutur-25, indicating a dominantly marine origin of organic matter. During the past 3.2kyrs, C_{org}/N_{total} ratios and $\delta^{13}C_{org}$ values vary only insignificantly in terms of organic matter provenance, implying a constant mixture of terrigenous and marine organic matter sources (Fig. 5.3C, D). No effects of the major historical climatic periods, such as Roman Warm Period, Dark Ages, Medieval Warm Period or the Little Ice Age, nor of anthropogenic impacts on the continental environment (e.g. by deforestation) are recorded by the organic matter provenance proxies. A reason for this may be the reworking and partial deposition of terrigenous organic material within the Tagus Estuary, leading to reported, high sedimentation rates inside the estuary (JOUANNEAU et al., 1998). A turbidity maximum in the uppermost estuary (CASTANHEIRO, 1982) indicates flocculation of dissolved riverine organic matter, triggered by the salinity increase, which can lead to the deposition of considerable parts of the riverine organic material inside the estuary. Furthermore, variations in freshwater discharge should be recorded in planktonic $\delta^{18}O$ data. The observation of constant SSS on the prodelta indicates thorough mixing of fresh- and seawater inside the estuary, diluting the terrigenous signal and leading to the relatively strong marine signature in the sediments close to the estuary mouth.

5.6.2.3 Grain Size Analyses

The similarity of the mean grain-size records of the bulk and terrigenous sediment fractions (i.e. carbonate, biogenic opal and organic matter removed) of core GeoB 8903 implies a dominance of lithic material. The positive correlation between $CaCO_3$ concentration and mean grain-size further suggests, that the calcareous material is relatively coarse, whereas the finer sediment has a higher MS (Fig. 5.4A).

This is supported by the downcore abundance of the finest end-member EM1 (6µm average grain size), which shows an excellent correlation with MS (R^2=0.9), indicating a continental origin (Fig. 5.4B, C). Further, the fine and poorly sorted grain size spectrum of EM1 supports a fluvial transport (KOOPMANN, 1981, STUUT et al., 2002, HOLZ et al., 2004). EM2 shows some similarity with C_{org} content (Fig. 5.4F, G), if the interval from 180 to 350cm is omitted (R^2=0.54), but as there are no clear correlations between EM2 and provenance proxies visible, no definite statements about the origin of EM2 can be made. The coarsest end-member EM3 (25µm) is strongly related to $CaCO_3$ content (R^2=0.92) (Fig. 5.4D, E). These

findings confirm, that the calcareous fraction is related to coarse sediment material (EM3) and that the MS signal is related to the fine fraction (EM1). The lithic character of EM3, as well as its coarse and relatively well-sorted grain-size spectrum indicate, that EM3 is of fluvial or aeolian origin. In case of the former, winnowing due to stronger bottom currents may concentrate and sort the EM3 fraction particularly prior to 2kyr BP (below 450cm core depth) (Fig. 5.3E, 5.5). Winnowing is supported by low sedimentation rates in the lower part of the sedimentary record, as well as by the reconstruction of stronger bottom-currents on the northwestern Portuguese shelf prior to 2.2kyr BP (MARTINS et al, 2006). A dry climate (Subboreal) at that time supports an input of dust, possibly originating from the central Iberian Peninsula, as suggested by the relatively coarse average grain-size. Dust may also be derived from the Saharan desert, from where dust is transported northwards over the Iberian peninsula (MORENO et al., 2002; GUERZONI et al., 1997), which is well observed by SeaWifs satellite images.

Both processes – winnowing and aeolian supply – imply the presence of stronger winds. Increased wind strength also results in stronger upwelling, producing the coevally high $CaCO_3$ content and thus explaining the excellent correlation between $CaCO_3$ and the lithic end-member EM3 (Fig. 5.4E, D). A high marine productivity should also lead to increased C_{org} content. This is not observed (Fig. 5.4F), because C_{org} is associated to a finer grain-size spectrum (i.e. EM2) and thus subject to winnowing due to stronger bottom currents.

Physical sediment properties show a high spatial variability on the Tagus Prodelta. This is evidenced by large differences in grain-size between core GeoB 8903 and a sediment record from the south-eastern prodelta, 17km away (LEBREIRO et al., 2006). The latter is characterised by grain-sizes between 30 and 100µm and sand content between 20 and 75%. Together with the differences regarding the record of the AD1755 tsunami, this emphasises the textural variability between sediments of the Tagus mud belt and shelf sediments.

5.6.2.4 Relation to NAO

On a short timescale, i.e. for the past 150 years the proxy records of GeoB 8903 can be compared to NAO reconstructions, to evaluate a potential influence of NAO variations on sediment properties. This is done by correlating time-related GeoB 8903-data, based on the age model, with the NAO reconstruction. Prior to AD1850 limitations of the age model and possible disturbances of the sedimentary record prevent a reliable correlation of the sediment record with NAO reconstructions. Furthermore slight offsets in sampling depth between MS measurements and grain-size analyses may lead to the observed shift between both records between 35 and 55cm.

MS shows a positive correlation with a reconstructed NAO index (COOK et al., 2002), i.e. low MS during NAO negative phases (Fig. 5.7). Simultaneously a negative correlation

between mean bulk grain size and NAO is evident. This observation is initially counterintuitive, when MS is interpreted as proxy for terrigenous sediment supply and should thus increase during negative NAO (i.e. high river runoff). However, the apparent contradiction can be explained by the existence of two distinct, lithic subpopulations, of which the finer carries the MS signal. The input of coarser, non-susceptible particles to the shelf by stronger currents and higher suspended sediment load during NAO negative phases dilutes the high-MS signal and leads to the observed positive correlation between NAO and MS as well as to the negative correlation between NAO and mean bulk grain-size (Fig. 5.7).

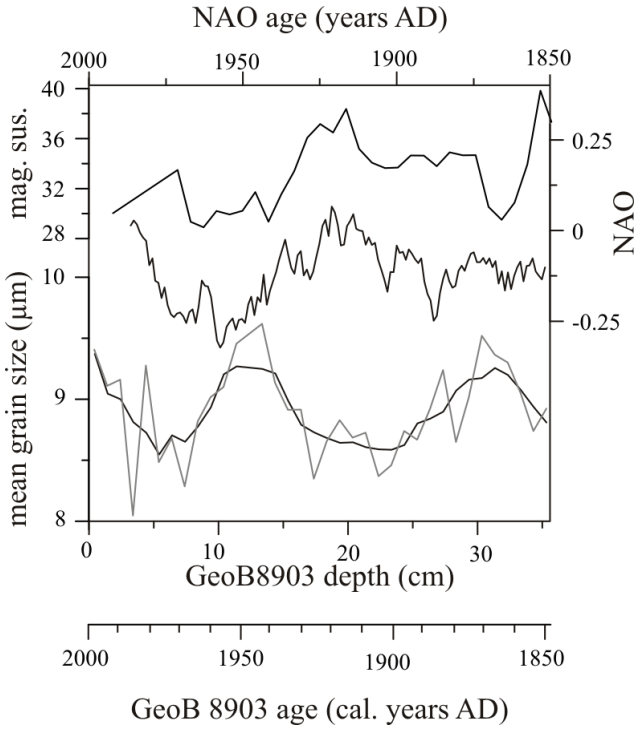

Fig. 5.7: Comparison of a NAO reconstruction (COOK et al., 2002: 33-point running average) with MS and mean grain-size (grey line: data in 1cm resolution; black line: 5-point running average), showing the positive correlation between NAO and MS and the negative correlation between NAO and grain-size. The two bottom axes give the age of the GeoB 8903 record at the respective depth. Prior to AD1850 the age model is uncertain, preventing a reliable correlation between the sediment record and NAO.

The furthermore excellent correlation between EM1 and MS allows the classification of EM1 as fine subpopulation, which appears to be supplied to the shelf constantly. The coarser, magnetically non-susceptible subpopulation is accordingly represented by EM2 (Fig. 5.5a).

This concept is further supported by weak, but evident correlations between NAO index and endmember abundance (Fig. 5.8). EM1 shows both a positive correlation with NAO, whereas EM2 correlates negatively with NAO. The correlation between EM3 and NAO is very weak, but best visible below 20cm depth. Due to the low relative abundance, this end-

member is most susceptible to small variations in sediment input. Hence, only slight fluctuations in the supply of EM3 can prevent an obvious correlation. Furthermore, as the abundances are given in a relative way, dilution effects also play a role and might weaken possible correlations with NAO. Thus, although these correlations are relatively weak, they substantiate the inferred dependence of individual sediment components on NAO.

A general conclusion from these observations is, that the sediment texture is an essential factor, which must be considered in paleoenvironmental interpretations. Typical proxies, which are used for paleoenvironmental reconstructions (MS, C_{org} content, $CaCO_3$ content), heavily depend on grain-size and are associated to distinctive components of the total sediment.

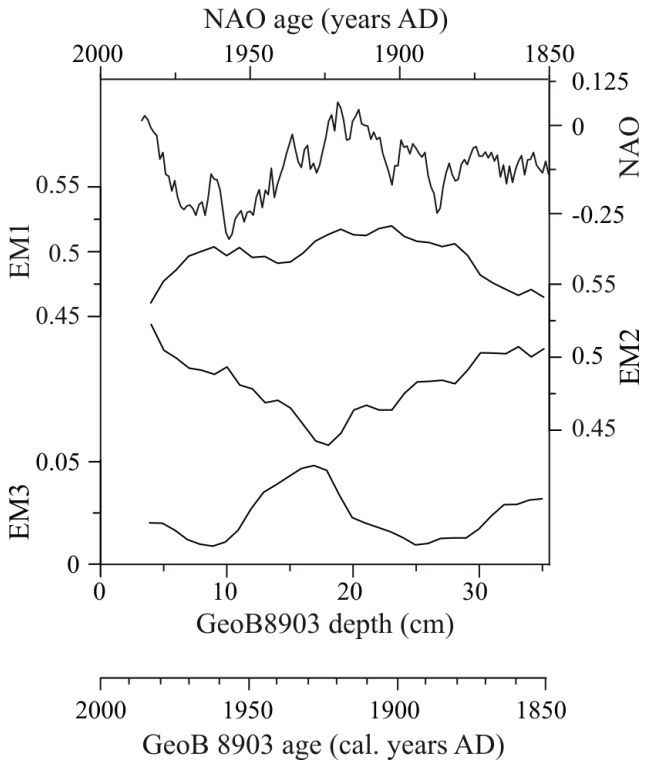

Fig. 5.8: Comparison of a NAO reconstruction (COOK et al., 2002: 33-point running average) with end-member abundances (7-point running average), showing a weak but significant positive correlation between EM1 and EM3 and NAO, whereas EM2 and NAO correlate negatively.

5.6.2.5 Long Term Variations

The part of the sediment record, which is not affected by the tsunami, shows three distinct phases. The oldest phase prior to 2kyr BP is characterised by enhanced $CaCO_3$ content, coarser grain-sizes and a dominance of EM3 against EM1 and EM2 on one hand and lower C_{org} content on the other hand (Fig. 5.4, 5.5). Interpreting EM3 as related to wind strength, regardless whether it is of aeolian origin or concentrated by winnowing due to strong shelf bottom currents, this observation implies stronger wind energy during this phase. An aeolian origin is supported by the high availability of dust due to the prevailing dry climate. Stronger wind-driven upwelling enhances marine productivity, which is evidenced by higher $CaCO_3$ content. Although an increase in marine productivity should also be observed by higher C_{org} content, the association of C_{org} to finer lithic material makes it more susceptible to winnowing. Increased shelf bottom-currents are additionally supported by a study from the northwestern Portuguese shelf (MARTINS et al., 2006).

The second period between 2 and 0.5kyr BP is characterised by lower $CaCO_3$ content, finer grain-sizes, less EM3 with respect to EM2 and slightly higher C_{org} concentrations (Fig. 5.4, 5.5). Corresponding to the above concept, this is explained by decreased wind energy, which results in weaker bottom-currents, hence less winnowing and a higher C_{org} concentration. Also dust supply is diminished and upwelling intensity is reduced, thus decreasing $CaCO_3$ input. Between 1.1kyr BP and 0.6kyr BP grain-sizes and $CaCO_3$ content decrease further, whereas MS increases slightly. Sedimentary records from the Eastern North Atlantic, e.g. from the Skagerrak (HEBBELN et al., 2006) and from other locations in the north-eastern North Atlantic (e.g. ERIÍKSSON et al., 2006) show a coincident change around 1.1kyr BP, evidenced by a coarsening and an increase in Ca/K ratio (HEBBELN et al., 2006). This is explained by a strengthening of bottom-currents (HEBBELN et al., 2006), induced by a reorganisation of atmospheric circulation patterns around 1.1kyr BP (SCOURSE et al., 2006). This reorganisation may affect sedimentary records from southwestern Europe in a complementary way.

The youngest phase is characterised by a strong increase in lithic, terrigenous supply between 0.6kyr BP and 0.5kyr BP, evidenced by an abrupt increase in MS, remaining on a high level until the core top (Fig. 5.6b). If this was a climatically induced change, e.g. by a temperature decline due to the onset of the Little Ice Age (e.g. LEBREIRO et al., 2006), MS should return to “warm” values in the top part, when temperatures are rising again. As this is not the case, the MS increase is interpreted as a permanent environmental change in the river catchment, e.g. caused by deforestation, which reached a maximum in the 15^{th} and 16^{th} century. During these times large amounts of timber were required, e.g. for shipbuilding. This interpretation is supported by a decreased influx of pollen from temperate trees (deciduous forests) since ca. 0.55BP (AD1400) in northwest Iberia (DESPRAT et al., 2003) indicating a regional decline in forest area. As a result, erosion rates and thus the discharge of lithic material through the Tagus River increased.

Consequently, the correlation of the GeoB 8903 record to historical climatic phases like Little Ice Age, Medieval Warm Period, Dark Ages or Roman Warm Period appears to be not appropriate. Instead, the observed changes in sediment parameters imply a different chronology of environmental changes, with the transition from the Subboreal to the Subatlantic period being dominating.

5.7 Summary

The sedimentary record of gravity core GeoB 8903 from the prodelta of the Tagus River on the central western Portuguese shelf shows environmental changes on a high temporal resolution, although the AD1755 tsunami possibly disturbed a minimum ca. 70cm long section of the core. Variations in environmental conditions are evident by changes in physical sediment properties, rather than changes in organic matter provenance. Detailed grain-size analyses exhibit three end-members of the lithic sediment fraction. The finest end-member EM1 carries the MS signal and is interpreted due to its fine grain-size of average 6µm to be of fluvial origin. A medium-sized end-member (EM2, mean grain-size 12µm) is associated to the C_{org} content, whereas the third end-member (EM3, 25µm) correlates strongly with $CaCO_3$ concentrations. The positive correlation between NAO and MS during the past 250 years and the coinciding negative correlation between mean bulk grain-size is explained by a perennial supply of EM1, diluted by an input of EM2 during NAO-negative phases. Hence, both sediment components are ascribed to fluvial, continental origin. The lithic composition and the relatively coarse, well-sorted grain-size spectrum of EM3 suggest an aeolian or fluvial origin. Generally the effect of NAO on the sediments appears to be minor and restricted to small variations in sediment composition. These are evident by slightly stronger EM2 inputs, related to increased precipitation rates during NAO negative phases or by a higher EM3 fraction during NAO positive phases, which are characterised by higher wind intensity. It becomes further evident, that proxies, that are commonly applied for paleoenvironmental reconstructions strongly depend on grain-size and that they are associated to specific sedimentary subpopulations.

The higher relative abundances of EM3, higher $CaCO_3$ content, coarser grain-sizes and the lower C_{org} content prior to 2kyr BP are interpreted to be results of stronger winds, combined with continental aridity (Subboreal), increasing the availability of dust. Stronger winds also lead to a higher marine productivity by more intense winds, increasing the $CaCO_3$ content. As C_{org} is connected to finer material, it is winnowed by increased bottom-currents.

Complementary, a more humid, less windy climate between 2 and 0.5ky BP is reflected by finer grain-sizes, less EM3, less $CaCO_3$ and a higher C_{org} content.

Around 0.6 to 0.5kyr BP increasing deforestation in the catchment of the Tagus River, possibly triggered by the increasing demand for timber for shipbuilding, results in an

increased supply of lithic material to the prodelta, indicated by strongly and permanently increased MS and by higher sedimentation rates.

The sedimentary record is possibly disturbed, as indicated by very high sedimentation rates between 69 and 140cm and by a questionable age model between 51cm and 198cm. This covers the AD1755 tsunami. However, no textural or geochemical difference is visible between disturbed and undisturbed sediments, which is in accordance to observations from inside the Tagus Estuary (ANDRADE et al., 2003), but contrary to observation from the southeastern prodelta (ABRANTES et al., 2005). This and a different sediment texture compared to the southeastern prodelta record (e.g. manifested by a considerably coarser grain-size in the southern cores, ABRANTES et al., 2005) emphasises the heterogeneity of sedimentation conditions and sediment properties on the Tagus Prodelta. Nevertheless, the timing of the observed change in sediment properties corresponds to the transition from the Subboreal to the Subatlantic. Additionally, variations in sediment properties appear to be synchronous to environmental changes, that have been reconstructed from eastern North Atlantic records (e.g. HEBBELN et al., 2006), evidenced by complementary patterns in sediment parameters, such as grain-size, in records from these locations. This emphasises the significance of the GeoB 8903 record although the chronology of Little Ice Age, Medieval Warm Period, Dark Ages or Roman Warm Period, which is commonly applied to the Portuguese shelf records, cannot be implemented here.

5.8 Acknowledgements

The work was conducted as a part of the SEDPORT project (Sedimentation Processes on the Portuguese Margin: The Role of Continental Climate, Ocean Circulation, Sea Level, and Neotectonics) and funded by the German Science Foundation (DFG) as part of the EUROMARGINS/EUROCORES program. Plutur samples were collected by the Hydrographic Institute of Portugal in cooperation with the Department of Geology and Oceanography (DGO) of the University Bordeaux during the European OMEX (Ocean Margin Exchange) program. We thank F. Abrantes, I. M. Gil, E. Salgueiro for thorough, valuable discussions, G.J. Weltje for providing the end-member modelling algorithm, Monika Segl, Birgit Meyer-Schack, Hella Buschhoff and the crew of RV POSEIDON during leg 304 for technical support and Phillip Franke for assistance with the grain-size measurements.

5.9 References

Abrantes, F., M.T. Moita (1999): Water column and recent sediment data on diatoms and coccolithophorids, off Portugal, confirm sediment record of upwelling events. Oceanologica Acta 22(3): 319-336.

Abrantes, F., S. Lebreiro, T. Rodrigues, I. Gil, H. Bartels-Jónsdóttir, P. Oliveira, C. Kissel, J.O. Grimalt (2005): Shallow-marine sediment cores record climate variability and earthquake activity off Lisbon (Portugal) for the last 2000 years. Quaternary Science Reviews 24(23-24): 2477-2494.

Altabet, M.A., R. Francois (1994): Sedimentary nitrogen isotopic ratio as a recorder for surface ocean nitrate utilization. Global Biogeochemical Cycles 8(1): 103-116.

Andrade, C., M.C. Freitas, J.M. Miranda, M.A. Baptista, M. Cachao, P. Silva, J. Munha. (2003): Recognizing possible tsunami sediments in the ultradissipative environment of the Tagus Estuary (Portugal). Coastal Sediments, Clearwater Beach, Florida, USA.

Baptista, M.A., J.M. Miranda, F. Chierici, N. Zitellini (2003): New study of the 1755 earthquake source based on multi-channel seismic survey data and tsunami modeling. Natural Hazards and Earth System Sciences 3: 333–340.

Bartels-Jónsdóttir, H.B., K.L. Knudsen, F. Abrantes, S. Lebreiro. J. Eiríksson (2006): Climate variability during the last 2000 years in the Tagus Prodelta, western Iberian Margin: Benthic foraminifera and stable isotopes. Marine Micropaleontology 59(2): 83-103.

Blott, S.J., K. Pye (2001): Gradistat: A grain-size distribution and statistics package for the analysis of unconsolidated sediments. Earth Surface Processes and Landforms 26: 1237-1248.

Bonway, H.C., A.C. Mix (2004): Oxygen isotopes, upper ocean salinity and precipitation sources in the eastern tropical Pacific. Earth and Planetary Science Letters 224: 493-507.

Castanheiro, J.M. (1982): Distribution, Transport and Sedimentation of Suspended Matter in the Tejo Estuary. Estuarine Processes: An Application to the Tagus estuary, Proceedings of a UNESCO/IOC/CNA workshop, Palácio Foz, Lisbon, Portugal.

Cook, E.R., R.D. D'Arrigo, M.E. Mann (2002): A Well-Verified, Multiproxy Reconstruction of the Winter North Atlantic Oscillation Index since A.D. 1400. Journal of Climate 15: 1754-1764.

Desprat, S., M.F. Sánchez-Goni, M.F. Loutre (2003): Revealing climatic variability of the last three millennia in northwestern Iberia using pollen influx data. Earth and Planetary Science Letters 213: 63-78.

Eiriksson, J., H.B. Bartels-Jonsdóttir, A.G. Cage, E.R. Gudmundsdóttir, D. Klitgaard-Kristensen, F. Marret, T. Rodrigues, F. Abrantes, W.E.N. Austin, H. Jiang, K.-L. Knudsen, H.-P. Sejrup (2006): Variability of the North Atlantic Current during the last 2000 years based on shelf bottom water and sea surface temperatures along an open ocean/ shallow marine transect in western Europe. The Holocene 16(7): 1017-1029.

Fiúza, A.F.G. (1983): Upwelling patterns off Portugal. In: Suess, E., J. Thiede (Eds.): Coastal Upwelling: Its Sediment Record. Plenum, New York: 85-98.

Folk, R.L., W.C. Ward (1957): Brazos River bar: a study in the significance of grain-size parameters. Journal of Sedimentary Petrology 27: 3-26.

Freitas, M.C., C. Andrade, J.C. Moreno, J.M. Munhá, M. Cachao (1999): The sedimentary record of recent (last 500 years) environmental changes in the Seixal Bay marsh, Tagus Estuary, Portugal. Geologie en Mijnbouw 77: 283-293.

Freudenthal, T., S. Neuer, H. Meggers, R. Davenport, G. Wefer (2001): Influence of lateral particle advection and organic matter degradation on sediment accumulation and stable nitrogen isotope ratios along a productivity gradient in the Canary Islands region. Marine Geology 177(1-2): 93-109.

Gil, I.M., F. Abrantes, D. Hebbeln (2006): The North Atlantic Oscillation forcing through the last 2000 years: Spatial variability as revealed by high-resolution marine diatom records from N and SW Europe. Marine Micropaleontology 60(2): 113-129.

Goñi, M.A., K.C. Ruttenberg, T.I. Eglinton (1998): A reassessment of the sources and importance of land-derived organic matter in surface sediments from the Gulf of Mexico. Geochim. Cosmochim. Acta 62(18): 3055-3075.

Guerzoni, S., E. Molinarolit, R. Chester (1997): Saharan dust inputs to the western Mediterranean Sea: depositional patterns, geochemistry and sedimentological implications. Deep Sea Research II 44(3-4): 631-654.

Hebbeln, D., K.-L. Knudsen, R. Gyllencreutz, P. Kristensen, D. Klitgaard-Kristensen, J. Backman, C. Scheurle, H. Jiang, I. Gil, M. Smelror, P. D. Jones and H.-P. Sejrup (2006): Late Holocene coastal hydrographic and climate changes in the eastern North Sea. The Holocene 16(7): 987-1001.

Holz, C., J.B.W. Stuut, R. Henrich (2004): Terrigenous sedimentation processes along the continental margin off NW Africa: implications from grain-size analysis of seabed sediments. Sedimentology 51: 1145-1154.

Hurrell, J.W. (1995): Decadal trends in the North Atlantic Oscillation: regional temperatures and precipitation. Science 269: 676-679.

Jouanneau J.M., C. Garcia, A. Oliveira, A. Rodrigues, J.A. Dias, O. Weber (1998): Dispersal and deposition of suspended sediment on the shelf off the Tagus and Sado estuaries, S.W. Portugal. Progress in Oceanography 42: 233–257.

Koopmann, B. (1981): Sedimentation von Saharastaub im subtropischen Nordatlantik während der letzten 25.000 Jahre. Meteor Forschungsergebnisse C(35): 23-59.

Lavik, G. (2001): Nitrogen Isotopes of sinking matter and sediments in the South Atlantic. Ph.D. Thesis, Fachbereich Geowissenschaften, Bremen: 140 pages.

Lebreiro, S.M., G. Francés, F.F.G. Abrantes, P. Diz, H.B. Bartels-Jónsdóttir, Z.N. Stroynowski, I.M. Gil, L.D. Pena, T. Rodrigues, P.D. Jones, M.A. Nombela, I. Alejo, K.R. Briffa, I. Harris, J.O. Grimalt (2006): Climate change and coastal hydrographic response along the Atlantic Iberian margin (Tagus Prodelta and Muros Ria) during the last two millennia. The Holocene 16(7): 1003-1015.

Liu, K.-K., I.R. Kaplan (1989): The eastern tropical Pacific as a source of 15N-enriched nitrate in seawater off southern California. Limnology and Oceanography 34(5): 820-830.

Mahowald, N., K. Kohfled, M. Hansson, Y. Balkanski, S. P. Harrison, I.C. Prentice, M. Schulz, H. Rodhe (1999): Dust sources and deposition during the last glacial maximum and current climate: A comparison of model results with paleodata from ice cores and marine sediments. Journal of Geophysical Research 104(D13): 15895-15916.

Mariotti, A. (1983): Atmospheric nitrogen is a reliable standard for natural N-15 abundance measurements. Nature 303(5919): 685-687.

Martins, V., J.M. Jouanneau, O. Weber, F. Rocha (2006): Tracing the late Holocene evolution of the NW Iberian upwelling system. Marine Micropaleontology 59(1): 35-55.

McCrea, J.M. (1950): On the isotopic chemistry of carbonates on a paleotemperature scale. Journal of Chemial Physics 18: 849-857.

Middelburg, J. J., J. Nieuwenhuize (1998): Carbon and nitrogen stable isotopes in suspended matter and sediments from the Schelde estuary. Marine Chemistry 60(3-4): 217-225.

Moreno, A., I. Cacho, M. Canals, M.A. Prins, M.-F. Sánchez-Goñi, J.O. Grimalt, G.J. Weltje (2002): Saharan dust transport and high-latitude glacial climatic variability: The Alboran Sea record. Quaternary Research 58(3): 318-328.

Müller, P., R.R. Schneider, G. Ruhland (1994): Late Quaternary pCO_2 variations the Angola Current: Evidence from organic carbon d13C and alkenone temperatures. In R. Zahn et al. (Eds.): Carbon Cycling in the Glacial Ocean: Constraints of the Ocean's Role in Global Change, NATO ASI Series, Vol. 1(17), Springer: 343-366.

Nadeau, M.-J., M. Schleicher, P.M. Grootes, H. Erlenkeuser, A. Gottdang, D.J.W. Mous, J.M. Sarnthein, H. Willkomm (1997): The Leibniz-Labor AMS facility at the Christian-Albrechts University, Kiel, Germany. Nuclear Instruments and Methods in Physics Research Section B 132(1-4): 22-30.

Niebler, H.-S., H.-W. Hubberten, R. Gersonde (1999): Oxygen Isotope Values of Planktonic Foraminifera: A Tool for the Reconstruction of Surface Water Stratification. In: Fischer, G., G. Wefer (Eds.): Use of Proxies in Paleoceanography: Examples from the South Atlantic. Berlin, Heidelberg, Springer Verlag: 165-189.

Oschlies, A. (2001): NAO-induced long-term changes in nutrient supply to the surface waters of the North Atlantic. Geophysical Research Letters 28(9): 1751-1754.

Owens, N.J.P. (1985): Variations in the natural abundance of 15N in estuarine suspended particulate matter: a specific indicator of biological processing. Estuarine, Coastal and Shelf Science 20: 505-510.

Schubert, C. J., B. Nielsen (2000): Effects of decarbonation treatments on δ13C values in marine sediments. Marine Chemistry 72: 55-59.

Scourse, J., H. P. Sejrup, P. D. Jones and HOLSMEER project participants (2006): Editorial: Late Holocene oceanographic and climate change from the western European margin: the results of the HOLSMEER project. The Holocene 16(7): 931-935.

Stuiver, M., P.J. Reimer (1993): Extended 14C database and revised CALIB radiocarbon calibration program. Radiocarbon 35: 215-230.

Stuut, J.B.W., M.A. Prins, R.R. Schneider, G.J. Weltje, J.H.F. Jansen, G. Postma (2002): A 300-kyr record of aridity and wind strength in southwestern Africa: inferences from grain-size distributions of sediments on Walvis Ridge, SE Atlantic. Marine Geology 180(1-4): 221-233.

Thornton, S. F., J. McManus (1994): Application of organic carbon and nitrogen stable isotope and C/N ratios as source indicators of organic matter provenance in estuary systems: evidence from the Tay Estuary, Scotland. Estuarine, Coastal and Shelf Sciences 38: 219-233.

Trigo R., D. Pozo-Vázquez, T. Osborn, Y. Castro-Diez, S. Ganiz-Fortis, M.J. Esteban-Parra (2004): North Atlantic Oscillation influence on precipitation, river flow and water resources in the Iberian peninsula. International Journal of Climatology 24: 925-944.

Vicente-Serrano, M., A. Heredia-Laclaustra (2004): NAO influence on NDVI trends in the Iberian peninsula (1982-2000). International Journal of Remote Sensing 25(14): 2871-2879.

Weltje, G.J. (1997): End-member modeling of compositional data: numerical-statistical algorithms for solving the explicit mixing problem. Journal of Mathematical Geology 29: 503–549.

Wolff, T., B. Grieger, W. Hale, A. Dürkopp, S. Mulitza, J. Pätzold, G. Wefer (1999): On the Reconstruction of Paleosalinities. In: Fischer, G., G. Wefer (Eds.): Use of Proxies in Paleoceanography: Examples from the South Atlantic. Berlin, Heidelberg, Springer Verlag: 207-228.

6 Holocene environmental conditions on the Portuguese margin

U. Alt-Epping[a], D. Hebbeln[a], R. Schneider[c], S. Lebreiro[b]

In Preparation

[a] DFG-Research Center Ocean Margins, University of Bremen, PO Box 330440, 28334 Bremen, Germany
[b] Department of Marine Geology, Instituto Nacional de Engenharia, Tecnologia e Inovação (INETI), Estrada da Portela, 2721-866 Alfragide, Portugal
[c] Department of Geosciences, Christian-Albrecht University Kiel, Ludewig-Meyn-Str. 10, 24118 Kiel, Germany

6.1 Abstract

Two sediment cores have been obtained from the western Portuguese margin to reconstruct variations in environmental conditions during the last deglaciation and the Holocene. A gravity core from the Tagus Prodelta allows an estimate of changes in terrigenous and marine sediment supply on a high temporal resolution, as well as variations in nutrient budget within the upwelling area. A piston core from the Lisbon Canyon levee resolves longer-term changes in oceanographic conditions and sediment supply to the deep sea.

The investigated proxies include elemental and isotopic carbon and nitrogen ratios (C_{org}/N_{total}, $\delta^{13}C_{org}$, $\delta^{15}N$), magnetic susceptibility, $CaCO_3$ content and mass accumulation rates. The deep sea record covers the past 17kyrs. It shows high sedimentation rates and a high portion of terrigenous sediment until 13kyrs BP. This is explained by a narrow shelf due to the low sea level. After the sea level rise around 8kyrs BP shelf sedimentation becomes continuous and the upwelling system shifts from the shelf edge towards the coast, which is reflected in sedimentary $\delta^{15}N$.

Holocene productivity is relatively low and organic matter provenance proxies indicate a maximum marine signature between 8 and 6kyrs BP. Subsequently increasingly terrigenous contributions are assigned to the cease of the sea level rise, leading to the supply of terrigenous material to more distal locations on the shelf. Since ca. 6kyrs, sedimentary $\delta^{15}N$ values approach similar values in shelf and deep sea core, possibly indicating an intensification of upwelling.

An instant increase in terrigenous signature around 2.5kyrs BP is explained by a climatic change from a warm, dry period (Subboreal) to a wetter period (Subatlantic), leading to a stronger discharge of terrigenous organic and lithic material onto the shelf.

Thus, environmental conditions at the central Portuguese margin have been rather constant during the Holocene and are mainly influenced by sea level variations and subsequent changes in hydrographical and sedimentological conditions. Except for the extreme climatic changes during the Deglaciation and for the inferred shift from the Subboreal to the Subatlantic climatic period, no effect of climatic variations are evident from the shelf or deep sea records.

6.2 Introduction

A way to reconstruct past variations in environmental conditions in marine and continental realms on a high temporal resolution is the analysis of marine shelf sediments, which are typically characterised by high sedimentation rates and by the integration of continental and marine signals, particularly when obtained from close to a river mouth. This is the case on the central shelf of the western Portuguese margin, where the Tagus River feeds into the Atlantic Ocean and supplies large amounts of sediment onto the shelf. A considerable fraction of sediment is also delivered to the deep sea through the nearby Lisbon and Setubal Canyons (JOUANNEAU et al., 1998). Combining a sediment record from the shelf with a deep sea record allows the distinction between type, spatial extent and temporal dimension of environmental changes.

Important indicators for paleoenvironmental changes are variations in sediment and organic matter provenance as well as variations in oceanographic conditions, e.g. upwelling, which is an important process in the study area. The former, being related to terrigenous sediment input, river runoff and hence precipitation in the hinterland, can be reconstructed by interpreting sedimentary C_{org}/N_{total} and $\delta^{13}C_{org}$ values (SACKETT and THOMPSON, 1963; MIDDLEBURG and NIEUWENHUIZE, 1998). This assumes conservative mixing of two endmembers with characteristic C_{org}/N_{total} and $\delta^{13}C_{org}$ ranges, e.g. organic matter of terrigenous origin (C_{org}/N_{total} ≥10, $\delta^{13}C_{org}$ 25-28‰, e.g. SMITH and EPSTEIN, 1971; MIDDLEBURG and NIEUWENHUIZE, 1998) and organic matter of marine origin (C_{org}/N_{total} around 7, $\delta^{13}C_{org}$ 18-22‰, e.g. REDFIELD et al., 1963; FONTUGNE and DUPLESSY, 1981).

Variations in the marine nutrient budget, which is a function of nutrient supply e.g. by upwelling or riverine input and nutrient consumption by marine primary production, can be inferred from sedimentary $\delta^{15}N$ values (ALTABET and FRANCOIS, 1994; FREUDENTHAL et al., 2001). The nutrient supply in a eutrophic upwelling region is directly related to upwelling intensity, providing deep water NO_3^- with a $\delta^{15}N$ of 5 to 6‰ to the shelf (LIU and KAPLAN, 1989). Preferential uptake of isotopically light nutrients by organisms leads to a spatial and

temporal gradient in sedimentary $\delta^{15}N$. Assuming Rayleigh fractionation during NO_3^- uptake, a sedimentary $\delta^{15}N$ of 5-6‰ indicates complete nutrient consumption and hence N-limitation of the marine production. A light $\delta^{15}N$ of ≤5‰ indicates strong nutrient supply and the removal of old, isotopically heavy NO_3^-, e.g. by offshore directed surface currents or an interruption of the marine production by other limiting nutrients or environmental conditions. A heavy $\delta^{15}N$ of ≥6‰ can be caused by the influx of isotopically heavy nutrients, e.g. from an estuary (OWENS, 1985) or from distant upwelling centers (ALTABET and FRANCOIS, 1994).

In this study a sediment core from the Tagus prodelta on the shelf (water depth 80m) has been investigated and compared to a piston core from the Lisbon Canyon levee (water depth 4602m). Thus Holocene variations of organic matter provenance and nutrient budget are reconstructed on a temporal and spatial scale by analysing C_{org}, $CaCO_3$ contents and respective mass accumulation rates, sediment C_{org}/N_{total}, $\delta^{13}C_{org}$ and $\delta^{15}N$ values and magnetic susceptibility. The results are interpreted in terms of interactions between upwelling intensity, marine primary production and sediment provenance, including external factors, such as the postglacial sea level rise and climatic variations.

6.3 Regional Setting

On the central western Portuguese margin the Tagus River feeds into the Atlantic close to the city of Lisbon (ca. 38.5°N) (Fig. 6.1). The Tagus River is ca. 1000km long and drains an 80600km^2 large watershed in the central and western part of the Iberian Peninsula. Although the discharge occurs through a large mesotidal estuary, which acts as a sediment trap and leads to extensive mixing of riverine and marine water masses, terrigenous sediment can be traced in surface sediments on the shelf (ALT-EPPING et al., 2007).

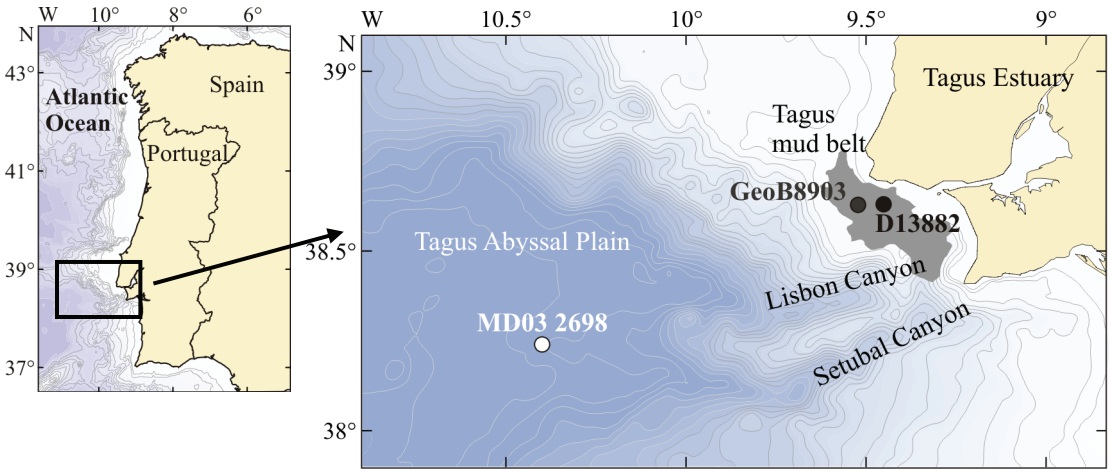

Fig. 6.1: Map of the investigated area and sampling locations. Additionally the location of core GeoB 8903, which is mentioned in the text, is shown.

The shelf off the Tagus River mouth is ca. 20-30km broad and southward bordered by the Lisbon and Setubal Canyons, which intersect the shelf and reach close to the coast (Fig. 6.1). The amount of material exported to the shelf through the Tagus estuary is between 0.4 and 1.0 x10^6t/yr (JOUANNEAU et al., 1998). A large fraction of river-discharged sediment is accommodated on the shelf in a ca. 560km^2 large mud patch in front of the river mouth; however, a considerable portion of sediment is transported through the Lisbon and Setubal Canyons to the Tagus Abyssal Plain. The pathway of continental sediments towards the canyons is detectable by geochemical properties of surface sediments from the river mouth towards the canyons (ALT-EPPING et al., 2007).

The hydrography and marine biological production is characterised by wind driven, seasonal upwelling between May and September, which results in a marine productivity of 60 to 90gC/m^{2}yr (FIÚZA, 1983; ABRANTES and MOITA, 1999). The upwelling is caused by the relocation of the Azores high-pressure system closer to the Iberian coast during summer (FIÚZA, 1983), leading to northwesterly winds, which drive the coastal upwelling. During most of the winter months the Azores High is located off the northwest African coast, resulting in southerly winds, which favour downwelling conditions. However, high marine productivity is also evident around January and February (DIAS et al., 2002a), which is triggered by the input of riverine nutrients. In front of the Tagus River mouth marine primary production is persistently high, which is shown by constantly high chlorophyll-a concentrations in SeaWifs satellite data (http://oceancolour.jrc.ec.europa.eu).

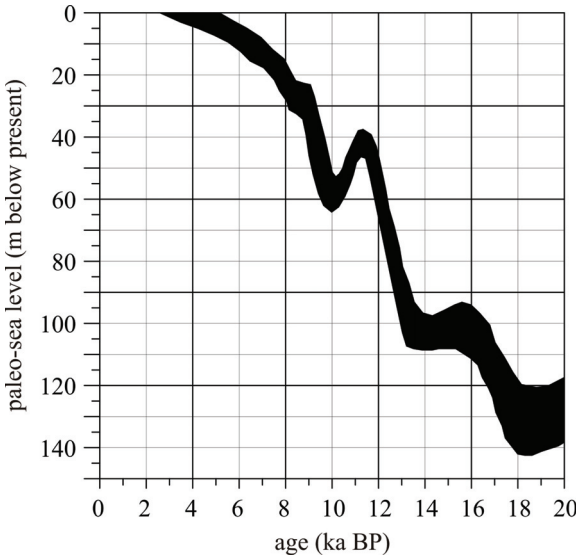

Fig. 6.2: Sea level curve for the Portuguese Margin since the Last Glacial Maximum, redrawn after DIAS et al. (2000). The width of the curve indicates the uncertainty with respect to timing and sea level.

Since the Last Glacial Maximum global sea level has risen by 140m along the Portuguese margin (DIAS et al., 2000). Especially between 11 and 13kyr BP a rapid sea level rise to 40m below present sea level led to the formation of estuaries and the entrapment of large amounts of sediment at the Portuguese Margin (DIAS et al., 2000). Around 10kyr a short regressive event led to a temporary sea level drop of 20m before between 10 and 8kyr a fast transgression flooded the paleo-shoreline, leading to a sea level rise by about 40m and to the formation of thick sediment beds at river mouths and estuaries. Between 5 and 2.5kyr the sea level reached the present level (DIAS et al., 2000) (Fig. 6.2).

6.4 Material and Methods

Core D13882 was obtained from the Tagus prodelta at 38.63°N and 9.45°W from a water depth of 80m (Fig. 6.1). It was sampled in intervals between 5 and 10cm down to a depth of 1370cm. The lowest section of core D13882 below 12m core depth was disturbed during coring and is thus omitted. Core MD03-2698 was obtained during an RV Marion Dufresne cruise in 2003 from the levee of the Lisbon Canyon at 38.24°N and 10.4°W from a water depth of 4 602m. This core was sampled in irregular intervals of 4 to 20cm down to a core depth of 866cm.

Measurements of elemental C and N contents were performed on discrete samples, following the procedure described by MÜLLER et al. (1994), using an Elementar Vario-EL3 element analyser. All samples were freeze-dried, ground and homogenized. 25mg of bulk sediment were filled into tin containers, folded and combusted to obtain total carbon (C_{total}) and nitrogen (N_{total}) content. Organic carbon (C_{org}) was measured on 25mg sample material, which was filled into silver containers, treated with 1-molar HCl to remove carbonate and dried at 60°C in an oven previous to combustion. Samples were not washed after treatment with HCl to prevent the loss of suspended material (SCHUBERT and NIELSEN, 2000). The analytical error is ca. 2%. Precision is ensured by continuous control measurements of a lab internal standard. The $CaCO_3$ content is calculated using the equation $CaCO_3 = 8.33*(C_{total}-C_{org})$.

The isotopic composition of organic carbon ($\delta^{13}C_{org}$) was measured on samples, which were decalcified following MÜLLER et al. (1994). The material was combusted to CO_2 in an HERAEUS elementar analyser, cleaned in a trapping box system and measured with a FINNIGAN DELTA E mass spectrometer against an internal standard gas, which was calibrated against NBS19. The error of measurements is ±0.1‰, based on long-term calibration curves. Isotopic values are given in standard notation with reference to PDB. The nitrogen isotope ratio ($\delta^{15}N$) was measured by combustion of bulk sediment in a CARLO-ERBA elementar analyser to N_2, which was then led into the FINNIGAN DELTA E mass spectrometer in a continuous flow mode, using He as carrier gas. Precision is ±0.2 to 0.3‰;

internal calibration was performed the same way as for $\delta^{13}C$. Isotopic values are given in standard notation against $\delta^{15}N_{air}$ (=0‰, MARIOTTI, 1983). The good agreement between the N_{total} content of $CaCO_3$ containing and $CaCO_3$ free samples legitimates the use of bulk sediment instead of decarbonized material, as the process of decarbonization has no apparent effect on $\delta^{15}N$ (LAVIK, 2001).

Magnetic susceptibility was measured in 1cm intervals with a GEOTEK Kappabridge.

Core MD03-2698 is radiocarbon dated on planktonic, multispecies foraminifera from eleven depth levels. The age model of core D13882 is based on eleven radiocarbon datings of shells, of which six yield reasonable results (Tab. 1, 2). All datings were done at the Leibniz Laboratory of the University Kiel, Germany. Radiocarbon dates are corrected for 400 years reservoir effect (ABRANTES et al., 2005) and calibrated with the software Calib 5.0.1 (STUIVER and REIMER, 1993) using the "intcal04" calibration curve.

6.5 Results

6.5.1 Core MD03-2698

The C_{org} content ranges from 0.46 to 1.03wt%, with highest values around 1% between 250 and 320cm depth and values increasing to 0.9wt% towards the core top (Fig. 6.3). C_{org}/N_{total} ratios vary around 8 between 900 and 250cm depth and decrease to around 6 between 250cm and core top (Fig. 6.3). The $CaCO_3$ content is around 20% until 400cm, increasing up to 30% between 400 and 300cm, before decreasing again to ca. 20% until 200cm. Above 200cm, the $CaCO_3$ content is slightly above 30%.

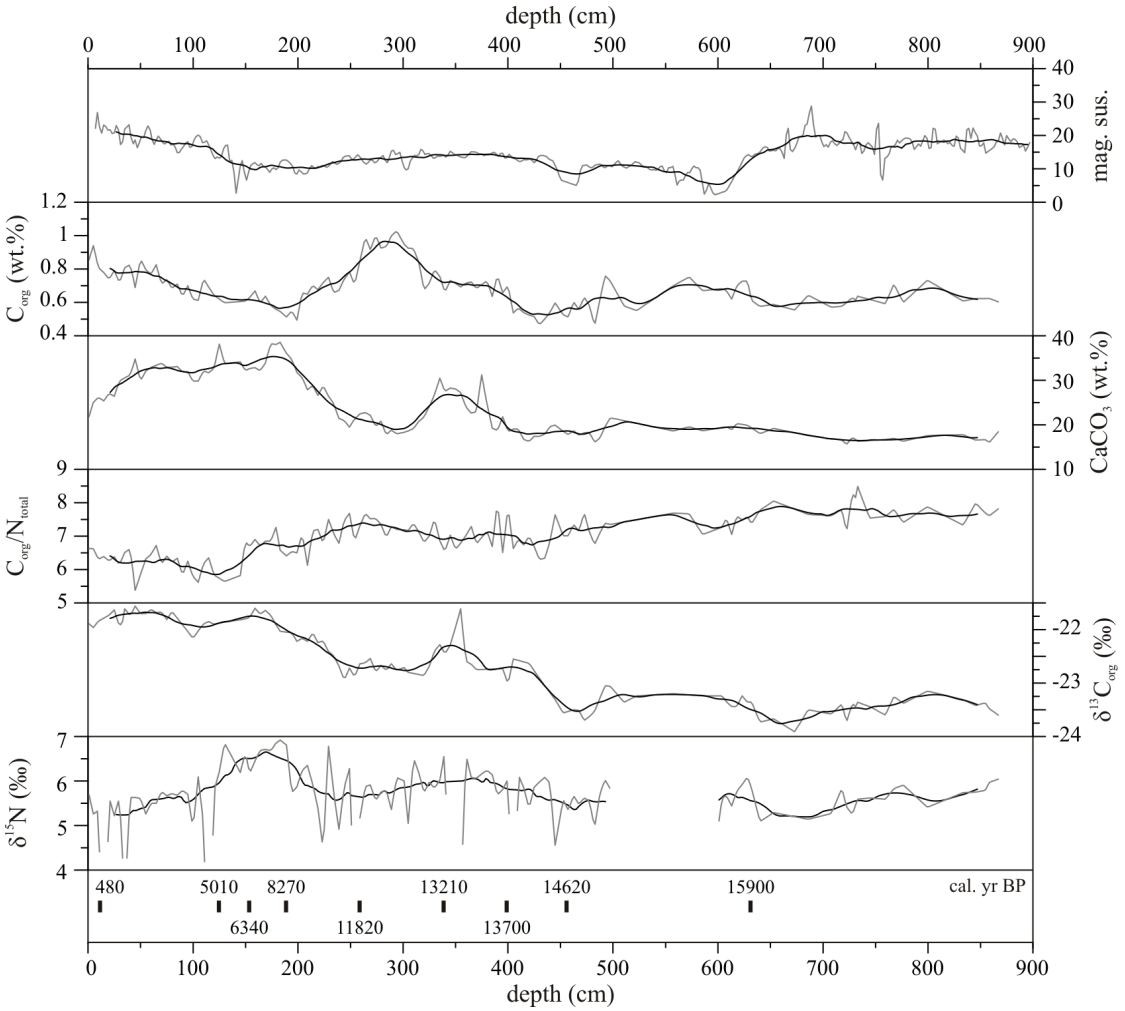

Fig. 6.3: Data versus depth of the deep sea core MD03-2698. Black lines show the 21-point running averages, bars in the bottom part mark the dating levels.

Stable organic carbon isotopes ($\delta^{13}C_{org}$) are between -23.9 and -21.6‰ (Fig. 6.3). Similar to $CaCO_3$ values, maxima of $\delta^{13}C_{org}$ values are found between 320 and 380cm and in the top 200cm. Sedimentary $\delta^{15}N$ values range in total between 3.5 and 6.9‰, with no measurements between 400 and 500cm. Slightly enhanced values of 6 to 7‰ are observed between 130 and 200cm (Fig. 6.3). No indications for early diagenetic alteration or effects of selective degradation of labile organic components are found in the C_{org}/N_{total}, $\delta^{13}C_{org}$ and $\delta^{15}N$ data.

Magnetic susceptibility (MS) is around $20*10^{-5}$ from 900 to 650cm and varies between 5 and $15*10^{-5}$ from 600 to 150cm. Between 150cm core depth and the core top, MS increases again to $20*10^{-5}$ (Fig. 6.3).

6.5.2 Core D13882

The C_{org} content of core D13882 varies around 0.7wt% from the core base (1400cm) to ca. 1050cm, before it decreases to ca. 0.5wt% until 800cm (Fig. 6.4). After a further decrease to ca. 0.3wt%, C_{org} content increases constantly to 1.3wt% between 600 and 350cm. Until the core top, C_{org} varies around between 1.2 and 1.6wt%. C_{org}/N_{total} ratios show values between 8 and 9 from the core base to 800cm, interrupted by a short interval of lower C_{org}/N_{total} ratios of below 7 between 1050cm and 1000cm (Fig. 6.4). Above 800cm, C_{org}/N_{total} values decrease to ca. 7.5, before they constantly increase to around 10.5 between 600 and 300cm, remaining constant around 10 until the core top (Fig. 6.4). The $CaCO_3$ content is between 20 and 30% from the core base to 700cm, showing a high variability. Lower values around 20% between 400 and 700cm are followed by a $CaCO_3$ content of around 10% from 400cm to the core top (Fig. 6.4). With ca. -24.6‰ is $\delta^{13}C_{org}$ very negative in the lowest 650cm, showing a high variability of 1‰. Above 750cm core depth, $\delta^{13}C_{org}$ values increase to ca. -22‰ at 650cm, before they decrease to ca. -24‰ at 400cm. From 400cm to the core top $\delta^{13}C_{org}$ remains relatively constant (Fig. 6.4). $\delta^{15}N$ varies between 5 and 6‰ through the entire record, with higher values between 650 and 750cm and in the top 100cm (Fig. 6.4). Selective degradation of isotopically light and labile organic components and a resulting biasing influence on C_{org}/N_{total}, $\delta^{13}C_{org}$ and $\delta^{15}N$ values, e.g. by simultaneously decreasing isotope ratios and increasing C_{org}/N_{total} ratios, is not observed. The magnetic susceptibility shows values around $10*10^{-5}$ from the core base to 1050cm, followed by values below $10*10^{-5}$ until ca. 450cm. Above 540cm, MS increases to around $20*10^{-5}$ between 400 and 100cm and further to $30*10^{-5}$ until 50cm. Very high values of up to $80*10^{-5}$ are measured in the top 30cm (Fig. 6.4).

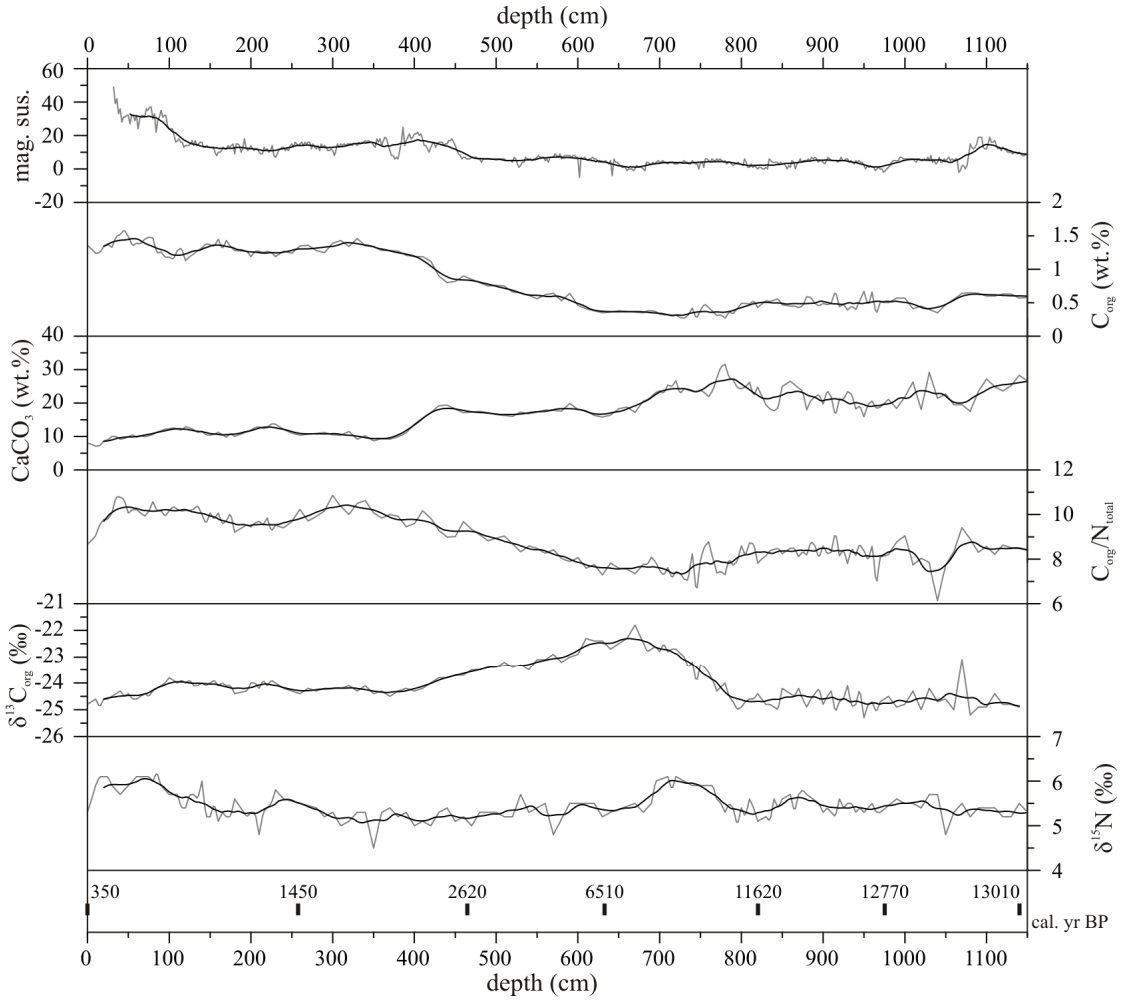

Fig. 6.4: Data versus depth of the shelf core D13882. Black lines show the 21-point running averages, bars in the bottom part mark the dating levels.

6.5.3 Age Models and Mass Accumulation Rates

All ages, obtained by AMS radiocarbon dating, are given in calibrated years before AD1950 (Tab. 6.1). Calculated sedimentation rates in core MD03-2698 are between 0.018cm/yr and 0.028cm/yr in the Holocene and reach a maximum value of 0.193cm/yr just after the LGM (Fig. 6.5).

To account for dilution effects on the C_{org} and $CaCO_3$ content, C_{org} and $CaCO_3$ mass accumulation rates (MAR) are calculated for core MD03-2698 by multiplying C_{org} and $CaCO_3$ wt% with sedimentation rate, acquired from linear interpolation between the calibrated datings, multiplied with GRAPE (Gamma-Ray Attenuation Porosity Evaluator) bulk density, acquired by shipboard measurements. As GRAPE density is influenced by sediment water content, absolute MAR values should be considered with care. C_{org} and $CaCO_3$ MAR show

very high values until 14.7kyr, followed by a period of lower MAR until 13.7kyr (Fig. 6.6). Between 13.7 and 13.2kyr MAR are again very high, decreasing after 13.2kyr and eventually reaching low values at 11.8kyr, which persist on that low level throughout the Holocene.

Table 6.1: Age model of core MD03-2698

Depth (cm)	Age (yrs BP)	half error (yrs)	probability	sigma
13	480	22	0.86	1
126	5008	48	0.7	1
155	6344	61	1	2
190	8260	84	1	2
260	11822	220	0.97	2
340	13207	98	1	2
400	13662	180	1	2
457	14592	359	1	2
632	15938	404	1	2
1185	18779	61	1	1
1295	19670	207	1	2

The correlation of the younger section of core D13882 (less than 3kyrs) with a nearby shelf record (GeoB 8903, ALT-EPPING et al., submitted) indicates, that the top part of core D13882, corresponding to ca. 350yrs, is missing. High sedimentation rates of 0.7cm/yr in the lowest part of the record (1140cm, 13kyrs) are followed by a decrease to 0.13cm/yr between 975cm (12.7kyrs) and 820cm (11.6kyrs). Between 820cm and 464cm (2.6kyrs), sedimentation rates decrease further to around 0.04cm/yr. Above 464cm sedimentation rates increase again to 0.18cm/yr until 257cm (1.5kyr) and further to 0.23cm/yr to the core top (Tab. 6.2). C_{org} and $CaCO_3$ mass accumulation rates are calculated by estimating an average bulk density of 1.5g/cm^3, which is based on the average density of a nearby gravity core (GeoB 8903, ALT-EPPING et al., submitted). The resulting MAR show very high values previous to 12.9kyrs BP (0.4-0.7gC/m^{2}yr; 20-30g$CaCO_3$/m^{2}yr), before they decrease to lower values around 0.1gC/m^{2}yr and 4g$CaCO_3$/m^{2}yr until 11.6kyrs BP and further to between 0.02-0.05gC/m^{2}yr and around 1.2g$CaCO_3$/m^{2}yr until ca. 2.6kyr BP. During the past 2.5kyrs, C_{org} MAR increase from 0.2 to around 0.5gC/m^{2}yr, whereas $CaCO_3$ MAR increase less strongly to 3-5g$CaCO_3$/m^{2}yr (Fig. 6.6).

Table 6.2: Age model of core D13882

Depth (cm)	Age (yrs BP)	half error (yrs)	probability	sigma
257	1446	92	1	2
464	2616	128	1	2
632	6505	63	0.89	1
820	11618	224	0.81	1
975	12773	45	1	1
1140	13012	67	1	1

6.6 Discussion

6.6.1 Provenance

Slightly decreased $\delta^{13}C_{org}$ ratios as well as high MS in core MD03-2698 indicate a slightly higher input of terrigenous organic and lithic material before ca. 16kyr BP (Fig. 6.5, solid lines). During the Deglaciation and the Holocene, variations in C_{org}/N_{total} and $\delta^{13}C_{org}$ are minor, indicating a constant fraction of terrigenous organic material. MS shows a strong decrease around 15.5kyrs BP and a slow but constant recovery to glacial values from ca. 6kyr to present.

The shelf sediment record of core D13882 begins around 13kyr with strong fluctuations in each dataset, probably indicating the onset of continuous sedimentation o the shelf due to the rising sea level. Slightly higher C_{org}/N_{total} ratios compared to core MD03-2698 indicate a higher terrigenous organic matter fraction until 11kyrs. This is basically supported by very negative $\delta^{13}C_{org}$ values (Fig. 6.5, dashed lines), which indicate an almost purely terrigenous organic matter fraction in the shelf sediment. However, the $\delta^{13}C_{org}$ values may be biased towards lower values by the effect of cooler temperatures (e.g. FONTUGNE and DUPLESSY, 1981). Assuming a North Atlantic SST difference of 5° between the Younger Dryas and the Holocene (PFLAUMANN et al., 2003), this would account for 1.5‰ lighter $\delta^{13}C_{org}$ (FONTUGNE and DUPLESSY, 1981) during the Younger Dryas. Hence, the low $\delta^{13}C_{org}$ values may lead to an overestimation of terrigenous input during cold periods, particularly, when seen in a context with C_{org}/N_{total} ratios, which indicate only small amounts of terrigenous organic matter. Furthermore, MS in the shelf core is lower than in the deep-sea sediments, suggesting a lower terrigenous lithic fraction in the sediment. An explanation for the low MS in the shelf sediments may be the association of MS-carrying particles to a very fine grain size spectrum, whereas organic matter is related to a coarser grain-size. This effect, which has been shown in a close-by sediment record from the Tagus prodelta (ALT-EPPING et al.,

submitted; see Chapter 5), would result in a farther transport of the MS signal across the shelf into the deep sea and to a subsequently higher MS in the deep-sea sediments.

Between ca. 11 and 8kyrs BP the $\delta^{13}C_{org}$ values decrease strongly to purely marine values, whereas C_{org}/N_{total} and MS remain relatively constant. As a purely marine organic matter source would also decrease C_{org}/N_{total}, this decrease in $\delta^{13}C_{org}$ is mainly assigned to the postglacial SST increase (e.g. FONTUGNE and DUPLESSY, 1981). A second option is a reduced export of terrigenous material to the shelf by trapping of terrigenous sediments in accommodation space in the hinterland, which has been created by the postglacial sea level rise. After a period of constant values until 6kyrs BP, increasing C_{org}/N_{total} and MS and decreasing $\delta^{13}C_{org}$ values indicate an increasing terrigenous sediment (organic and lithic) fraction (Fig. 6.5). This also coincides with a slow but constant increase in MS in the deep core MD03-2698 as well as with an increase in sedimentation rate. A possible explanation for this increase in terrigenous supply is the slowdown of the postglacial sea level rise (DIAS et al., 2000), which results in the filling of the sediment accommodation space, which was generated by the sea level rise. Subsequently, more terrigenous material will be delivered onto the shelf and into the deep sea.

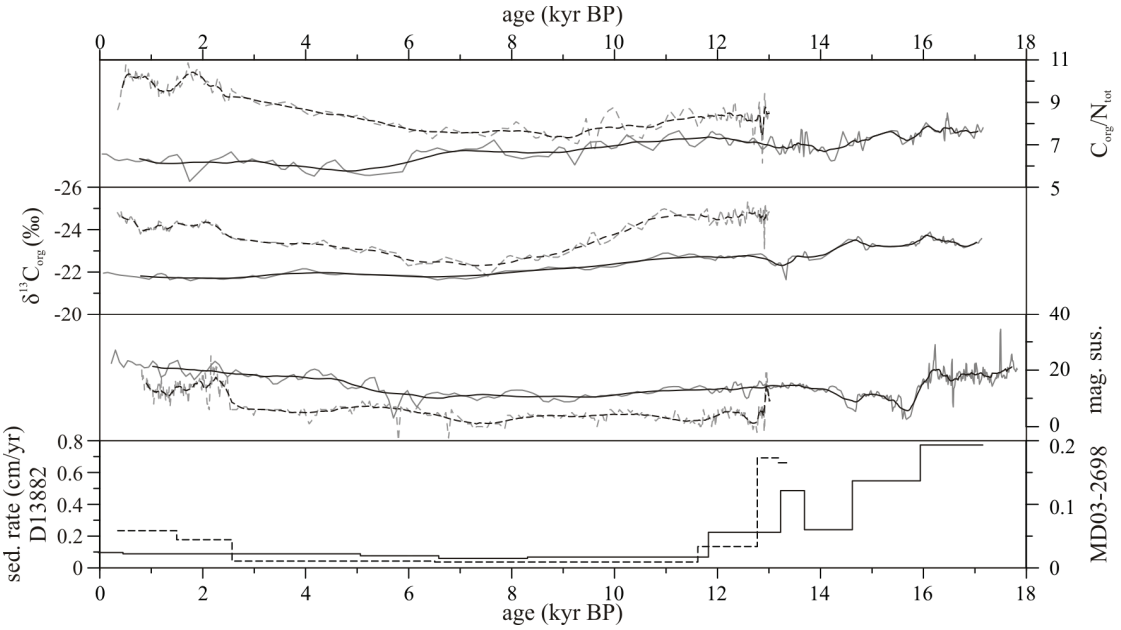

Fig. 6.5: Provenance proxies (C_{org}/N_{total}, $\delta^{13}C_{org}$, MS) and sedimentation rates of core MD03-2698 (solid lines) and core D13882 (dashed lines). Grey lines indicate raw data; black lines show a 21-point running average.

The increase in the terrigenous source signature in C_{org}/N_{total}, $\delta^{13}C_{org}$ and MS reaches its maximum level at ca. 2.5kyr BP, remaining constant on this high level until present (Fig. 6.5). The high level of terrigenous input may be an effect of increased riverine sediment supply, related to a change in climatic conditions from dry to wetter conditions. This may be

e.g. the change from the warm, dry Subboreal to the cold, wet Subatlantic climate period, which occurred around 2kyr BP (GIL GARCÍA et al., 2002; GARCÍA-AMORENA et al., 2007).

6.6.2 Nutrient Budget and Marine Productivity

Sedimentary $\delta^{15}N$ values in core MD03-2698 vary between 5 and 6‰ between 17 and 13kyr BP (Fig. 6.6, solid lines). This is within the range of the NO_3^- source (deep water $\delta^{15}NO_3^-$ = 5-6‰, LIU and KAPLAN, 1989), indicating a balanced NO_3^- budget, i.e. NO_3^- consumption equals NO_3^- supply, assuming closed system Rayeigh fractionation. Around 13.5kyr, a period of increased $CaCO_3$ content and higher $CaCO_3$ MARs is observed, indicating a higher marine, calcareous input or a better carbonate preservation at that time.

The shelf record begins around 13kyrs BP and shows only minor variations of $\delta^{15}N$, $CaCO_3$ and C_{org} values throughout the Deglaciation and the Holocene until 6kyrs BP. Core MD03-2698 however shows an increasing $CaCO_3$ content, which doubles from 12.5kyrs to 8kyrs BP, remaining on that high level until present. This increase in accompanied by a synchronous decrease in C_{org} and is therefore probably not a result of an increase in marine productivity, but rather the result of improving carbonate preservation until 8kyrs BP, which leads to relative, compositional changes in the marine sediment fraction.

Although still in the range of marine $\delta^{15}NO_3^-$ and hence not indicative of changes in marine nutrient budget, $\delta^{15}N$ values show a slight increase in both cores from 11 to 9kyrs BP (Fig. 6.6). Around 9kyrs BP, the course of the $\delta^{15}N$ records in both cores separates, showing a decrease to lower values in the shelf record and a continuing increase in the deep sea sediments until around 7‰ between 8kyrs and 5kyrs BP.

This separation and the resulting offset between $\delta^{15}N$ of shelf sediments and deep sea sediments of more than 1‰ is interpreted as an effect of the relocation of the upwelling centre from the shelf break onto the shelf due to the rising sea level (Dias et al., 2000, Fig. 6.2). A result of this reorganisation is the advection of depleted and isotopically light NO_3^- to the shelf edge, which is eventually reflected in the sediments by heavier $\delta^{15}N$.

After 5.5kyr, $\delta^{15}N$ values in the deep core MD03-2698 decrease to 5-6‰, similar to $\delta^{15}N$ in the shelf sediments (Fig. 6.6). As C_{org} and $CaCO_3$ MAR and content remain constant, the decrease in $\delta^{15}N$ in the deep core MD03-2698 possibly reflects a change in NO_3^- source, e.g. caused by a shift in the upwelling pattern.

Around 2.5kyrs BP core D13882 shows a strong increase in C_{org} content, which coincides with a decline in $CaCO_3$. This supports the reconstruction of an increased supply of terrigenous organic and lithic material at that time (see previous paragraph), resulting in a higher organic carbon supply, which is of mainly terrigenous origin and which dilutes the $CaCO_3$ in the shelf sediments.

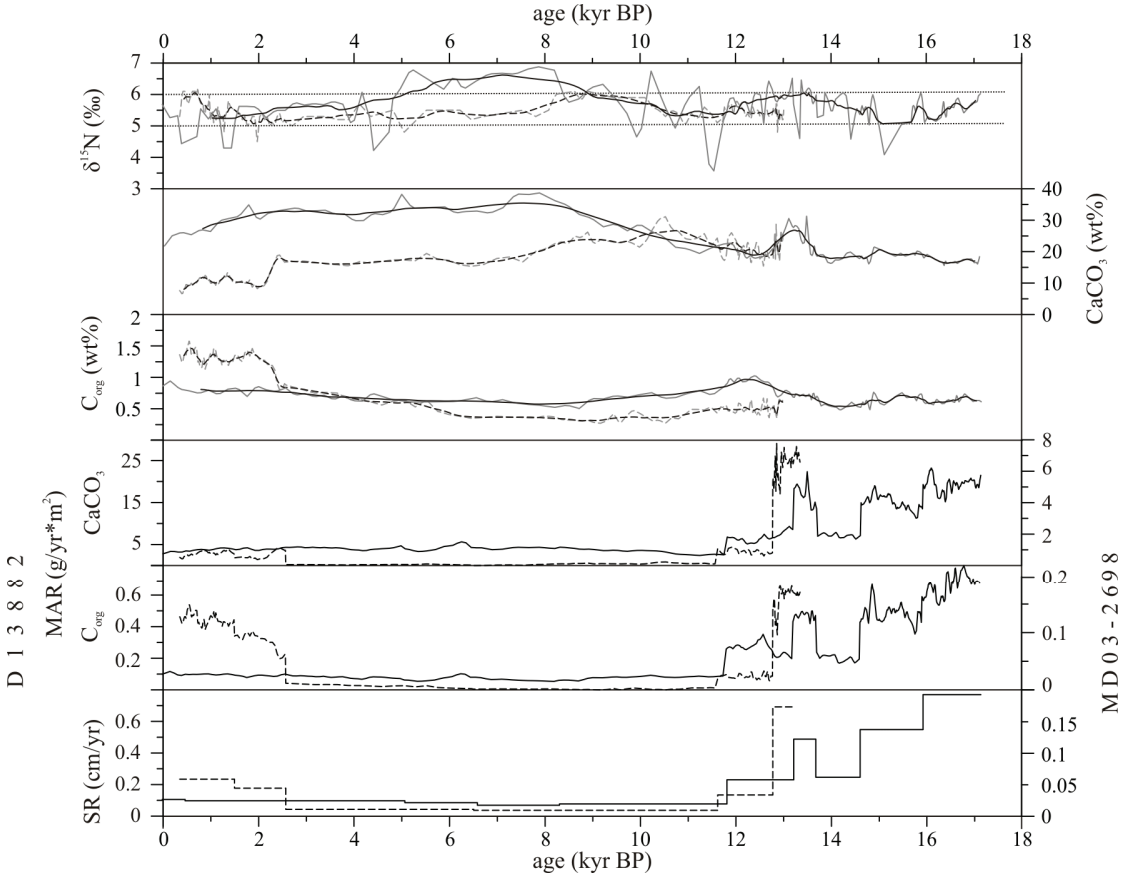

Fig. 6.6: Sedimentary $\delta^{15}N$ values, C_{org} and $CaCO_3$ content, respective MARs and sedimentation rates of cores MD03-2698 (solid lines) and D13882 (dashed lines). $\delta^{15}N$ is interpreted as proxy for nutrient budget, $CaCO_3$ content, C_{org} and MARs are interpreted to reflect marine productivity, the latter two are also used as indicators for terrigenous input, particularly during the last 2.5kyrs. Grey lines show raw data, black lines a 21-point running average.

6.7 Environmental Implications

Generally, variations in organic matter provenance, nutrient budget and marine productivity during the Holocene are minor. Main influences on the sediment records from the deep sea as well as from the shelf arise from variations in sea level and subsequent changes in hydrographic and sedimentological conditions. The low, glacial sea level results in a higher terrigenous organic matter supply to the deep sea, whereas on the shelf, no continuous sedimentation is evident until ca. 13kyrs BP. During the Deglaciation and the increase of sea surface temperatures, the $\delta^{13}C_{org}$ values increase over-proportionally strong, compared to C_{org}/N_{total} ratios. This is interpreted as a temperature effect on $\delta^{13}C_{org}$ values, according to e.g. FONTUGNE and DUPLESSY (1981).

The ongoing increase in sea level during the first part of the Holocene becomes evident in the hydrographic setting, as the upwelling centre is shifted from the shelf edge onto

the shelf. This is evidenced by relatively heavy $\delta^{15}N$ values in the deep sediments, compared to shelf sediments, due to the offshore advection and assimilation of isotopically heavy and thus depleted NO_3^-. The convergence of both $\delta^{15}N$ records between 5 and 4kyrs BP is interpreted to reflect a change in the upwelling pattern, e.g. by a supply of fresh NO_3^- to the shelf edge.

Simultaneously, the input of terrigenous organic matter and bulk sedimentation rates increase in the shelf record since 6kyrs BP. The decreasing velocity of the sea level rise may result in a filling of the postglacial created sediment accommodation space and the more efficient delivery of terrigenous sediments into the shelf. Around 2.5kyrs BP this increase in terrigenous organic matter fraction coincides with an instant increase in MS, which is interpreted to reflect an increase in lithic, terrigenous material supply. This general increase in terrigenous sediment (organic and lithic) remains on a constant, high plateau until present and is explained by a climatic shift from a drier to a wetter climate (e.g. from the Subboreal to the Subatlantic).

6.8 Acknowledgements

This study is part of the SEDPORT project (Sedimentation Processes on the Portuguese Margin: The Role of Continental Climate, Ocean Circulation, Sea Level, and Neotectonics) and funded by the German Science Foundation (DFG) as part of the EUROMARGINS/ EUROCORES program. We thank F. Abrantes, I.M. Gil, E. Salgueiro for thorough, valuable discussions, Monika Segl, Birgit Meyer-Schack, Hella Buschhoff and the crew of RV POSEIDON during leg 304 and RV Marion Dufresne during leg PICABIA for technical support.

6.9 References

Abrantes, F., M.T. Moita (1999): Water column and recent sediment data on diatoms and coccolithophorids, off Portugal, confirm sediment record of upwelling events. Oceanologica Acta 22(3): 319-336.

Abrantes, F., S. Lebreiro, T. Rodrigues, I. Gil, H. Bartels-Jónsdóttir, P. Oliveira, C. Kissel, J.O. Grimalt (2005): Shallow-marine sediment cores record climate variability and earthquake activity off Lisbon (Portugal) for the last 2000 years. Quaternary Science Reviews 24: 2477–2494.

Altabet, M.A., Francois, R. (1994): Sedimentary nitrogen isotopic ratio as a recorder for surface ocean nitrate utilization. Global Biogeochemical Cycles 8(1): 103-116.

Balsam, W. (1981): Late Quaternary Sedimentation in the Western North Atlantic: Stratigraphy and Paleoceanography. Palaeogeography Palaeoclimatology Palaeoecology 35: 215-240.

Dias, J.M.A., T. Boski, A. Rodrigues, F. Magalhaes (2000): Coast line evolution in Portugal since the Last Glacial Maximum until present – a synthesis. Marine Geology 170: 177-186.

Dias, J.M.A., J.M. Jouanneau, R. Gonzalez, M.F. Araujo, T. Drago, C. Garcia, A. Oliveira, A. Rodrigues, J. Vitorino, O. Weber (2002): Present day sedimentary processes on the northern Iberian shelf. Progress in Oceanography 52: 249-259.

Fiúza, A.F.G. (1983): Upwelling patterns off Portugal. In: Suess, E., J. Thiede (eds.): Coastal Upwelling: Its Sediment Record: 85-98. Plenum, New York.

Fontugne, M.R., J.C. Duplessy (1981): Organic carbon isotopic fractionation by marine phytoplankton in the temperature range -1 to 31°C. Oceanologica Acta 4(1): 85-90.

Freudenthal, T., S. Neuer, H. Meggers, R. Davenport, G. Wefer (2001): Influence of lateral particle advection and organic matter degradation on sediment accumulation and stable nitrogen isotope ratios along a productivity gradient in the Canary Islands region. Marine Geology 177(1-2): 93-109.

García-Amorena, I., F. Gómez Manzaneque, J.M. Rubiales, H.M. Granja, G. Soares de Carvalho, C. Morla (2007): The Late Quaternary coastal forests of western Iberia: A study of their macroremains. Palaeogeography, Palaeoclimatology, Palaeoecology 254(3-4): 448-461.

Gil García, M.J., M. Dorado Valiño, A. Valdeolmillos Rodríguez, M.B. Ruiz Zapata (2002): Late-glacial and Holocene palaeoclimatic record from Sierra de Cebollera (northern Iberian Range, Spain). Quaternary International 93-94: 13-18.

Hall, I.R., G.G. Bianchi, J.R. Evans (2004): Centennial to millennial scale Holocene climate-deep water linkage in the North Atlantic. Quaternary Science Reviews 23: 1529-1536.

Jouanneau J.M., C. Garcia, A. Oliveira, A. Rodrigues, J.A. Dias, O. Weber (1998): Dispersal and deposition of suspended sediment on the shelf off the Tagus and Sado estuaries, S.W. Portugal. Progress in Oceanography 42: 233–257.

Lavik, G. (2001): Nitrogen Isotopes of sinking matter and sediments in the South Atlantic. Ph.D. Thesis, Fachbereich Geowissenschaften, Bremen: 140 pages

Liu, K.-K., I.R. Kaplan (1989): The eastern tropical Pacific as a source of ^{15}N-enriched nitrate in seawater off southern California. Limnology and Oceanography 34(5): 820-830.

Mariotti, A. (1983): Atmospheric nitrogen is a reliable standard for natural N-15 abundance measurements. Nature 303: 685-687.

Martins, V., J.M. Jouanneau, O. Weber, F. Rocha (2006): Tracing the late Holocene evolution of the NW Iberian upwelling system. Marine Micropaleontology 59(1): 35-55.

Middelburg, J. J., J. Nieuwenhuize (1998): Carbon and nitrogen stable isotopes in suspended matter and sediments from the Schelde estuary. Marine Chemistry 60(3-4): 217-225.

Müller, P. J. (1977): C/N ratios in Pacific deep-sea sediments: effect of inorganic ammonium and organic nitrogen compounds sorbed by clays. Geochimica et Cosmochimica Acta 41: 765-776.

Müller, P., R. Schneider, G. Ruhland (1994): Late Quaternary pCO_2 variations the Angola Current: Evidence from organic carbon $\delta^{13}C$ and alkenone temperatures. In: Zahn, R., T.F. Pedersen (eds.): Carbon Cycling in the Glacial Ocean: Constraints of the Ocean's Role in Global Change. NATO ASI Series, Vol. 1(17): 343–366. Springer.

Owens, N.J.P. (1985): Variations in the natural abundance of ^{15}N in estuarine suspended particulate matter: a specific indicator of biological processing. Estuarine, Coastal and Shelf Science 20: 505-510.

Pflaumann, U., M. Sarnthein, M. Chapman, L. de Abreu, B. Funnell, M. Hüls, T. Kiefer, M. Maslin, H. Schulz, J. Swallow, S. van Kreveld, M. Vautravers, E. Vogelsang, M. Weinelt (2003): Glacial North Atlantic: Sea-surface conditions reconstructed by GLAMAP 2000, Paleoceanography, 18(3), 1065, doi:10.1029/2002PA000774.

Redfield, A.C., B.H. Ketchum, F.A. Richards (1963): The influence of organisms on the composition of seawater. In: Hill, M.N. (Ed.): The Sea, Vol. 2, Wiley, New York: 26-79.

Sackett, W.M., R.R. Thompson (1963): Isotopic organic carbon comnposition of recent continental derived clastic sediments of the East Gulf Coast, Gulf of Mexico. American Association of Petroleum Geologists Bulletin 47: 525-532.

Schubert, C. J., B. Nielsen (2000): Effects of decarbonation treatments on $\delta^{13}C$ values in marine sediments. Marine Chemistry 72: 55-59.

Smith, B.N., S. Epstein (1971): Two categories of $^{13}C/^{12}C$ ratio for higher plants. Plant Physiology 47: 380-384.

Stuiver, M., P.J. Reimer (1993): Extended ^{14}C database and revised CALIB radiocarbon calibration program. Radiocarbon 35: 215-230.

7 Sedimentological record of tsunamis on shallow-shelf areas: The case of the AD1969 and AD1755 on the Portuguese Shelf off Lisbon

F. Abrantes[a] (corresponding author), U. Alt-Epping[b], S. Lebreiro[a], A. Voelker[a], R. Schneider[c]

Marine Geology 249 (2008)

[a] Department of Marine Geology, Instituto Nacional de Engenharia, Tecnologia e Inovação (INETI), Estrada da Portela, 2721-866 Alfragide, Portugal

[b] DFG-Research Center Ocean Margins, University of Bremen, PO Box 330440, 28334 Bremen, Germany

[c] Department of Geosciences, Christian-Albrecht University Kiel, Ludewig-Meyn-Str. 10, 24118 Kiel, Germany

7.1 Abstract

One of the objectives of the SEDPORT project (ESF Euromargins EUROCORES program) major objective was to investigate the depositional features on the shelf and upper slope of the Portuguese Margin - Tagus System, during the Holocene. To fulfill the objectives, two shallow box-cores and two sedimentary sequences were studied; PO287-26B and the spliced sequence of sites D13902, PO287-26G recovered on the Portuguese Continental Shelf SSW off the Tagus River mouth, and the box PO287-28B and gravity core GeoB 8903 collected towards the W of the river mouth.

Magnetic susceptibility, grain-size and XRF Fe data as well as ^{210}Pb and AMS ^{14}C dating of these sedimentary sequences have allowed the identification of a "instantaneous deposit" at about 20cm in the box-cores. Downcore we could establish: a hiatus corresponding to 355years of sedimentation at both sites; a 39cm "instantaneous deposit" of coarse material including carbonate broken shells on the SSW site; and a 1.5m "instantaneous deposit" of fine material on the W site. Both hiatus and instantaneous deposits are considered to be of tsunamigenic origin. The box-cores deposit has an estimated age of AD1969 and it is attributed to the AD1969 earthquake caused tsunami.

The hiatus and deposits found downcore are, due to the age limits encountered, believed to represent the AD1755 Lisbon major earthquake related tsunami. These data further indicate a sediment deposit similar in type and thickness on both SSW and W sites in AD1969,

while the AD1755 record indicates a higher energy backwash along the SSW and a preferential deposition of fine suspended matter towards the W.

7.2 Introduction

In recent years, much research on modern and palaeotsunami deposits, in particular the ones found on land, has been published. To reconstruct past and pre-historic tsunamis, including a determination of tsunami size, extent and recurrence interval, is the fundamental goal of such work whose final objective is to contribute directly to tsunami-mitigation and risk- assessment programs.

As shown by the December 2004 Indian Ocean tsunami and other historic tsunamis, erosion is widespread as well as deposition both at sea, shallow and abyssal basins, and inland along the world's coastal areas. "Fine to coarse debris, at times including boulders, peat masses, trees, uprooted vegetation, and man-made materials, can be moved by the force and run-up of a tsunami (TELLER et al., 2005)".

Whereas research focusing on geologic evidences of tsunami has shown a broad variety of tsunami depositional traces inland along the coastlines of the world, very little (VAN DER BERGH et al., 2003; PARESCHI et al., 2006) has been done on tsunami transport and deposition in the offshore zones or in shallow shelf areas as recognized by DAWSON and STEWART (2007). Such studies are particularly important in regions prone to earthquakes and with an historical record of tsunamis. Portugal and the Lisbon area have suffered from several historical earthquakes, of which AD1531, 1755, 1761 and 1969 were associated to tsunami events (NOAA National Geophysical Data Center; Portuguese/European GITEC database; BAPTISTA et al., 1988a).

On the basis of historical records, the most destructive tsunamis listed are the AD1531 as a local tsunami in Lisbon and AD1755 and AD1761 transatlantic events. Some authors consider the AD1531 event even more catastrophic for the city of Lisbon than the AD1755 one (MENDONÇA, 1758). However, the AD1755 earthquake, ranked 8.75 to 9.0 on the Richter scale, was one of the strongest in human history (CAMPOS, 1991; MADER, 2001), and the effects of the earthquake related tsunami, not only over the city of Lisbon but also over 52 other locations on both Atlantic coasts, turned it into the most catastrophic of the historical tsunamis.

The source of this historical event is uncertain, the AD1531 earthquake inferred source has been placed both offshore Iberian and north of Lisbon, up the Tagus estuary (JUSTO and SALWA, 1998). The similarities between the isoseismals for the AD1969 and AD1755 earthquakes have led to the construction of several models using as a source for the AD1755 the AD1969 instrumentally defined Gorringe Bank source. However, many other models have been suggested and except for a SSW located epicenter no consensus has yet been reached

(MACHADO, 1966; ZITELINI et al., 2001; TERRINHA et al., 2003). An epicenter SSW of Lisbon agrees with historical eyewitness reports that indicate a NNE/SSW direction for the tsunami water transport in/out the Tagus Estuary mouth area (Charles Davy in Tappan, 1914; SOUSA, 1928).

Without doubt, the tsunami triggered by these earthquakes and the AD1755 in particular, must have had a substantial height. The AD1761 tsunami influence has propagated all the way up to Ireland and to Barbados, and 2.4m is its estimated maximum water height (NOAA National Geophysical Data Center). The AD1969 event, maximum water height in the area of Lisbon has only reached a ±0.50m (BAPTISTA et al., 1992). As for the AD1755 event, historical accounts indicate maximum water heights of 30 m in the Algarve and 12-15m in Lisbon, heights confirmed by BAPTISTA (1988b). Off Oeiras, BAPTISTA et al. (2003) modeled a 5m wave, and WHELAN and KELLETAT (2005) defend that tsunami waves responsible for the transport of the boulders encountered at Trafalgar had to have run up heights in the order of 19m or more.

Historical sources mention tsunami waves and the inundation in Lisbon both in AD1531 and AD1755 (BAPTISTA et al., 2006), but inland field evidence such as the presence of large littoral debris and geomorphic features and their relationship, found at the Algarve coast (south Portugal – HINDSON et al., 1996; DAWSON et al., 1991; DAWSON et al., 1995; ANDRADE et al., 1992), northwest of Lisbon (SCHEFFERS and KELLETAT, 2005) and at Cabo de Trafalgar (southern Spanish Atlantic coast - WHELAN and KELLETAT, 2005) have been interpreted as tsunami deposits generated by the AD1755 event.

Major problems in studies of inland paleotsunamis are related to the positive identification of a tsunami deposit, due to their variable character, and the dating difficulties, two aspects that are possibly easier to deal with in marine sediments, where distinctive deposits may be left by such events, and the dating of marine carbonate microorganisms by AMS ^{14}C is possible. The Tagus upper shelf offers a natural laboratory to scrutinize in detail deposits associated with the Lisbon historical tsunamis.

In this paper, we revisit the published characteristics of the record found in a core located SSW of the Tagus River mouth and that has been attributed to the AD1755 tsunami (ABRANTES et al., 2005), and present new data from a core located on the W extreme of the shelf mud deposit often labeled as Tagus prodelta, as well as box-core record from both locations.

7.3 Materials and Methods

The material used in this study is a suite of 6 cores recovered from the upper shelf off the Tagus river mouth (Tab. 7.1, Fig. 7.1); however, we concentrate mostly on the two best-dated and studied sedimentary sequences. That is, a spliced sequence of cores D13902 and box and gravity cores PO287-26B, G positioned SSW of the Tagus River mouth, and cores GeoB 8903 and PO287-28B collected to the west, offshore of the river mouth (Tab. 7.1).

Tab. 7.1: List of cores used in this work. Numbers in bold refer to the best dated cores used as a basis in this paper.

Core name	Type	Latitude (°W)	Longitude (°N)	depth (m)	length (m)	ship	cruise
D13902	**Long Piston**	**38º 33.24'**	**9º 20.13'**	**90**	**6.00**	**Discovery**	**D249**
D13882	Long Piston	38º 38.07'	9º 27.25'	88	13.61	Discovery	D249
PO287-26G	**Gravity**	**38º 33.49'**	**9º 21.84'**	**97**	**3.05**	**Poseidon**	**PO287**
GeoB 8903	**Gravity**	**38° 37.86'**	**9° 30.84'**	**102**	**5.40**	**Poseidon**	**PO304**
MD99-2333	Calypso	38º 33.51'	9º 21.85'	91	3.47	M. DuFresne	IMAGES V
PO287-26B	**Box-core**	**38º 33.49'**	**9º 21.84'**	**96**	**0.52**	**Poseidon**	**PO287**
PO287-28B	**Box-core**	**38º 37.47'**	**9º 30.87'**	**105**	**0.52**	**Poseidon**	**PO287**

Magnetic susceptibility was measured on a multi-parameter logging system at the Southampton Oceanography Center for core D13902 and D13882, while all other cores were measured at the Bremen Core Repository. Iron (Fe) content as counts per second (cps) was determined, at 1cm intervals for all other cores by X-ray fluorescence core scanning for non-destructive semi-quantitative analysis of major elements (from K to Sr) developed at the Netherlands Institute for Sea Research (JANSEN et al., 1998) and was carried out at the Bremen Core Repository of the University of Bremen (Fig. 7.1).

For grain size determination, sediments were sliced at 1cm intervals and 5-8cc of sediment prepared through organic matter removal with basic H_2O_2 (130 vol.) and dispersed with sodium hexametaphosphate (0.033M), prior to being analyzed with a Coulter LS230 laser instrument. On gravity core GeoB 8903, analysis was done on bulk sediment collected every 1cm for the top 55cm and every 5cm below that, and run trough a Coulter LS200 after dispersion with sodium pyrophosphate. Mean grain-sizes were calculated with the software GRADISTAT (BLOTT and PYE, 2001) after the FOLK and WARD (1957) method.

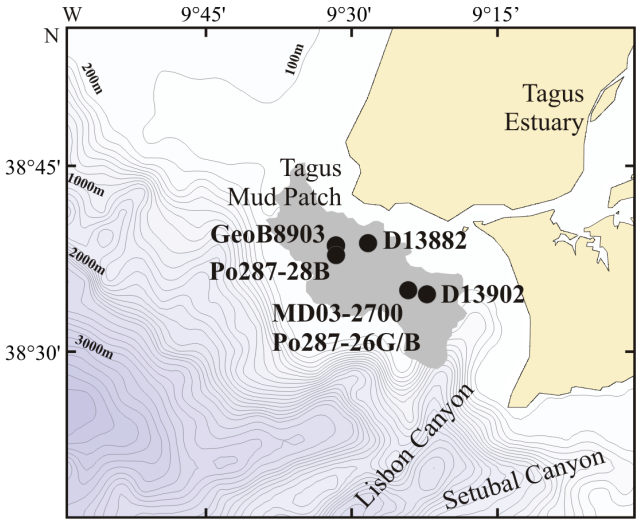

Fig. 7.1: Sites location on the inner shelf, offshore the Tagus River mouth on a bathymetric map. Sites D13902 and PO287-26 SSW of the river mouth and sites GeoB 8903 and PO287-28, west of the river mouth.

7.4 Chronology

The age models proposed for the box-cores are based on ^{210}Pb determinations done at NIOZ for 9 levels in both cores, and three deeper samples from core D13902 for base activity determinations, and considering a CF:CS model (A Constant Flux and Constant Sedimentation rate).

For the longer cores, age models were constructed on the basis of accelerator mass spectrometry (AMS) radiocarbon dating performed at 16 levels in core D13902, 3 levels in PO287-26G and 9 levels in core GeoB 8903 (Tab. 7.2). AMS ^{14}C ages are corrected for a marine reservoir effect of 400 years, as determined for the area (ABRANTES et al., 2005) and converted to calendar ages with the INTCAL04 data set (REIMER et al., 2004). Calibrated ages are presented in years Anno Domini (AD).

The definition of the spliced sequence age model (D13902 and PO287-26B, G) followed the line of reasoning presented by ABRANTES et al., (2005) although for the conversion of the conventional AMS ^{14}C ages into calendar ages was based on the new INTCAL04 data set. As presented by those authors, a splice of the above referred cores was constructed using the AD1896 age found at 51.5cm of box-core PO287-26B, assuming the top of the box-core to represent AD2001, in conjunction with a simple correlation of the MST data of the cores, which revealed that piston core D13902 failed to recover the uppermost 48cm of the seafloor at this location (Tab. 7.2).

Of the 16 AMS ^{14}C dates of core D13902, a sequence of 3 ages, between 95 to 76cm deviates considerably from the remaining 9 dates (Fig. 7.2). Those strange ages coincide with

an abnormally high peak in magnetic susceptibility (MS) and grain size (GS), and are assumed to represent older reworked material (Fig. 7.2).

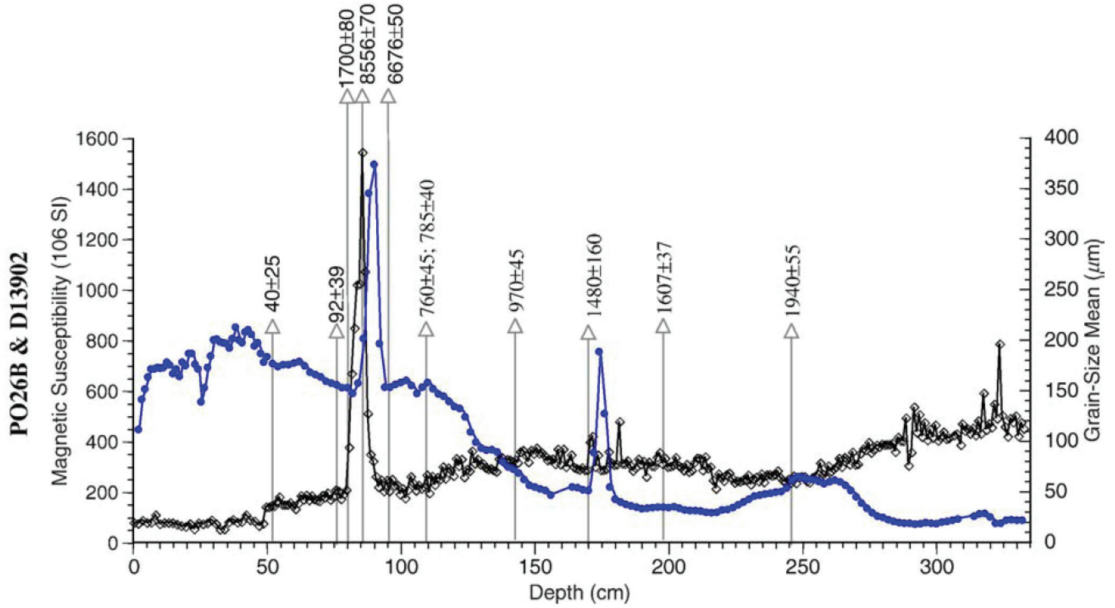

Fig. 7.2: Magnetic susceptibility, grain-size mean, and radiocarbon chronology along PO287-26B and D13902 composite depth. Ages as calendar yr BP; magnetic susceptibility (10^6 SI – full dots) and mean grain-size (μm – open diamonds).

In core GeoB 8903, 4 of the 9 AMS ^{14}C dates obtained between 198 and 65cm core depth, are not only very close to each other as there is even a slight inversion. Within 2 s these ages are not independent of each other implying a nearly instantaneous sedimentation of this interval (Fig. 7.3).

In order to avoid major changes in the sedimentation rate resulting from the traditional linear interpolation between two sequential ^{14}C dated levels in such a short time interval (2 000 years), it was chosen to interpolate linearly between all the accepted ages. The equations on the figure represent the age/depth relationship defined for each one of the best-fit lines (Fig. 7.3). From the observation of the age vs. depth plot (Fig. 7.4) a major change in sedimenttation rate is obvious for cores D13902 and PO287-26G below and above the interval with older ages, implying a hiatus or a major change in the sedimentation regime at this level. As for core GeoB 8903, besides the observation of the same age gap, also pointing to the occurrence of a hiatus, the existence of 143cm with similar and non-independent ages can only be explained by an almost instantaneous sedimentation (Fig. 7.4).

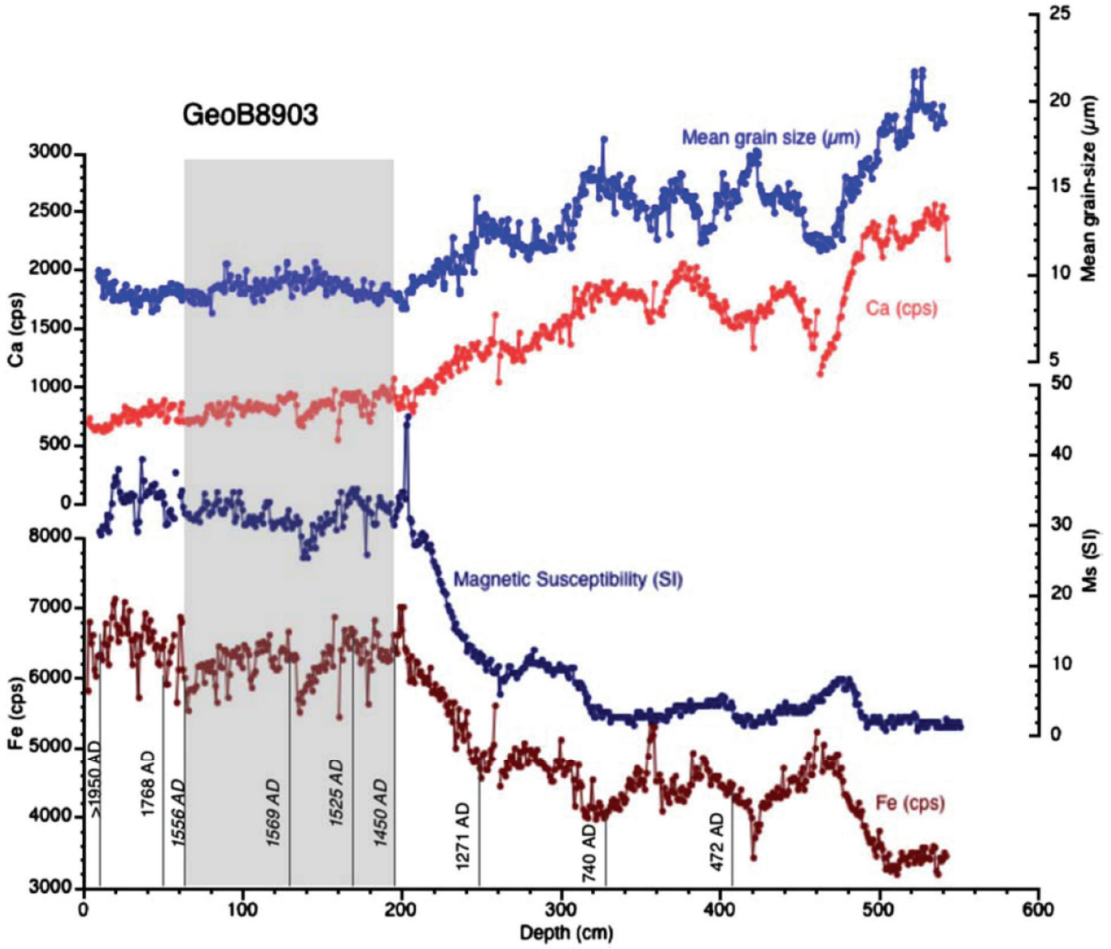

Fig. 7.3: Magnetic susceptibility, XRF-Fe, grain-size mean, XRF-Ca and radiocarbon chronology along GeoB 8903. Magnetic susceptibility (10^6 SI), mean grain-size (μm), Fe and Ca (cps).

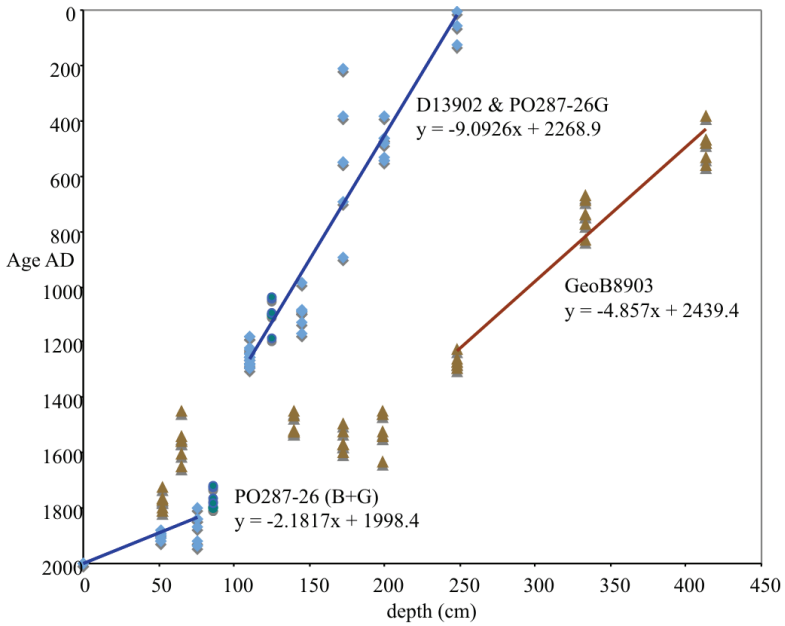

Fig. 7.4: Age versus depth model for box- and gravity-core PO287-26B, G and piston core D13902 and gravity core GeoB 8903 based on the AD ages calibrated from AMS ^{14}C ages as listed in Tab. 1 (upper, lower and most probable ages at both 1 and 2 s). Dark circles correspond to Box-core PO287-26 1B and piston core D13902; light circles represent the ages obtained along core PO287-26 3G, and triangles the age for gravity core GeoB 8903. Equations represent the age/depth relationship given by the best-fit line for each set of dates.

Tab. 7.2: Results of AMS dating. Ages were reservoir corrected by 400 yrs. Levels in *italic* correspond to ages not considered for the age model.

Sample Name and Depth	Sample Type	^{14}C Age BP	1 or 2 sigma	no. of ranges	cal. AD/BC ranges		relative probability
					lower	upper	
PO287-26B	Mollusk shell	40 ±25	1	4	1890	1909	0.71
32-33cm			2	5	1877	1917	0.60
D13902	Mollusk shell	92 ±39	1	5	1867	1918	0.41
27-28cm			2	5	1802	1938	0.69
D13902	*Mollusk shell*	*1700* ±80	1	1	*240*	*425*	1.00
31-32cm			2	2	*206*	*535*	0.93
D13902	*Mollusk shell*	*8555* ±70	1	2	*-7611*	*-7524*	0.97
37-38cm			2	1	*-7733*	*-7490*	1.00
D13902	*Mollusk shell*	*6675* ±50	1	1	*-5637*	*-5556*	1.00
46-47cm			2	2	*-5671*	*-5508*	0.99
D13902	Mollusk shell	760 ±45	1	1	1226	1279	1.00
62-63cm			2	2	1178	1297	1.00
D13902	Turritela	785 ±40	1	1	1221	1269	1.00
62-63cm			2	1	1178	1283	1.00
D13902	Mollusk shell	970 ±45	1	3	1081	1127	0.47
96-97cm			2	1	988	1167	1.00
D13902	Foraminifera	1480 ±160	1	2	386	692	0.97
124-125cm			2	2	214	895	1.00

D13902	Mollusk shell	1607 ±37	1	3	483	533	0.54
151-152cm			2	2	382	547	1.00
D13902	Mollusk shell	1940 ±55	1	1	4	125	1.00
199-200cm			2	1	-49	217	1.00
PO287-26G	Mollusk shell	*-345* ±25	*1*	*0*	modern	modern	
21-22cm			2	0			
PO287-26G	Mollusk shell	145 ±25	1	9	1726	1766	0.33
86-87cm			2	6	1718	1781	0.32
PO287-26G	Turritella	910 ±25	1	3	1045	1094	0.59
125-126cm			2	2	1035	1186	0.99
GeoB 8903	Foraminifera	> AD1950	1	0	modern	modern	
8-12cm			2	0			
GeoB 8903	Foraminifera	210 ±35	1	3	1764	1801	0.47
52-53cm			2	3	1727	1812	0.52
GeoB 8903	*Foraminifera*	335 ±55	1	3	1540	1603	0.49
65-70cm			2	1	1449	1650	1.00
GeoB 8903	*Foraminifera*	285 ±30	1	2	1523	1572	0.62
171-173cm			2	3	1494	1601	0.63
GeoB 8903	*Foraminifera*	360 ±25	1	3	1467	1521	0.62
139-141cm			2	2	1452	1527	0.52
GeoB 8903	*Foraminifera*	360 ±45	1	0	1523	1542	0.52
198-199cm			2	0	1636	1542	1.00
GeoB 8903	Foraminifera	735 ±30	1	1	1261	1285	1.00
248-249cm			2	1	1224	1293	1.00
GeoB 8903	Foraminifera	1260 ±35	1	1	687	776	1.00
333-334cm			2	2	668	829	0.94
GeoB 8903	Foraminifera	1600 ±40	1	2	482	533	0.56
413-414cm			2	1	383	560	1.00
MD99 2333	Mollusk shell	1845 ±45	1	2	233	169	1.00
240-241cm			2	2	257	169	0.98
MD99 2333	Mollusk shell	295 ±40	1	2	1591	1568	0.69
115.5-116.5cm			2	2	1664	1568	0.99

7.5 Results and Discussion

The studied material corresponds to two sedimentary sequences recovered off Lisbon, right at the mouth of the longest Iberian river, the Tagus River, at ≈ 100m water depth from the extremes of an organic-rich clayey silty deposit located on the inner shelf and that represents the area of preferential deposition of continental materials transported in suspension by the river (MONTEIRO and MOITA, 1971; GASPAR and MONTEIRO, 1977).

7.5.1 Last Century Record

The analysis of the total ^{210}Pb record of both box-cores reveals a minimum at about 20cm (Fig. 7.5). ^{210}Pb is widely used in the study of sedimentary environments on a temporal scale up to 150 years, and its total concentration profile along an undisturbed sediment sequence is characterized by an exponential decrease with depth. Deviations from the expected exponential profile can be due to bioturbation, when values are higher than expected, but when the observed values are lower than expected, as it is the case, they can't be attributed to bioturbation in situ, and are more likely due to the presence of older reworked material. However, no specific mark can be seen on either the core description or the MS and grain-size records for this level, which, on the basis of our age model corresponds to 1970 ± 4 (Fig. 7.5). The same trend in total ^{210}Pb has been described for a few sites collected in the SW Iberian Margin, between 2173 and 4900m water depth, and the ^{210}Pb age model for the shallower and higher resolution site (MC1), recovered from 36º56'N, 9º45'W, indicates an age of AD1971 ± 3 for this minimum in total ^{210}Pb (GARCIA-ORELLANA et al., 2006). Again, no specific sedimentological or geochemical mark has been found at this level in the MC1 core.

^{137}Cs is another radionuclide that can be used as a time stratigraphic marker, since its presence in the sediments is associated to the atmospheric nuclear tests and has its onset in the 1950's. ^{137}Cs determinations in MC1 reveal first appearance at a level that agrees with the ^{210}Pb age model prediction. That is, the minimum in total ^{210}Pb represents an otherwise unidentifiable turbidite, composed of material of the same type/origin with an age close to AD1970 ± 4. Considering the age model uncertainty, this turbidite can be attributed to the AD1969 earthquake related tsunami felt in the Lisbon area (NOAA National Geophysical Data Center; HEINRICH et al., 1994; GARCIA-ORELLANA et al., 2006). A tsunami that reached a maximum water height of about 50cm in Lisbon and that caused reworking of older material and the instantaneous deposition of a fine turbidite with a thickness of ≈ 8 and 5cm respectively at the SSW and W extremes of the clayey silty deposit off the Tagus River mouth.

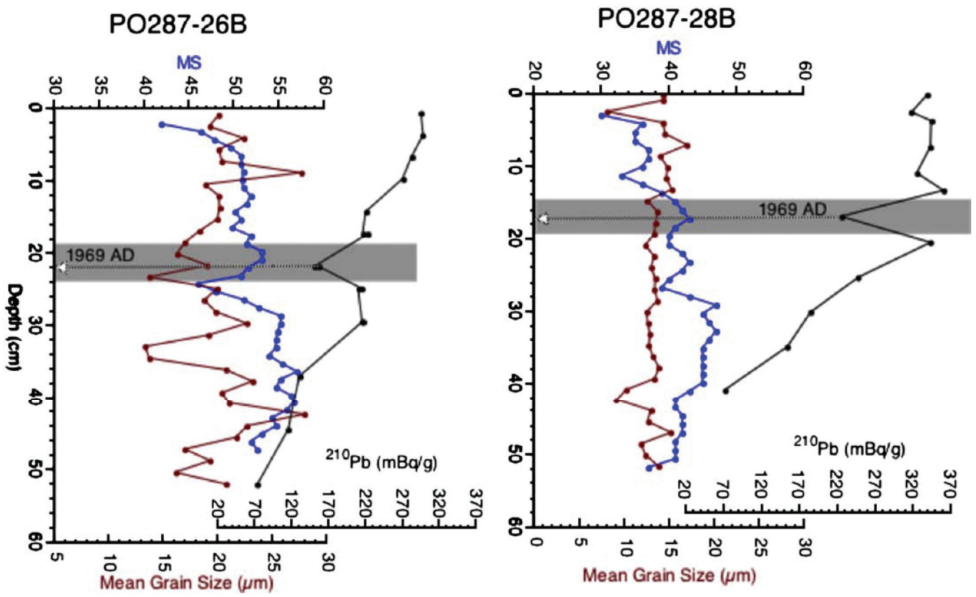

Fig. 7.5: Magnetic Susceptibility, mean grain size and total ^{210}Pb records along box-cores PO287-26B and 28B. Grey bands represent the thickness of the deposit of reworked sediment generated by the 1969 tsunami.

7.5.2 Historical (last 2 000 yr) Record

Along piston-core D13902, MS and mean grain size show extremely high magnetic susceptibility values centered at 90cm, followed by contemporary maxima in mean grain size (up to 386μm) at around 85cm (Fig. 7.2). As discussed in the chronology section and in ABRANTES et al. (2005), the coincidence of the 3 much older ages with the abnormal peaks in MS and mean grain size suggest deposition of older and coarser material by an event that has also caused important erosion of the existing sediments. Considering the age model described in section 3 (Tab. 7.1, Figs. 7.4, 7.6), this reworked deposit is imbedded between AD1253±45 and AD1838±39, a time that encompasses AD1531, 1755, and 1761, the dates of the major earthquakes and tsunamis felt in Lisbon (AD1531) and the Iberian Peninsula (AD1755, 1761) during historical times. Considering the ages below and above the "abnormal deposit" a loss by erosion of 355years worth of sediment and the instantaneous deposition of the 49cm of reworked material is estimated (Fig. 7.6).

Site GeoB 8903 magnetic susceptibility record (Fig. 7.3) shows a hint of a rapid increase at about 200cm, immediately followed by quite homogeneous values upward, and, a XRF Fe content that mimics the MS record. As for mean grain size and XRF Ca, their records are like a mirror image of the MS or Fe records, indicating that Ca is mainly in coarser particles, while Fe is in the finer sediment fractions. Furthermore, all records show quite homogeneous sediments between 198 and 65cm, the depth interval in which the AMS ^{14}C ages get undifferentiated at 2 s (Figs. 7.4, 7.6). A 143cm sedimentary body that apart from the

strange ages does not contain any of the characteristics anticipated for a turbidite of tsunami provenance (DAWSON and STEWART, 2007).

On shallow shelf regions strong tsunami events are expected to cause important erosion from the depth at which the wave(s) start feeling the seabed, resuspending and transporting sand and other fine materials more than 1km inland or even single boulders or boulder assemblages several meters above sea level and 100–400m inland as defended by SCHEFFERS and KELLETAT (2003; and literature cited within). As to the backflow, Dawson (1994) and NAMAYAMA et al. (2000), consider that although its carrying capacity is unknown, they are certainly erosive enough to rework the onshore deposits, which, becoming part of the outflow, will in turn lead to an increase of the rip currents erosional capacity.

Concerning the deposition of the eroded material, LE ROUX and VARGA (2005) picture the sediment seaward transport as gravity flows increasing in sediment concentration in near shore channels, while COLEMAN (1968), proposes the deposition of poorly sorted sediments close to the shore due to the outflow's rapid loss of energy. But, he also predicts the possibility of the bulk of deposition in the deeper offshore water beyond the shelf.

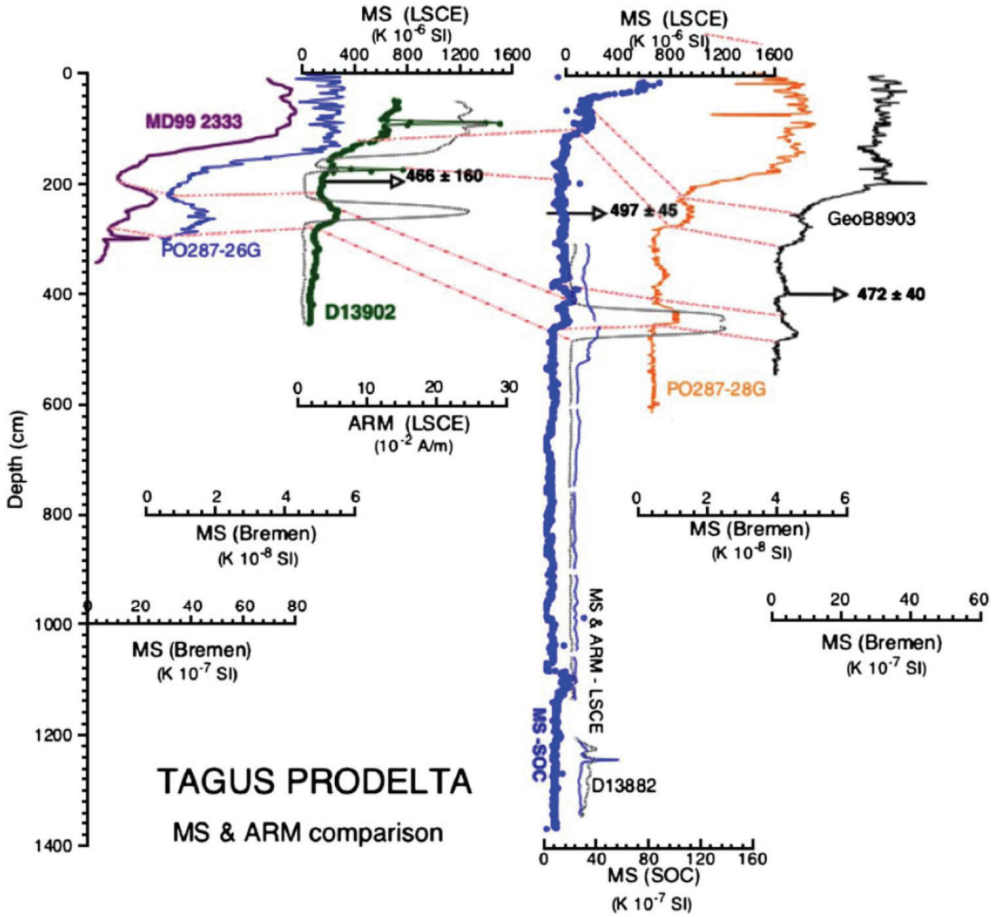

Fig. 7.6: Magnetic susceptibility and ARM comparison of the cores collected on the Tagus Prodelta (Tab. 1). (Centers where measurements were done: LSCE - Laboratoire des Sciences du Climat et de l'Environnement; SOC – Southampton Oceanographic Center; Bremen – University of Bremen).

Spatial comprehensive studies of shallow marine tsunami deposits are scarce, however, data from a shallow marine embayment NW of Java, that suffered a tsunami caused by the Krakatau eruption, revealed major variability both in the composition and thickness of the tsunamite with lack of a record on the north open sea facing part of the bay (VAN DER BERGH et al., 2003).

Off the Tagus River mouth, the correlation of the MS for the existing sites recovered from the shelf clayey silty deposit (Fig. 7.7), reveals a general increase in magnetic susceptibility ≈ AD1200 at all sites (Figs. 7.2, 7.3, 7.7), but neither the sites located to the west of the Tagus mouth (D13882, PO287-28 and GeoB 8903), nor SSW site PO287-26, located to the west of site D13902, show the strong magnetic susceptibility peak found in the easternmost core (D13902) (Fig. 7.7).

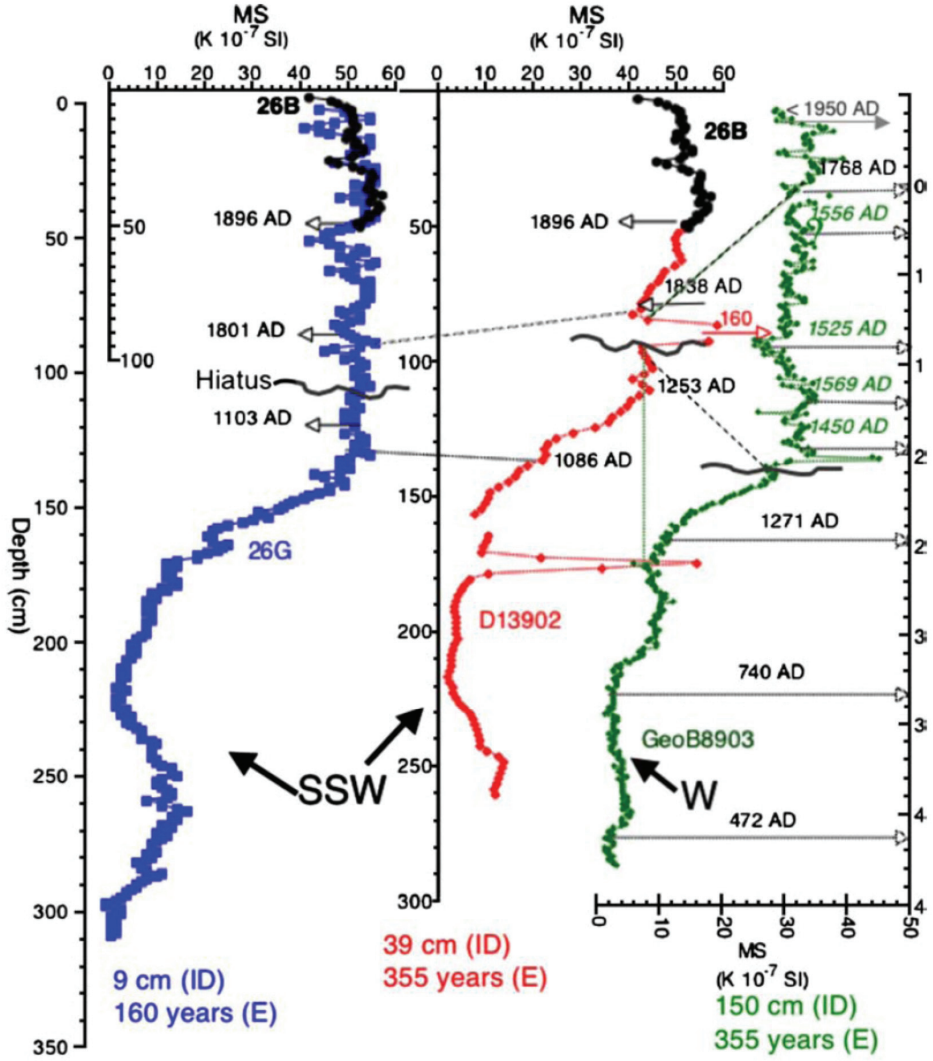

Fig. 7.7: Magnetic susceptibility and dated levels comparison of the best dated cores PO287-26G and D13902 located to the SSW of the Tagus River mouth, and GeoB 8903 positioned to the W side. Numbers in italic identify non-independent ages at the 2 s; ID refers to the height of sediment, in cm, estimated as deposited instantaneously at each site; E relates to the number of years represented by the sediment eroded by the event.

Visual examination of the D13902 archive half did not reveal major perturbations and magnetic susceptibility measurements done on U-channels, sampled from the central part of the archive core, confirmed the occurrence of a major magnetic susceptibility peak, while the Anhysteretic Remanent Magnetization (AMR*) data validates the existence of an exceptionnally high concentration of magnetic minerals in the fine-grained sediment (KISSEL et al., 1999).

As to the sites recovered to the W, only site GeoB 8903 was carefully dated. Determined ages reveal a sediment body of uniform age that did not stand out from the sediment above and below it during core description. Its homogeneous character both in terms of grain-size (silt-clay) and composition (Fig. 7.3) reminds the observed in the box-cores for the AD1969 tsunami record, as well as the described meter-thick 'homogenite' that blankets much of the central Mediterranean and that was interpreted by CITA et al (1996) as a result of the Thera tsunami. As a possible mechanism to explain this homogenite's origin, the same authors consider both: (1) the erosional process of the near-bottom currents and (2) the increase in suspended load generated by the spontaneous liquefaction of seabed slopes overloaded by cyclic pressure pulses of the passing tsunami. Although the mechanism proposed might still be considered speculative (DAWSON and STEWART, 2007) and in need of further investigation, the resuspension of material by the backwash has been proved by the great plumes of turbid water moving offshore observed in the video footage of the 26th December 2004 Indian Ocean tsunami.

The AD1755 earthquake is generally referred to as the major historic earthquake, and had associated tsunami waves that reached maximum water heights, at Lisbon, 6 times higher than the ones estimated for the AD1761 event (NOAA National Geophysical Data Center). Relatively to the AD1351 event, even though this earthquake might have been strong in the Lisbon area, it had a localized effect. On this basis, we assume the major AD1755 earthquake and tsunami as the determinant one for any sedimentary process recorded in the area in study.

Different epicenters have been proposed for the 1755 Lisbon earthquake, the Gorringe Bank by MACHADO (1966), the Marquês de Pombal Fault by ZITELLINI et al. (2001) and TERRINHA et al. (2003), but all agree with a southward origin as also indicated by the deposits found in the southern part of Portugal (Andrade, 1992), as well as with a NNW direction of water transport by the tsunami as indicated by eyewitness reports (NOZES, 1990; SOUSA, 1928). However, using the analysis of the contemporary accounts and intensity data from other more recent earthquakes, VILANOVA et al. (2003) defend that although the main shock was offshore (Goringe Bank), the resulting stress changes induced the rupture of the Lower Tagus Valley Fault (LTVF in Fig. 1 of VILANOVA et al., 2003) a few minutes after the main shock resulting in a sequence of high-energy tsunami waves, or a tsunami-like wave in the Tagus followed by the arrival of the offshore-generated tsunami wave. Either way, enormous alteration must have occurred on both the bed of the Estuary and the shallow shelf area.

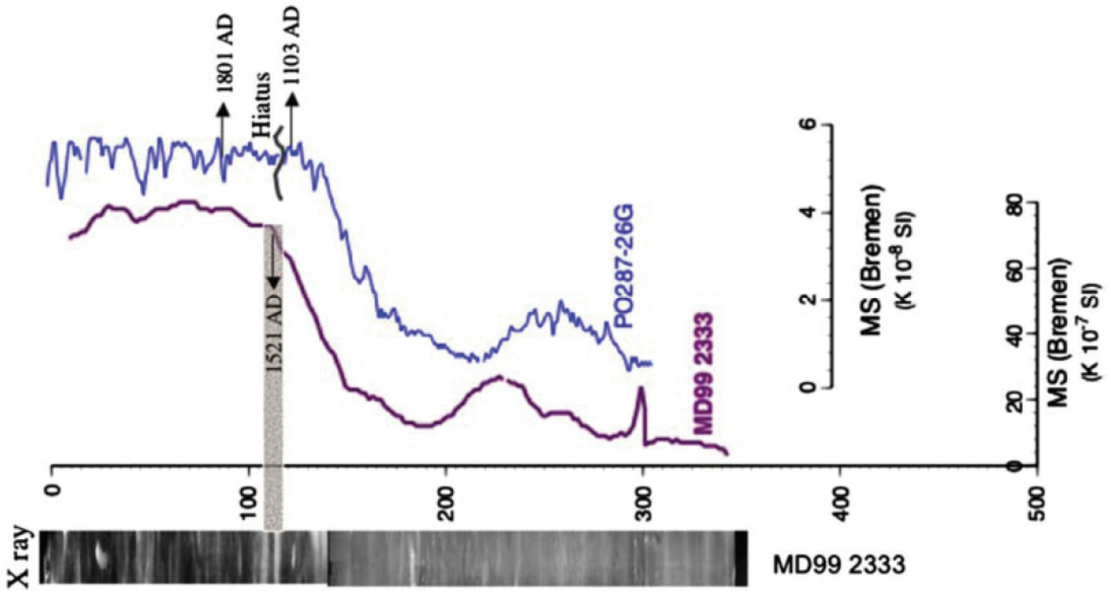

Fig. 7.8: Comparison of the magnetic susceptibility records along cores MD99 2333 and PO287-26G to the X-ray image of MD99 2333. Shadow band marks the ≈ 9 cm layered sediments depicted in the X-ray image.

According to the above referred information, and the model of VILANOVA et al. (2003), the western area of the Tagus prodelta is likely to have received more inland/estuarine and shallow-shelf fine materials transported out in suspension, by the tsunami-like wave generated in the Estuary by the rupture of the LTVF, or by the backwash current of the offshore tsunami wave. A stronger impact by the offshore tsunami wave is likely to have occurred southwestwards of the Tagus mouth where the coarse shell and heavy fine material ended up as a lag deposit formed as the water receded seaward through a SSW direction.

At site PO287-26, located to the W of D13902 at a minor canyon of the Setubal Canyon system, there is indication of a hiatus but no clear instantaneous deposit was identified. Core MD99-2333 has also been retrieved close to this site location (Tab. 1) and although MS and mean grain size are not indicative of any major change in sedimentation regime or sediment's origin, X-ray images of this sedimentary sequence reveal a thin disturbed mud sediment level within somewhat sandier levels reaching a total of 9cm (Fig. 7.8), that may be interpreted as the tsunami record at a minor canyon of a system which is likely to have functioned as a washout pathway of material towards the deeper Abyssal Plain. In fact records found at the Tagus abyssal basin (THOMPSON and WEAVER, 1994), certainly represent the sand sized destabilized sediments that have flown down slope and contributed to the formation of turbidity currents that very probably escaped via the Lisbon and Setubal canyons (Fig. 7.8).

While the erosion of the whole area by the tsunami as well as the deposition of sediment on the SSW site is likely to have been caused by bottom currents occurring quickly, the deposition of the fine resuspended material reworked from within the same sedimentary

environment in a somewhat fast mode, and that ended up on the W site, might be attributed to either a less vigorous Tagus tsunami-like wave as proposed in the VILANOVA et al. (2003) model, or to a somewhat slower sedimentation determined by the water column and circulation conditions after the event, and that might have happen within hours of the initial tsunami impact.

The major difference between the AD1969 record, constituted by a sediment level similar in composition and thickness on both the SSW and W sites, and the quite heterogeneous record associated to the AD1755 event, might be attributed not only to the major differences in wave run-up, but also to changes in the estuary mouth and coastal morphology and bathymetry caused by human action through the centuries, and possibly also by the AD1755 tsunami itself, which must have resulted in heavy changes in the waves' propagation and resulting effects.

7.6 Conclusions

The most important conclusion is that both the AD1969 and the AD1755 earthquake-originated tsunami left a sedimentary imprint in the shallow-shelf environment off Lisbon. However, the tsunamite levels correspond mainly to fine turbidites no different either chemically or texturally from the rest of the sequence, and so, most likely to be overlooked in an environment where the occurrence of fine sediments is normal. As a result, paleotsunami identification will require special attention and detailed dating, given that, such as in the Lisbon area, sediments attributed to a tsunami cause can originate and redeposit within a sedimentary environment that is maintained the same before and after the event.

The variability of the record found in such a small area can be significant and appears dependent of the wave height, coastal morphology, shelf bathymetry, relative importance of the bottom currents effect, the backwash suspended load and circulation characteristics.

Paleotsunami studies in shallow-shelf areas beyond historical times will be difficult due to the lack of clear criteria for tsunami evidence.

7.7 Acknowledgements

We thank the captain and crew of RV Discovery and RV Poseidon for their help in collecting the samples and the EU PALEOSTUDIES project for supporting the XRF measurements. Financial support was provided by the EU project HOLSMEER (EVK2-CT-2000-00060) and the ESF EUROCORES EUROMARGINS project SEDPORT (PDCTM/40017/2003).

7.8 References

Abrantes, F., S. Lebreiro, I. Gil, T. Rodrigues, H. Bartels-Jónsdóttir, P. Oliveira, C. Kissel, J.O. Grimalt (2005): Shallow marine sediment cores record climate variability and earthquake activity off Lisbon (Portugal) for the last 2000 years. Quaternary Science Reviews 24: 2477-2494.

Andrade, C. (1992): Tsunami generated forms in the Algarve barrier islands. Science of Tsunami Hazards 10: 21-34.

Baptista, M.A., P. Miranda, L.M. Victor (1988a): Constraints on the source of the 1755 Lisbon tsunami inferred from numerical modeling of historical data. Journal of Geodynamics 25: 159-174.

Baptista, M.A., S. Heitor, J.M. Miranda, P. Miranda, L.M. Victor (1988b): The 1755 Lisbon tsunami; evaluation of the tsunami parameters. Journal of Geodynamics 25: 143-157.

Baptista, M.A., P. Miranda, l.M. Mendes (1992): Maximum Entropy Analysis of Portuguese Tsunami: The Tsunamis of 28/02/1969 and 26/04/1975. Science of Tsunami Hazards 10(1): 9-20.

Baptista, M.A., J.M. Miranda, F. Chierici, N. Zitellini (2003): New study of the 1755 earthquake source based on multi-channel seismic survey data and tsunami modelling. Natural Hazards and Earth System Sciences 3: 333-340.

Baptista, M.A., P.M. Soares, J.M. Miranda, J.F. Luis (2006): Tsunami Propagation along Tagus Estuary (Lisbon, Portugal) Preliminary Results. Science of Tsunami Hazards 24: 329-338.

Blott, S.J., K. Pye. (2001): Gradistat: A grain-size distribution and statistics package for the analysis of unconsolidated sediments. Earth Surface Processes and Landforms 26: 1237-1248.

Cabeçadas, G., M.J. Rogueira, M. Nogueira, L. Cabeçadas, H. Cavaco, P. Nogueira (2003): Coastal phytoplankton productivity associated with different stability and Nutrient patterns. Geophysical Research Abstracts 5: 09277.

Campos, M.L. (1991): Tsunami hazard on the Spanish coast of the Iberian Peninsula. Science of Tsunami Hazards 9(1): 83-90.

Cita, M.B., A. Camerlenghi, B. Rimoldi (1996): Deep-sea tsunami deposits in the eastern Mediterranean: new evidence and depositional models. Sedimentary Geology 104: 155-173.

Coleman, P.J. (1968): Tsunamis as geological agents. Journal of Geological Society of Australia 15: 267-273.

Dawson, A.G., I.D.L. Foster, S. Shi, D.E. Smith, D. Long (1991): The identification of tsunami deposits in coastal sediment sequences. Science of Tsunami Hazards 9: 73-82.

Dawson, A.G. (1994): Geomorphological processes associated with tsunami runup and backwash. Geomorphology 10: 83-94.

Dawson, A.G., R.A. Hindson, C. Andrade, C. Freitas, R. Parish, M. Bateman (1995): Tsunami sedimentation associated with the Lisbon earthquake of 1 November AD1755: Boca do Rio, Algarve, Portugal. The Holocene 5(2): 209-215.

Dawson, A.G., I. Stewart (2007 in press): Tsunami Deposits in the Geological Record. Sedimentary Geology: doi: 10.1016/j.sedgeo.2007.01.002.

Folk, R.L., W.C. Ward (1957): Brazos River bar: a study in the significance of grain-size parameters. Journal of Sedimentary Petrology 27: 3-26.

Garcia-Orellana, J., E. Gràcia, A. Vizcaino, P. Masqué, C. Olid, F. Martinez-Ruiz, H. Piñero, J.-A. Sanchez-Cabeza, J. Dañobeitia (2006): Identifying instrumental and historical earthquake records in the SW Iberian margin using ^{210}Pb turbidite chronology. Geophysical Research Letters 33: L24601, doi:10.1029/2006GL028417.

Gaspar, L., H. Monteiro (1977): Matéria Orgânica nos sedimentos da plataforma continental portuguesa entre os cabos Espichel e Raso. Comunicações dos Serviços Geológicos de Portugal, LXII: 69-83.

Heinrich, P., M.A. Baptista, P.M. Miranda (1994): Numerical Simulation of 1969 Tsunami along the Portuguese Coasts. Preliminary Results. Science of Tsunami Hazards 12(1): 13-23.

Hindson, R.A., C. Andrade, A.G. Dawson (1996): Sedimentary processes associated with the tsunami generated by the 1755 Lisbon earthquake on the Algarve coast, Portugal. Physics and Chemistry of the Earth 21: 57-63.

Jansen, J.H.F., S.J. Van der Gaast, B. Koster, A.J. Vaars (1998): CORTEX, a shipboard XRF-scanner for element analyses in split sediment cores. Marine Geology 151(1-4): 143-153.

Justo, J.L., C. Salwa (1998): The 1531 Lisbon Earthquake. Bulletin of the Seismological Society of America 88(2): 319-328.

Kissel, C., C. Laj, L. Labeyrie, T. Dokken, A. Voelker, D. Blamart (1999): Magnetic signature of rapid climatic variations in North Atlantic sediments. In Abrantes, F., A. Mix (Eds.): Reconstructing Ocean History: a Window into the Future: 419-437. Plenum Publishing, London.

Le Roux, J.P., G. Vargas (2005): Hydraulic behavior of tsunami backflows: insights from their modern and ancient deposits. Environmental Geology 49(1): 65-75. doi: 10.1007/s00254-005-0059-2.

Machado, F. (1966): Contribuição para o Estudo do Terramoto de 1 de Novembro de 1755, Revista da Faculdade de Ciências de Lisbon Series C, 14: 19-31

Mader, C.L. (2001): Modelling the 1755 Lisbon tsunami. Science of Tsunami Hazards 19(2): 93-98.

Mendonça, M. (1758): Historia Universal dos Terramotos que tem havido no mundo de que ha noticia desde a sua creção até ao século presente. Biblioteca Nacional de Lisboa, Portugal.

Monteiro, H., I. Moita (1971): Morfologia e sedimentos da plataforma continental e vertente continental superior ao largo da Peninsula de Setúbal. In "Congresso de Geologia": 301-330.

Nozes, J. (1990): O Terramoto de 1755: Testemunhos Britânicos; British Accounts of the Lisbon Earthquake of 1755, The British Historical Society of Portugal, Lisbon.

Pareschi, M.T., E. Boschi, M. Favalli (2006): Lost tsunami. Geophysical Research Letters 33: L22608. doi:10.1029/2006GL027790.

Reimer P.J., M.G.L Baillie, E. Bard, A. Bayliss, J.W. Beck, C. Bertrand, P.G. Blackwell, C.E. Buck, G. Burr, K.B. Cutler, P.E. Damon, R.L. Edwards, R.G. Fairbanks, M. Friedrich, T.P. Guilderson, K.A. Hughen, B. Kromer, G. McCormac, S. Manning, C.B. Ramsey, R.W. Reimer, S. Remmele, J.R. Southon, M. Stuiver, S. Talamo, F.W. Taylor, J. van der Plicht, C.E. Weyhenmeyer (2004): INTCAL04 terrestrial radiocarbon age calibration, 0-26 cal. kyr. BP. Radiocarbon 46: 1029-1058.

Scheffers, A., D. Kelletat (2003): Sedimentologic and geomorphologic tsunami imprints worldwide - a review. Earth-Science Reviews 63(1): 83-92.

Scheffers, A., D. Kelletat (2005): Tsunami Relics on the Coastal Landscape West of Lisbon, Portugal. Science of Tsunami Hazards 23(1): 3-16.

Sousa, F.P.D. (1928): Distritos de Lisboa. Serviços Geológicos de Portugal, Lisboa.

Tappan, E.M. (Editor), 1914. The World's Story: A History of the World in Story, Song and Art, 14 Vols. (Boston: Houghton Mifflin, 1914), Vol. V: Italy, France, Spain, and Portugal, Source: Modern History Sourcebook: Historical Depictions of the 1755 Lisbon Earthquake Rev. Charles Davy: The Earthquake at Lisbon, 1755, pp. 618-628.

Teller, J.T., T. Murty, N. Nirupama, P. Chittibabu (2005): A Possible Tsunami in the Labrador Sea Related to the Drainage of Glacial Lake Agassiz ~8400 Years BP. Science of Tsunami Hazards 23(3): 3-16.

Terrinha, P., L.M. Pinheiro, J.-P. Henriet, L. Matias, M.K. Ivanov, J.H. Monteiro, A. Akhmetzhanov, A. Volkonskaya, T. Cunha, P. Shaskin, M. Rovere (2003): Tsunamigenic-seismogenic structures, neotectonics, sedimentary processes and slope instability on the southwest Portuguese Margin. Marine Geology 195: 55-73.

Thomson, J., P.P.E. Weaver (1994): An AMS radiocarbon method to determine the emplacement time of recent deep-sea turbidites. Sedimentary Geology 89: 1-7.

Van der Bergh, G.D., W. Boer, H. Haas, T. van Weering, R. van Wijhe (2003): Shallow marine tsunami deposits in Telik Banten (NW Java, Indonesia), generated by the 1883 Krakatau eruption. Marine Geology 197: 13-34.

Vilanova, S., C. Nunes, J. Fonseca (2003): Lisbon 1755: A case of Triggered Onshore Rupture? Bulletin of the Seismological Society of America 93: 2056-2068.

Whelan, F., D. Kelletat (2005): Boulder Deposits on the Southern Spanish Atlantic Coast: Possible Evidence for the 1755 AD Lisbon Tsunami. Science of Tsunami Hazards 23(3): 25-38.

Zitellini, N., L. Mendes, D. Córdoba, J.J. Dañobeitia, R. Nicolich, G. Pellis, A. Ribeiro, R. Sartori, L. Torelli and BIGSETS Team (2001): Source of the 1755 Lisbon Earthquake and Tsunami Investigated. EOS, Transactions of AGU 82(26): 285-291.

8 General Conclusion

Present day conditions and past changes of marine and continental environmental conditions on the Iberian Peninsula are recorded in shelf sediments of the western Portuguese margin. Variations in environmental parameters can be identified and distinguished by the analysis of multiple proxies and the integration of the obtained datasets into one synoptic interpretation. The different temporal resolutions of environmental processes can be accounted for by appropriate sample acquisition, which considers the temporal resolution of the sediment archives. Thereby, surface samples are interpreted in terms of the status quo of sediment properties, high-resolution records are used for reconstructing centennial climate variations and lower resolution records are applied for millennial environmental reconstructions. Additionally, the detailed analysis of the sediment's grain-size spectra of the high-resolution record allows an evaluation of the influence of sediment texture on organic and inorganic proxies.

8.1 Present Day Setting

The spatial distribution of provenance proxies (C_{org}/N_{total}, $\delta^{13}C_{org}$, $CaCO_3$) in surface sediments reflects the present day input of terrigenous versus marine material to the shelf. Additionally, sedimentary $\delta^{15}N$ values indicate spatial variations of the nutrient budget by either local variations of upwelling patterns or by variations in marine primary production.

Off the Douro and Tagus Rivers, the riverine discharge of terrigenous organic matter can be traced on the shelf, where it dominantly accumulates on coast-parallel mud belts. A part of the terrigenous sediment accumulates close to the Nazaré Canyon, as evidenced by a significant fraction of terrigenous organic matter in surface samples. As river inputs in the vicinity are absent, this material seems to be transported southwards along the coast. Off the Tagus Estuary, a gradient form a continental to a marine source signature reflects increasing marine contributions to shelf sediments. Inside the Estuary, no clear gradient can be established, as the surface sediments are subject to constant reworking by natural and anthropogenic causes. A turbidity maximum in the uppermost estuary coincides with increased salinity and is thus possibly caused by flocculation of suspended organic matter. On the southern shelf off Cape Sines sedimentary organic matter is of marine origin.

Spatial variations of the coastal upwelling are reflected by $\delta^{15}N$ values in the surface sediments. The Douro region, which according to satellite images is characterised by broad, temporally static upwelling, has a correspondingly homogenous $\delta^{15}N$ distribution with a marine NO_3^- utilisation between 80 and 95%. In the Nazaré region, sedimentary $\delta^{15}N$ and water column NO_3^- concentrations indicate complete NO_3^- consumption with slightly higher $\delta^{15}N$ values further offshore. This fractionation gradient is interpreted to reflect the assimilation of freshly upwelled NO_3^- with lower $\delta^{15}N$ closer to the coast, but it is blurred by

the averaging of sedimentary $\delta^{15}N$ signals over several years. In the Tagus region, sedimentary $\delta^{15}N$ values are biased by the input of agriculturally affected, isotopically heavy DIN. The distribution of $\delta^{15}N$ in the Sines region reflects the stronger upwelling and higher marine productivity in the southern part of the sampling region, extending also towards Cape S. Vicente. Denitrification plays no role, as oxygen concentrations inside the estuary and along the coast are high enough to prevent denitrification. Relatively high $\delta^{15}N$ values indicate further, that N_2-fixation is no relevant process.

The sediment texture, which is known to affect the organic matter content of bulk sediment by biasing it towards higher values in finer sediment, has no significant effect on organic matter provenance proxies (i.e. C_{org}/N_{total} and $\delta^{13}C_{org}$), nor on $\delta^{15}N$ in the surface samples. Low correlation coefficients between provenance proxies and grain-size allow an interpretation of C_{org}/N_{total} and $\delta^{13}C_{org}$ in terms of organic matter source and of $\delta^{15}N$ in terms of nutrient budget.

8.2 Centennial Variations

A high-resolution record GeoB 8903 from the Tagus Prodelta shows no variations in organic matter provenance during the past 3200 years. This is possibly caused by trapping and reworking of organic material inside the Tagus Estuary, blurring the source signatures of the organic matter. Further, no major variations in the NO_3^- budget are evident.

However, two major changes in environmental conditions become obvious in sediment properties. A decrease in $CaCO_3$, in mean bulk grain-size and in coarse end-member abundance around 2000 years BP is interpreted as a shift from a dry and windy climate to a wetter and less windy climate. This coincides with the transition from the warm, dry Subboreal to the cooler, wet Subatlantic period. Stronger winds after 2000 years BP lead to stronger upwelling, as well as to winnowing of the surface sediment, which concentrates the coarse sediment fraction and results in the observed better sorting of the coarsest end-member. Although increased upwelling should also result in a higher C_{org} content, the association of organic matter to a finer sediment fraction results in winnowing of the organic matter by the stronger, wind-driven shelf currents. The relatively good sorting of the coarse lithic end-member may also be an effect of increased aeolian input, i.e. dust from e.g. the central Iberian Peninsula or from the Saharan desert. This cannot be clearly distinguished, however, the general driving mechanism would be wind energy for both cases. A second, more recent change is evident around AD1400 by an increase in fine, lithic terrigenous fraction and a simultaneous, strong increase in magnetic susceptibility. A coincident change in MS of equal magnitude is observed in other Tagus prodelta records, whereas such a change is absent in more distant records along the shelf. This implies a driving mechanism, which is restricted to the Tagus Prodelta region and hence this shift is explained by an environmental shift in the

Tagus River catchment. The timing of this change is synchronous to major deforestation on the Iberian Peninsula, possibly caused by an increased demand for timber for shipbuilding.

For the past 250 years a relation between MS and grain-size and the North Atlantic Oscillation can be established, showing low MS and slightly coarser bulk grain-sizes during NAO negative phases. This apparent contradiction – negative NAO results in high precipitation rates and should thus increase MS – is explained by the association of MS to the finest lithic sediment component. The finest end-member is delivered to the shelf constantly, whereas this input is diluted by the input of a coarser end-member with lower MS during NAO negative phases. As this coarser end-member has a low MS, negative NAO phases coincide with lower MS and coarser bulk grain-size. This is supported by a positive correlation between the abundance of the finest end-member with NAO and a negative correlation between the medium sized end-member with NAO. The additional slight positive correlation of the coarsest end-member with NAO emphasises its relation to wind strength, as a positive NAO is characterised by stronger winds, supporting the above interpretation of higher wind energy prior to 2000 years BP.

8.3 Long-Term Changes

On a long-term view the shelf environment is dominantly affected by sea level variations, which change the sedimentological setting and are thus reflected in the sediment properties. The varying width of the shelf changes the sediment accommodation space and affects the delivery of terrigenous sediment to either sampling location. During transgressive periods, accommodation space is generated close to the coast, trapping terrigenous sediment, possibly in an early estuarine environment and resulting in a stronger marine organic matter source signature in the shelf record D13882. The comparison of $\delta^{15}N$ signatures between the shelf record and the deep-sea core MD03-2698 shows the relocation of the upwelling centre from the shelf edge on the shelf, due to the increasing water depth. Generally the sediment supply changes more quantitatively than qualitatively, as observed in accumulation rates, because the effect of sea level variations seems to exceed the impact of climatic changes in the continental hinterland.

8.4 Grain-Size Effects

The reconstruction of lithic subpopulations of the sediment – in this case of core GeoB 8903 – shows the importance of the relation between individual proxies and the associated grain-size spectra. Modelling results suggest the existence of three end-members, which constitute the sediment's grain-size spectrum. This is supported by correlations between:

- the finest end-member and magnetic susceptibility,
- the coarsest end-member and $CaCO_3$,
- an intermediate end-member and C_{org}, although this correlation is less clear.

These different end-members as well as the associated proxies are subject to sorting processes during transport or after deposition. An example for that is a probably longer transport of the finest end-member by currents, leading to a transfer of the terrigenous MS-signal farther offshore, whereas the C_{org}-signal, which is associated to slightly coarser material, is deposited in a more proximal realm. An example for postdepositional influences is the stronger resistance of the coarse, $CaCO_3$-containing fraction to winnowing, compared to the fine, MS-carrying sediment fraction. It is hence important to include sedimentological information into the environmental interpretation.
The relative abundances of each end-member show additionally a correlation with the NAO, which is probably the most relevant environmental driving process in that region. The relation between end-member and environmental processes on one hand and proxies on the other hand allows an evaluation of sources and transport pathways of the sediment's components and e.g. a distinction between fluvial, terrigenous material and marine, biogenic material.

8.5 Tsunami

Although considerable effort has been spent on unravelling the impact of tsunamis on the shelf sediments, particularly of the AD1755 event, the extend of a possible sediment disturbance is unclear. Summarising, several facts are worth a more detailed discussion, balancing the pro and contra arguments.

- Age model: Four radiocarbon ages between 68 and 198cm in core GeoB 8903 cover a similar range of possible calibrated ages around and prior to the AD1755 event. At a first glance this implies reworking of 1.3m sediment. However, it is possible to construct a linear age model through the four anomalous ages between 68 and 198cm (see Fig. 5.4), except for the 68.5cm dating, which yields an age reversal. Resulting sediment accumulation rates are within the range of normal values for the Tagus Prodelta (ABRANTES et al., 2005; JOUANNEAU et al., 1998) and the possible tsunamigenic interval is reduced to some decimeters.

  A possible alternative explanation for the anomalies in the age model may be variations of upwelling intensity, which changes the reservoir age of the seawater. This effect has been reconstructed for the Holocene, yielding a variable offset between marine and continental ^{14}C ages of some hundred years (SOARES et al., 2006). An additional impact on the marine reservoir age may be exerted by variable riverine freshwater discharge, thus leading to deviations from the 400 years reservoir age, which is used in this study (ABRANTES et al., 2005). Particularly during the past centuries, strong upwelling and high river discharge could

be reconstructed (see Fig. 2.9, chapter 5). Therefore, these biasing factors may have a significant impact on the dating results, leading to deviations in the age model.

- Sediment Data: In a sediment record from the southern prodelta, a dm-sized sand layer with a high magnetic susceptibility was observed and assigned to the AD1755 tsunami. Such a change in sediment properties is absent in GeoB 8903 from the western prodelta, as well as in sediments from inside the Tagus Estuary (ANDRADE et al., 2003). A possible explanation for this is dissipation of the tsunami energy during its course on the Tagus Prodelta from the South, moving counter-clockwise on the shelf, leading to stronger erosion on the southern prodelta and to increased deposition on the western prodelta. However, a change in grain-size should then also be observable in sediments from the western prodelta.
  Baptista et al. (2003) modelled a tsunami wave height of 5m off Oeiras, close to Lisbon off the Tagus Estuary mouth. This is considerably less, than at other locations along the Iberian coast (e.g. Cadiz: 15m; BAPTISTA et al., 1988) and may indicate, that the effect of the AD1755 tsunami on the Tagus Prodelta was relatively low. This is supported by the absence of any evidence for older tsunamis in any of the sediment records, although this would be expected in an area, which is frequently affected by earthquakes and associated tsunamis. Furthermore, the GeoB 8903 shelf record shows changes in environmental proxies, which are synchronous to variations in North East Atlantic records (e.g. HEBBELN et al., 2006, EIRÍKSSON et al., 2006). This would most probably not be observable, if 1.3m of sediment were reworked and it thus implies a largely undisturbed stratigraphy of GeoB 8903 and its significance in terms of a paleoenvironmental reconstruction.

Hence, a definite conclusion from the presented data about the extend of a tsunamigenic sediment disturbance cannot be drawn, but the presented data suggests, that the effect of tsunamis and accompanied sediment reworking is not traceable in the sediments from the western prodelta.

9 Perspectives

For assessing environmental conditions in the continental hinterland and interactions between marine and continental environmental processes, specific information about the continental environment is required. Continental datasets, such as pollen data or sediment records from the river floodplain are under preparation by SEDPORT project partners and will in the future be combined with the marine datasets. With that, the until now underrepresented data of continental environmental parameters will be supplemented.

This would also help to assess the bias, which is exceeded by the presence of the Tagus Estuary on the chemical and physical properties of shelf sediments. Large amounts of terrigenous, river transported material are trapped and reworked inside the estuary, as evidenced by properties of estuarine surface sediments. Although it is extremely difficult, to obtain continuous records from inside the estuary, because the sediment surface is subject to frequent natural or anthropogenic disturbances e.g. by channel migration or dredging, the investigation of estuarine sediment cores would be a way to account for inner estuarine processes, that blur the terrigenous signal in prodelta sediments.

As described in the previous chapter, the impact of tsunamis, particularly the AD1755 event, cannot be clearly confined. To ensure the continuity of the Tagus Prodelta records, it is important to identify the tsunamigenic influence and to confine hiati or intervals of reworked sediment. Therefore a more detailed age model is needed, covering not only the AD1755 event, but also the other known tsunamis, e.g. the AD1531, AD880 and 220BC events on a higher resolution., e.g. by additional radiocarbon dating. An additional improvement of the age model can be obtained by correlating the various prodelta records. Also the acquisition of additional and supplementary information about sediment structures and sediment properties, e.g. by X-Ray photography or high-resolution grain-size analyses of other shelf cores would contribute to a more reliable identification of possible tsunami layers.

Despite this potential for improvements, the sampling location is a promising area for investigating the effects of marine and continental environmental changes on sediments, as well as for reconstructing the interactions between marine and continental environmental processes. The Tagus Prodelta combines inputs from continental and marine sources on an overall high temporal resolution. If it is possible to confine the tsunamigenic disturbances and to account for the estuarine bias, the Tagus Prodelta sediments are valuable archives for past environmental variations.

Particularly the integration of the Tagus Prodelta data into a larger spatial context – e.g. on a continental or hemispheric scale – would allow a more significant interpretation in terms of large-scale environmental changes. This would allow a distinction between local and regional signals and an attempt for this is the comparison between Tagus Prodelta records to records from the North Atlantic (see e.g. HOLSMEER project, The Holocene, Issue 16). This broad view yields coincident changes of environmental parameters in both realms and it would be a future task to identify common driving mechanisms and teleconnections.

Appendix 1

–

Complementary Data

10 Complementary Data

Several datasets, which were acquired within the framework of the SEDPORT project, have not been published, because they are of a rather descriptive character or require more intense analytical efforts. This data is presented in the following and consists of

- visual and hydroacoustic investigations with a remotely operated vehicle (ROV) and an SES echosounder system
- a box core PO287-1 from inside the Tagus Estuary
- three box cores PO287-26, -27, -28 from the Tagus prodelta
- a foraminifera $\delta^{18}O$ record of gravity core GeoB 8903
- XRF data of core GeoB 8903.

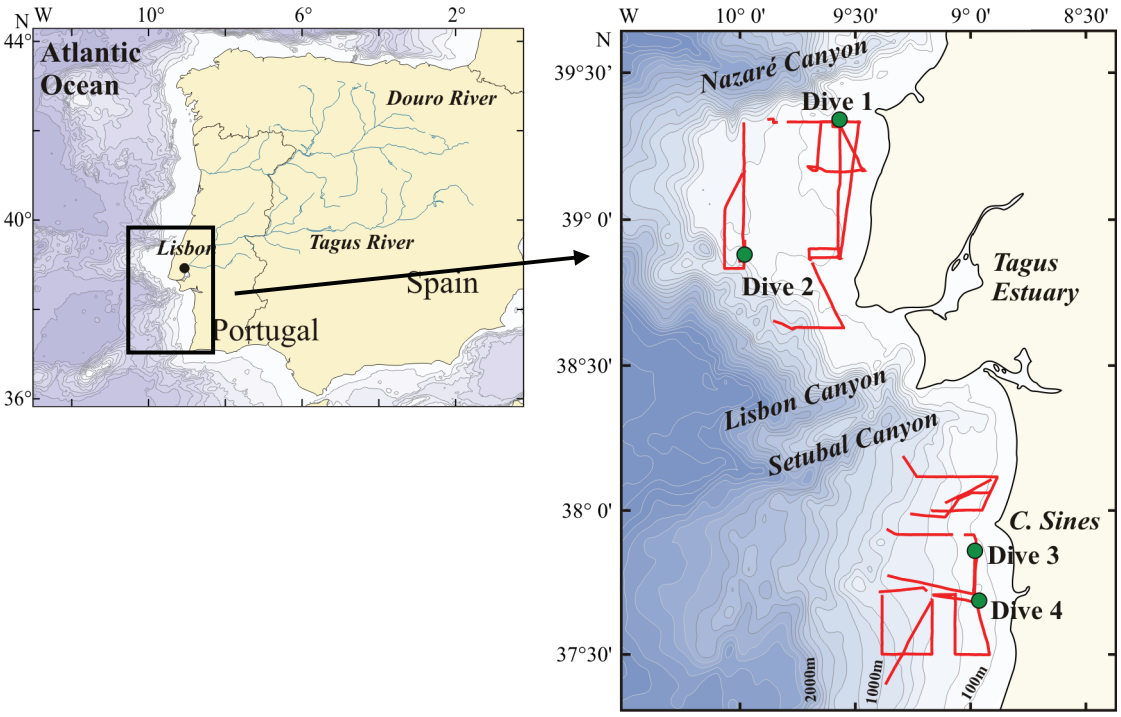

Fig. 10.1: The enlarged map shows the obtained echosounder profiles along the Portuguese margin (red lines) and the four ROV deployment sites (circles).

10.1 Visual and Seismic Observations

For obtaining a direct impression of the sea floor in the sampling regions, acoustic and visual techniques have been employed. These include a parametric echosounder system SES-96 and a remotely operated vehicle, type Subatlantic CHEROKEE, owned by the Research Center

Ocean Margins Bremen. 25 profiles of variable length were obtained with the SES-96, including previous acoustic investigation of the four deployment sites of the ROV (Fig. 10.1).

10.1.1 Echosound Profiles

The parametric echosounder system SES-96, provided by the Institut für Ostseeforschung Warnemünde of the University Rostock, was used to obtain seismic sections of the sea floor along the cruise track (Fig. 10.1). The SES operates with 100kHz or 8kHz, depending on water depth, providing high resolution profiles of the sea floor morphology with a low penetration depth. Sedimentological properties, such as the Tagus mud patch as well as bathymetric features such as canyons or rocky outcrops can be observed (Figs. 10.2-10.10). It was thus possible to assess suitable locations for coring and the deployment of the Remotely Operated Vehicle (ROV). As an example, Fig. 10.2 shows the SES profile across the boundaries of the Tagus prodelta mud patch, revealing a sharp boundary between the mud patch sediments, which show a good layering, and the surrounding shelf sediments. In the northwestern part of the northern profile rocky outcrops appear, which may diminish bottom currents in their current shade and lead to trapping of fine material. The southern profile shows the onset of the continental slope westwards, which is separated towards the mud patch by a shallow elevation.

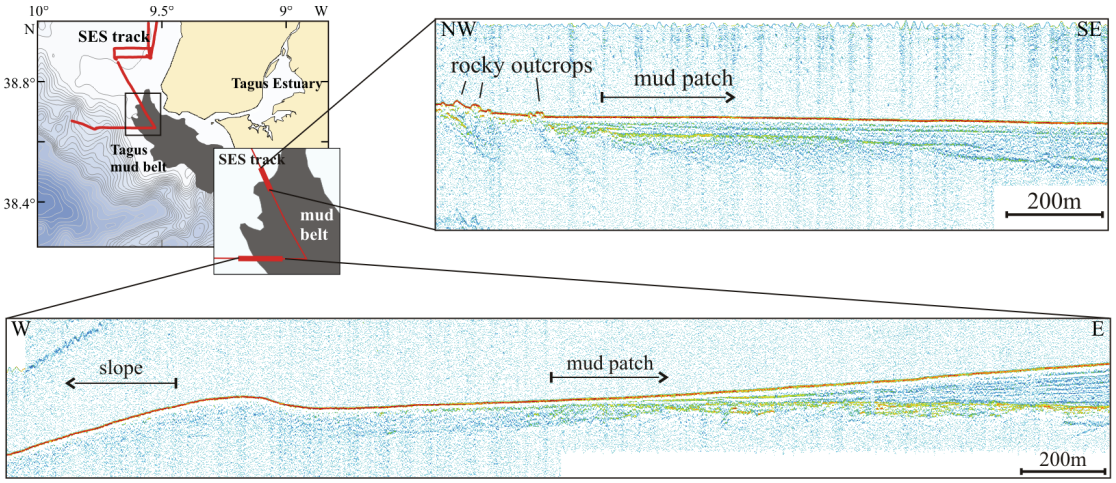

Fig. 10.2: The two echosounder profiles show the sharp boundaries of the Tagus mud patch, which is drawn after JOUANNEAU et al. (1998). Thickened red lines in the map indicate the track of the echosounder profiles. Vertical scale: thickness of mud patch on the right hand side of the profiles is ca. 15m.

10.1.2 Remotely Operated Vehicle

A remotely operated vehicle (ROV) of the Research Center Ocean Margins (RCOM), Bremen, type Subatlantic CHEROKEE, was deployed at four different locations along the shelf to obtain a visual impression of the sea floor.

The heterogeneity of the sediment has consequences for the interpretation of surface sediment properties and must be accounted for, when comparing sediment properties along the shelf. Different grain-sizes almost certainly affect organic matter properties (e.g. GEARING et al., 1977; MÜLLER, 1977; RANSOM et al., 1998) and several sediment types (e.g. gravel) may not be characteristic for the shelf sedimentation. The high spatial variability of sedimentological conditions must also be considered, when correlating neighbouring sediment records, which may consequently show significant differences despite an immediate proximity.

10.1.3 Dive 1

Dive 1 was done on the southern rim of the Nazaré Canyon at 39°20'N and 9°34'W in around 90m water depth, recording a West-East profile of 285m length. The SES profile shows a variable sea floor morphology with a relief of up to 30m (Fig. 10.3). In the eastern part of the section the relief becomes shallower and a sharp reflector, which is eastwards bordered by a ca. 5m high elevation, becomes evident. This area was considered as suitable for the ROV deployment (red square in Fig. 10.3).

The enlarged SES profile of the ROV dive location (Fig. 10.4B) shows a horizontal surface in the West, which merges into a gently dipping, flat surface in the centre along the ROV track and which is eastwards bordered by irregular structures of some meters height.

Due to strong bottom currents and resulting navigation problems, the ROV camera survey was restricted to the eastern section of the profile. Nevertheless the images show a highly variable sediment texture, with grain-sizes ranging from cm-sized shell debris (Fig. 10.5, images A and E) to silty material (Fig. 10.5, image D). The transition between both textures occurs abruptly (Fig. 10.5, image F). Images B and C (Fig. 10.5) show rocky outcrops, which resemble in shape and texture beach rock. These may thus be part of a submerged shore line, which formed during the sea level low stand 8-10 kyrs BP (DIAS et al., 2000). The sharp reflector in the centre of the SES profile is interpreted as a patch of silty sediment and the bordering elevations as outcrops of probably in-situ rocks.

The presence of silty sediments may be a result of the protection against strong bottom currents by rocky outcrops eastwards (Fig. 10.3, 10.4). This mechanism has been

reported to be an explanation for the formation of mud belts along the northern shelf (DIAS et al., 2002a).

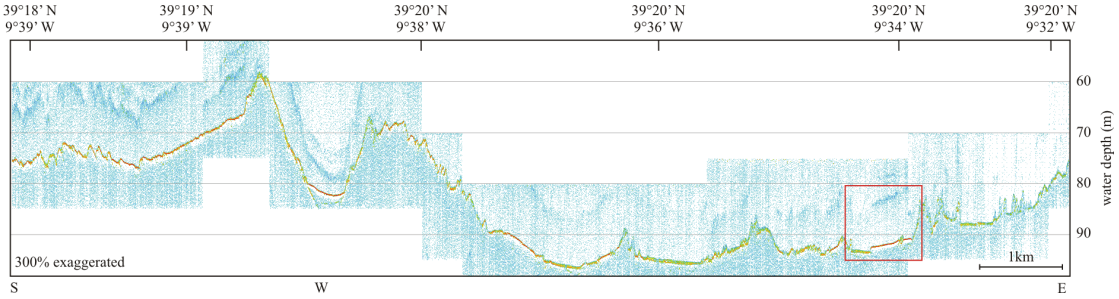

Fig. 10.3: Echosound profile, covering the area of ROV dive 1 along the Nazaré Canyon rim. Red rectangle indicates the enlargement in Fig. 10.4B.

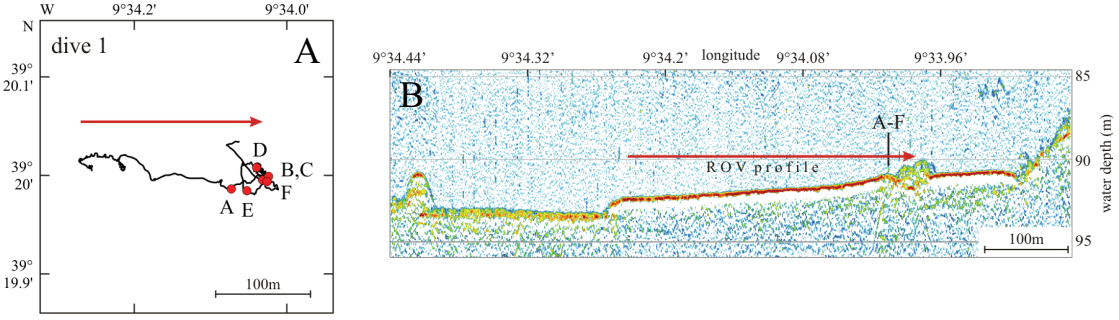

Fig. 10.4A & B: Map (A) and enlarged echosound section (B) of ROV dive 1. Letters in the graphs indicate the location of the pictures, shown in Fig. 10.5.

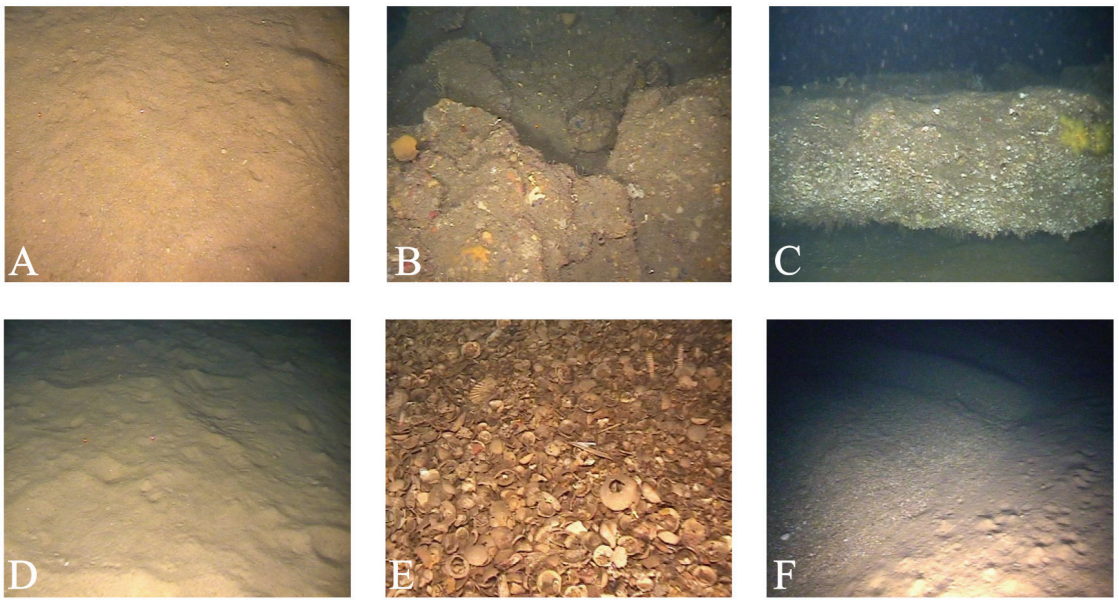

Fig. 10.5: Photographs taken during ROV dive 1. Letters in images correspond to letters in Figure 10.3A and B.

10.1.4 Dive 2

The second ROV dive was done on the Estremadura Spur at 38°52'N and 9°59'W in 300m water depth, recording a north-south profile of 1665m length. The relief on the sea floor ranges up to 70m (Fig. 10.6), showing an apparent dip northwards, which is interrupted by a ca. 20m high elevation in the northern part of the SES section. An alternation between sharp and fuzzy reflectors in the southern part of the SES profile was chosen as a location for ROV deployment (red box in Fig. 10.6, 10.7).

The ROV images show mainly coarse material, which is made up of shell fragments (Fig. 10.8, image C) and forms large ripples with a wavelength of 30-40cm (Fig. 10.8, image A). These sediments are interrupted by rocky outcrops (Fig. 10.8, image B), whose surface appears eroded and abraded.

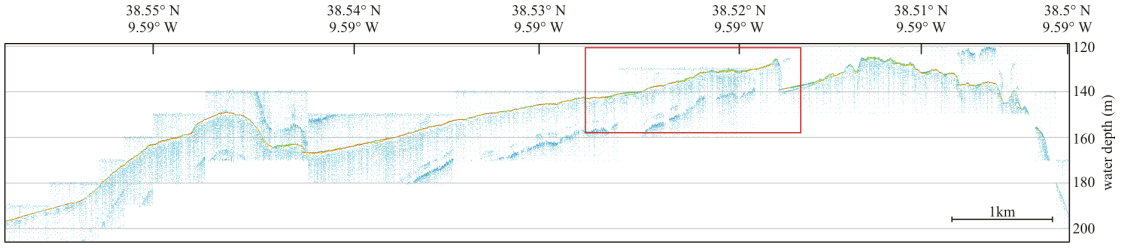

Fig. 10.6: Echosound profile, covering the location of ROV dive 2 on the Estremadura Spur. Red rectangle indicates the enlargement in Fig. 10.7B.

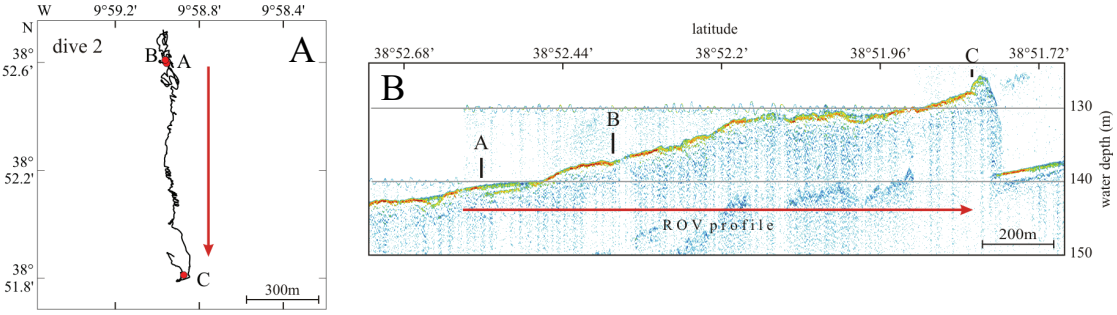

Fig. 10.7A & B: Map (A) and enlarged echosound section (B) of ROV dive 2. Letters in the graphs indicate the location of the pictures, shown in Fig. 10.8.

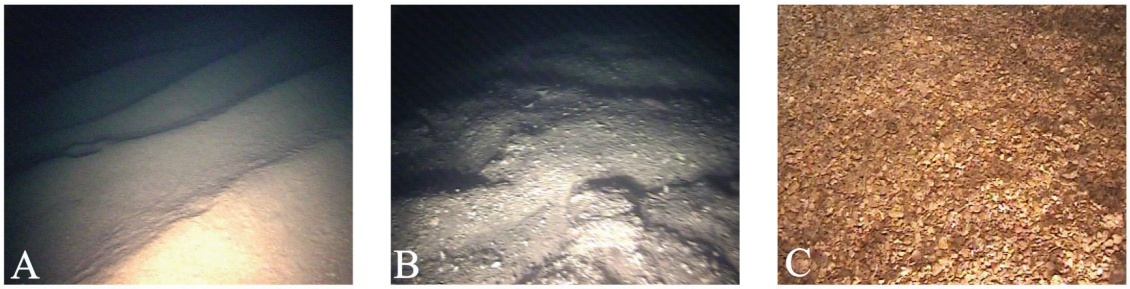

Fig. 10.8: Photographs taken during ROV dive 2. Letters in images correspond to letters in Figure 10.7A and B.

10.1.5 Dive 3

The location of the third ROV deployment is southwest of Cape Sines at 37°51'N and 8°59'W in around 130m water depth, covering a south-north profile of 1180m length. The SES profile shows along its latitudinal section a relatively flat sea floor except for ca. 20m high elevations in the northern part. Westwards the water depth increases, which can be observed in the northern, longitudinal part of the SES section (Fig. 10.1).

The SES profile, which shows the ROV dive (Fig. 10.10B), differs from the large scale SES profile (Fig. 10.9), because the former was separately recorded during the ROV dive. This leads to a spatial offset of some tens of meters. The ROV images show the whole range of sediment textures from fine, silty material (Fig. 10.11, image A) to coarse shell fragments (Fig. 10.11, image B). Well rounded rocks of dm-size are observed (Fig. 10.11, images C, F, H), that are loosely distributed on the sandy surface. Occasionally, in situ outcrops of rock with explicit bedding appear (Fig. 10.11, image G).

Bedforms range from flat surfaces (Fig. 10.11, images A, I) to large ripples of almost meter-sized wave length and crest heights on a decimetre scale (Fig. 10.11, image E).

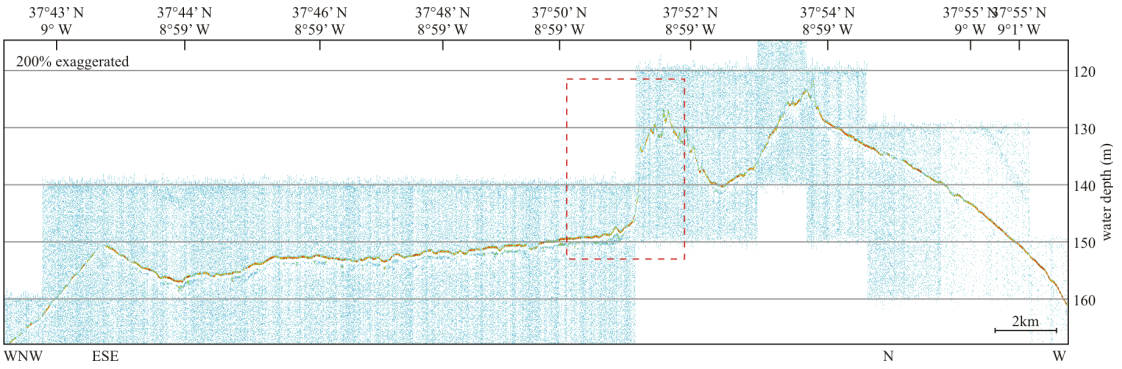

Fig. 10.9: Echosound profile, covering the location of ROV dive 3 close to Cape Sines. Red rectangle indicates the enlargement in Fig. 10.10B.

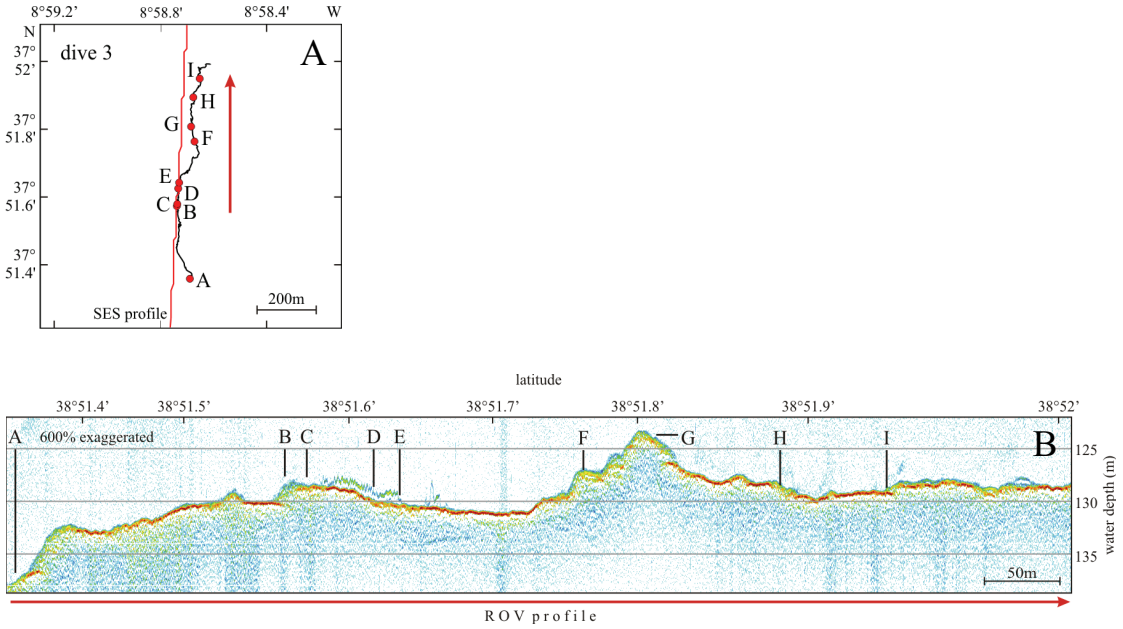

Fig. 10.10A & B: Map (A) and enlarged echosound section (B) of ROV dive 3. Letters in the graphs indicate the location of the pictures, shown in Fig. 10.11.

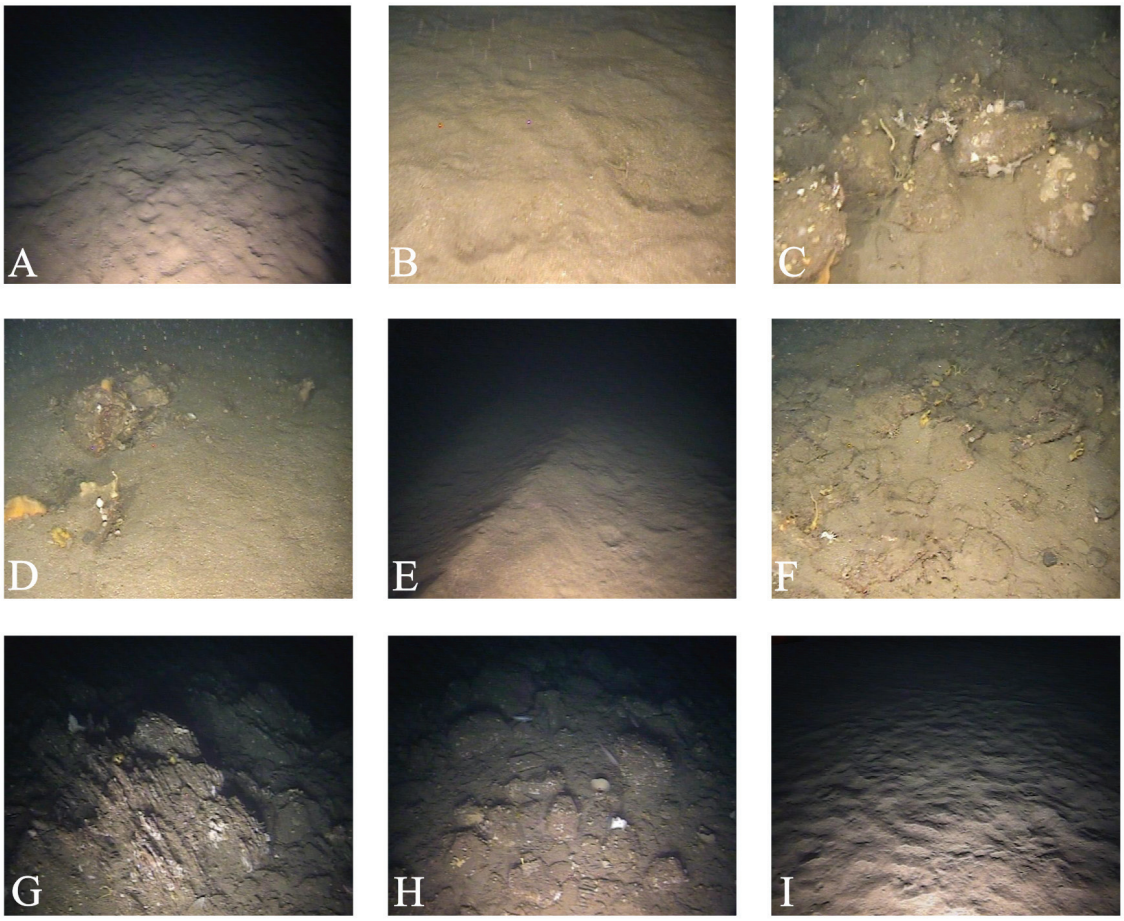

Fig. 10.11: Photographs taken during ROV dive 3. Letters in images correspond to letters in Figure 10.10A and B.

10.1.6 Dive 4

The fourth ROV dive is close to the third dive southwest of Cape Sines at 37°41'N and 8°58'W between 100 and 140m water depth, covering a South-North profile of 1740m length. The long SES profile shows a large and steep elevation, extending ca. 60m high over an otherwise flat sea floor (Fig. 10.12). This feature, that might be part of the Principes d'Avis Spur, was inspected more closely by the ROV (Fig. 10.13). Similar to the third ROV dive, the sediment textures cover the entire spectrum from flat, fine grained sediments (Fig. 10.14, image A) to coarse material, forming decimeter and meter-scale ripples (Fig. 10.14, images B, I). Well rounded boulders are observed, particularly close to an outcrop of rocks (Fig. 10.14, images D, F, G, J), which can be identified as sedimentary by their decimetre scale layering (Fig. 10.14, image H).

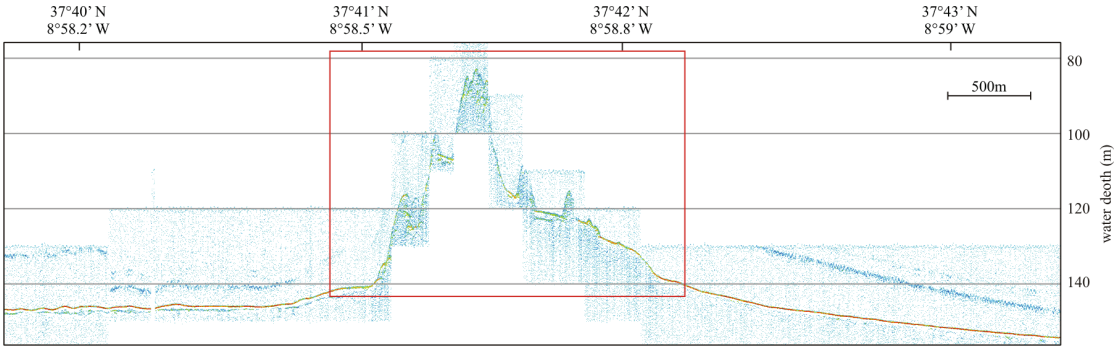

Fig. 10.12: Echosounder profile, covering the location of ROV dive 4 (Fig. 10.1). Red rectangle indicates the enlargement in Fig. 10.13B.

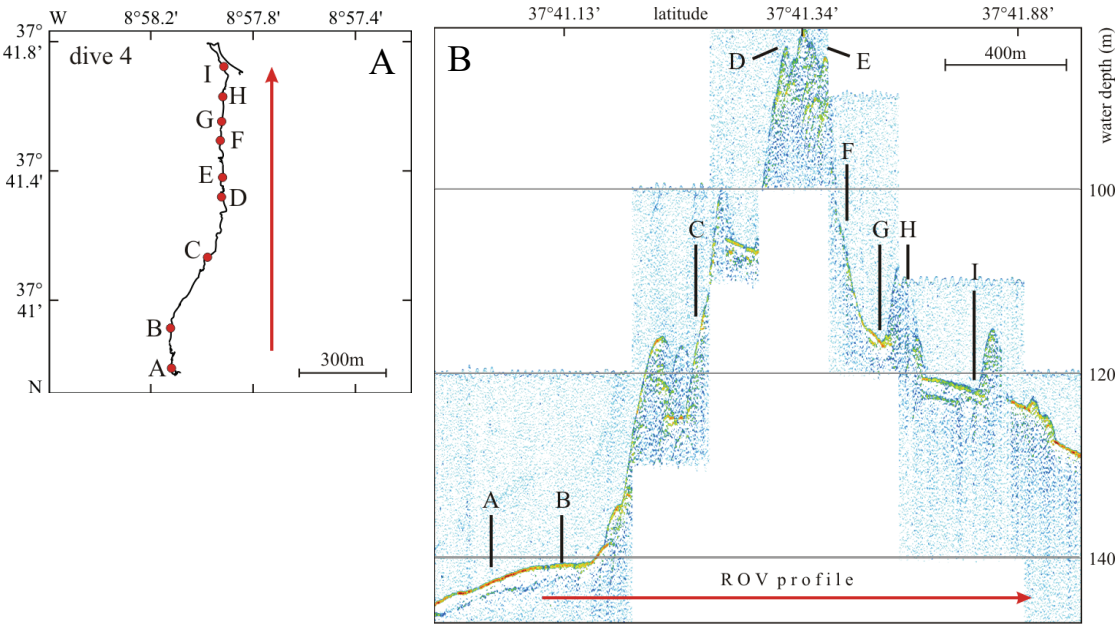

Fig. 10.13A & B: Map (A) and enlarged echosound section (B) of ROV dive 4. Letters in the graphs indicate the location of the pictures, shown in Fig. 10.14.

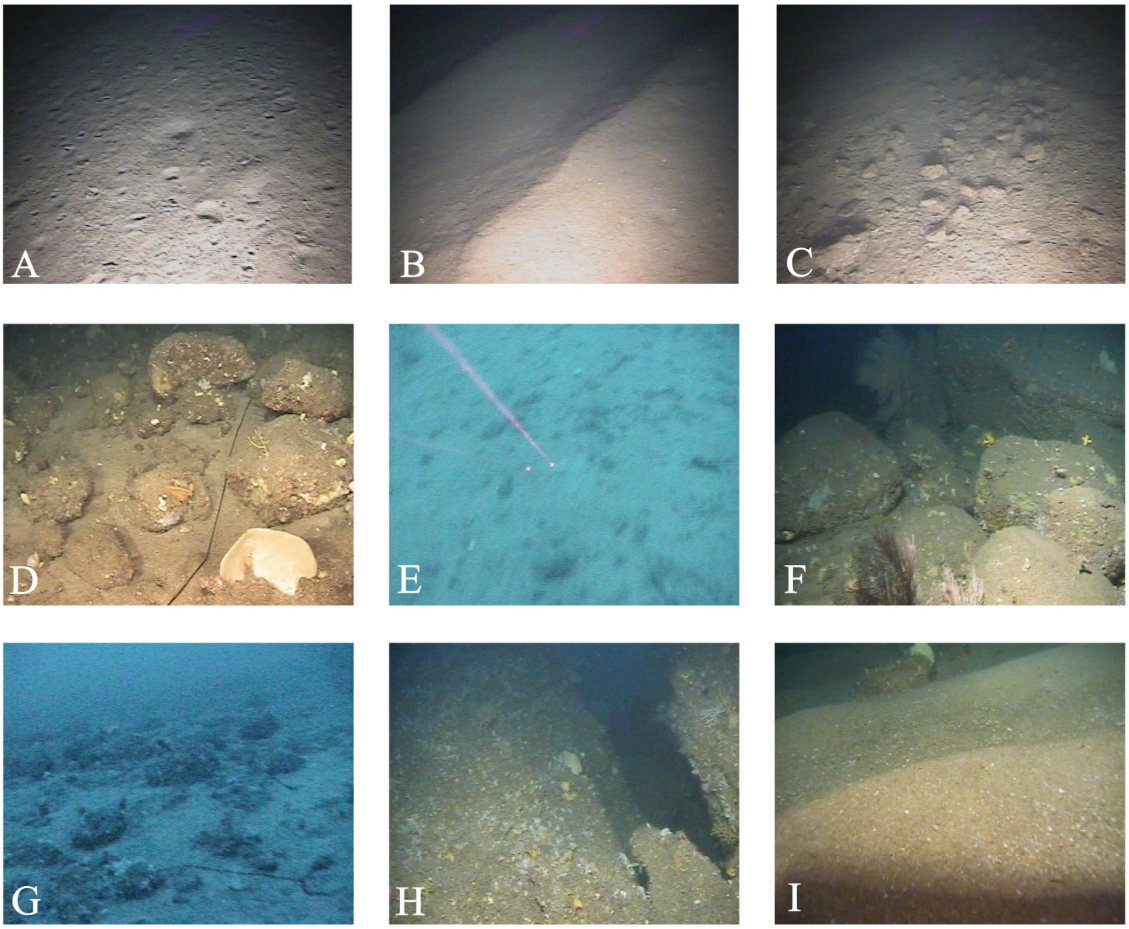

Fig. 10.14: Photographs taken during ROV dive 4. Letters in images correspond to letters in Figure 10.13A and B.

10.2 Estuary Core PO287-1

One box core (PO287-1B) was obtained from inside the Tagus Estuary (Fig. 3.2: sample Po1). Low $CaCO_3$ content, high C_{org}/N_{total} ratios and negative $\delta^{13}C_{org}$ values reveal a terrigenous source signature (Fig. 10.15). The heavy $\delta^{15}N$ signal is explained by the influence of agriculturally derived DIN (see Chapter 4, ALT-EPPING et al., 2007). However, downcore changes in the data must be considered carefully, as a large bridge was built next to the sampling location in AD1966. This most probably disturbed the sediment surface additional to natural and anthropogenic sediment reworking inside the estuary, e.g. by channel migration or dredging. This may also explain the relatively high variability of C_{org}/N_{total} ratios (±6 within the 25cm long box core) and $\delta^{13}C_{org}$ values (±1‰ within the box core), compared to e.g. box cores from the Tagus prodelta (Fig. 10.16: C_{org}/N_{total} variability maximal ±3, $\delta^{13}C_{org}$ ±0.5‰). Hence, data from this core is not used for paleoenvironmental interpretation, except for the statement, that the sediments at that location are derived from a mainly terrigenous source.

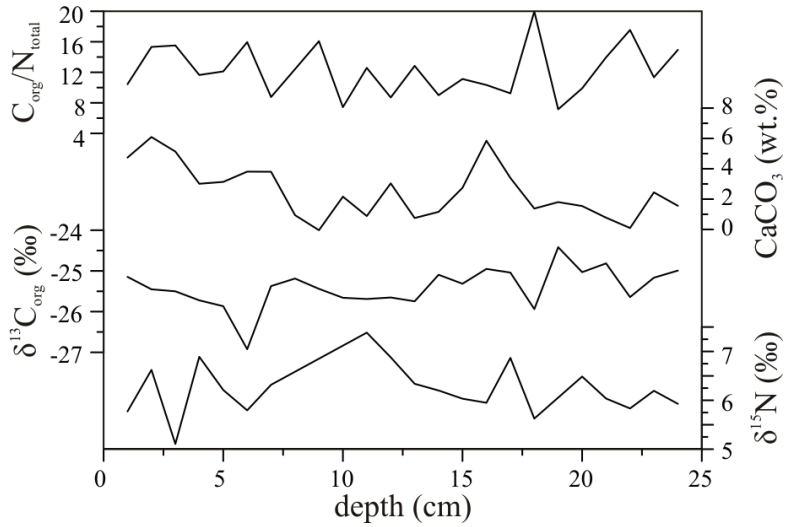

Fig. 10.15: Data of box core PO287-1 from the Tagus Estuary (for location see Fig. 3.2).

10.3 Prodelta Box Cores

Three box cores from the Tagus prodelta (Fig. 3.2: samples Po26, Po27, Po28) were analysed with respect to various biogenic sediment properties. Core PO287-26 has an age of AD1896 at 51.5cm depth, assuming full recovery of the core top (ABRANTES et al., 2006), whereas the other box cores have not been dated. Downcore variations show no significant and consistent variations in organic matter provenance, nor in the nutrient budget (Fig. 10.16). However, cores PO287-26 and PO287-27 show a higher terrigenous sediment fraction, whereas core

PO287-28 shows a strong marine organic matter source signature (Fig. 10.16). The relatively high content of terrigenous organic material in core PO287-27 is due to its closer proximity to the estuary mouth, which thus receives most continental material. Although cores PO287-26 and -28 are more or less equally far away from the estuary mouth, the higher terrigenous organic matter content in core PO287-26 may be due to the preferential southward transport of continental and estuarine organic matter. Core PO287-26 is therefore under a direct influence of the estuarine discharge and receives more continental organic matter, than core PO287-28.

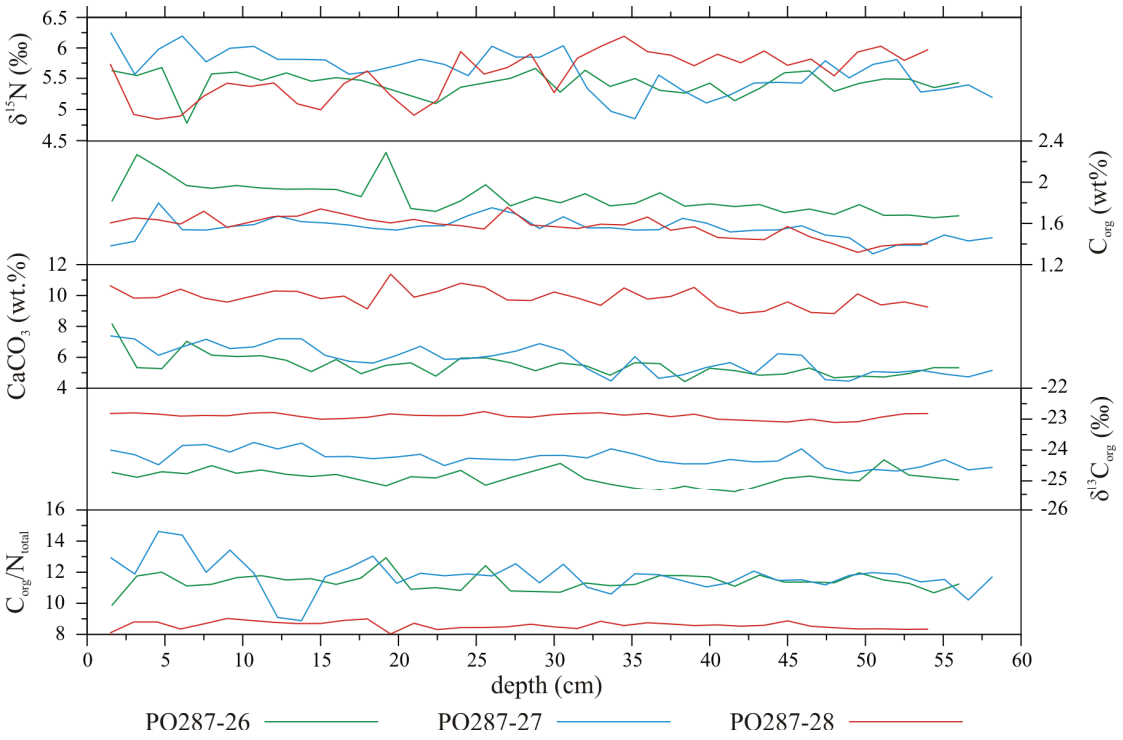

Fig. 10.16: Biogenic data of the box cores from the Tagus prodelta (PO287-26, -27, -28).

10.4 GeoB 8903: Oxygen Isotopes and Alkenones

The acquired $\delta^{18}O$ curve of core GeoB 8903 is shown in Fig. 10.17. $\delta^{18}O$ records are commonly applied for reconstructions of sea surface temperature (SST) and salinity (SSS) variations. However, in regions with a combined influence of temperature and salinity changes, such as a prodelta setting with varying freshwater discharge rates, $\delta^{18}O$ values become ambiguous, because the effect of SST or SSS changes in $\delta^{18}O$ can not be distinguished. To solve this problem, a second, salinity-independent SST proxy is required, which is here provided by an alkenone index $U^{k'}_{37}$, obtained by the IFM-Geomar, Kiel (Fig. 10.17). With this index, which is assumed to be independent on salinity (e.g. SONZOGNI et al.,

1997), it is possible to reconstruct past SSS variations by calculating $\delta^{18}O$ of the surrounding seawater according to BEMIS et al. (1998) (eq. 1),

$$SST = 16.5 - 4.8*(\delta^{18}O_{sample} - \delta^{18}O_{seawater}) \quad 1)$$

and the subsequent calculation of SSS by rearranging the equation $\delta^{18}O_{seawater} = 0.497*SSS - 17.05$ (GEOSECS data, valid for mid-latitudes, PAUL et al., 1999) to

$$SSS = (\delta^{18}O_{seawater} + 17.05)*2.012 \quad 2)$$

The results are shown in Fig. 10.13, including also an SST-reconstruction, which is based on calcareous $\delta^{18}O$. The differences between the $\delta^{18}O$-SST and alkenone-SST can be explained by changes in SSS. However, the alkenone-SST shows an instant jump from ca. 20°C to almost 24°C around 60cm core depth, followed by several other, strong fluctuations, which are – due to their magnitude – hard to explain. Additionally, the alkenone-SST record shows no correlations with other regional SST reconstructions from the Tagus prodelta (a compilation is given by BARTELS-JÓNSDÓTTIR et al., 2006). Due to this and the uncertain influence of salinity variations, caused by variations in riverine freshwater discharge through the Tagus River, the presentation of $\delta^{18}O$ and alkenone data and their application for SST and SSS reconstructions is not included into the publications.

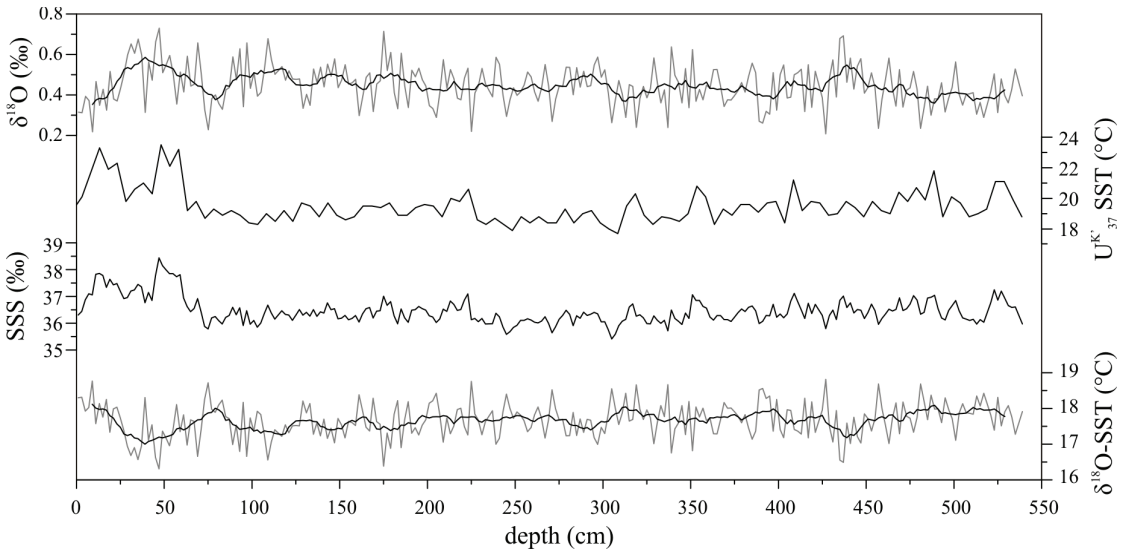

Fig. 10.17: $\delta^{18}O$ and alkenone based SST records, as well as SSS and $\delta^{18}O$-based SST reconstruction for core GeoB 8903.

10.5 GeoB 8903: Element Abundance

Except for Fe and Ca content, the results of XRF scanning (Fig. 10.14) were not integrated into a paleoenvironmental interpretation, because element abundances are very low or/and the use of the elements as paleoenvironmental proxies is not established.

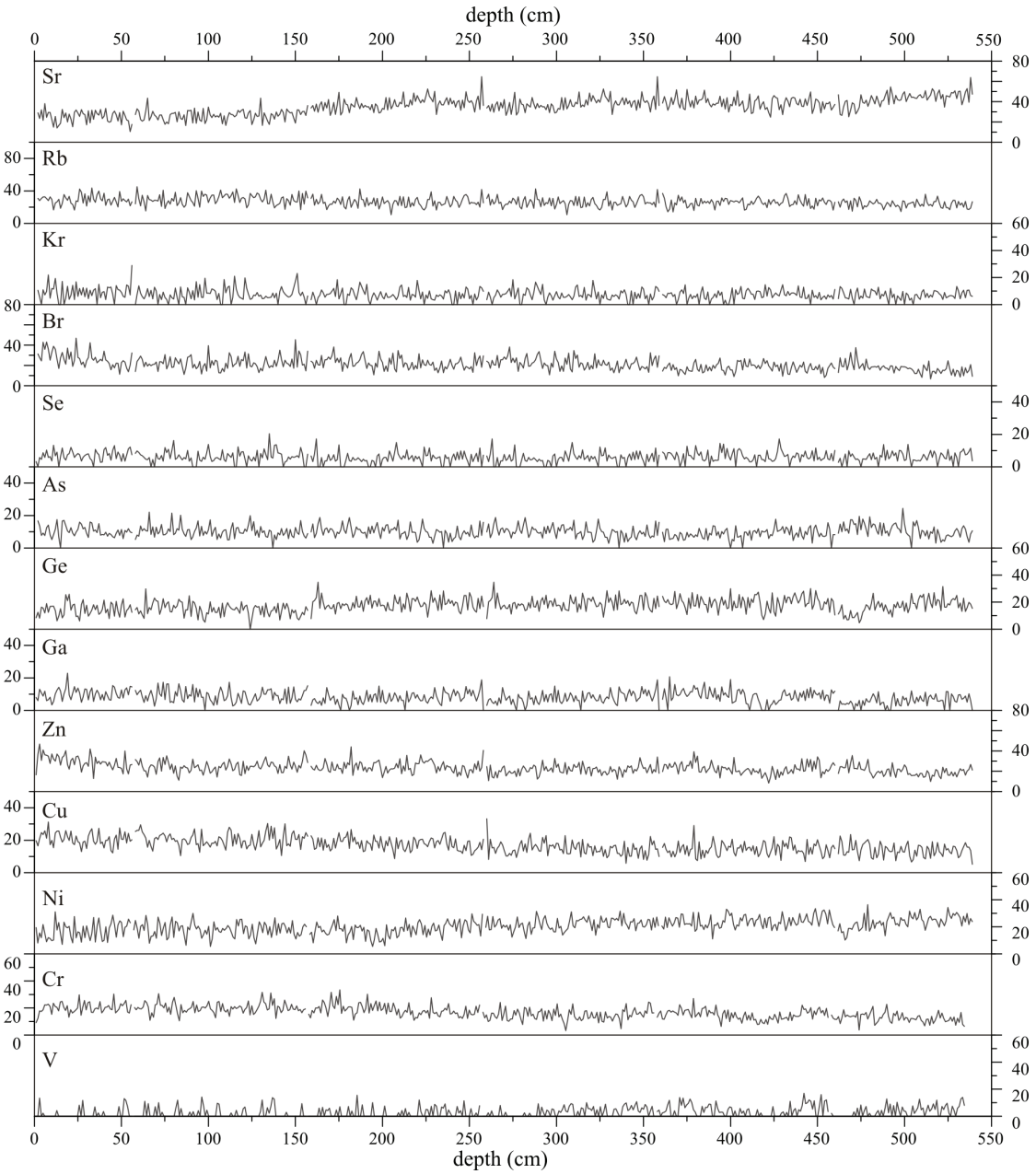

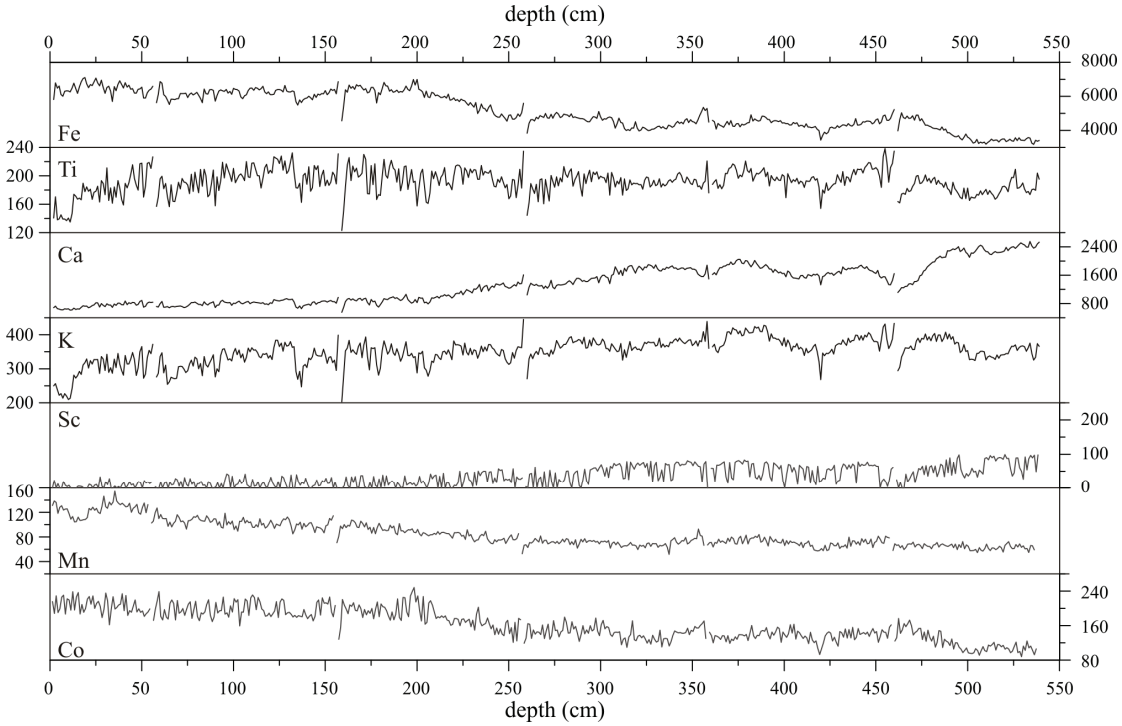

Fig. 10.18: XRF data of core GeoB 8903. Units are counts per second (cps). Breaks and associated outliers in the plot are caused by section breaks in the sediment record.

Appendix 2

–

Literature Values of Selected Proxies

Table A-1: Literature values of elemental and isotopic parameters of marine organic material

	C_{org} and N_{total} (%)	C/N	$\delta^{13}C$ (‰)	$\delta^{15}N$ (‰)
Marine realm	0.3 % C_{org} generally	8 [30, 33]	-18 [30]; -21.5 [53]; -18.5 to -20.5 [19]; -21 [33]	9 [30]; "heavy" [52]; 7.5 [33]
	0.29 to 1.37 % C_{org} on shelf [32]	intermediate and deep waters 8-10	-25.4 (sediment); -21.9 to -22.2 (suspended) [43]	deep water NO_3^-: +5 to +6 [2, 24]
		shelf 10.7±1.3; slope 8.3±0.4 [32]	-20 to -21.5 (shelf); -24 (off large rivers) [16]	POM-pre-bloom: -3 [2]
		bulk plankton 6 [37]	-16 to -23 [48]	dissolved N_2: +1, POM: -2 to +11 [35]
		shelf sediments 5-7 [39]	Beauford Sea: -22.6; Gulf of Mexico: -21.1; Bay of Bengal: -19.2 [15]	ocean water: -6 to +10 [25]
		phytoplankton 5.9; zooplankton 6.3; bacteria 4 to 5; diatoms 7.5; copepods 4.6; benthos 4.2 [all 4]	slope: -20.9±0.1; shelf sed. -21.7 to -24.5 [32]	marine plants: 1-10 [25]
			Bicarbonate (HCO_3^-) in seawater: 0 [42, 48]	marine animals: 11-24 [25]
			deep ocean: +0.6; surface ocean: +1.8 [22]	diatoms: physically protected against degradation 0 to 4 lower than bulk sediment $\delta^{15}N$ [27]; diatom bound OM southern ocean) 3.5 to 5 [7]
			dissolved marine CO_2: -8 (equilibrium with air) [26b]	
			diatoms -21 to -23 [7]	phytoplankton: "high" [5]
				chl-*a*: 5‰ lower than total cell $\delta^{15}N$ [40]

Table A-2: Literature values of elemental and isotopic parameters of continental material

	C_{org} and N_{total} (%)	C/N	$\delta^{13}C$ (‰)	$\delta^{15}N$ (‰)
Upper Estuary	1.3 to 4 % C_{org} [32]	8 (sediment: 17; suspended: 8.9) [30]	-29 (sediment: -26.3; suspended: -28.9) [30]	15 (sediment: 6.9; suspended matter: 8.9) [30]
		16.4±2.6 (sediment) [32]	-25 (suspended) [8]	
			-30 [12]; -25 to -27.3 [32]	
			saltmarsh: -15 to -9; freshwater marsh: -33 to -23 [10]	
Lower Estuary			-18.7 to -21.7 (suspended) [8]	
			-18 [12]	
Riverine Organic Matter	1.3 to 4 % C_{org} [32]	7.5 [30]	-30 [30]	9 [30]
		9.6±1.2 (suspended) [32]	-28 (sediment) [43]	detrital: 2.8 [45]
		10 to 11 (fine suspended) [39]	-25 to -27.3 (suspended) [32]	polluted by agriculture: ca. 15 [51]

Table A-3: Literature values of elemental and isotopic parameters in the terrestrial and atmospheric realms

	C_{org} and N_{total} (%)	C/N	$\delta^{13}C$ (‰)	$\delta^{15}N$ (‰)
Terrestrial organic matter/Plants		21 [30]; 18 [33] 10 to 24 (average) [38] C3 plants: 12 [50]; >20 [54] C4 plants: >30 [26]	-26 [30, 53, 33]; -27.1 [49]; -26.5 [52] C3 plants: -28 to -26 [50]; >-28 [54]; -27.6 [47]; -23 to -34 [48] C4 plants: -13 [44]; -10 to -18 [48] lipids: "+8 comp. to whole plant" [34]	3.5 [30]; "light" [52]; 1 [33]; 3 [51] plants: -8 to +10; animals: 2 to 15 [25] -1.8±0.8 (land plants) [52]; -10 to +10 [29]; -8 to +10 [25] leafs: -8 to +3 [35] N_2-fixers: 0±2 [35]
Soil organic matter		6-14 [21]	-26 [21]	4.1±.0.4 [52]; -4 to +14 [35]; -1 to +18 [25] "higher in cultivated soil compared to virgin soil" [6] bulk: <2; NH_4^+: >3; NO_3^-: 3 to 18; N_2: -2 to +15 [29]
Atmosphere			CO_2: -7 [42]; 8 [55]; -7 to -9 [48] CO_2: -7.5 [22]; decrease of 1.5 since AD1800 [14]	N_2: 0 [29] NH_4^+: +10 to -2 [29] NO_3^-: +3 to -7 [29] precipitation: NH_4^+: -18 to +8; NO_3^-: -15 to +3 [35] NO_3^- and NH_4^+ in rainwater: -17 to +4 [25]

Table A-4: Elemental and isotopic properties of other materials and important, biasing processes

	C_{org} and N_{total} (%)	C/N	$\delta^{13}C$ (‰)	$\delta^{15}N$ (‰)
Terrestrial organic matter/Plants	bacteria 4-6 % N [39b] proteins: 15 to 19% N on average (protein content of: higher terr. plants: 1 to 10%; algae 20 to 30%; phytoplankton 34%; zooplankton 57%; bacteria 80%) [4]	bacteria: 4 [4]	dust Sahara: -19 [11] fossil fuel burning emissions: -28; coal: -24; oil/gas: -27.3 [22] labile components (amino acids, carbohydrates, proteins [20, 17]) enriched in ^{13}C = high $\delta^{13}C_{org}$ [9, 28] refractory compounds (lignin in vascular vegetation, lipids, cellulose): depleted in ^{13}C =low $\delta^{13}C_{org}$ [23, 36, 9, 28]	treated sewage: ~10 [18] animals: 5-15 [29] sediment NO_3^-: -8 to 0 [29] petroleum: >2 [29]; coal/oil: 3 to 15 [25] fertilizer: 10 to 12 [3]; NH_4^+: 0; NO_3^-: 3 [35] fossil fuel emission: NOx: -2 to +4; NH_3: -8 to -4 [35] bacteria "high" [39] proteins: 3 higher than total δN [33]
Soil organic matter	N is generally preferentially remineralized, inorganically sorbed and assimilated by benthos [31]	preferential degradation of N commonly increasing C/N with depth [31], but… …C_{org}/N_{total} ratios potentially lowered by adsorption of N to clay lattices [31] (especially in Illite: NH_4^+ substitutes for K^+) [e.g. 46]	decrease by early loss of labile components (may account for 2 to 6‰) temperature effect: decreasing $\delta^{13}C_{org}$ with decreasing water temperature [15] (0,2‰/°C [41]; 0.5‰/°C below 28°C [13]), at least partly attributed to higher CO_2 solubility in cold water [16]	decrease early loss of labile components, e.g. deeper trap material: -1‰ due to protein degradation [1]

Tables A-1 to A-4: Compilation of literature values for C_{org}, N_{total}, C_{org}/N_{total}, $\delta^{13}C_{org}$ and $\delta^{15}N$. Several values must be seen in the context of the respective study. Particularly average values are shown with decimal places, implying a precision, which is not achieved by analytical methods and thus false. Nevertheless typical ranges for the proxies become roughly evident, but also the various processes and parameters, that affect each proxy, such as dependencies on temperature, grain-size, specific organic compound or chemical species, that has been analysed.

References

1. Altabet, M.A., W.G. Deuser, S. Honjo, C. Stienen (1991): Seasonal and depth-related changes in the source of sinking particles in the North Atlantic. Nature 354: 136–139.

2. Altabet, M.A. (1996): Nitrogen and carbon isotopic tracers of the source and transformation of particles in the deep sea. In: (Ittekkot, V., P. Schäfer, S. Honjo, P.J. Depetris (Eds.): Particle Flux in the Ocean. Scientific Committee On Problems of the Environment (SCOPE). John Wiley & Sons Ltd., London, pp. 155-184 (chapter 8).

3. Amberger, A., H.-L. Schmidt (1987): Natürliche Isotopengehalte von Nitrat als Indikatoren für dessen Herkunft. Geochimica et Cosmochimica Acta 51: 2699-2705.

4. Bordovskiy, O.K. (1965): Accumulation of organic matter in bottom sediments. Marine Geology 3: 33-82.

5. Brabandere, L.D., F. Dehairs, S.V. Damme, N. Brion, P. Meire, N. Daro (2002): $\delta^{15}N$ and $\delta^{13}C$ dynamics of suspended organic matter in freshwater and brackish waters of the Scheldt estuary. Journal of Sea Research 48: 1-15 (p. 9 and references therein).

6. Bremner, J.M., M.A. Tabatabai (1973): Nitrogen-15 enrichment of soils and soil derived nitrate. Journal of environmental Quality 2 (3): 363-365.

7. Crosta, X., A. Shemesh (2002): Reconciling down core anticorrelation of diatom carbon and nitrogen isotopic ratios from the Southern Ocean. Paleoceanography 17 (1): 101-108.

8. Dauby, P., F. Mosora, M. Frankignoulle, J.M. Bouquegneau (1992): La matière en suspension de la couche de surface du plateau continental nord-ouest européen. I. Distribution spatial de la biomasse et du rapport $^{13}C/^{12}C$. Bulletin de la Société Royale des Sciences de Liège 61 (1-2) : 63-70 (cited from [1]).

9. Degens, E.T. (1969): Biogeochemistry of Stable Carbon Isotopes. In: Eglinton, E., M.T.J. Murphy (Eds.): Organic Geochemistry. Berlin, Springer: 304-329 (cited from [51]).

[10] Deines, P. (1980): The isotopic composition of reduced organic carbon. In: P. Fritz and J.Ch. Fontes (Eds.): Handbook of Environmental Isotope Geochemistry, Vol. 1. Elsevier, New York, pp. 329-406 (cited from [10] and [51]).

[11] Eglinton T.I., G. Eglinton, L. Dupont, E.R. Sholkovitz, D. Montluçon, C.M. Reddy (2002): Composition, age, and provenance of organic matter in NW African dust over the Atlantic Ocean. Geochemistry, Geophysics, and Geosystems 3 (8): 1050, doi:10.1029/2001GC000269.

[12] Fichez, R., P. Dennis, M.F. Fontaine, T.D. Jickells (1993) : Isotopic and biochemical composition of particulate organic matter in a shallow water estuary (Great Ouse, North Sea, England). Marine Chemistry 43: 263–276 (cited from [10]).

[13] Fontugne, M.R., J.C. Duplessy (1981): Organic carbon isotopic fractionation by marine phytoplankton in the temperature range -1 to 31°C. Oceanologica Acta 4 (1): 85-90.

[14] Friedli, H., H. Lötscher, H. Oeschger, U. Siegenthaler, B. Stauffer (1986): Ice core record of the $^{13}C/^{12}C$ ratio of the atmosphere in the past two centuries. Nature 324: 237-238 (cited from "Isotope Geochemistry Lecture Notes", Fig. 37.3: http://www.geo.cornell.edu/geology/classes/GEO656.html).

[15] Gearing, P.J. (1975): Organic carbon stable isotope ratios of continental margin sediments. PhD Thesis, University of Texas, 154 pages (cited from Tan, F.C., P.M. Strain (1979): Organic carbon isotope ratios in recent sediments in the St. Lawrence Estuary and Gulf of St. Lawrence. Estuarine and Coastal Marine Science 8: 213-225).

[16] Gearing, P., F.E. Plucker, P.L. Parker (1977): Organic carbon stable isotope ratios of continental margin sediments. Marine Chemistry 5: 251-266.

[17] Harvey H.R., J.H. Tuttle, J.T. Bell (1995): Kinetics of phytoplankton decay during simulated sedimentation: Changes in biochemical composition and microbial activity under oxic and anoxic conditions. Geochimica et Cosmochimica Acta 59 (16): 3367–3377 (cited from [51]).

[18] Heaton, T.H.E. (1986): Isotopic studies of nitrogen pollution in the hydrosphere and atmosphere: A review. Chemical Geology 59: 87-102.

[19] Hedges, J.I., P.L. Parker (1976): Land-derived organic matter in surface sediments from the Gulf of Mexico. Geochimica et Cosmochimica Acta 40: 1019-1029 (cited from [27]).

[20] Hedges J.I., W.A. Clark, G.L. Cowie (1988): Fluxes and reactivities of organic matter in a coastal marine bay. Limnology and Oceanography 33 (5): 1137-1152 (cited from [51]).

[21] Hedges, J.I., J.M. Oades (1997): Comparative organic geochemistries of soils and marine sediments. Organic Geochemistry 27 (7/8): 319-361.

[22.] Heimann, M., E. Maier-Reimer (1996): On the relations between the oceanic uptake of CO_2 and its carbon isotopes. Global Biogeochemical Cycles. 10: 89-110 (cited from "Isotope Geochemistry Lecture Notes", Fig. 37.1: http://www.geo.cornell.edu/geology/classes/GEO656.html).

[23.] Hillaire-Marcel, G. (1989): Isotopes and Food. In: P. Fritz, J.C. Fontes (Eds.): Handbook of Environmental Isotope Geochemistry. Elsevier, Amsterdam, The Netherlands: 507-547.

[24.] Holmes, E., P. Müller, R.R. Schneider, M. Segl, G. Wefer (1998): Spatial variations in euphotic zone nitrate utilization based on d15N in surface sediments. Geo-Marine Letters 18: 58-65.

[25.] Kelly, S.D., C. Stein, T.D. Jickells (2005): Carbon and nitrogen isotopic analysis of atmospheric organic matter. Atmospheric Environment 39: 6007–6011.

[26.] Lamb, A.L., G.P. Wilson, M.J. Leng (2006): A review of coastal palaeoclimate and relative sea-level reconstructions using $\delta^{13}C$ and C/N ratios in organic material. Earth-Science Reviews 75: 29– 57 (cited from Meyers, P.A. (1994): Preservation of elemental and isotopic source identification of sedimentary organic matter. Chemical Geology 114: 289-302).

[26b] Lamb, A.L., G.P. Wilson, M.J. Leng (2006): A review of coastal palaeoclimate and relative sea-level reconstructions using $\delta^{13}C$ and C/N ratios in organic material. Earth-Science Reviews 75: 29– 57 (cited from Keeley, J.E., D.R. Sandquist (1992): Carbon: freshwater plants. Plant, Cell and Environment 15, 1021- 1035.

[27.] Lavik, G. (2001): Nitrogen Isotopes of sinking matter and sediments in the South Atlantic. Fachbereich Geowissenschaften. Universität Bremen: 140; Sigman, D.N., M.A. Altabet, R. Francois, D.C. McCorkle, J.-F. Gaillard (1999): The isotopic composition of diatom-bound nitrogen in Southern Ocean sediments. Paleoceanography 14 (2): 118-134.

[28.] Lehmann, M.F., S.M. Bernasconi, A. Barbieri, J.A. McKenzie (2002): Preservation of organic matter and alteration of its carbon and nitrogen isotope composition during simulated and in situ early sedimentary diagenesis. Geochimica et Cosmochimica Acta 66 (20): 3573–3584.

[29.] Létolle, R. (1980): Nitrogen-15 in the natural environment. In: Fritz, P.-L., J.-C. Fontes (Eds.): Handbook of environmental isotope geochemistry. Elsevier, Amsterdam, The Netherlands: 545 pages.

[30.] Middelburg, J.J., J. Nieuwenhuize (1998): Carbon and nitrogen stable isotopes in suspended matter and sediments from the Schelde estuary. Marine Chemistry 60 (3/4): 217-225.

[31.] Müller, P.J. (1977): C/N ratios in Pacific deep-sea sediments: effect of inorganic ammonium and organic nitrogen compounds sorbed by clays. Geochimica et Cosmochimica Acta 41: 765-776.

[32.] Nagao, S., T. Usui, M. Yamamoto, M. Minagawa, T. Iwatsuki, A. Noda (2005): Combined use of $\delta^{14}C$ and $\delta^{13}C$ values to trace transportation and deposition processes of terrestrial particulate organic matter in coastal marine environments. Chemical Geology 218: 63-72.

[33.] Ogrinc, N., G. Fontolan, J. Faganeli, S. Covelli (2005): Carbon and nitrogen isotope compositions of organic matter in coastal marine sediments (the Gulf of Trieste, N Adriatic Sea): indicators of sources and preservation. Marine Chemistry 95 (3-4): 163-181 (cited from various literature).

[34.] Park, R., S. Epstein (1961): Metabolic fractionation of ^{12}C and ^{13}C in plants. Plant Physiology 36 (2): 133-138.

[35.] Peterson, B., B. Fry (1987): Stable Isotopes in Ecosystem Studies. Annual Review of Ecology and Systematics 18: 293-320 (and various references therein).

[36.] Prahl, F.G., G.J. de Lange, S. Scholten, G.L. Cowie (1997): A case of post-depositional aerobic degradation of terrestrial organic matter in turbidite deposits from the Madeira Abyssal Plain. Organic Geochemistry 27 (3/4): 141-152.

[37.] Redfield, A.C., B.H. Ketchum, F.A. Richards (1963): The influence of organisms on the composition of seawater. In: Hill, M.N. (Ed.), The Sea, Vol. 2, Wiley, New York: 26-79 (cited from [27]).

[38.] Romankevich, E.A. (1990): Biogeochemical problems of living matter of the present-day biosphere. In: Ittekkot, V., S. Kempe, W. Michaelis, A. Spitzy (Eds.): Facets of modern Biogeochemistry: 39-51 (cited from [27]).

[39.] Ruttenberg, K.C., M.A. Goñi (1997): Phosphorous distribution, C/N/P ratios and $\delta^{13}C_{org}$ in arctic, temperate and tropical coastal sediments: Tools for characterizing bulk sedimentary organic matter. Marine Geology 139: 123-145 (cited from Holtvoeth, J. (2004): Terrigenous organic matter in sediments of the eastern equatorial Atlantic - distribution, reactivity and relation to Late Quaternary climate. Department of Geosciences. Bremen, University of Bremen: 149, page 85).

[39b] Ruttenberg, K.C., M.A. Goñi (1997): Phosphorous distribution, C/N/P ratios and $\delta^{13}C_{org}$ in arctic, temperate and tropical coastal sediments: Tools for characterizing bulk sedimentary organic matter. Marine Geology 139: 123-145 (cited from Goñi, M.A., J.I. Hedges (1995): Sources and reactivities of marine-derived organic matter in coastal sediments as determined by alkaline CuO oxidation. Geochimica et Cosmochimica Acta 59 (14): 2956–2981).

[40.] Sachs, J.P., D.J. Repeta, R. Goericke (1999): Nitrogen and carbon isotopic ratios of chlorophyll from marine phytoplankton. Geochimica et Cosmochimica Acta 63(9): 1431-1441.

[41.] Sackett, W.M., W.R. Eckelmann, M.L. Bender, A.W.H. Bé (1965): Temperature dependence of carbon isotope composition in marine plankton and sediments. Science 148: 235-237.

[42.] Sackett, W.M. (1989): Stable carbon isotope studies on organic matter in the marine environment. In: P. Fritz, J.C. Fontes (Eds.): Handbook of Environmental Isotope Geochemistry. Elsevier, Amsterdam, The Netherlands: 139-169.

[43.] Salomons, W., W. Mook (1981): Field observations of the isotopic composition of particulate organic carbon in the southern North Sea and the adjacent estuaries. Marine Geology 41: 11-20 (cited from [1])

[44.] Schlünz, B. (1998): Riverine organic carbon input to the ocean in relation to late quaternary climate change. PhD Thesis, Fachbereich Geowissenschaften, Universität Bremen 116: 136 pages.

[45.] Schubert, C.J., S.E. Calvert (2001): Nitrogen and carbon isotopic composition of marine and terrestrial organic matter in Arctic Ocean sediments: Implications for nutrient utilization and organic matter composition. Deep-Sea Research I 48: 789-810.

[46.] Schwertmann U. E.-A. Niederbudde (1993): Tonminerale in Böden. In: Jasmund K., G. Lagaly (Eds.): Tonminerale und Tone: Struktur, Eigenschaften, Anwendungen und Einsatz in Industrie und Umwelt: pp. 212-262. Steinkopf, Darmstadt.

[47.] Showers, W.J., D.G. Angle (1986): Stable isotopic characterization of organic carbon accumulation on the Amazon continental shelf. Continental Shelf Research 6 (1/2): 227-244 (cited from [14])

[48.] Smith, B.N., S. Epstein (1977): Two categories of 13C/12C ratio for higher plants. Plant Physiology 47: 380-384.

[49.] Thornton, S.F., J. McManus (1994): Application of organic carbon and nitrogen stable isotope and C/N ratios as source indicators of organic matter provenance in estuary systems: evidence from the Tay Estuary, Scotland. Estuarine, Coastal and Shelf Sciences 38: 219-233 (cited from [1]).

[50.] Tyson, R.V. (1995): Sedimentary Organic Matter: Organic Facies and Palynofacies. Chapman & Hall, London (cited from [10]).

[51.] Voss, M., U. Struck (1997): Stable nitrogen and carbon isotopes as indicator of eutrophication of the Oder river (Baltic Sea). Marine Chemistry 59: 35-49 (terrigenous $\delta^{15}N$ values cited from [43] and [6]).

[52.] Wada, E., M. Minagawa, H. Mizutani, T. Tsuji, R. Imaizumi, K. Karasawa (1987): Biogeochemical studies on the transport of organic matter along the Otsuchi River watershed, Japan. Estuarine, Coastal and Shelf Sciences 25: 321-336 (cited from [1]).

[53.] Westerhausen, L., J. Poynter, G. Eglinton, H. Erlenkeuser, M. Sarnthein (1993): Marine and terrigenous origin of organic matter in modern sediments of the equatorial East Atlantic: The $\delta^{13}C$ and molecular record. Deep-Sea Research I 40: 1087-1121.

[54.] Wilson, G.P., A.L. Lamb, M.J. Leng, S. Gonzalez, D. Huddart (2005): $\delta^{13}C$ and C/N as potential coastal palaeoenvironmental indicators in the Mersey Estuary, UK. Quaternary Science Reviews 24: 2015-2029.

[55.] Yeh, H.-W., W.-M. Wang (2001): Factors Affecting the Isotopic Composition of Organic Matter. (1) Carbon Isotopic Composition of Terrestrial Plant Materials. Proclamations of the National Science Council, China 25 (3): 137-147.

12 References for Chapters 1 – 10

Abrantes, F., M.T. Moita (1999): Water column and recent sediment data on diatoms and coccolithophorids, off Portugal, confirm sediment record of upwelling events. Oceanologica Acta 22(3): 319-336.

Abrantes, F., N. Lancaric, J. Moreno, M. Mil-Homens, U. Pflauman (2001): Paleoceanographic conditions along the Portuguese Margin during the last 30ka: a multiple proxy study. Comunicações do Instituto Geológico e Mineiro 88: 161-184.

Abrantes, F., S. Lebreiro, T. Rodrigues, I. Gil, H. Bartels-Jónsdóttir, P. Oliveira, C. Kissel, J.O. Grimalt (2005): Shallow-marine sediment cores record climate variability and earthquake activity off Lisbon (Portugal) for the last 2000 years. Quaternary Science Reviews 24: 2477–2494.

Alt-Epping, U., M. Mil-Homens, D. Hebbeln, F. Abrantes, R.R. Schneider (2007): Provenance of organic matter and nutrient conditions on a river- and upwelling influenced shelf: A case study from the Portuguese Margin. Marine Geology 243: 169-179.

d'Abreu, L., N.J. Shackleton, J. Schoenfeld, M. Hall, M. Chapman (2003): Millennial-scale oceanic climate variability of the Western Iberian margin during the last two glacial periods. Marine Geology 196: 1-20.

van Aken, H.M. (2000a): The hydrography of the mid-latitude northeast Atlantic Ocean I: The deep water masses. Deep-Sea Research I 47: 757-788.

van Aken, H.M. (2000b): The hydrography of the mid-latitude Northeast Atlantic Ocean II: The intermediate water masses. Deep-Sea Research I 47: 789-824.

Altabet, M.A., R. Francois (1994): Sedimentary nitrogen isotopic ratio as a recorder for surface ocean nitrate utilization. Global Biogeochemical Cycles 8(1): 103-116.

Andrade, C., M.C. Freitas, J.M. Miranda, M.A. Baptista, M. Cachao, P. Silva, J. Munha (2003): Recognizing possible tsunami sediments in the ultradissipative environment of the Tagus Estuary (Portugal). Coastal Sediments, Clearwater Beach, Florida, USA.

Araujo, M.F., J.M. A. Dias, J.M. Jouanneau (1994): Chemical characterisation of the main fine sedimentary deposit at the northwestern Portuguese shelf. Gaia 9: 59-65.

Baas, J.H., J. Mienert, F. Abrantes, M.A. Prins (1997): Late Quaternary sedimentation on the Portuguese continental margin: climate-related processes and products. Paleogeography, Paleoclimatology, Paleoecology 130: 1-23.

Baptista, M.A., S. Heitor, J.M. Miranda, P. Miranda, L.M. Victor (1988): The 1755 Lisbon tsunami; evaluation of the tsunami parameters. Journal of Geodynamics 25: 143-157.

Baptista, M.A., J.M. Miranda, F. Chierici, N. Zitellini (2003): New study of the 1755 earthquake source based on multi-channel seismic survey data and tsunami modeling. Natural Hazards and Earth System Sciences 3: 333-340.

Bartels-Jónsdóttir, H.B., K.L. Knudsen, F. Abrantes, S. Lebreiro, J. Eiríksson (2006): Climate variability during the last 2000 years in the Tagus Prodelta, western Iberian Margin: Benthic foraminifera and stable isotopes. Marine Micropaleontology 59(2): 83-103.

Bemis, B.E., H.J. Spero, J. Bijma, D.W. Lea (1998): Reevaluation of the oxygen isotopic composition of planktonic foraminifera: Experimental results and revised paleotemperature equations. Paleoceanography 13(2): 150-160.

Benito, G., A. Sopena, Y. Sanchez-Moya, M.J. Machado, A. Perez-Gonzalez (2003): Palaeoflood record of the Tagus River (Central Spain) during the Late Pleistocene and Holocene. Quaternary Science Reviews 22: 1737-1756.

Benner, R., M.L. Fogel, E.K. Sprague, R.E. Hodson (1987): Depletion of 13C in lignin and its implications for stable carbon isotope analysis. Nature 329(22): 708-710.

Bianchi, G.G., I.N. McCave (1999): Holocene periodicity in North Atlantic climate and deep-ocean flow south of Iceland. Nature 397: 515-517.

Blott, S.J., K. Pye (2001): Gradistat: A grain size distribution and statistics package for the analysis of unconsolidated sediments. Earth Surface Processes and Landforms 26: 1237-1248.

Bordovskiy, O.K. (1965): Sources of organic matter in marine basins. Marine Geology 3: 5-31.

Brandes, J.A., A.H. Devol (1997): Isotopic fractionation of oxygen and nitrogen in coastal marine sediments. Geochimica et Cosmochimica Acta 61(9): 1793-1801.

Cabecadas, L. (1999): Phytoplankton production in the Tagus estuary (Portugal). Oceanologica Acta 22(2): 205-214.

Castanheiro, J.M. (1982): Distribution, transport and sedimentation of suspended matter in the Tejo Estuary. In: Estuarine processes: an application to the Tagus Estuary. Proceedings of a UNESCO/IOC/CAN workshop. Palácio Foz, Lisbon, Portugal, pp. 75-90.

DeNiro, M.J., S. Epstein (1978): Influence of diet on the distribution of carbon isotopes in animals, Geochimica et Cosmochimica Acta 42: 495-506.

DeNiro, M.J., S. Epstein (1981): Influence of diet on the distribution of nitrogen isotopes in animals, Geochimica et Cosmochimica Acta 45: 341-351.

Desprat, S., M.F.S. Goni, M.F. Loutre (2003): Revealing climatic variability of the last three millennia in northwestern Iberia using pollen influx data. Earth and Planetary Science Letters 213: 63-78.

Dias, J.M.A. (1987): Dinamica sedimentar e evolucao recente da plataforma continental portuguesa setentrional. Lisbon, Universidade clássica de Lisboa.

Dias, J.M.A., T. Boski, A. Rodrigues, F. Magalhaes (2000): Coast line evolution in Portugal since the Last Glacial Maximum until present – a synthesis. Marine Geology 170: 177-186.

Dias, J.M.A., J.M. Jouanneau, R. Gonzalez, M.F. Araujo, T. Drago, C. Garcia, A. Oliveira, A. Rodrigues, J. Vitorino, O. Weber (2002a): Present day sedimentary processes on the northern Iberian shelf. Progress in Oceanography 52: 249-259.

Dias, J.M.A., R. Gonzalez, C. Garcia, V. Diaz-del-Rio (2002b): Sediment distribution patterns on the Galicia-Minho continental shelf. Progress in Oceanography 52: 215-231.

Drago, T., A. Oliveira, F. Magalhaes, J. Cascalho, J.M. Jouanneau, J. Vitorino (1998): Some evidence of northward fine sediment transport in the Portuguese continental shelf. Oceanologica Acta 21(2): 223-231.

Drago, T., F. Araujo, P. Valerio, O. Weber, J.M. Jouanneau (1999): Geomorphological control of fine sedimentation on the northern Portuguese shelf. Boletin Instituto Espanol de Oceanografia 15(1-4): 111-122.

Eiriksson, J., H.B. Bartels-Jonsdóttir, A.G. Cage, E.R. Gudmundsdóttir, D. Klitgaard-Kristensen, F. Marret, T. Rodrigues, F. Abrantes, W.E.N. Austin, H. Jiang, K.-L. Knudsen, H.-P. Sejrup (2006): Variability of the North Atlantic Current during the last 2000 years based on shelf bottom water and sea surface temperatures along an open ocean/shallow marine transect in western Europe. The Holocene 16(7): 1017-1029.

Field, C.B., Behrenfeld, M.J., Randerson, J.T., Falkowski, P. (1998): Primary production of the Biosphere: Integrating Terrestrial and Oceanic Components. Science 281: 237-240.

Fiúza, A.F., M.E.d. Macedo, M.R. Guerreiro (1982): Climatological space and time variation of the Portuguese coastal upwelling. Oceanologica Acta 5(1): 31-40.

Fiúza, A.F.G. (1983): Upwelling patterns off Portugal. In: Suess, E., J. Thiede (eds.): Coastal Upwelling: Its Sediment Record. New York, NATO Conference Series IV: 85-98.

Fiúza, A.F.G., M. Hamann, I. Ambar, G.D.d. Rio, N. Gonzales, J.M. Cabanas (1998): Water masses and their circulation off western Iberia during May 1993. Deep-Sea Research I 45: 1127-1160.

Folk, R.L., W.C. Ward (1957): Brazos River bar: A study in the significance of grain-size parameters. Journal of Sedimentary Petrology 27: 3-26.

Fontugne, M.R., J.C. Duplessy (1981): Organic carbon isotopic fractionation by marine phytoplankton in the temperature range -1 to 31°C. Oceanologica Acta 4(1): 85-90.

Freitas, M.C., C. Andrade, J.C. Moreno, J.M. Munhá, M. Cachao (1999): The sedimentary record of recent (last 500 years) environmental changes in the Seixal Bay marsh, Tagus Estuary, Portugal. Geologie en Mijnbouw 77: 283-293.

Freudenthal, T., S. Neuer, H. Meggers, R. Davenport, G. Wefer (2001a): Influence of lateral particle advection and organic matter degradation on sediment accumulation and stable nitrogen isotope ratios along a productivity gradient in the Canary Islands region. Marine Geology 177(1-2): 93-109.

Freudenthal, T., T. Wagner, V. Wenzhöfer, M. Zabel, G. Wefer (2001b): Early diagenesis of organic matter from sediments of the eastern subtropical Atlantic: evidence from stable nitrogen and carbon isotopes. Geochimica et Cosmochimica Acta 65(11): 1795-1808.

Gearing, P.J. (1975): Organic carbon stable isotope ratios of continental margin sediments. PhD Thesis, University of Texas: 154 pages.

Gearing, P., F.E. Plucker, P.L. Parker (1977): Organic carbon stable isotope ratios of continental margin sediments. Marine Chemistry 5: 251-266.

Gil, I.M., F. Abrantes, D. Hebbeln (2006): The North Atlantic Oscillation forcing through the last 2000 years: Spatial variability as revealed by high-resolution marine diatom records from N and SW Europe. Marine Micropaleontology 60(2): 113-129.

Gunn, D.E., A.I. Best (1998): A new automated nondestructive system for high resolution multi-sensor core logging of open sediment cores. Geo-Marine Letters 18: 70-77.

Hebbeln, D., K.-L. Knudsen, R. Gyllencreutz, P. Kristensen, D. Klitgaard-Kristensen, J. Backman, C. Scheurle, H. Jiang, I.M. Gil, M. Smelror, P.D. Jones, H.-P. Sejrup (2006): Late Holocene coastal hydrographic and climate changes in the eastern North Sea. The Holocene 16(7): 987-1001.

Hedges, J.I., R.G. Keil (1995): Sedimentary organic matter preservation: an assessment and speculative synthesis. Marine Chemistry 49: 81-115.

Holmes, E., P. Müller, R.R. Schneider, M. Segl, G. Wefer (1998): Spatial variations in euphotic zone nitrate utilization based on $\delta^{15}N$ in surface sediments. Geo-Marine Letters 18: 58-65.

Holz, C., J.B.W. Stuut, R. Henrich (2004): Terrigenous sedimentation processes along the continental margin off NW Africa: implications from grain-size analysis of seabed sediments. Sedimentology 51: 1145-1154.

Hurrell, J.W., H.v. Loon (1997): Decadal variations in climate associated with the North Atlantic Oscillation. Climatic Change 36: 301-326.

Ittekkot, V., R.W.P.M. Laane (1991): Fate of Riverine Particulate Organic Matter. In: Degens, E.T., S. Kempe, J.E. Richey (eds.): SCOPE 42: Biogeochemistry of major world rivers. Chichester, U.K., Wiley: Chapter 10.

Jansen, J.H.F., S.J. Van der Gaast, B. Koster, A.J. Vaars (1998): CORTEX, a shipboard XRF-scanner for element analyses in split sediment cores. Marine Geology 151(1): 143-153.

Jouanneau, J.M., C. Garcia, A. Oliveira, A. Rodrigues, J.A. Dias, O. Weber (1998): Dispersal and deposition of suspended sediment on the shelf off the Tagus and Sado estuaries, S.W. Portugal. Progress in Oceanography 42: 233-257.

Jouanneau, J.M., O. Weber, T. Drago, A. Rodrigues, A. Oliveira, J. M. A. Dias, C. Garcia, S. Schmidt, J.L. Reyss (2002): Recent sedimentation and sedimentary budget on the western Iberian shelf. Progress in Oceanography 52: 261-275.

Kendall, C., E.A. Caldwell (1998): Fundamentals of Isotope Geochemistry. In: C. Kendall, J.J. McDonnell (eds.): Isotope Tracers in Catchment Hydrology, Elsevier, Amsterdam, 839 p: Chapter 2. (http://wwwrcamnl.wr.usgs.gov/isoig/isopubs/itchch2.html)

Lavik, G. (2001): Nitrogen Isotopes of sinking matter and sediments in the South Atlantic. Ph.D. Thesis, Fachbereich Geowissenschaften, Bremen: 140 pages.

Lebreiro, S.M., G. Francés, F.F.G. Abrantes, P.Diz, H.B. Bartels-Jónsdóttir, Z.N. Stroynowski, I.M. Gil, L.D. Pena, T. Rodrigues, P.D. Jones, M.A. Nombela, I. Alejo, K.R. Briffa, I. Harris, J.O. Grimalt (2006): Climate change and coastal hydrographic response along the Atlantic Iberian margin (Tagus Prodelta and Muros Ria) during the last two millennia. The Holocene 16(7): 1003-1015.

Lehmann, M.F., S.M. Bernasconi, A. Barbieri, J.A. McKenzie (2002): Preservation of organic matter and alteration of its carbon and nitrogen isotope composition during simulated and in situ early sedimentary diagenesis. Geochimica et Cosmochimica Acta 66(20): 3573-3584.

Lemos, P.A.F. (1984): Tagus Estuary. Lisboa, Administracao-Geral do Porto de Lisboa.

Liu, K.-K., I.R. Kaplan (1989): The eastern tropical Pacific as a source of 15N-enriched nitrate in seawater off southern California. Limnology and Oceanography 34(5): 820-830.

Loureiro, J.M. (1979): Curvas de duracao dos caudais medios diarios no rio Tejo. Technical report, Servico Hidraulico (DGRAH), Lisbon.

Loureiro, J.J.M., M.E. Macedo (1986): Bacia Hidrográfica do Rio Tejo. In: Monografias Hidrológicas dos Principais Cursos de Água de Portugal continental, Servico Hidraulico (DGRAH), Lisbon: 281-335.

Mariotti, A. (1983): Atmospheric nitrogen is a reliable standard for natural N-15 abundance measurements. Nature 303: 685-687.

Martins, V., J.M. Jouanneau, O. Weber, F. Rocha (2006): Tracing the late Holocene evolution of the NW Iberian upwelling system. Marine Micropaleontology 59(1): 35-55.

Meyers, P.A. (1994): Preservation of elemental and isotopic source identification of sedimentary organic matter. Chemical Geology 114: 289-302.

Milliman, J.D. (1990): River Discharge of Water and Sediment to the Oceans: Variations in Space and Time. In: Ittekkot, V., S. Kempe, W. Michaelis, A. Spitzy (eds.): Facets of Modern Biogeochemistry, Festschrift for the 60th anniversary of E.T. Degens. Berlin, Heidelberg: 83-90.

Miltner, A., K.-C. Emeis, U. Struck, T. Leipe, M. Voss (2005): Terrigenous organic matter in Holocene sediments from the central Baltic Sea, NW Europe. Chemical Geology 216: 313-328.

Müller, P.J. (1977): C/N ratios in Pacific deep-sea sediments: effect of inorganic ammonium and organic nitrogen compounds sorbed by clays. Geochimica et Cosmochimica Acta 41: 765-776.

Müller, P.J., E. Suess (1979): Productivity, sedimentation rate and sedimentary organic matter in the oceans - I. organic carbon preservation. Deep-Sea Research 26A: 1347-1362.

Müller, P., R.R. Schneider, G. Ruhland (1994): Late Quaternary pCO_2 variations the Angola Current: Evidence from organic carbon $\delta^{13}C_{org}$ and alkenone temperatures. In: Zahn, R., T.F. Pedersen (eds.): Carbon Cycling in the Glacial Ocean: Constraints of the Ocean's Role in Global Change. NATO ASI Series, Vol. 1(17), Springer: 343-366.

Ogrinc, N., G. Fontolan, J. Faganeli, S. Covelli (2005): Carbon and nitrogen isotope compositions of organic matter in coastal marine sediments (the Gulf of Trieste, N Adriatic Sea): Indicators of sources and preservation. Marine Chemistry 95(3-4): 163-181.

Oliveira, I., A. Valle, F. Miranda (1982): Littoral problems in the Portuguese west coast. Coastal Engineering Proceeding III: 1951-1969.

Oliveira, A., A. Rodrigues, J.M. Jouanneau, O. Weber, J.M. Alveirinho-Dias, J. Vitorino (1999): Suspended particulate matter distribution and composition on the northern Portuguese margin. Boletino del Instituto Espanol de Oceanografia 15(1-4): 101-109.

Oliveira, A., F. Rocha, A. Rodrigues, J.M. Jouanneau, A. Dias, O. Weber, C. Gomes (2002): Clay minerals from the sedimentary cover from the Northwest Iberian shelf. Progress in Oceanography 52: 233-247.

Owens, N.J.P. (1985): Variations in the natural abundance of ^{15}N in estuarine suspended particulate matter: a specific indicator of biological processing. Estuarine, Coastal and Shelf Science 20: 505-510.

Paul, A., S. Mulitza, J. Pätzold, T. Wolff (1999): Simulation of oxygen isotopes in a global ocean model. In: Fischer, G., G. Wefer (eds.): Use of Proxies in Paleoceanography: Examples from the South Atlantic. Springer, Heidelberg: 655-686.

Park, R., S. Epstein (1961): Metabolic fractionation of ^{12}C and ^{13}C in plants. Plant Physiology 36(2): 133-138.

Peliz, A.J., A.F.G. Fiúza (1999): Temporal and spatial variability of CZCS-derived phytoplankton pigment concentrations of the western Iberian Peninsula. International Journal of Remote Sensing 20(7): 1363-1403.

Ransom, B., D. Kim, M. Kastner, S. Wainwright (1998): Organic matter preservation on continental slopes: Importance of mineralogy and surface area. Geochimica Et Cosmochimica Acta 62(8): 1329-1345.

Redfield, A.C., B.H. Ketchum, F.A. Richards (1963): The influence of organisms on the composition of seawater. In: Hill, M.N. (ed.): The Sea, Vol. 2, Wiley, New York: 26-79.

Sackett, W.M., W.R. Eckelmann, M.L. Bender, W.H. Bé (1965): Temperature dependence of carbon isotope composition in marine plankton and sediments. Science 148: 235-237.

Scheffer, F., P. Schachtschabel (2002): Lehrbuch der Bodenkunde, 15. Edition. Spektrum Akademischer Verlag, Heidelberg: 528 pages.

Schönfeld, J. (1997): The impact of the Mediterranean Outflow Water (MOW) on benthic foraminiferal assemblages and surface sediments at the southern Portuguese continental margin. Marine Micropaleontology 29(3): 211-236.

Schubert, C.J., B. Nielsen (2000): Effects of decarbonation treatments on $\delta^{13}C_{org}$ values in marine sediments. Marine Chemistry 72: 55-59.

Schubert, C.J., S.E. Calvert (2001): Nitrogen and carbon isotopic composition of marine and terrestrial organic matter in Arctic Ocean sediments: implications for nutrient utilization and organic matter composition. Deep-Sea Research I 48: 789-810.

Silva, S., A. Ré, P. Pestana, A. Rodrigues, V. Quintino (2004): Sediment disturbance off the Tagus Estuary, Western Portugal: chronic contamination, sewage outfall operation and runoff events. Marine Pollution Bulletin 49: 154–162.

Skinner, L.C., N.J. Shackleton (2004): Rapid transient changes in northeast Atlantic deep water ventilation age across Termination I. Paleoceanography 19(2): PA2005. doi:10.1029/ 2003PA000983.

Smith, B.N., S. Epstein (1977): Two categories of $^{13}C/^{12}C$ ratio for higher plants. Plant Physiology 47: 380-384.

Soares, A.M.M., J.M.A. Dias (2006): Coastal upwelling and radiocarbon - evidence for temporal fluctuations in ocean reservoir effect off Portugal during the Holocene. Radiocarbon 48(1): 45-60.

Sonzogni, C., E. Bard, F. Rostek, D. Dollfus, A. Rosell-Mele and G. Eglinton (1997): Temperature and Salinity Effects on Alkenone Ratios Measured in Surface Sediments from the Indian Ocean. Quaternary Research 47(3): 344-355.

Stuut, J.B.W., M.A. Prins, R.R. Schneider, G.J. Weltje, J.H.F. Jansen, G. Postma (2002): A 300-kyr record of aridity and wind strength in southwestern Africa: inferences from grain-size distributions of sediments on Walvis Ridge, SE Atlantic. Marine Geology 180(1-4): 221-233.

Trigo, R.M., T.J. Osborn, J.M. Corte-Real (2002): The North-Atlantic Oscillation influence on Europe: climate impacts and associated physical mechanisms. Climate Research 20: 9-17.

Trigo, R., D. Pozo-Vazquez, T. Osborn, Y. Castro-Diez, S. Ganiz-Fortis, M.J. Esteban-Parra (2004): North Atlantic oscillation influence on precipitation, river flow and water resources in the Iberian Peninsula. International Journal of Climatology 24: 924-944.

Vale, C., B. Sundby (1987): Suspended Sediment Fluctuations in the Tagus Estuary on Semi-Diurnal and Fortnightly Time Scales. Estuarine Coastal and Shelf Science 25(5): 495-508.

Vicente-Serrano, M., A. Heredia-Laclaustra (2004): NAO influence on NDVI trends in the Iberian Peninsula (1982-2000). International Journal of Remote Sensing 25(14): 2871-2879.

Vieira, M.E.C., A.A. Bordalo (2000): The Douro estuary (Portugal): a mesotidal salt wedge. Oceanologica Acta 23(5): 585-594.

Visbeck, M.H., J.W. Hurrell, L. Polvani, H.M. Cullen (2001): The North Atlantic Oscillation: Past, Present and Future. Proceedings of the National Academy of Sciences 98(23): 12876-12877.

Weaver, P.P.E., R.B. Wynn, N.H. Kenyon, J. Evans (2000): Continental margin sedimentation, with special reference to the north-east Atlantic margin. Sedimentology 47(6-Supplement 1): 239-256.

Weltje, G.J. (1997): End-member modeling of compositional data: numerical-statistical algorithms for solving the explicit mixing problem. Journal of Mathematical Geology 29: 503-549.

Zenk, W., L. Armi (1990): The complex spreading pattern of Mediterranean Water off the Portuguese continental slope. Deep Sea Research I: Oceanographic Research Letters 37(12): 1805-1823.